2 March 2012 | $10

Science

AAAS

CONTENTS

Volume 335 Issue 6072

EDITORIAL

1019 The Flame Challenge
Alan Alda

NEWS OF THE WEEK

1024 A roundup of the week's top stories

NEWS & ANALYSIS

1027 Loose Cable May Unravel Faster-Than-Light Result

1028 Scientists Rush to Find Clues on New Animal Virus

1029 Potential Egg Stem Cells Reignite Debate

1030 Is Motherhood the Biggest Reason for Academia's Gender Imbalance?
Half-Time Jobs, Full-Time Scientists

1032 Overhaul of U.S. Child Health Study Concerns Investigators

NEWS FOCUS

1033 Sound and Fury in the Microbiology Lab
Giant Viruses Revive Old Questions About Viral Origins

1036 'Killjoys' Challenge Claims of Clever Animals

1038 Is the World Tottering on the Precipice of Peak Gold?
>> Science *Podcast*

LETTERS

1040 Editors' Note
C. Norman and J. Sills

Saudi University Policy: King Saud Response
A. A. Al-Khedhairy

Saudi University Policy: King Abdulaziz Response
A. Zahed

Saudi University Policy: Meaningful Cooperation
U. Becker

Saudi University Policy: Overvalued Rankings
G. Miley

1042 TECHNICAL COMMENT ABSTRACTS

1042 CORRECTIONS AND CLARIFICATIONS

BOOKS *ET AL.*

1043 The Major Transitions in Evolution Revisited
B. Calcott and K. Sterelny, Eds., reviewed by D. H. Erwin

1044 Dispersed Radiance
A. Sur, reviewed by A. Gopinathan

POLICY FORUMS

1045 Reconsidering the Consequences of Selective Fisheries
S. M. Garcia et al.

1047 The Limits of Government Regulation and Science
J. D. Kraemer and L. O. Gostin
>> See all H5N1 coverage online at http://scim.ag/_h5n1

PERSPECTIVES

1050 Reconfiguring Regulation
G. Chalancon et al.
>> Reports pp. 1099 and 1103

1051 Probing the Mantle Past
V. C. Bennett
>> Research Article p. 1065

1052 Facing Extinction in Real Time
D. B. Wake

1054 Roaming Reaction Pathways Along Excited States
M. J. T. Jordan and S. H. Kable
>> Report p. 1075

1055 Structural Origins of Receptor Bias
S. R. Sprang and J. Chief Elk
>> Report p. 1106

1056 Origins of Cumulative Culture
R. Kurzban and H. C. Barrett
>> Report p. 1114

CONTENTS continued >>

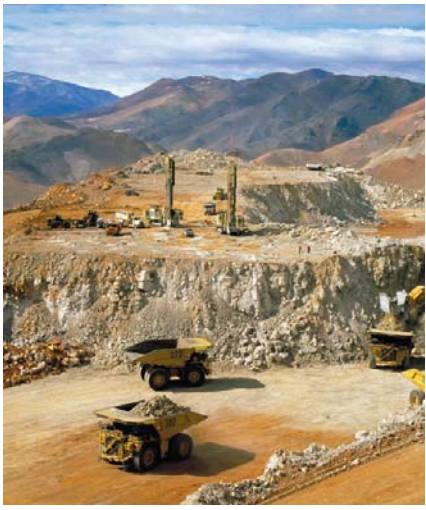

page 1038

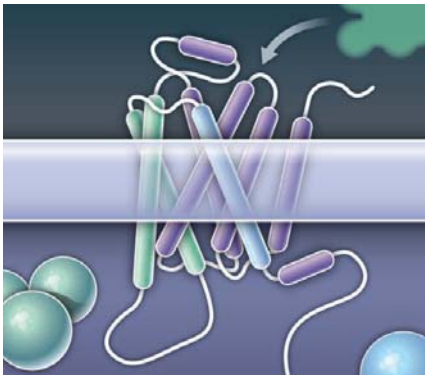

pages 1055 & 1106

COVER

An adult male brown anole, *Anolis sagrei* (length ~150 millimeters from snout to tail), perches atop a branch. The diameter of the vegetation used by brown anoles is a strong selective force on limb length. Lizards inhabiting previously unoccupied islands in the Bahamas show genetic and morphological differences due to random and selective processes. See page 1086.

Photo: Neil Losin, University of California, Los Angeles, www.neillosin.com

DEPARTMENTS

1017 This Week in *Science*
1020 Editors' Choice
1022 *Science* Staff
1126 New Products
1127 *Science* Careers

Published by AAAS

CONTENTS

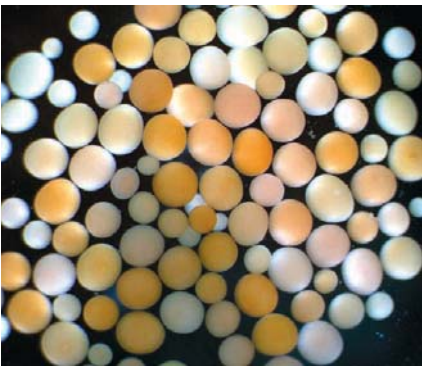

page 1064

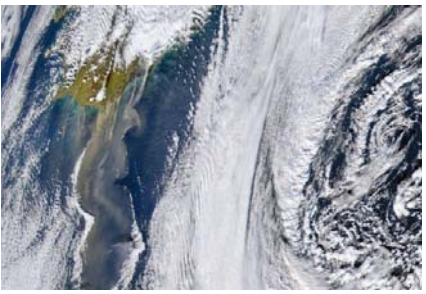

page 1078

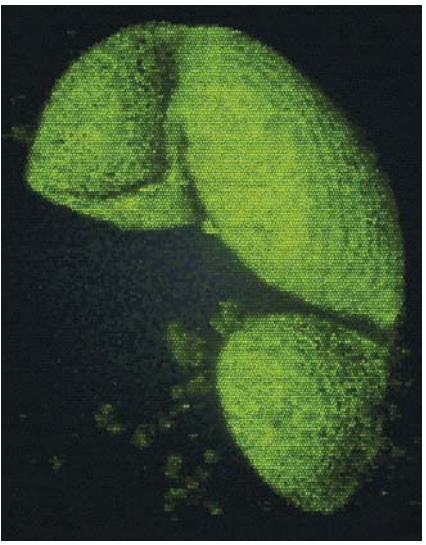

page 1083

REVIEW

1058 The Geological Record of Ocean Acidification
B. Hönisch et al.

BREVIA

1064 Turbulence, Cleavage, and the Naked Embryo: A Case for Coral Clones
A. J. Heyward and A. P. Negri
The embryos of pelagic corals break up in waves yet survive to form smaller colonies.

RESEARCH ARTICLE

1065 ^{182}W Evidence for Long-Term Preservation of Early Mantle Differentiation Products
M. Touboul et al.
Tungsten isotopes in ancient volcanic rocks suggest sluggish mixing processes in the primitive mantle.
>> Perspective p. 1051

REPORTS

1070 Observation of Quantum Criticality with Ultracold Atoms in Optical Lattices
X. Zhang et al.
Trapped low-temperature atoms model the transition between insulating and superfluid states in a more complex material.

1072 Reactions of Solvated Electrons Initiated by Sodium Atom Ionization at the Vacuum-Liquid Interface
W. A. Alexander et al.
Electrons at a deuterated glycerol surface can liberate deuterium atoms that escape into the gas phase before reacting further.

1075 No Straight Path: Roaming in Both Ground- and Excited-State Photolytic Channels of $NO_3 \rightarrow NO + O_2$
M. P. Grubb et al.
A chemical reaction proceeds exclusively by mechanisms that do not pass through a conventional transition state.
>> Perspective p. 1054

1078 High-Latitude Dust Over the North Atlantic: Inputs from Icelandic Proglacial Dust Storms
J. M. Prospero et al.
Cold, higher-latitude regions—not just low-latitude arid regions—can be substantial sources of dust.

1083 Glacial Survival of Boreal Trees in Northern Scandinavia
L. Parducci et al.
DNA from modern and ancient spruce and pine indicate that both survived in ice-free areas during the last glaciations.

1086 Founder Effects Persist Despite Adaptive Differentiation: A Field Experiment with Lizards
J. J. Kolbe et al.
Introduced populations of anoles retain characteristics of their founders and acquire adaptations to their new environment.

1090 Pollinator-Mediated Selection on Flower Color Allele Drives Reinforcement
R. Hopkins and M. D. Rausher
Butterfly behavior reduces hybridization and reinforces speciation among *Phlox* plants.

1092 Generation of Leaf Shape Through Early Patterns of Growth and Tissue Polarity
E. E. Kuchen et al.
A model for the development of leaf shape describes how it arises through oriented growth and tissue deformation.

1096 Elastic Domains Regulate Growth and Organogenesis in the Plant Shoot Apical Meristem
D. Kierzkowski et al.
New leaves emerge where they are allowed.

1099 Global Network Reorganization During Dynamic Adaptations of *Bacillus subtilis* Metabolism
J. M. Buescher et al.
A vertical analysis reveals that a simple switch of one food for another evokes changes at many levels.

1103 Condition-Dependent Transcriptome Reveals High-Level Regulatory Architecture in *Bacillus subtilis*
P. Nicolas et al.
A horizontal analysis reveals the breadth of genes turned on and off as nutrients change.
>> Perspective p. 1050

1106 Biased Signaling Pathways in β_2-Adrenergic Receptor Characterized by ^{19}F-NMR
J. J. Liu et al.
Selective effects of different ligands provide insights into the structural plasticity of receptor signaling.
>> Perspective p. 1055

1110 Catalysis and Sulfa Drug Resistance in Dihydropteroate Synthase
M.-K. Yun et al.
Structures of a target enzyme in the bacteria that cause anthrax and bubonic plague may lead to effective drugs.

1114 Identification of the Social and Cognitive Processes Underlying Human Cumulative Culture
L. G. Dean et al.
Humans not only watch and imitate each other but also learn from each other in multiple ways.
>> Perspective p. 1056; Science *Podcast*

1118 The Effects of Experience and Attrition for Novice High-School Science and Mathematics Teachers
G. T. Henry et al.
New teachers face a steep learning curve, and those who fall off tend to leave teaching.

Published by AAAS

SCIENCEONLINE

SCIENCEXPRESS
www.sciencexpress.org

Energy Capture from Thermolytic Solutions in Microbial Reverse-Electrodialysis Cells
R. D. Cusick et al.
Thermally induced salt gradients could augment the electricity generated by microbial fuel cells from wastewater.
10.1126/science.1219330
>> Science *Podcast*

Silicon Isotope Evidence Against an Enstatite Chondrite Earth
C. Fitoussi and B. Bourdon
Earth accreted from materials with a heterogeneous mix of chondritic meteorite compositions.
10.1126/science.1219509

Niche and Neutral Effects of Acquired Immunity Permit Coexistence of Pneumococcal Serotypes
S. Cobey and M. Lipsitch
The human immune response preserves antigenic variation in a bacterial pathogen.
10.1126/science.1215947

Interleukin-22 Drives Endogenous Thymic Regeneration in Mice
J. A. Dudakov et al.
Damage to the thymus caused by infection or radiation is reversed by a cytokine.
10.1126/science.1218004

Crystal Structure of Human Enterovirus 71
P. Plevka et al.
The structure of a virus linked to neurological disease reveals how drugs targeting viruses in this family can be modified.
10.1126/science.1218713

TECHNICALCOMMENTS

Comment on "Phonemic Diversity Supports a Serial Founder Effect Model of Language Expansion from Africa"
T. F. Jaeger et al.
Full text at www.sciencemag.org/cgi/content/full/335/6072/1042-a

Response to Comment on "Phonemic Diversity Supports a Serial Founder Effect Model of Language Expansion from Africa"
Q. D. Atkinson
Full text at www.sciencemag.org/cgi/content/full/335/6072/1042-b

SCIENCENOW
www.sciencenow.org
Highlights From Our Daily News Coverage

Shame on the Rich
Unethical behavior more common in upper classes.
http://scim.ag/Shame_Rich

The Red-Dress Effect
Men see women wearing red as more open to romantic advances.
http://scim.ag/Red-Dress

Bacteria-Killing Viruses Wield an Iron Spike
Researchers figure out how bacteriophages gain entry into cells.
http://scim.ag/Viral_Attack

SCIENCESIGNALING
www.sciencesignaling.org
The Signal Transduction Knowledge Environment
28 February issue: http://scim.ag/ss022812

EDITORIAL GUIDE: Focus Issue—A Cell's Sense of Direction
W. Wong
Research reveals new mechanisms for cell migration and chemotaxis.

RESEARCH ARTICLE: Diverse Sensitivity Thresholds in Dynamic Signaling Responses by Social Amoebae
C. J. Wang et al.

PERSPECTIVE: Chemoattractant Signaling in *Dictyostelium*—Adaptation and Amplification
P. A. Iglesias
Dictyostelium cells sense and interpret gradients by combining an incoherent feedforward loop and an amplification step.

RESEARCH ARTICLE: PTEN Protein Phosphatase Activity Correlates with Control of Gene Expression and Invasion, a Tumor-Suppressing Phenotype, But Not with AKT Activity
P. Tibarewal et al.
The lipid and protein phosphatase activities of PTEN are both required for glioma cell invasion and many of its effects on gene expression.

PERSPECTIVE: How Actin Gets the PIP
S. E. Moss
The relative concentrations of different phosphoinositide species may dictate whether actin comets or membrane ruffles are formed.

SCIENCETRANSLATIONAL MEDICINE
www.sciencetranslationalmedicine.org
Integrating Medicine and Science
29 February issue: http://scim.ag/stm022912

RESEARCH ARTICLE: A Biophysical Indicator of Vaso-occlusive Risk in Sickle Cell Disease
D. K. Wood et al.

PODCAST
J. M. Higgins and M. L. Frisk
An ex vivo microfluidic device can stratify sickle-cell patients on the basis of dynamic blood properties.

RESEARCH ARTICLE: Productive Replication of Ebola Virus Is Regulated by the c-Abl1 Tyrosine Kinase
M. García et al.
Ebola virus growth is regulated by a c-Abl tyrosine kinase, which modulates the viral protein VP40, and can be blocked by c-Abl antagonists.

RESEARCH ARTICLE: HIV-Specific Cytolytic CD4 T Cell Responses During Acute HIV Infection Predict Disease Outcome
D. Z. Soghoian et al.

PERSPECTIVE: $CD4^+$ T cells and HIV—A Paradoxical Pas de Deux
N. R. Klatt and G. Silvestri
A robust $CD4^+$ T cell response during early HIV infection predicts a slower progression to overt disease.

PERSPECTIVE: Toward a Meningitis-Free World
S. Black et al.
New vaccines against serotypes A, C, W, Y, and B of meningococcal meningitis may allow elimination of the disease.

SCIENCECAREERS
www.sciencecareers.org/career_magazine
Free Career Resources for Scientists

Taken for Granted: Foreign Invasion
B. L. Benderly
What happens when an influx of established talent invades a small research field?
http://scim.ag/TFG_Invasion

Young Spanish Scientists in Limbo
E. Pain
Tighter research budgets and bureaucratic delays threaten to derail the careers of many young scientists in Spain.
http://scim.ag/SpanishLimbo

Perspective: Preparing for a PUI Career
R. N. Austin
A chemistry professor at a top liberal arts college offers advice on preparing for jobs at colleges like hers.
http://scim.ag/PUI_Prep

SCIENCEPODCAST
www.sciencemag.org/multimedia/podcast
Free Weekly Show

On the 2 March *Science* Podcast: the roots of human cumulative culture, microbes that transform waste into energy, peak gold, and more.

SCIENCEINSIDER
news.sciencemag.org/scienceinsider
Science Policy News and Analysis

SCIENCE (ISSN 0036-8075) is published weekly on Friday, except the last week in December, by the American Association for the Advancement of Science, 1200 New York Avenue, NW, Washington, DC 20005. Periodicals Mail postage (publication No. 484460) paid at Washington, DC, and additional mailing offices. Domestic individual membership and subscription (51 issues): $149 ($74 allocated to subscription). Domestic institutional subscription (51 issues): $990; Foreign postage extra: Mexico, Caribbean (surface mail) $55; other countries (air assist delivery) $85. First class, airmail, student, and emeritus rates on request. Canadian rates with GST available upon request, GST #1254 88122. Publications Mail Agreement Number 1069624. **Printed in the U.S.A.**

Change of address: Allow 4 weeks, giving old and new addresses and 8-digit account number. **Postmaster:** Send change of address to AAAS, P.O. Box 96178, Washington, DC 20090–6178. **Single-copy sales:** $10.00 current issue, $15.00 back issue prepaid includes surface postage; bulk rates on request.

AAAS
ADVANCING SCIENCE, SERVING SOCIETY

EDITED BY CAROLINE ASH

The Constant Pollinator

In ecology, reinforcement is the process by which species prevent hybridization and maintain species boundaries, but the underlying genetic mechanisms are unclear. **Hopkins and Rausher** (p. 1090, published online 2 February) examined reinforcement between two species of a wild flowering plant called *Phlox* that show incomplete hybrid sterility. Down-regulation of a flavonoid gene produces red flowers and operates in concert with a color intensity locus to adjust flower color and tone. A distinct geography of flower color has emerged in which it appears that dark coloration causes less hybridization between the species because the butterfly pollinators tend to favor light-blue flower color variants. If pollinators visit flowers with similar phenotypes more frequently than flowers with dissimilar phenotypes, this will decrease gene flow between the unlike flowers.

Acid History

As human activity continues to pump nearly 50-fold more CO_2 into the atmosphere than any existing natural sources, the oceans absorb it. Over time, this vast quantity of excess oceanic CO_2 is expected to decrease oceanic pH and have marked effects on calcifying marine species. Looking to the past for records of the consequences, other instances of ocean acidification in geologic history caused by large natural events, such as volcanism, may help predict the oceans' response to contemporary CO_2 levels. **Hönisch *et al.*** (p. 1058) review the geological events that potentially altered oceanic pH, from the last deglaciation to the largest mass extinction in Earth's history. The current rate of anthropogenic CO_2 input into the oceans is much faster than at any other instance in the past, but yet it is unclear whether or not future ocean pH will be significantly affected.

Earth's Sluggish Past

Based on their affinity for iron or silicon, some elements partition into different compartments of Earth's interior. In the early stages of the formation of the solar system, when Earth was rapidly accreting and differentiating to form a core and mantle, elements such as tungsten and hafnium went along for the ride. By studying the signatures of these elements and their isotopes in ancient volcanic rocks from the mantle, **Touboul *et al.*** (p. 1065, published online 16 February; see the Perspective by **Bennett**) reveal that there was a long-lived ^{182}W reservoir that formed deep within Earth during the first 30 million years of the solar system. Because the reservoir persisted for over 1.7 billion years, it appears the mantle was poorly mixed and indeed it was so sluggish that it did not even homogenize during the massive collision that formed the Moon.

Cold Dust

Atmospheric dust affects air quality, air and ocean chemistry, ocean biology, and climate, so understanding its origins is important to many fields. Hot, dry, desert regions at low latitudes are well-understood sources, but the role of higher-latitude regions in dust production has not been considered. **Prospero *et al.*** (p. 1078) present a 6-year record of measurements made on an island south of Iceland, which revealed frequent episodes of dust-production associated with glacial outwash plains and outburst floods. Much of this dust is transported southward and deposited in the North Atlantic, making it a potentially important supply of iron to drive ocean production in that region.

Tree Refugia

Ideas of how and when boreal plants spread to the formerly glaciated parts of the world following the retreat of the glaciers 9000 years ago are long debated. Models of the postglacial spread of boreal plants argue for dispersal from southern refugia; however, **Parducci *et al.*** (p. 1083) have shown that both spruce and pine were present in small ice-free regions of Scandinavia much earlier than thought. DNA haplotyping confirmed that a remnant mitochondrial type of spruce, once unique to Scandinavia, now lives alongside the more common spruce originating from Eastern Europe. Evidence from lake cores collected from central and northern Norway indicated the survival of conifers as early as 22,000 years before the present, when apart from ice-free pockets, most of Scandinavia was covered by ice.

Setting Atoms Free

In a plasma, gaseous atoms and molecules accumulate so much energy that they fall apart into electrons and all manner of bigger charged fragments. Free electrons can also wreak a degree of havoc within a liquid environment as they generate local reactive fragments, which then couple with the surrounding solvent to form a slew of products. **Alexander *et al.*** (p. 1072) explored what happens if reactive electrons emerged at the surface of such a liquid. To generate these conditions, they bombarded a shallow film of deuterated glycerol with sodium atoms that ionized on impact and discovered, in contrast with bulk liquid, that solvent-derived deuterium atoms escaped from the surface into the gas phase before they could react any further.

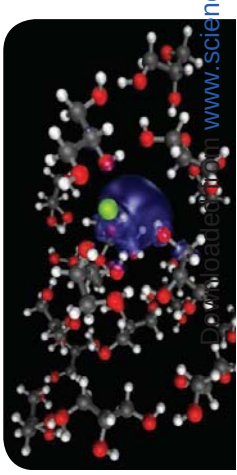

Random and Directed

Natural selection drives populations to adapt to new environments; the raw material or "founder effects" provided by the first colonizing individuals can thus have a formative influence on the population's future. **Kolbe *et al.*** (p. 1086, published online 2 February; see the cover) tested the relative contributions of selection and founder effects in Bahamian lizards. Founders were taken from an island covered in forest:

Continued on page 1018

Continued from page 1017

These lizards had long hindlimbs for sprinting across the broad expanses of tree trunks. Long-limbed lizards were introduced to seven smaller islands covered in scrub that, before hurricane Frances in 2004 swept them away, had been populated by lizards with short hindlimbs better suited for navigating a twiggy habitat. After several generations, all the new lizard populations had adapted to their new habitats by evolving shorter hindlimbs but they also retained other morphological and genetic signatures from their founding ancestors. Thus, evolution occurs by a combination of arbitrary events, as well as those shaped by selection.

Shape-Shifting Signals

Although orthogonal signaling systems seem to direct various developmental processes, few tissues remain in the same shape as they are at initiation to that of the final form. *Arabidopsis* leaves are free of the cell migrations that complicate animal development, and thus allowed **Kuchen *et al.*** (p. 1092) to track and model the trajectory of leaf growth under a variety of perturbations. Varying the values of parameters in their model produced outputs of different leaf shapes ranging from obcordate, ovate, and oval to elliptic, and offered predictions for genes that regulate the developmental process. The meristem at the growing tip of plants is home to stem cells and is the source of newly differentiating shoots and leaves. New leaves make their first appearance as bulges at the side of the dome-shaped meristem. Although these developmental events are under hormonal control, they also seem to be constrained by the physical properties of the meristem. **Kierzkowski *et al.*** (p. 1096) tested physical effects acting on the shoot apical meristem of growing tomato shoots that alter turgor pressure. Again, mathematical modeling combined with observations of plant tissue helped to define the different zones in the meristem that respond to diverse mechanical stimuli.

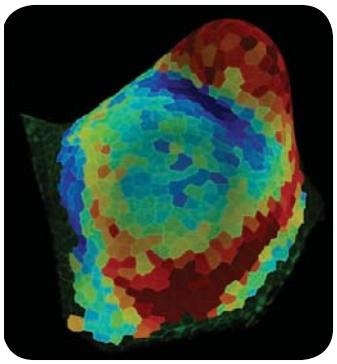

CREDIT: DANIEL KIERZKOWSKI, ANNE-LISE ROUTIER-KIERZKOWSKA, AND RICHARD S. SMITH

Sulfa's Crystal View

The sulfonamide antibiotics (sulfa drugs) have been used to treat infections for over 70 years; however, emerging resistance has eroded their clinical utility. Sulfa drugs target dihydropteroate synthase, a key enzyme in the bacterial folate pathway. By performing the reaction in the crystalline form of the enzyme, **Yun *et al.*** (p. 1110) have characterized the key structural intermediates. In combining structural data with theoretical and mutagenesis studies, they propose a detailed mechanism for dihydropteroate synthase catalysis. By resolving this structure with a sulfa drug bound to the enzyme, they showed how inhibition occurred and indicated how resistance could emerge.

Acquire and Share

Few would argue with the stance that human social cognition supports an unequaled capacity to acquire knowledge and to share it with others. **Dean *et al.*** (p. 1114; see the Perspective by **Kurzban and Barrett**) compared the extent to which these social and cognitive psychological processes can be elicited in children, capuchins, and chimpanzees through the use of a three-level puzzlebox task. Incentivized by improving rewards, 3- to 4-year-old children progressed from the first to the third level by imitating observed actions, taught other members of their social group how to solve the problem, and shared the rewards obtained. By contrast, neither the capuchins nor chimpanzees, very few of which ever reached the third level, exhibited these charactertistics.

New Teacher Syndrome

The employment retention of high-school science and math teachers in the United States has diminished over recent decades, such that now many students are being taught by novice teachers. **Henry *et al.*** (p. 1118) have analyzed the effectiveness of teachers by examining data collected from North Carolina public schools. Less-effective teachers seem to have a greater tendency to leave teaching and the greatest gains in teacher effectiveness are when the teacher is new—within the first 3 years on the job. Some subject areas are more likely to be affected by the preponderance of novice teachers than other subjects, including math and science.

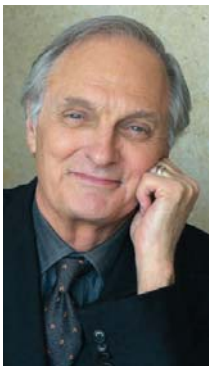

Alan Alda is an actor, writer, and founding board member of the Center for Communicating Science.

The Flame Challenge

I WAS 11 AND I WAS CURIOUS. I HAD BEEN THINKING FOR DAYS ABOUT THE FLAME AT THE END of a candle. Finally, I took the problem to my teacher. "What's a flame?" I asked her. "What's going on in there?" There was a slight pause and she said, "It's oxidation." She didn't seem to think there was much else to say. Deflated, I knew there had to be more to the mystery of a flame than just giving the mystery another name. That was a discouraging moment for me personally, but decades later I see the failure to communicate science with clarity as far more serious for society. We feel the disconnect all around us, from a common misimpression that evolution is the theory that we're descended from monkeys, to the worry that physicists in Geneva might suck the universe into a teacup—or something uncomfortably smaller.

Scientists have recognized for some time that there is a harmful gap in understanding between their work and much of the rest of the world—one that can hold back scientific progress. Scientists urgently need to be able to speak with clarity to funders, policy-makers, students, the general public, and even other scientists. (Not to mention the poignant wish of some young researchers to be able to explain their work to their grandmothers.) I first got insight into this problem while interviewing hundreds of scientists on the television program Scientific American Frontiers, produced for the Public Broadcasting Service in the United States. On that show, rather than doing conventional interviews, I had conversations with the scientists in which I kept barraging them with questions until I finally understood their answers. As a result, their work became more accessible to the audience (and to me) than if I had stuck to a standard interview format. Having to talk with someone who was truly trying to understand caused an actual human interaction to take place in these interviews. There was more warmth, and the real person behind the scientist in the white lab coat could emerge. Suddenly, both young people and adults could see that scientists were like them, with a natural way of speaking and even a sense of humor.

I began to think that clarity in communicating science is at the very heart of science itself. And I wondered if written and oral communication skills could be taught systematically throughout the entire length of a student's science education. The State University of New York at Stony Brook picked up on this idea, founding the Center for Communicating Science. I became part of the teaching faculty, and we began experimenting. We are now teaching communication courses for credit to graduate students in the sciences. Students learn to distill their message and write without jargon. They also experience an innovative course in improvisation, which teaches them to communicate with a live audience with the ease and familiarity of an animated conversation. The intention, of course, is not to turn scientists into actors but to allow them to be more authentically themselves in public interactions. Most of all, we discourage any form of "dumbing down" the science. The goal is to achieve clarity and vividness.

As serious as this question is, I'd like to try a playful experiment. Would you be willing to have a go at writing your own explanation of what a flame is—one that an 11-year-old would find intelligible, maybe even fun? The Center for Communicating Science is looking for new ways to light up people's minds with science, and you might point the way. We'll try out the entries on real 11-year-olds and see which work best. For information about this Flame Challenge contest, see http://flamechallenge.org.

So here I am—I'm 11 years old and looking up at you with the wide eyes of curiosity. What is a flame? What's going on in there? What will you tell me?

– Alan Alda

10.1126/science.1220619

EDITORS' CHOICE

EDITED BY KRISTEN MUELLER AND JAKE YESTON

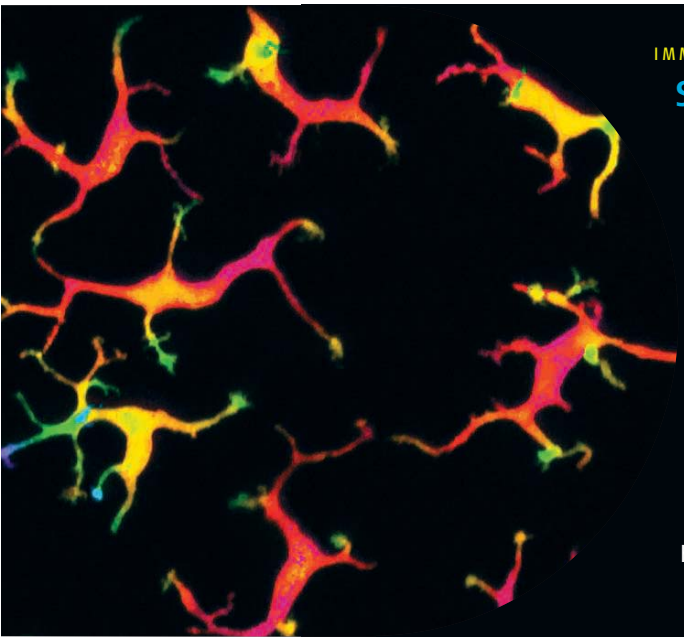

IMMUNOLOGY

Skin Surveyors

A specialized population of T cells that reside in the skin are important for responding to stress, such as that caused by wounding or malignancy. In mice, most of these cells express the γδ T cell receptor (TCR), and it is thought that they recognize stress when the TCR itself engages stress-induced ligands. Whether the TCR of skin γδ T cells is engaged in the steady state, however, is not well understood. Chodaczek *et al*. used a combination of intravital microscopy and immunohistochemistry of recently imaged mouse skin fragments to obtain a better picture of the actions of epidermal γδ T cells in the steady state. They found that these cells had specific orientations: They were positioned along squamous keratinocyte tight junctions and had multiple dendrites that extended toward the apical epidermis. The γδ TCR as well as other TCR signaling molecules localized to the tips of the dendrites in a TCR-specific manner. Epidermal stress caused γδ T cells to reorient toward the basal epidermis and Langerhans cells, but did not substantially alter the strength of the TCR signals. These results suggest that active TCR signaling in the basal state may help to prime γδ T cells to respond to a secondary stress signal. — KLM

Nat. Immunol. **13**, 272 (2012).

CHEMISTRY

The Ends Control the Means

Changing the balance of weak intermolecular forces can change the types of phases that molecules form. Cortese *et al*. explored the ordering of polypropylene (PPO) oligomers (either 460 or 2200 g/mol) bearing either thymine (Thy) or diaminotriazine (DAT) end groups, as well as mixtures of these molecules. The better-defined hydrogen bonding complementarity of Thy caused those associated oligomers to arrange in both a crystalline phase and a lamellar phase, in which the Thy groups formed an ordered two-dimensional crystal but the PPO chains were disordered. In contrast, DAT-terminated oligomers formed only glasses; the stronger affinity of PPO for DAT than Thy and the multiple hydrogen bonding motifs provided less driving force for microphase separation. In mixtures of the oligomers, the stronger Thy-DAT versus Thy-Thy interactions actually disrupted the lamellar ordering. In these systems, the ability of the end groups to crystallize appeared to be the main driver of mesoscopic ordering. — PDS

J. Am. Chem. Soc. **134**, 10.1021/ja2119496 (2012).

ENGINEERING

Lightening the Load

One clear-cut method of raising the fuel efficiency of a car is to reduce its weight. Of course, that's easier said than done, given competing constraints such as safety and performance. Alonso *et al.* focus on a more subtle aspect of the problem. In principle, an overall reduction in gross vehicle mass (GVM) enables an associated reduction in the masses of many individual components that now bear and act on a lighter load. In practice, such secondary mass savings (SMS) may go unrealized because the subsystems are designed and manufactured separately—

and in some cases are used in a range of car models that vary in GVM. The authors therefore empirically analyze the subsystems in a set of 77 vehicles (representing 13 different manufacturers) currently marketed in North America and Europe to pinpoint sources and scope of SMS, with the ultimate goal of facilitating consideration of these factors earlier in the overall design process. Their statistics indicate prospective mean SMS as high as 0.95 kg per kg of primary mass reduction. — JSY

Environ. Sci. Technol. **46**, 10.1021/es202938m (2012).

CLIMATE SCIENCE

Soon It's Gonna Rain

As climate warms, the atmosphere holds more moisture, and increased global precipitation is expected even while deserts may expand or move as areas receiving precipitation shift. This physics is captured in global climate models, and their results show changes even for warming over the 20th century. However, observational data seem to show an even greater increase in precipitation. Noake *et al.* take a closer look, comparing three data sets of on-land precipitation covering the latter half of the 20th century with the output from 54 climate model runs. Their analysis shows that precipitation increased most noticeably at higher latitudes in the Northern Hemisphere from December through May and over a wider belt in the fall; summer precipitation decreased slightly at lower latitudes. The model results are consistent with the pattern seen, but underestimate the spring increases seen at higher latitudes. Most useful for planning are estimates of the likely extremes in precipitation, as these affect flood forecasts and mitigation contingencies. Mishra *et al.* conduct an analysis comparing regional climate models and observations of urban extreme

Published by AAAS

precipitation events across the United States. Their comparison similarly implies that regional models generally underestimate short-lived precipitation extremes but do somewhat better (about 25% success) with daily averages. — BH

Geophys. Res. Lett. **39**, L03706; L03407 (2012).

ECOLOGY

Behold My Triumph

Triumph displays are something we regularly associate with professional athletes, who often celebrate their victories in sometimes quite memorable ways. Such displays also occur widely among animals—for example, as loud calls that follow a victory over a competitor for territory or a mate. The functions of these displays, however, are not well understood. This is because understanding a display's function requires knowing something about how it influences its potential receivers, and characterizing a receiver's impression of a display is challenging. Mouterde *et al.* use a clever approach to try to characterize the internal response of nesting little blue penguins to the call of a triumphant male. They briefly replaced the eggs of nesting birds (both males and females) with egg-shaped heart monitors and then experimentally exposed them to calls simulated to represent winners and losers. When later exposed to the same calls, the heart rates of males rose significantly in the presence of winners, but not losers. The heart rates of females rose in response to both types of calls. These results suggest that triumph calls operate to establish a dominance reputation for individuals, particularly among males, and may help animals avoid conflict. This may be especially important in animals like little blue penguins whose contact with other individuals is relatively infrequent. — SNV

Anim. Behav. **83**, 605 (2012).

IMMUNOLOGY

Biased for the Better

Bacterial infections can turn deadly when components of the bacterial membrane, such as lipopolysaccharide (LPS), cause runaway activation of the host immune system. LPS binds to Toll-like receptor 4 (TLR4) on the surface of host cells and activates two major signaling pathways. One, which acts through an adaptor protein known as TRIF, leads to production of interferon and chemokines that beneficially stimulate the adaptive immune system. The problematic side is mediated by the adaptor known as MyD88, which stimulates inflammatory responses that can lead to toxicity. Bowen *et al.* report that a very small structural change in a mimetic molecule that acts like LPS, analogous to changing just one phosphate group on the lipid A portion of LPS, effectively separates the two signaling pathways. Binding of the mimetic to TLR4 activated TRIF-mediated signals but caused little or no activation of the MyD88-mediated pathway. The results confirm that it may be possible to design therapeutic agents that can harness beneficial signaling from the TLR4—for example, to promote a strong response to vaccination, but avoid the normally concomitant, potentially toxic inflammatory response. — LBR

Sci. Signal. **5**, ra13 (2012).

CELL BIOLOGY

A Forced Opening

Mechanical forces on bone stimulate intracellular signaling pathways in osteocytes that promote remodeling. Signaling molecules that drive such remodeling are likely transmitted between cells through the connexin 43 (Cx43) hemichannel (HC). Integrins are focal adhesion proteins that provide support to the cell by connecting the cytoskeleton to extracellular matrix (ECM) components like fibronectin. Integrins have also been proposed to be mechanosensors in bone cells. Batra *et al*. now show that the cytoplasmic domain of the α subunit of integrin $\alpha_5\beta_1$ interacts with the cytoplasmic domain of Cx43, that the interaction is strengthened by fluid flow, and that this interaction is required for HC opening. The opening required osteocyte attachment to the ECM but was independent of integrin $\alpha_5\beta_1$ binding to its ligand, fibronectin. Direct forces applied to integrin $\alpha_5\beta_1$ by magnetic beads induced the opening of the HC, and such mechanical stress–induced opening required phosphatidylinositol 3-kinase (PI3K), which has been implicated in fluid-flow–induced activation of integrins in epithelial cells. It is likely that PI3K is responsive to fluid flow and transmits this to integrins, leading to opening of the HC and bone remodeling. — VV

Proc. Natl. Acad. Sci. U.S.A. **109**, 10.1073/pnas.1115967109 (2012).

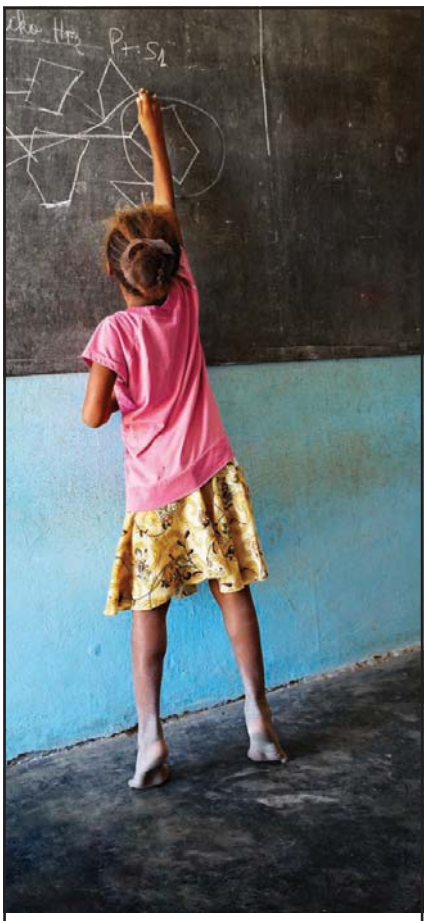

AROUND THE WORLD

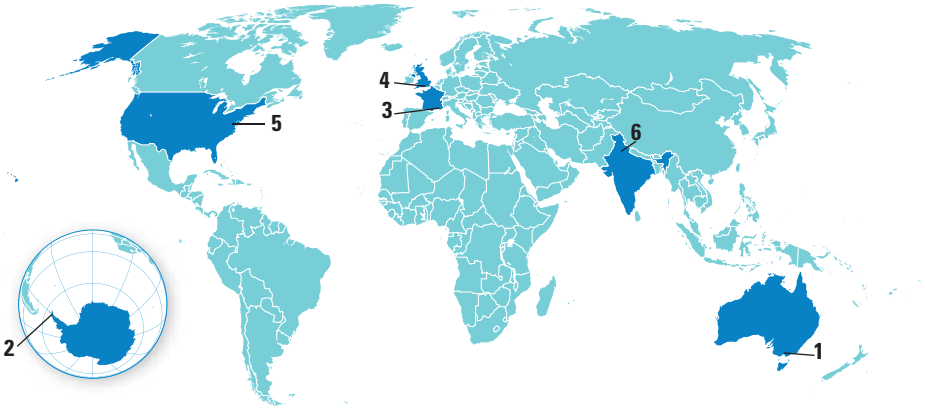

Melbourne, Australia **1**

Salvation in Sight for Synchrotron

After months of uncertainty, a deal is taking shape to save the Australian Synchrotron, one of two such facilities in the Southern Hemisphere. The synchotron has given Australian scientists access to powerful beams of light to probe new materials, proteins, and other substances. But last May, the synchrotron's major backers—the federal government and the government of Victoria State, which hosts the facility—omitted funds for the synchrotron in their budgets beyond 30 June 2012.


The Australian Synchotron

Under a new agreement about to be inked, federal support for the synchrotron will be extended through the Australian Research Council's Special Research Initiative, which awards large grants to university consortia. Monash University will lead the bid for the funds, says Ian Smith, the university's pro vice-chancellor for research and research infrastructure. Smith says that the synchrotron will need at least AUS $100 million to operate over the next 4 years. The Special Research Initiative would provide a quarter of the funds; universities would match that amount, and the remainder would come from the Victorian government, the New Zealand government, and three Australian government agencies.

Admiralty Bay, Antarctica **2**

Fire at Brazil's Antarctic Station

A fire sweeping through a generator room at Brazil's Comandante Ferraz Antarctic Station caused an explosion that killed two people, injured another, and destroyed about 70% of the station on 25 February. The Brazilian Air Force has evacuated 45 people from the base, including the injured man.

The station is in the South Shetland Islands near the tip of the Antarctic Peninsula, where scientists studied coastal and shelf marine ecosystems and the impact of climate change. "The assessment is that we really lost virtually everything," Brazilian Defense Minister Celso Amorim told reporters on 25 February, noting that the loss of the base—Brazil's only permanent research station on the continent—is a major blow to Brazil's scientific community. Amorim added that plans for reconstructing the base would begin almost immediately.

Cadarache, France **3**

ITER Dodges Trouble With Superconducting Cables

A potential problem that threatened to delay construction of the huge ITER fusion reactor looks like it has been resolved. Tests last year on samples of superconductor cable for the facility's magnets indicated the cable would last only one-tenth as long as required. That prompted a scramble to identify the cause and come up with a solution. Recent tests at a high-magnetic-field facility in Switzerland show that engineers have succeeded.


Wrapped up. Superconductor for ITER's magnets.

The superconducting cables consist of multiple "triplets" of three strands. The cables that failed contained triplets made up of two niobium-tin strands and one of copper; the copper is a safeguard against "quenching," when the niobium-tin material suddenly loses its superconducting ability. In normal operation, the two strands shoulder the large magnetic forces that the conductors experience. The new configuration would consist of three strands made of a combination of copper and niobium-tin, so that all three share the load of magnetic forces.

This has delayed the start of conductor manufacture, but other delays—including last year's earthquake and tsunami in Japan—had already forced ITER managers to push back the scheduled start of the reactor by 1 year to late 2020. **http://scim.ag/_ITER**

Southampton, U.K. **4**

Declassified Sub Data To Shed Light on Arctic

The U.K. Minister of Defense is declassifying data collected by Royal Navy submarines in the Arctic and handing them over to scientists to help track the region's changing climate. The subs' data will include temperature and salinity measurements that may span time periods of anywhere from 10 to 20 years. Scientists are eager for information about how the Arctic has been changing over the past few decades, but the harsh conditions make it hard to collect traditional oceanographic measurements in the region, says John Allen, an oceanographer at the National Oceanography Centre, Southampton, which will receive the data.

Because of the classified nature of the data, it's not yet clear how much there is, Allen says, or even exactly what will be made available. Before the scientists can begin to analyze the data, the ministry's Defense Science and Technology Laboratory

Published by AAAS

will first remove the exact locations where the data were collected. But, even without precise locations, the data can provide a valuable, long-term series of snapshots of the changing chemistry of Arctic waters. In particular, Allen says, they will help scientists compare the time scales of temperature changes in ice-covered waters with those in ice-free waters.

Washington, D.C. **5**

World Bank, NGOs Partner For Ocean Health

The World Bank is teaming up with major environmental groups and international non-governmental organizations to raise $1.5 billion to improve ocean health. The Global Partnership for Oceans, announced 24 February, will attempt to speed progress on overfishing, marine pollution, and destruction of ocean habitats such as coral reefs.

Top goals for the next decade include rebuilding more than half of the depleted fish stocks around the world and expanding marine protected areas from about 1% of the oceans to cover 5%. In addition, aquaculture should provide two-thirds of the global fish supply rather than half, and it should be made more sustainable by relying less on fish meal for feed, for example. "All these points are well thought out," says ecologist Carl Safina of Blue Ocean Institute in Cold Spring Harbor, New York, who says he welcomes the announcement. "The biggest criticism of the World Bank is that it increases ability of people to exploit nature and does not emphasize the need for sustainability, but this does."

Last gasp. Many stocks of Patagonian toothfish, also called Chilean sea bass, are depleted.

To help accomplish these goals, the partnership says it will raise $300 million for initial actions, such as ramping up efforts to fight government corruption. These efforts, they hope, will leverage another $1.2 billion from donors over 5 years. Details of the partnership will be worked out at a meeting next month.

New Delhi **6**

Space Scientists Protest Colleagues' Blacklisting

India's scientific community is turning up the heat on the government over its controversial sanctions of four former officials of the Indian Space Research Organisation (ISRO) for alleged missteps in a satellite deal. Last month the goverwnment banned four scientists—including former ISRO head G. Madhavan Nair, who oversaw India's successful Chandrayaan-1 lunar probe in 2008—from holding a government position for the rest of their lives. The punishment cited "procedural lapses" during negotiations to lease two communication satellites to a private company.

Senior Indian scientists have blasted the ban. Roddam Narasimha, an aerospace scientist at Jawaharlal Nehru Centre for Advanced Scientific Research in Bangalore, resigned on 24 February from the Space Commission, India's top space policy body. Narasimha wrote in a letter to Prime Minister Manmohan Singh that the "actions taken against the scientists could demoralize the Indian Space Research Organization's scientific community, and adversely affect its ability to take the kind of technological initiatives … that are the hallmark of an innovative organization."

http://scim.ag/Indiaspace

THEY SAID IT

"I suspect … that both Einstein's theory and my boxer shorts are safe."

—Physicist Jim Al-Khalili of the University of Surrey in the United Kingdom, who had promised to eat his boxers on live TV if neutrinos were shown to travel faster than light (see p. 1027).

CREDITS (TOP TO BOTTOM): PZUMA PRESS/NEWSCOM; M. VAN LUNENBURG/OWL MONKEY PROJECT

Double-Duty Dads

In the primate world, owl monkeys are unusual because the dads play a big role in bringing up baby. Now, the unprecedented births of two sets of twins in a population of owl monkeys that researchers have been studying for 15 years in Argentina is offering a "rare, exciting, and fascinating" research opportunity, says behavioral primatologist Eduardo Fernandez-Duque of the University of Pennsylvania.

"Few aspects of primate behavior are so intriguing, yet so poorly understood, as the intense care of infants by males," he explains. And owl monkey fathers (like the one pictured at left) are especially unusual, in that they "do it all—carrying the infants, feeding them, playing with them." Now, a recent grant from the U.S. National Science Foundation will enable Fernandez-Duque and colleagues to see how the dads handle double duty as the twins, born late last year, grow up. The study may offer insight into why this rare child-rearing arrangement evolved.

Published by AAAS

Random Sample

A Cold July in Baghdad

Researchers in Spain are tapping a new database in their search for historic climate patterns: medieval Arab history. Physicist Fernando Domínguez-Castro of the University of Extremadura in Badajoz, Spain, and his colleagues, including a historian of Arab culture, examined references to droughts, floods, and hail in ten Arab sources written between 816 C.E. and 1009 C.E.. One text told of nights during a Baghdad summer that were so cold that residents bundled up inside their homes rather than sleeping on roofs as was the custom, the team reported in *Weather.*

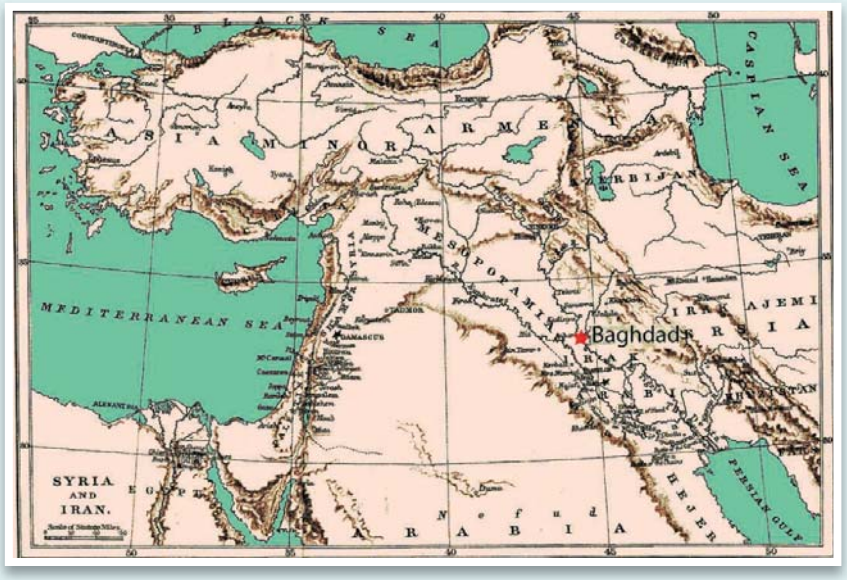

The texts, the team concluded, suggest that 10th century Baghdad had more cold spells than it does now. That conclusion agrees with previous hemisphere-wide temperature reconstructions by climate scientists—but it's the first time this has been demonstrated for Baghdad.

Understanding how global climate trends play out close to home is a priority for many climatologists. Yet extracting useful climate information from medieval records will require trust and cooperation between researchers with little in common. "People are reticent," Domínguez-Castro says of the historians closest to medieval archives. "They think, 'These crazy physicists are here to steal my job.' "

Still, the large geographic and historic span of Arab record-keeping is attracting funding from Spanish and German research organizations. Comparing historical records from German monasteries with those from Andalusian courts might also generate fresh insights. "Most climate reconstructions are from the north of the Mediterranean," Domínguez-Castro explains."The southern Mediterranean is climatically very interesting but also very little studied."

FINDINGS

Genetically Engineered Bacteria Could Help Fight Climate Change

Some researchers believe that capturing atmospheric CO_2 and trapping it in buried rocks could lower the risk of catastrophic climate change. Now researchers have found that bacteria can speed that process up.

CO_2 pumped into underground rocks combines with metal ions in the salty water that fills the rock pores and mineralizes into mineral carbonates such as calcium carbonate ($CaCO_3$). That can take thousands of years. To see if they could speed things up, biochemist Jenny Cappuccio and colleagues at the Lawrence Berkeley National Laboratory's Center for Nanoscale Control of Geologic CO_2 put a mix of common bacterial species in a calcium chloride solution in the lab and pumped in CO_2. They found that calcium carbonate formed faster where the bacteria were living than in sterile solutions.

The team guessed that the surfaces of the bacteria were helping the CO_2 hook up with calcium ions. They modified one of the bacterial species, *Caulobacter vibrioides*, inserting a sequence of DNA that reshaped the bacteria's surface to attract calcium ions.

It worked. When the researchers pumped CO_2 into the tanks where the modified bacteria were living, even more $CaCO_3$ solidified than in tanks with unmodified bacteria. Cappuccio reported the team's results 26 February at a meeting of the Biophysical Society in San Diego, California. **http://scim.ag/CO2gen**

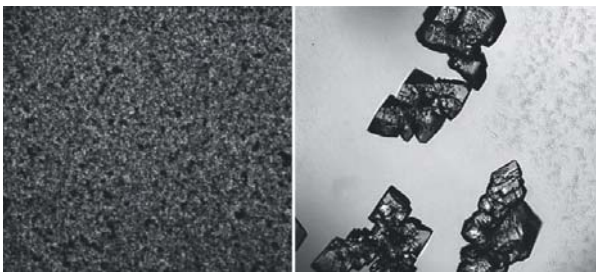

Taking shape. Initially amorphous in sterile solutions (*left*), calcium carbonate quickly forms crystals (*right*) when bacteria are present.

BY THE NUMBERS

149 Potential sources of human error in fingerprint analysis, according to a National Institute of Standards and Technology report.

198 kg of CO_2 The estimated carbon footprint—equivalent to burning 90 liters of gasoline—of a shrimp cocktail made with shrimp grown in former mangroves, according to ecologist Boone Kauffman of Oregon State University, Corvallis, reporting at February's AAAS meeting.

Science LIVE

Join us on Thursday, 8 March at 3 p.m. EST for a live chat on the **Science of Forensics**. How are researchers helping police solve tough crimes? **http://scim.ag/forensiclive**

CREDITS (TOP TO BOTTOM): FERNANDO DOMÍNGUEZ-CASTRO *ET AL.*, *WEATHER* 67 (27 FEBRUARY 2012); JENNY CAPPUCCIO/LAWRENCE BERKELEY NATIONAL LABORATORY

SUPERLUMINAL NEUTRINOS

Loose Cable May Unravel Faster-Than-Light Result

Anomalous data suggesting that neutrinos can travel faster than light probably resulted from a faulty connection in a GPS timing system, physicists from the OPERA collaboration revealed last week. Scientists who wish not to be identified say a few persistent OPERA researchers spotted the problem during tests the collaboration's leaders at first opposed.

OPERA, or Oscillation Project with Emulsion tRacking Apparatus, is a particle detector housed under the Gran Sasso mountain in central Italy. In September 2011, 171 scientists from the international collaboration announced that thousands of measurements made between 2009 and 2011 seemed to show that neutrinos from the CERN laboratory near Geneva, Switzerland, were reaching Gran Sasso some 60 billionths of a second (60 nanoseconds) earlier than light would—a finding at odds with Einstein's special theory of relativity (*Science*, 30 September 2011, p. 1809). In November, measurements with shorter, easier-to-time pulses confirmed the anomaly, but many physicists remained skeptical (*Science*, 2 December 2011, p. 1200).

That skepticism has grown with the latest announcement. From December 2011 until a couple of weeks ago, a small group of OPERA researchers carefully measured how much time it takes light pulses to travel along an 8-kilometer optical fiber that connects an external GPS receiver to the Gran Sasso laboratory. The "time stamps" encoded by these pulses are also sent to CERN to synchronize timing at the two labs, but the time that the pulses take to travel along the fiber must be added to the time stamp to ensure that the neutrinos' arrival times are recorded accurately.

The investigators discovered that the pulses' transit time varied by several tens of nanoseconds depending on how tightly the coaxial fiber cable was plugged into a socket attached to a card inside the experiment's master-clock computer. The card converts the light pulses into electronic signals. Any loose connection was supposed to stop the pulses from being registered, but instead it appears that the card allowed the delayed pulses to get through. So a loose connection during the experiment would have stamped neutrino pulses with arrival times suggesting faster-than-light travel. Although researchers can't be sure the cable was loose during the experiment, the size of the delays involved is highly suggestive.

The travel times of pulses along the fiber had been measured in 2008 by collaboration member Dario Autiero of the University of Lyon in France. A source familiar with the experiment says some researchers thought the measurement should have been rechecked before the neutrino velocity results were submitted to a journal in November, but OPERA's scientific management resisted carrying out such a check. (Autiero and collaboration spokesman Antonio Ereditato of the University of Bern in Switzerland were unavailable for comment before this story went to press.)

In December, the researchers finally got the go-ahead to test the fiber. Last week, OPERA issued a written statement confirming that the possible fiber delay, combined with a second potential source of error, could "substantially influence" the velocity results. This other potential error—on an electronic card in the oscillator used to provide the fine-grain timing for individual neutrino events between GPS pulses—would cause the stamp to show a later time than it should. But Lucia Votano, director of the Gran Sasso lab, says researchers consider the connection problem more significant. "This is the main suspicion because it is in the right direction for explaining the anomaly and is also bigger than the other effect," she says.

A technical report on these two possible sources of error is being prepared for discussion at a forthcoming collaboration meeting. But the final word should come in May, when CERN will send a high-precision pulsed neutrino beam to OPERA and three other Gran Sasso detectors. The test will use two independent timing systems. "If none of these experiments detected the anomaly, then that would be definite proof that neutrinos can't travel faster than light," Votano says. Meanwhile, physicists in the United States will be measuring the speed of neutrinos sent from Fermilab near Chicago to the MINOS detector in a mine in northern Minnesota.

David Wark of Imperial College London, a physicist who works on the T2K neutrino experiment in Japan, says it was "reasonable" for OPERA to release its results when it did. "If they sit on it for [too] long, inevitably it will come out on someone's blog, and they will have no control over that," he says. "Instead, they said to the scientific community, 'Look, we have something weird. Can you explain it?' "

But one OPERA scientist believes the error should have been caught. "What's happened here is an accident, something unexpected, but identifying these things is part of the scientific procedure," the researcher says. "In recent years, there has been too much pressure in science to be first. This has made us go faster than we should have done."

–EDWIN CARTLIDGE

Edwin Cartlidge is a writer based in Rome.

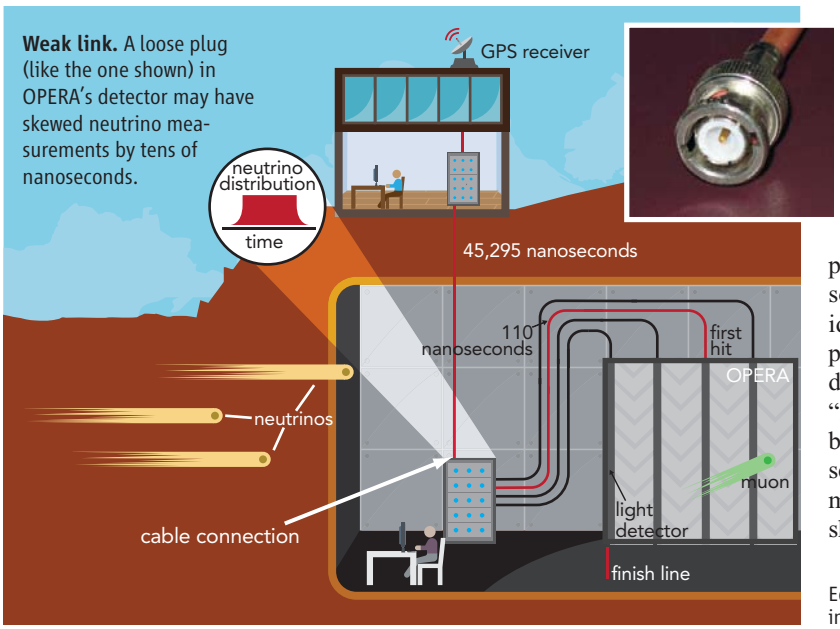

CREDITS: (ILLUSTRATION) G. GRULLÓN/*SCIENCE*; (INSET) PHOTO BY MEGGAR/WIKIMEDIA COMMONS

Published by AAAS

Investigation. Pathologists here in Krefeld, Germany, and across Europe are examining lambs and other livestock born dead or deformed for signs of the Schmallenberg virus.

INFECTIOUS DISEASE

Scientists Rush to Find Clues On New Animal Virus

A new animal virus first detected in Germany and the Netherlands late last year is taking a heavy toll on livestock across Europe, causing the birth of dead or deformed animals. Scientists are scrambling to figure out where the virus has come from and exactly how it is transmitted. Named Schmallenberg after the German town where it was first detected, the virus has now also been found in France, Belgium, the United Kingdom, and most recently, Italy and Luxembourg. Animal health experts are bracing for an uptick in cases in the next few weeks.

Scientists working at the Friedrich Loeffler Institute (FLI), the German federal animal health lab, first identified the novel virus in November 2011 in blood samples taken from cows that had shown a slight infection in late summer. Now, months after the initial infections, more than 1400 farms across Europe are reporting severe symptoms in newborn sheep, goats, and cows. The virus seems to have infected the fetuses of pregnant animals last summer—with catastrophic consequences for the offspring that are becoming apparent only now. Many of them are born with stiff and twisted limbs, a curved spine, shortened tendons, and severe brain malformations such as hydrocephalus, in which parts of the brain are replaced by sacs filled with fluid.

So far, most cases have occurred in sheep, but that might be due to their shorter gestation period, says Thomas Mettenleiter, head of FLI. In the coming weeks, cows that were in the early stages of pregnancy last summer and might have been infected will give birth. "We are worried that we will see an increase in the number of affected calves," Mettenleiter says.

Schmallenberg virus belongs to a group called orthobunyaviruses, found mainly in Asia, Africa, and Australia; they are usually transmitted by midges and mosquitoes. The new virus most closely resembles the sequence of three viruses that were all isolated from cattle in Japan: Shamonda, Akabane, and Aino. They belong to a subgroup of orthobunyaviruses called Simbu serogroup that has not been seen in Europe before. "We know almost nothing about Schmallenberg virus and very little about the viruses most closely related to it," says Martin Beer, an expert on animal viruses at FLI. Although some orthobunyaviruses infect people, there is no evidence to date that this one does.

Virologists say it is hard to speculate on the pathogen's origin or how long it has been circulating in Europe without any data on where it is found in the rest of the world. But its spread is reminiscent of the bluetongue disease, which emerged in the same area on the borders of Germany, Belgium, and the Netherlands in 2006. "It is a very interesting coincidence," says Peter Mertens, who heads the vector-borne viral disease program at the Institute for Animal Health in Pirbright, U.K. "We don't know exactly how bluetongue or Schmallenberg arrived in Europe, but there are a number of hypotheses." They could have come with insects imported on aircraft, or with an infected animal, or with cut flowers from Africa. Many cut flowers are imported into Europe from sub-Saharan Africa; to keep them cool they are packed at night under bright lights that might attract insects. "We know so little, we cannot rule out anything," Mertens says.

The outbreak has sparked a furious genome-sequencing effort to see exactly where the Schmallenberg virus fits into the Simbu subgroup and thus where it might have come from. Early on, scientists were hampered by the paucity of sequence information from other viruses that could be compared with the Schmallenberg DNA. For most viruses in the subgroup, only the smallest of the three genome segments had been sequenced, and for some there was no sequence information at all. So far, researchers at FLI have sequenced the complete genomes of nine related viruses provided by the Center for Biodefense and Emerging Infectious Diseases at the University of Texas Medical Branch in Galveston. But the data are "generating more questions than answers at the moment," Beer says. "We might have to rethink the classification of this group."

To Mettenleiter, the extent of the virus's spread suggests that it may have been in Europe for more than one season: "To spread over such a big area in one season is not impossible, but it is difficult." He and others are trying to find out whether this is Schmallenberg's second season by testing samples taken from animals in 2010. So far none has tested positive. They have also teamed up with entomologists from affected countries in Europe to identify the vector carrying the pathogen. Thousands of insects caught for other reasons are being screened for the virus; again, none has tested positive.

Both efforts are hampered by the lack of a good diagnostic test. FLI developed a PCR assay that is already being used by affected countries, but it can detect an infection only while the viral DNA is in the blood—apparently just a few days in most cases. Developing an ELISA test, which detects antibodies against the virus, is among the top priorities of the labs working on Schmallenberg. "We need a system that can detect animals that have been infected at any time after that," Mertens says. "Without it we are blind."

Schmallenberg seems to have spread very efficiently, affecting most animals in many herds. "The best guess is that this is insect-transmitted," Mertens says. "But we have to ask whether there are other routes of transmission," such as fecal-oral trans-

CREDIT: FEDERICO GAMBARINI/EPA/LANDOV

Published by AAAS

mission between animals; it might also be spread as an aerosol or by direct contact between animals, he suggests.

Scientists are also puzzled by the virus's ability to infect the fetus without killing it. "It is unusual that a pathogen that kills mammalian cells in the petri dish can stay in an organism as sensitive as a fetus for such a long time without causing an abortion," Beer says. He suggests that this trait might be the virus's way of surviving the winter, when no insects are around.

With biting midges expected to take off again in May or sooner, animal health experts are preparing for the next season of Schmallenberg infection. Preliminary data from two cows show that the animals that had been infected earlier are immune to the virus. "But of course we don't know whether this goes for all cows or how long this protection will last," Mettenleiter says.

Work is already under way on a vaccine. At FLI, scientists are trying the classical approach: inactivating the virus chemically and adding an adjuvant. Although the vaccine might be easy to produce, the rigorous testing demands—scientists have to be sure it is safe in pregnant animals—will probably take a long time. "It's very unlikely that this will be ready this year," Mettenleiter says. "But it might be ready in 2013."

–KAI KUPFERSCHMIDT

Kai Kupferschmidt is a science writer in Berlin.

REPRODUCTIVE BIOLOGY

Potential Egg Stem Cells Reignite Debate

Since 2004, reproductive biologist Jonathan Tilly of Massachusetts General Hospital in Boston has fought a relatively lonely battle to overturn one of the central dogmas of his field. Men typically produce working sperm as long as they live, but most textbooks say female mammals are born with all the egg cells, or oocytes, they will ever have. Tilly has challenged that conventional wisdom, arguing that in mice—and perhaps also in humans—there must be an ongoing source of new eggs.

The proposal, it's safe to say, hasn't been warmly received by fellow reproductive biologists. And Tilly didn't help his case in 2005 when he proposed that bone marrow was a source of eggs in mice. (That idea was discredited a year later.) But this week online in *Nature Medicine*, Tilly and colleagues report isolating rare cells in ovarian tissue from adult women that can grow in lab dishes and form immature oocytes.

This latest claim is earning some cautious acceptance. "As an egg biologist, I'm juiced about this," says David Albertini of the University of Kansas Medical Center in Kansas City. The potential egg stem cells could provide a lab-based model for understanding how oocytes develop. And they may help scientists devise new ways to rescue the fertility of women who undergo cancer treatments or who suffer from premature menopause.

Tilly's battle to win over colleagues is far from over, however. "There is no evidence that these cells actually exist in vivo," says Jock Findlay, a reproductive biologist at Prince Henry's Institute of Medical Research in Clayton, Australia.

Since the 1950s, reproductive biologists have thought that egg precursor cells stop dividing about halfway through mammalian fetal development, giving a newborn female a finite number of potential eggs. A baby girl, for example, is born with an estimated 1 million oocytes. By puberty, that number has declined to roughly 400,000. During a woman's fertile years, follicles, the structures that host an oocyte and help it to mature, are activated at a rate of about 1000 per menstrual cycle. (Typically, only one mature egg is released into the fallopian tubes each cycle.) And once the oocyte supply runs low, menopause begins.

Green egg. A human oocyte derived from oogonial stem cells expressing green fluorescent protein.

CREDIT: VINCENT CENTER FOR REPRODUCTIVE BIOLOGY, MASSACHUSETTS GENERAL HOSPITAL

In 2004, Tilly and his colleagues published data in *Nature* that indicated that in mice, too many oocytes die during each menstrual cycle to sustain the supply of eggs for the animal's lifetime fertility. New eggs, presumably from an unidentified stem cell, must be coming from somewhere, they proposed (*Science*, 12 March 2004, p. 1593). Other researchers dismissed that conclusion, saying the team had drastically overestimated the rate of oocyte death.

Tilly persevered and in 2005, based on bone marrow–transplant experiments in mice, he and colleagues proposed in *Cell* that new oocytes might come from the marrow and travel to the ovary via the bloodstream. A paper in *Nature* quickly discredited that idea (*Science*, 16 June 2006, p. 1583). In 2009, however, Tilly's original idea got a boost when reproductive biologist Ji Wu and his colleagues at Shanghai Jiao Tong University in China reported in *Nature Cell Biology* that they had isolated "female germline stem cells" from adult mouse ovaries. To prove their case, the team genetically modified the putative stem cells so that they produced green fluorescent protein (GFP) and then injected them into the ovaries of sterilized mice. Those females gave birth to green-glowing pups, demonstrating that the injected cells had given rise to mature oocytes (*Science*, 17 April 2009, p. 320).

It was still not clear, however, whether normal fertility and reproduction depend on such cells—or whether they exist in humans. And initial attempts by other labs to find the mouse cells failed. Tilly says he, too, was frustrated at first. "I put a person on the protocol the day the paper was published. It took 10 months to get it to work. I still don't know why," he says.

In the new paper, Tilly and his colleagues report that they have refined Wu's cell-collection methods to isolate a more pure cell population from mouse ovaries. And they further describe fishing out similar cells from human ovary tissue that Yasushi Takai, who works at the Saitama Medical Center in Japan, had previously collected from six women who had sex-reassignment surgery. The women were healthy and young—between 22 and 33 years old—and all agreed to have their frozen tissue used for the project. ▶

Published by AAAS

The cells, which Tilly calls oogonial stem cells (OSCs), are very rare—only about 1 out of 10,000 ovarian cells. The OSCs grow quickly in the lab, and they spontaneously form cells that visually and molecularly resemble immature oocytes. To find out how the cells would behave in an ovary, the scientists injected OSCs engineered to make GFP into a piece of donated human ovarian tissue and then implanted the tissue under the skin of a mouse. When they looked at the grafts 1 and 2 weeks later, they found immature follicles with green oocytes at their center.

Finding a human version of the cells Wu isolated is "very exciting," says Evelyn Telfer, who studies oocyte development at the University of Edinburgh in the United Kingdom. But she and Albertini note that the current experiments don't address what, if any, role the apparent stem cells play in normal ovaries. And Findlay says the cells might be an artifact of the purification or culture methods the team used. Even the green oocytes should be viewed with caution, as GFP-tagged cells can fuse with unrelated cells, says Renee Reijo-Pera, a reproductive biologist at Stanford University in Palo Alto, California.

The oocyte-like cells that grew from the human OSCs were far too immature to try fertilizing them, Tilly notes. And attempting such an experiment would need special ethical oversight, he says. He and Telfer have plans to see whether her techniques for maturing oocytes in vitro work with OSC-derived cells. Whether the stem cells themselves could be a source of fertile oocytes for in vitro fertilization attempts is doubtful, Albertini says. He points out that expanding cells in culture almost always leads to accumulation of potentially harmful mutations.

Still, Albertini says, studying the cells could help researchers. "I think it's a great model. It could help us move toward understanding how these incredible cells [oocytes] are born and how they develop."

Tilly holds a patent on the OSCs, and he has started a biotech company to explore ways to use the cells to help improve fertility treatments. The company will screen for compounds that encourage the cells' growth and development and will test whether compounds in the cells might be able to boost the fertility of aged eggs. But even Tilly admits that the controversy is unlikely to settle down anytime soon: "Whether the cells represent what we believe they do? That's going to take a while to weed through."

–GRETCHEN VOGEL

SCIENTIFIC CAREERS

Is Motherhood the Biggest Reason For Academia's Gender Imbalance?

A new paper by two developmental psychologists on the dearth of women in academic science argues that the cause of the gender imbalance is much easier to identify than most researchers have posited. The solution is also more obvious, they say, although that doesn't mean it will be easy to implement (see sidebar). Not surprisingly, their provocative assertions, in a paper titled "When Scientists Choose Motherhood," have stirred the pot in an already contentious field.

Writing in the March/April issue of *American Scientist*, Wendy Williams and Stephen Ceci of Cornell University argue that the traditional view of female underrepresentation as a complex mixture of discrimination, differential abilities, and career preferences misses the mark. Instead, say the husband-and-wife team, the evidence from studies stretching back more than a decade points overwhelmingly to the primacy of "the dynamics of family formation in Western society," or, in a word, motherhood.

Family matters. Cornell psychologists Stephen Ceci and Wendy Williams with two of their three daughters.

CREDIT: COURTESY OF W. WILLIAMS AND S. CECI

Williams and Ceci are certainly not the first to note that the desire to have a family hives off a significant fraction of women who have made it through graduate school and postdoctoral training in STEM (science, technology, engineering, and mathematics) fields and who stand at the brink of an academic career. Despite their clear interest and talent, the authors say, women in their prime childbearing years are often forced to make a stark choice between having a family and pursuing a career for which they have trained all their adult lives. "Why is it that women are given one 7-year interval in which to amass a research portfolio and have two kids?" Williams asks, referring to the typical time frame for an assistant professor to earn tenure at a major research university. "That's crazy. Men don't have to do that. It's this societal-designed unfairness that's rooted in biology."

Researchers from nearly every scientific discipline have spent decades examining the reasons behind gender differences in math and science, from the nursery to the Nobel Prize. Some studies have found systemic bias and discrimination, whether deliberate or inadvertent, to be a major factor in the imbalance. Others argue that the slight edge for boys in mathematical ability among highly gifted students translates into a significant difference in adult success in math-intensive STEM fields. A third camp sees personal preferences—"working with people versus things," as some describe it—as the driving force behind the divergent career choices by men and women.

In their new article, which builds on a 2011 paper in the *Proceedings of the National Academy of Sciences*, the authors assert that a "misdirection" of resources toward problems that no longer exist has slowed progress. In particular, they take issue with those who say that correcting the gender imbalance will require a wholesale revamping of societal attitudes toward women and a reworking of the nation's educational system. What is more important, they say, is to change the current rigid system at universities of rewarding academic excellence. "More flexibility in the early years would allow them to have a family and become full-fledged researchers, too," says Williams, who notes that having three daughters influenced the couple's decision in 2005 to jump into this contentious field. "But the current system doesn't let them back in."

It's no surprise that an aggressive attack on those analyses would trigger strong rebuttals from researchers who are passionate about the topic. In particular, many researchers think Williams and Ceci have oversimplified what they say is a very complex issue and selectively chosen data to bolster their case.

Published by AAAS

Half-Time Jobs, Full-Time Scientists

Even if Wendy Williams and Stephen Ceci are right that the way to improve the gender balance is to alter the academic reward system (see main text), how would you do it?

Matthew Pritchard and Rowena Lohman are accidental subjects in a natural experiment testing one ingredient in the authors' recipe for change: half-time tenure-track slots that would allow women to be productive researchers while giving them more time to raise a family. The arrangement is so rare at top-tier U.S. research universities that there are no data, only anecdotes. Even so, the couple's experience raises questions about whether the approach can be scaled up.

Since 2007, the husband-and-wife volcanologist and earthquake specialist at Cornell University have split a tenure-track slot—and one salary—within the department of earth and atmospheric sciences (EAS). They are taking advantage of the relatively low cost of living in Ithaca, New York, to carve out coequal careers. Pritchard, now 37, joined the faculty in 2003, and 4 years later the university hired Lohman, now 36, after agreeing to divide the position. The arrangement has allowed them to start a family—the couple has a 2½-year-old daughter and is expecting a second child in July—while continuing to be productive members of a top-rated department.

It is a sweet deal for the department. Despite earning a half-time salary, the couple figure they work pretty much full-time. "We don't view ourselves as half-time," Lohman says. "We're basically each half-time teaching and half-time research." As an example, Lohman stayed out for only a week after the birth of her daughter, and the infant was a constant presence within the department. "Never once did anyone complain about her crying," Lohman recalls with gratitude about her colicky child.

At the same time, Lohman sees a psychological benefit in holding a part-time position. "I think we're under less stress," Lohman says. "When my daughter is sick, and I have to pick her up from [on-campus] day care, I don't worry about taking the time off. And even if we're not working any less, the perception is that we're a little more relaxed."

Although Pritchard officially went part-time in 2007, he was still able to meet the requirements for tenure within the traditional 6-year window. Lohman will be up for review in the summer of 2013 after requesting a 1-year extension. Still, she feels her productivity is nearly indistinguishable from that of any full-time faculty member.

Pritchard and Lohman are actually the third couple in the EAS department currently splitting a single tenured position. Hearing about the two older couples during his initial job interview helped to convince him that such an arrangement could work, Pritchard says, as well as sending the message that the department is very family-oriented.

On the job. Their daughter, Jeanne Roanne, is no stranger to the department where Matthew Pritchard and Rowena Lohman split a tenure-track position.

But some academics see a downside to modifying the traditional tenure process. Although Cornell geoscientists seem comfortable with split tenure positions, the option is rarely exercised by other departments and colleges within the university. In fact, it took 2 years for higher-level university administrators to sign off on the deal for Pritchard and Lohman. "I'm not sure why there was a delay, but the dean told us it was part of a larger issue and not about us," Pritchard explains.

In fact, some on campus had objected on the grounds that employing Lohman at 50% of the regular faculty salary was a form of discrimination against women and made her a second-class citizen. "I think that's a narrow perspective," says Teresa Jordan, who pioneered the arrangement 30 years ago with her geologist husband, Richard Allmendinger, and who was department chair at the time. "For every young woman taking the job at 50% salary, there's a man doing the same thing."

Jordan says the ruckus surrounding the hiring of Lohman could well make it harder for department chairs to win approval for split positions even if new faculty members request the arrangement. And if that's the case at a place with a track record of success, then a university without any such history may be wary of taking the plunge. **–J.D.M.**

"There are many reasons why women are not succeeding at the same rate as men in academic math-related fields," says Diane Halpern, a prominent scholar on sex differences and cognitive abilities and a psychologist at Claremont McKenna College in California. Although she agrees that "tenure and biological clocks run in the same time zone," she questions how Williams and Ceci can place motherhood above the other factors, especially when those factors don't lend themselves to a quantitative comparison.

Halpern, a former president of the American Psychological Association, was lead author of a widely cited 2007 paper that took a sober look at the science of sex differences. "People were very unhappy with us when we concluded that lots of things are very important," she notes. "They said, 'So you mean you don't really know?' But our response was, 'That's the answer.' "

Donna Nelson, a chemistry professor at the University of Oklahoma, Norman, has spent 2 decades collecting data on hiring and promotion practices among U.S. research universities. She says she's worried that Williams and Ceci are making the same mistake that they accuse their critics of making: putting all their eggs in one basket.

"I think this article does have merit, for a subset of women, during one part of their lives," Nelson says. "However, it has not uncovered a problem which, when solved, will create an equal environment for women." Nelson says it would be unfortunate if departments "were to invest millions of dollars in things like in-house daycare centers" only to find that such investments improved conditions for "a relatively small number of women."

At the same time, most researchers applaud Williams and Ceci for shining a light on an issue important not just to U.S. academic science but also to the country's economic well-being. And they welcome their call to action. "There has to be a sense that the outcome—more women in math-related fields—is desirable," Halpern says. "There also has to be people willing to stand up and speak out on their campuses. Academia is really the only profession where people are faced with this early up or out. And it's incredibly expensive to lose talented people."

–JEFFREY MERVIS

CREDIT: JULIE ELLIOTT

Published by AAAS

EPIDEMIOLOGY

Overhaul of U.S. Child Health Study Concerns Investigators

A controversial health study of 100,000 U.S. children that has struggled for years hit another rough patch last month when the National Institutes of Health (NIH) announced that it may modify its sampling plan in 2013 to save money. NIH officials also surprised academic researchers who run some early study sites by telling them last week that they will soon be replaced with a new contractor.

The two changes have upset National Children's Study (NCS) investigators, who fear that scientific quality will be compromised—and that shrinking the study's geographical footprint could erode political support. Several study investigators say that NCS seems to be scrapping its 6-year partnership with the academic community. "The news is devastating," says Maureen Durkin of the University of Wisconsin, Madison, whose directorship of an NCS site in Waukesha County will end. "It's disheartening to see the lost opportunity for children's health, and the vast investment that the country has made in the NCS now being frittered away."

NCS Director Steven Hirschfeld says the original academic contractors like Durkin should not have expected to remain with the study through its lifetime. He said in an e-mail that the contractor—not yet named—will help NIH study how to "transition" a site to a new contractor "in the event that it is needed." NIH's goal, he says, is to "configure the entire study so that it can conduct high-level science in a fiscally prudent manner."

Alan Guttmacher, director of the National Institute of Child Health and Human Development (NICHD), which is managing the project, acknowledges that NIH's new sampling plan is causing "angst" among investigators. But he says the strategy will still yield a group of 100,000 children "very broadly representative of the American population." And NIH won't go forward with all the changes until it has examined the "scientific tradeoffs," he says.

Requested by Congress 12 years ago, NCS aims to study links between environmental factors and child health by following 100,000 children from before birth to age 21. Early in planning, NCS leaders decided to recruit pregnant women by knocking on household doors in a statistical sample of 105 U.S. sites (mostly single counties)—a costly approach but the gold standard in epidemiology because it yields results that apply to all U.S. children, including diverse ethnic, socioeconomic, and geographic groups (*Science*, 10 December 2004, p. 1883).

Three years ago, when only 510 pregnant women had been recruited at seven "vanguard" sites and the study's cost had doubled to a projected $6 billion, NIH replaced NCS's leadership and began pilot-testing other ways to recruit subjects at 30 more sites, such as going through health care providers to find pregnant women. By the end of last year, the 37 vanguard sites had recruited a total of about 6700 families, including 2200 babies.

"It would still be very broadly representative of the American population."

—ALAN GUTTMACHER, NICHD

But NIH has now decided that even that approach is too expensive. Instead, for the main part of the study, NIH proposes to cut $28 million (15%) from NCS's $193 million budget, possibly by recruiting women through providers that participate in health plans. This would be cheaper and easier "but would abandon the geographic based probability sample," according to an NIH budget document. The resulting sample would be "robust" for studying biological relationships but affect the "generalizability of some" socioeconomic relationships, NIH says.

Guttmacher says by turning to large providers such as health maintenance organizations (HMOs), NCS could take advantage of electronic health records and the "voluminous data points on participants" they would yield. But some planned recruiting sites may disappear. "It doesn't necessarily mean we're going to go to all 105 of [the original] sites. It means we're going to include the vast population of the United States, but we may be in different geographic areas," Guttmacher says. "We still need to figure out what the right number will be and the locations."

This plan has NCS investigators worried. Epidemiologist Nigel Paneth of Michigan State University in East Lansing says that if NCS recruits only through HMOs, "it will be very hard to create a nationally representative sample" because those providers inevitably underrepresent certain groups, such as the poor. "We do need a probability sample," says sociologist Barbara Entwisle of the University of North Carolina, Chapel Hill, who agrees with Paneth. "To me it's premature to choose" the sampling strategy, she adds.

Researchers are also concerned about Guttmacher's suggestion that the main study may not take place at the original 105 sites, where investigators have spent years building community participation. This has made recruitment easier and has helped secure funding from Congress, Paneth suggests: "What possible advantage is there to lose all that goodwill?"

Already reeling from the change in sampling plan, NCS investigators were stunned to learn from the NCS program office late last week that the seven initial vanguard centers will be turned over to a single contractor this summer. Hirschfeld told researchers on an NCS conference call that 30 or so other vanguard centers with contracts that end in the next 18 months could also be "transitioned" to a new contractor. Researchers expressed concerns about how the handover will affect scientific input into the study, relationships with participants, and the handling of follow-up visits and biological samples. "It was hard news," says Entwisle, who told her seven-person Duplin County team Friday that their project will soon end.

Some NCS researchers are discussing whether to take their concerns to the broader scientific community or perhaps Congress. "Our concern is the quality of the science," Paneth says.

–JOCELYN KAISER

CREDIT: NIH

Published by AAAS

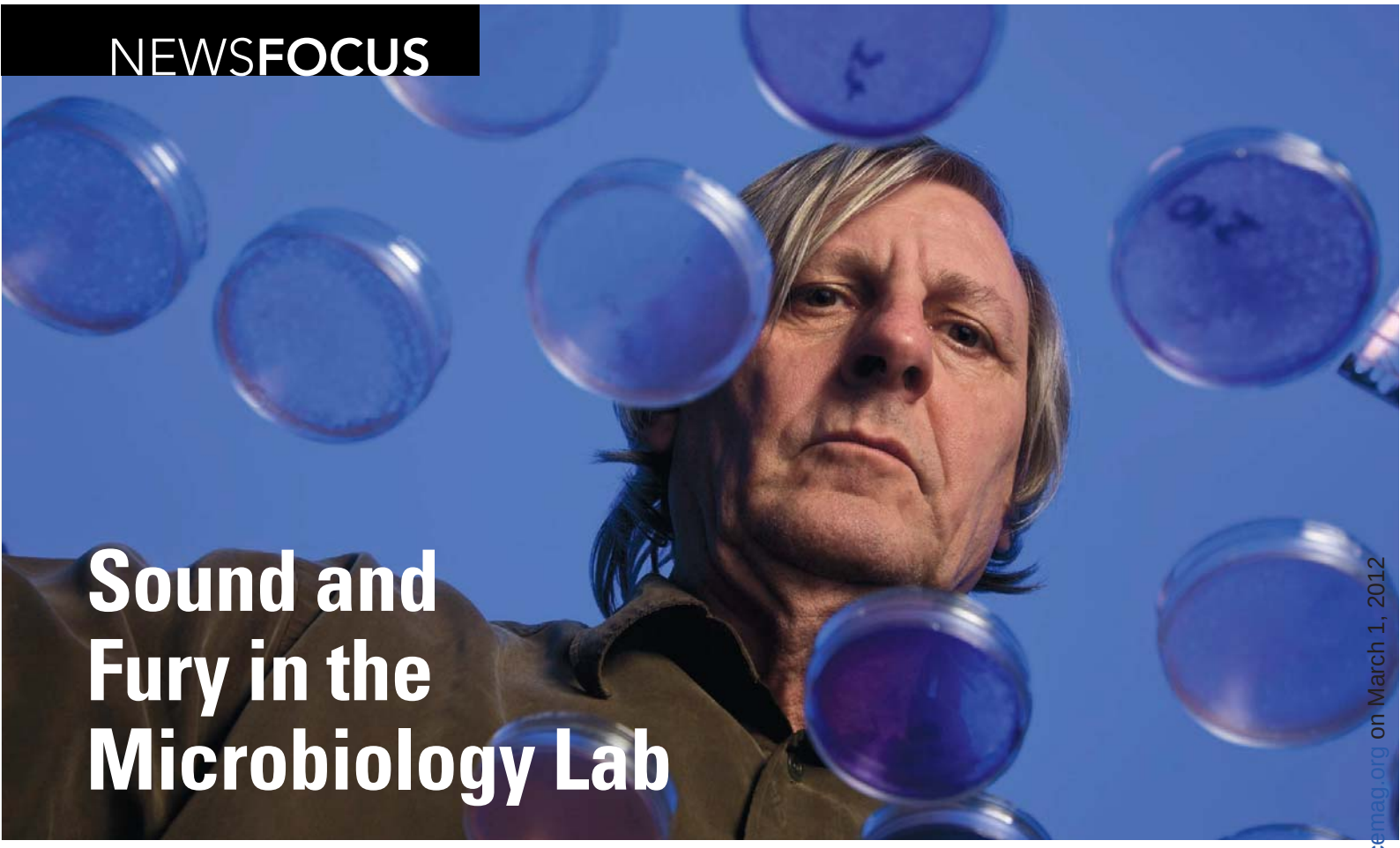

Sound and Fury in the Microbiology Lab

He's imaginative, rebellious, and often disdainful. Above all, France's most productive microbiologist loves a good fight

MARSEILLE, FRANCE—Didier Raoult has come a long way, even though he hasn't really strayed far from home. As an unruly, rebellious teenager in this port city with a reputation for toughness, Raoult was suspended from high school several times. But today, at 59, he's the most productive and influential microbiologist in France, leading a team of 200 scientists and students at the University of Aix-Marseille, here in the city where he came of age. He has discovered or co-discovered dozens of new bacteria, and in 2003, he stunned colleagues with a virus of record size, dubbed *Mimivirus*, the first member of a family that sheds an intriguing new light on the evolution of viruses and the tree of life.

But Raoult hasn't lost his edge. Long-haired and tall, his piercing eaglelike eyes sometimes cloud over in an expression of apparent fear, and he has a sense of provocation that many find irritating. Controversial and outspoken, Raoult last year published a popular science book that flat-out declares that Darwin's theory of evolution is wrong. And in an episode reminiscent of his teenage days, he was temporarily banned from publishing in a dozen leading microbiology journals in 2006, an episode that still enrages him. Raoult likes to say that "life is full of sound and fury," in a reference to the novel by William Faulkner—and in his case, it's true. "If my wife hadn't been a psychiatrist, I would be even crazier," he says.

Raoult's craziness may be a key element to his success. "He's very imaginative, a very hard worker, and very enthusiastic," says Jérôme Etienne, dean of the medical faculty at the University of Lyon and a longtime collaborator and friend. Despite its mammoth size, scientists at Raoult's lab say they wouldn't want to work anywhere else. "He's my boss because he's one of the greatest microbiologists in the world," says Philippe Brouqui, who has conducted research under Raoult for more than 20 years.

Yet Raoult is also known for his enmities and his disdain for those who disagree with him. "People don't like to talk about him because he has a lot of influence. He can make life hard for you," says one of several French researchers contacted by *Science* who would only talk about Raoult if they could remain anonymous. "Few of his science colleagues will find the thought of another profile story about him particularly appealing," geneticist Jean-Michel Claverie of Aix-Marseille University—who severed ties with Raoult in 2006 after a 5-year collaboration—wrote in an e-mail to *Science*.

A magical period

Raoult's career has always been tightly linked to Marseille, a city where his family settled when he was 8 and whose rough-and-tumble reputation matches his character. He trained as a physician and obtained a Ph.D. in human biology here; in 2004, he would name a rickettsia species, *Afipia quartiernordensis,* in honor of Quartiers Nord, a local neighborhood of ill repute.

Rickettsias, intracellular Gram-negative bacteria transmitted by ticks, fleas, lice, and acarids, have become Raoult's specialty. He worked on a disease called Mediterranean spotted fever, or Marseille fever, and studied typhus for 6 months at the National Naval Medical Center in Bethesda, Maryland. When he came back to Marseille in 1984, the university president offered him an assistant professorship. He combined his work as a physician with basic research and the development of new diagnostic methods. In 1987, Raoult's lab became France's national reference center for rickettsias, and in 1988, a collaborating center for the World Health Organization for arthropod-transmitted bacteria.

He owes many of his discoveries to well-chosen collaborations. From heart valve

samples provided by cardiologists in Lyon, for instance, he managed to isolate *Coxiella burnetii*, a bacterium already known to cause a zoonosis transmitted by cattle, goats, and sheep called Q fever. He showed that *C. burnetii* was also involved in endocarditis, an inflammation of the inner layer of the heart. He went on to discover several other microbes that cause endocarditis. "One of the keys to Raoult's success is his ability to make bacteria grow where others fail," says Michel Drancourt, who has worked in Raoult's group since 1984.

When the genomics revolution arrived, Raoult jumped to apply it in microbiology. In 1992, he bought his first DNA sequencing machine and started to fish for typical bacterial sequences in various samples with the aim of identifying new species. He sees "metagenomics," the analysis of microbial DNA in environmental samples such as seawater or soil, as a window on entirely new worlds in microbiology. "We're in a magical scientific period, an era of discoverers," he says.

Fatherly spirit

One afternoon in August, during the ritual Friday meeting, a young Ph.D. student in Raoult's genomics group delivers a 10-minute talk about the sequence of a newly isolated bacterium. Raoult listens intently and then, in a warm voice, tells her how to proceed with the research. The Asian woman nods shyly. The other students of the group—many of them non-French as well—appear to be listening with deference.

"For foreign students, Raoult's lab is a springboard [to a career]," says microbiologist Patricia Renesto of Joseph Fourier University in Grenoble, who spent several years in Raoult's lab and admires him. "The flip side is that he controls everything. He can behave odiously," she adds. "Raoult has that fatherly family spirit, which some people don't understand," Brouqui says.

After the meeting, back at his office, Raoult boasts that the newly isolated microbe was one of 225 different bacterial species found in a single stool sample from Dakar. "The world record was 80 species. We beat it by a factor of two and a half," he says. "Half of those species have never been isolated from the gut before, and 21 are completely unknown."

Raoult's entire opus appears to be written in big numbers. A recent PubMed search showed him as an author on more than 1400 papers, including the description of more than 60 new bacterial species and one new bacterial genus, which Drancourt named *Raoultella*. But some scientists grumble that manuscripts out of Raoult's lab often contain errors, for instance, as a result of unchecked genetic sequences.

Indeed, problems in a paper about a mouse model for typhus got his lab in hot water in 2006. A reviewer for *Infection and Immunity*, a journal published by the American Society for Microbiology (ASM), discovered that four figures in a revised manuscript were identical to figures in the original manuscript, even though they were supposed to describe a different experiment.

In letters to ASM, made available by Raoult, second author Christian Capo and last author Jean-Louis Mège, a group leader, accepted "full responsibility" for the problem, which they said involved only two figures. Capo, in his letter, wrote that he had made an innocent mistake; Mège wrote that Capo had subsequently failed to show the revised manuscript to other authors, who were on vacation, before resubmitting it. But after consulting its ethics panel, ASM banned all five authors, including Raoult, from publishing in its journals for a year. "We are not entirely comfortable with the explanation provided," ASM officials wrote to Mège. "Misrepresentation of data … is an affront to the ethical conduct of scientific inquiry."

Big surprise. Raoult's team initially mistook the giant *Mimivirus* (illustration), discovered in a cooling tower, for a bacterium.

CREDIT: MIEKE ROTH/ WWW.MIEKEROTH.COM

Capo and Mège accepted the decision, but Raoult wrote ASM that he wasn't at fault and that the "collective punishment" was "very unfair." He appealed the ban, also on behalf of two other co-authors, but lost. Furious, he resigned from the editorial board of two other ASM journals, canceled his membership in the American Academy of Microbiology, ASM's honorific leadership group, and banned his lab from submitting to ASM journals, in which he had published more than 230 studies. His name has been on only two ASM journal papers since, both published in 2010. To clear his name, Raoult sent his ASM correspondence to French colleagues in 2007, along with a letter defending himself. "If I had been in the United States, I would have sued," he wrote.

Still, the affair does not appear to have dented Raoult's career. From 2013 onward, he will head a new government-funded academic medical center of excellence that will combine the expertise of various research and medical agencies in infectious and tropical diseases in Marseille.

Charlatans

Despite his long career in bacterial research, Raoult has become best known for the discovery of giant viruses. The story began in the late 1980s, when Timothy Rowbotham, a bacteriologist at the Public Health Laboratory in Leeds, U.K., isolated amoebae that had *Legionella* bacteria living inside them. In one amoeba, Rowbotham discovered another putative bacterium that he could not identify.

He later sent the amoeba collection to Richard Birtles, a Ph.D. student in the United Kingdom. Always interested in new microbes, Raoult invited Birtles to come work in Marseille. Even there, the unknown amoeba resident initially defied identification—until the team looked at it using an electron microscope. It was not a bacterium at all but a novel virus bigger than any known virus. With a diameter of 700 nm—including its hairy crown—*Mimivirus* was also stuffed with a genome of 1.2 million DNA base pairs, six times bigger than any known DNA virus and bigger than some bacteria. Genetic comparisons showed that the unusual virus belonged to the group of nucleocytoplasmic large DNA viruses, which also includes the poxviruses. Raoult baptized it *Mimivirus*, short for "mimicking microbe," and the new family Mimiviridae.

Mimivirus turned out to have an interesting genome. An analysis performed with Claverie's team showed that it includes genes involved in DNA processing and protein production that were until then considered to be unique to living organisms. The finding revived the old debate about viruses' place in the tree of life, and Raoult has now staked out a strong position (see sidebar, p. 1035). But David Moreira of the University of Paris-Sud in Orsay says Raoult is out of his depth: "He has a tendency to throw himself into a field he doesn't know well."

Some scientists argue that the same is true for epidemic modeling, a field that has seen tremendous growth but which Raoult

Giant Viruses Revive Old Questions About Viral Origins

Where did viruses come from? And are they alive? Didier Raoult's 2004 discovery of the *Mimivirus*—and several other giant viruses identified since then—has brought those questions, debated for a century, back to the scientific fore.

When viruses were discovered in the early 20th century, some scientists saw them as the missing link between the inanimate world and living organisms—a group that predated and perhaps gave rise to cells. But genetic data collected later supported an opposing view, in which viruses emerged from pieces of genetic material and other molecules broken out of cells; they would evolve further by stealing more genes from cellular organisms. This view suggests that viruses aren't part of the tree of life but are an ever-changing sideshow to its three domains: the Archaea, Bacteria, and Eukarya. In 2000, the International Committee on Taxonomy of Viruses officially declared that viruses are not alive.

The genetic makeup of the *Mimivirus* has challenged this view. The viral giant is endowed with many genes encoding the enzymes that repair DNA, correct errors occurring during its replication, produce mRNA transcripts from genes, and translate those mRNAs into proteins. These so-called informational genes had so far been considered hallmarks of living things. Known viruses hijack the products of these genes from the cells they infect to replicate; the *Mimivirus* genes had never been found in viruses before. Based on the genome, Raoult and others have concluded that this class of virus has likely inherited its giant genome from an ancient viral ancestor endowed with the entire protein-translation machinery rather than picking up the genes piece by piece.

Not everybody was convinced. In 2008, David Moreira of the University of Paris-Sud in Orsay and his colleagues published an analysis showing that 126 *Mimivirus* genes have counterparts in cellular organisms, which they said supported the view that, despite its extreme size, *Mimivirus* has evolved by picking up genes here and there.

Raoult stuck to his guns, and in a paper published in 2010 proposed a theory that went further: Not only does *Mimivirus* belong in the tree of life, but nucleocytoplasmic large DNA viruses (NCLDVs), the class to which it belongs, trace their origin to the very beginning of life on Earth, forming a fourth domain alongside the three well-established ones. His view was based on a phylogenetic analysis of eight DNA-processing genes shared by NCLDVs and the three known branches of life, in which the NCLDVs' versions seemed to form a separate cluster.

But constructing such phylogenies reaching back eons is tricky business, because similarities in genes don't always reflect shared ancestry; the same DNA sequence may have arisen independently in genes of different origins, a process called convergent evolution. In a paper published in June 2011, a team led by Eva Heinz of Newcastle University in the United Kingdom repeated Raoult's analysis but used different models of evolution that take this phenomenon into account. In their phylogenetic trees, the fourth domain evaporated, and the NCLDV genes were spread out over the other branches of life.

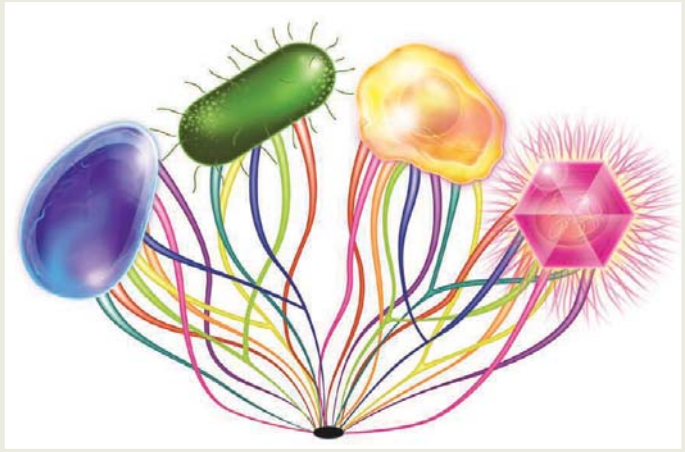

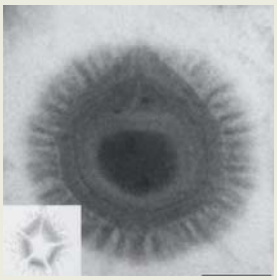

Even bigger. *Megavirus chilensis* (*left*) strengthened the case that giant viruses share a common ancestor. Didier Raoult believes they form a fourth domain, pictured here in magenta in a drawing from his lab.

For now, Raoult's position in this debate has few supporters. But the idea that giant viruses share ancient common ancestors was bolstered by a paper published in the *Proceedings of the National Academy of Sciences* last October by Jean-Michel Claverie of the University of Aix-Marseille—once Raoult's collaborator but no longer on speaking terms with him. Claverie recently isolated *Megavirus chilensis*, a virus distantly related to *Mimivirus* but even bigger, off the coast of Chile. In the paper, he reported that *Megavirus* shares 53% of its genes with *Mimivirus*; of seven genes encoding key steps in protein translation, four have a homolog in *Mimivirus* and had never been found in a virus before. "This rules out the scenario whereby those genes were acquired independently by both viruses," Claverie says. Even Moreira says the paper won him over for a common viral ancestor between the two viruses.

Edward Holmes, a virus evolution specialist at Pennsylvania State University, University Park, notes that ongoing fishing expeditions for new viruses—not just the giant ones—are likely to resolve the origins of these infectious agents. "It's naïve to say that we understand the history of the evolution of viruses based on current samples," Holmes says. "There may be undiscovered viruses on our planet, some completely novel." **–C.M.**

has repeatedly attacked as useless. Epidemic modelers are "charlatans," he says. "There are zero examples in infectious diseases of something that has been predicted by a model."

And then there is his popular science book *Dépasser Darwin* (*Beyond Darwin*). "Darwin was a priest," Raoult says, claiming that the image of the tree of life that Darwin proposed is inspired from the Bible. "It also is too simplistic." Raoult questions several other tenets of modern evolutionary theory, including the importance of natural selection. He says recent discoveries in genetics show how frequently genes are exchanged not just between different microbial species but also between microbes and complex organisms, for instance, in the human gut. That means de novo creation of entirely new species is possible, Raoult argues, and Darwin's branching tree of life should be replaced by a network of interconnected species.

"It's dangerous to say those things," says Moreira, who worries that Raoult is providing creationist groups with ammunition. "He goes a bit too far," says Eugene Koonin, an evolutionary biologist at the National Center for Biotechnology Information in Bethesda. "Darwin's theory is relevant but is incomplete. It does not apply to the evolution of microorganisms."

Raoult says he doesn't really care what other people think, and he relishes the constant storm around him. "An amazing thing I discovered when I arrived in Marseille was that the people there are fighters," he recalls. It's why he feels at home here. For Raoult, the fights never stop. **–CATHERINE MARY**

Catherine Mary is a writer in Caluire, France.

ANIMAL COGNITION

'Killjoys' Challenge Claims Of Clever Animals

Sharing the wealth. Chimps aren't quick to help each other but may do so under some conditions.

Despite recent claims of advanced intelligence in animals, researchers still debate how to test whether their abilities reflect humanlike cognition

LONDON AND CHICHELEY—It seems that hardly a week goes by without a new report about animals performing marvelous feats we once thought only humans could do: Crows make tools, chimpanzees seem to mourn their dead, and rats supposedly empathize with one another's pain.

Charles Darwin, were he alive today, might approve this trend. "The difference in mind between man and the higher animals," he wrote in *The Descent of Man*, "… is one of degree and not kind." For many researchers, the new evidence represents a welcome shift from behaviorist paradigms often associated with psychologist B. F. Skinner, which denied nonhuman species anything approaching advanced cognition (*Science*, 25 January 2008, p. 404). Yet recently, some researchers have been pushing back against attributing humanlike qualities to other animals without considering cognitively simpler explanations.

This more skeptical contingent was present in force at two recent back-to-back meetings* sponsored by the Royal Society in London and Chicheley. At both, researchers explored what animals are really doing when they engage in seemingly complex behaviors, rather than reported still more discoveries of their impressive abilities. "There's an arms race to identify the most clever animals," Lars Chittka, an animal psychologist at Queen Mary, University of London, said at the London meeting. "But what are we trying to demonstrate?"

Attempts to measure the gap between human and nonhuman minds have become like a "party game," said experimental psychologist Cecilia Heyes of the University of Oxford in the United Kingdom. Some researchers blamed the news media, and even some scientists, for exaggerated interpretations of animal behavior. "People in the field often gravitate into two camps," Daniel Dennett, a philosopher at Tufts University in Medford, Massachusetts, told *Science*. "There are the romantics," those who are quick to see humanlike traits in animals, "and the killjoys," who prefer more behaviorist explanations. "I think the truth is almost always in the middle."

Crinkly bananas

In a talk at the London meeting titled "Simple Minds," Heyes argued that many researchers discount associative learning—the expectation that two events, for example, a stimulus and reward, are connected. Heyes argued that this type of learning is ubiquitous among both animals and humans and remains a "contender" when interpreting animal experiments. As a case study, Heyes critiqued a paper on chimp altruism published last year in the *Proceedings of the National Academy of Sciences*. Researchers have been hard put to show that chimps have much desire to help each other out; unlike humans, they seem to do so only when pressured or pleaded with rather than spontaneously.

In the study, led by primatologists Victoria Horner and Frans de Waal of Emory University in Atlanta, chimps were given a choice between two different colored tokens. One color prompted the human experimenter to give a banana to both the subject chimp and another chimp in an adjacent enclosure whereas the other color resulted in food for the first chimp only. Chimps showed a significant preference for the token that led to a banana for both themselves and their partners. The team concluded that chimps are more altruistic than usually given credit for.

But Heyes pointed out that the bananas were wrapped in crinkly paper, so chimps could both hear and see when the partner got a reward. She suggested that the chimps may have begun to like the sound of the crinkly paper, "just as Pavlov's dogs got to like the sound of a bell." Thus they might have opted for the color choice that yielded a double shot of the noise.

Psychologist Sara Shettleworth of the University of Toronto in Canada says she "totally agrees" with Heyes's reservations, and even Horner calls the arguments "thought-provoking." But Horner argues that the chimps got only one reward no matter "how many rustling papers they heard." Had associative learning been the primary mechanism operating, she says, the chimps would not have preferred one token color over another.

Although researchers still debate what's behind the behavior of close human relatives such as chimpanzees, there was wide agreement with points made at the Chicheley meeting by cognitive scientist Derek Penn of the University of California, Los Angeles. His talk, titled "Animals Aren't People," included a blistering critique of a 9 December 2011 *Science* paper (p. 1427) that claimed that rats are capable

*"Animal minds: from computation to evolution," London, 16–17 January, and "Theories of minds: the theoretical bases of comparative cognition," Chicheley, 18–19 January.

CREDIT: NICK BIEMANS/ALAMY

Published by AAAS

of empathy—or, as *Science*'s online news coverage headlined the story, "Rats Feel Each Other's Pain."

In the study, neurobiologist Peggy Mason of the University of Chicago in Illinois and her colleagues trapped one rat in a small plastic restrainer that could be opened only from the outside; trapped rats gave alarm calls roughly 20% of the time. A second, free rat was placed nearby, and it soon learned to free its compatriot by opening the door. Free rats did not open the door when the trap was empty. The authors concluded that the helping rat reacted empathically to the distress of its fellow.

But Penn argued that the team hadn't shown that either rat was truly in distress. The team didn't perform at least one other important control, he said: using trapped rats that were not distressed. Playing videos of the experiments to the meeting, he pointed out that once the door was open, the free rat entered the trap and explored it with the trapped rat, suggesting that being in the trap was not that stressful.

Mason, who was not at the meeting, counters that once the trap was open, it became "an object to be explored, and in fact rats might prefer it to staying out in the open." As for the lack of an unstressed control rat, Mason says the team now has an experiment under way suggesting that the more anxious the trapped rat, the more helping behavior is evoked. She agrees that rats probably are not aware of one another's mental states, as humans are, but says the behavior her team observed is the "rodent homolog of empathy."

Nevertheless, Penn argued that this and many other recent papers suffer from what is called "folk psychology": interpreting animal and human behavior in "commonsense" rather than strictly scientific terms. Folk psychology, Penn said, gives animals humanlike reasons for what they do, such as "the rats helped free their cagemates because the caged rats were feeling scared."

Penn's talk evoked murmurs of agreement in the meeting room. "Our folk psychological labels carry a lot of specifically human baggage," Dennett says, "which can be gradually jettisoned as we come to understand other ways of accomplishing many of the same basic cognitive tasks."

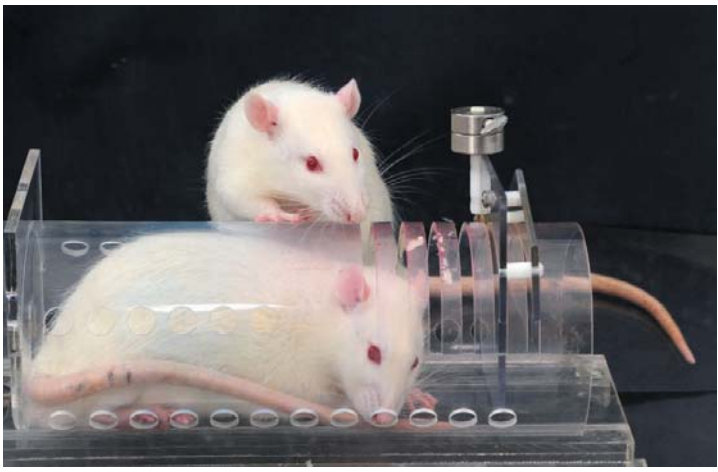

Feeling his pain? A study concluding that rats have empathy for one another came under fire at the meeting.

Do birds have theory of mind?

Are there alternative ways of explaining remarkable animal feats? A talk in Chicheley by cognitive scientist Rineke Verbrugge of the University of Groningen in the Netherlands explored that question in the case of birds such as rooks and jays. Recent findings suggest that these birds can make tools and understand the mental states of others, often called "theory of mind"—behavior once reserved for humans.

Research suggests that the western scrub jay is no "birdbrain" cognitively, for example. In work by Nicola Clayton of the University of Cambridge in the United Kingdom and colleagues, the jays appear to plan for the future by caching food where it is most likely to be needed later. And in an elegant 2006 *Science* paper (16 June, p. 1662), Clayton's team showed that these birds might even have theory of mind. The team found that the jays alter their caching behavior—for example, moving food, called recaching—if other birds are watching. Because jays routinely steal one another's caches, this raises the possibility that the birds are aware of one another's mental state.

In her talk, Verbrugge described computational modeling work carried out by graduate student Elske van der Vaart, which was published online this week in *PLoS ONE*. Van der Vaart created "virtual scrub jays" whose behavior was governed by simple behavioral rules. In the model, the birds recached more when they were stressed, for example, by the presence of another bird, especially one more dominant in the pecking order. The model also took into account the scrub jays' superb memories.

Van der Vaart's simulations closely duplicated the behavior of real scrub jays. "Their model fits some of the data really well," says psychologist Amanda Seed of the University of St. Andrews in the United Kingdom. "Even better, it provides some testable predictions," such as that boosting birds' stress levels should spark more recaching.

Clayton agrees that the model "provides a powerful explanation for some of the studies," but she argues that it leaves some data unexplained, a point Heyes also makes. For example, Clayton's team showed that "it takes a thief to know a thief": Jays that have previously pilfered others' caches are more likely to recache themselves. Van der Vaart's model does not explain that result, but theory of mind could. Further experiments are needed, Clayton says, and she and the Groningen team are now discussing collaborating on them.

Van der Vaart and colleagues emphasize that they haven't proved that scrub jays don't have theory of mind, only that theory of mind is not necessary to produce the findings. Indeed, meeting attendees discussed at length where the burden of proof should lie: on those who claim animals have more advanced, or less advanced, cognition. "Part of me hopes they will prove the model wrong," Van der Vaart says. "But I think it's important to exclude as many simpler explanations as possible." **–MICHAEL BALTER**

Cache as catch can. Scrub jays hide food more often if they are aware that another bird has been watching them.

CREDITS (TOP TO BOTTOM): DAVID CHRISTOPHER; NICKY CLAYTON, UNIVERSITY OF CAMBRIDGE

Published by AAAS

MINERAL RESOURCES

Is the World Tottering on The Precipice of Peak Gold?

Seventeen-hundred-dollar-an-ounce gold is driving a mining frenzy, but analysts are concerned that miners can't extract gold any faster than they have the past decade

Gold miners are worried. In the past 40 years, they've seen a slew of developments favoring their business. Gold's price has risen so that on average it's been worth several times what it was. Investment in the search for new gold deposits doubled and then doubled again, making gold more intensively sought after than any other metal or mineral group. Technologists have come up with better and cheaper ways to find and extract gold. And gold mining has spread throughout the planet.

And yet worldwide, production of the glittering element has hardly budged in the past decade. It's not for lack of demand. Gold may not fuel economies the way oil does, but gold for jewelry—its primary use—has been much in demand, and that demand will likely increase. Investors' interest could be intense for years longer. But to judge by the mining industry's modest success of late in finding new deposits of gold, production will not be much higher in the next decade.

Miners and analysts agree that most of the easy-to-find, easy-to-develop gold has been found. To discover still-hidden deposits and at least maintain production, let alone increase it, miners will need continued high or even higher gold prices, revolutionary new technology, and the cooperation of often reluctant host countries.

"It's a huge amount of new [gold] deposits that has to be found," says resource geochemist Stephen Kesler of the University of Michigan, Ann Arbor. "That is an issue of considerable concern" because no one wants to see the world's first mineral resource peak anytime soon.

A golden age

The times may be challenging in gold mining, but you don't have to go back to California's '49ers to find an exuberant heyday for gold. In a 2010 article, three experts—Tommy D. McKeith, vice president for exploration and development for Gold Fields Ltd. in Perth, Australia; Richard Schodde, managing director of MinEx Consulting Pty. Ltd. in Melbourne, Australia; and Ed Baltis of Gold Fields, Perth—pointed to a confluence of forces in the 1970s and '80s that drove an eventual doubling of production.

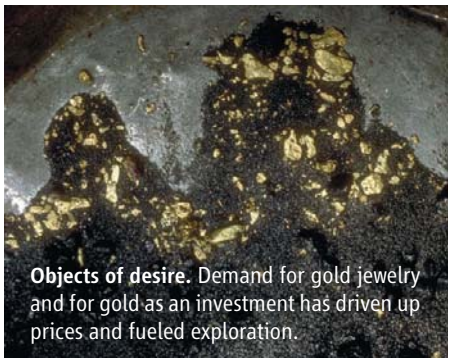

Objects of desire. Demand for gold jewelry and for gold as an investment has driven up prices and fueled exploration.

First of all, in 1971, governments stopped fixing their currencies to gold at a price of $35 an ounce ($185 in 2009 dollars). As the unleashed gold price rose through the 1970s toward a 1980 peak above $1500 an ounce, so too did investment in exploration for gold. Exploration expenditures soared in the 1980s by an order of magnitude, never again falling below double the spending of the 1970s.

Technical and scientific breakthroughs fed gold mining fever as well. Recognition of new types of gold deposits—such as the Carlin deposits of Nevada, which have no visible gold grains—aided exploration. So did new technology, from more-sensitive sample analyses that detect low levels of gold to orbiting satellites that use spectra to map promising mineral terrains. New, cheaper gold-extraction techniques—such as leaching gold from heaps of ore with a cyanide solution—made ores worth mining even when they contained less than a gram of gold per ton of rock.

By the 1980s and especially in the 1990s, those changes greatly broadened the gold mining club. They made the United States, Australia, and China major producers in a business previously dominated by South Africa. They also drew in more than a dozen new countries. And production soared. From a low of 1200 metric tons of gold in 1975, the industry's output more than doubled to 2600 tons in 2001.

End of an age

The exuberance of the 1980s and '90s has definitely cooled, and now it is tinged with anxiety. Production immediately began dropping from its 2001 record high to a low of

Published by AAAS

Big mining. Part-per-million gold ores require large-scale operations (note people in red, *center*).

2260 tons in 2008. Miners have since clawed their way back to record-equaling production, spurred by gold prices rocketing to the (inflation-adjusted) levels of 1980.

That resurgence isn't heartening gold miners much, though, because their best indicator of future production—the amount of gold discovered in the past 10 years or so—is showing no signs of life. As he reported at the 2011 NewGenGold Conference in Perth last November (http://www.minexconsulting.com/publications/nov2011b.html), Schodde has compiled reports of the amounts of gold discovered per year from 1950 to 2010 (see figure). Using history as a guide, he increased the size of recent discoveries to account for the inevitable growth in the apparent size of a newly discovered deposit as geologists explore it.

By Schodde's reckoning, gold discoveries peaked in the 1980s. That presumably led to the 2001 production peak. Since the 1980s, discoveries have been something like 20% lower. Is that enough to sustain production over the next decade or two? "Yes," Schodde says, "but it's a struggle, it really is." A bolstered exploration effort has been yielding meager returns; the average gold content of ore mined has steadily fallen by a factor of 4 since 1979. So to produce an ounce of gold, four times the tonnage of rock has to be moved and processed.

The golden age seems to be over. "It's becoming harder and harder to find" gold, concludes minerals analyst Michael Chender, CEO of Metals Economics Group in Halifax, Canada. "There's a general sense that most of what's easily available has been found and picked up." Andrew Lloyd agrees; the industry "has increased exploration, but they're not finding a lot of new deposits, especially the large ones," says the spokesperson for the world's largest gold mining company, Barrick Gold Corp., headquartered in Toronto, Canada. "The industry as a whole is really struggling to keep up with demand."

Pause or peak?

How the struggles of the gold mining industry will play out depends on whose crystal ball you are consulting. Those who have been predicting that the world's production of oil will shortly peak, if it hasn't already done so, are pessimistic about gold's prospects as well. Applying a standard peaking analysis to the history of gold production, retired oil geologist Jean Laherrère concluded in 2009 that 2001 was the peak and that production would soon plummet.

Some analysts and explorationists are considerably more optimistic. They point to the three production peaks in the 20th century, each of which was followed by a higher peak. Each time, the gold price went up, new territory opened to mining, or new technology made it easier to find or process gold ore. "I'm sure we'll discover something in the next 10 years that will change the picture," Kesler says. A can-do spirit goes with the turf, says resource geochemist Gavin Mudd of Monash University, Clayton, in Australia. "It's never say never" in the mining industry, he notes. "Part of this business is the business of hope."

Others come down on a middle ground. "Our view is that mine supply is not likely to increase from present levels," Barrick's Lloyd says. Schodde, too, sees another decade, at least, of more or less unchanging gold production. That would be reminiscent of the "undulating plateau" of recent world oil production (*Science*, 3 February, p. 522). Shifts in price or demand or the politics in a producing country might swing annual production up or down for a few years, but over a decade or so the supply would be little changed.

Gold plateauists tend to see greater challenges in gold production now than ever before, but no good solutions in the offing. For example, all the exploration innovations of the past 50 years have not let geologists find deposits any deeper in Earth's crust. Hot, briny solutions deposited gold not at the surface but several kilometers below it. But Schodde finds that the depth to gold deposits discovered in virgin territory has averaged a mere 30 meters in each of the past 5 decades. In every decade, almost half of those discoveries were deposits now exposed at the surface by erosion. Even the generally optimistic Kesler "cannot think of any major processing, mining, or exploration method that is very recent in appearance" that could help out anytime soon.

While these "belowground" issues loom large, the aboveground ones are looking equally daunting. Getting all the required permits for a new mine is taking longer, miners say. Resource economist Keith Long of the U.S. Geological Survey in Tucson, Arizona, has found that in the United States it has taken on average 7 years from requesting a permit to opening a mine. Remote sites in Alaska or deposits in a country new to large-scale mining can take much longer. And overseas, the big global mining companies must delicately, and slowly, navigate the tricky political and social waters of the countries holding the remaining gold.

Litigation further stretches out the development process and increases costs. The gold mining industry produces hundreds of millions of tons of waste rock a year and uses tons of cyanide, Mudd notes. The mass of potential pollution is already increasing as the grade of gold ores has declined, he has found. "The big constraints [on gold production] will be environmental and social," Mudd believes, "not so much discoveries."

Gold, mined as it has been for 6000 years, may be a harbinger of production challenges in other metal industries. Analysts often mention economically essential copper as another element encountering mining constraints. But trends in mineral discovery in general suggest to Kesler that "we are approaching some sort of wall in materials to support our way of life." So watch gold's price and production figures for clues to how close the world may be to the first such wall.

–RICHARD A. KERR

Online

sciencemag.org

Podcast interview (http://scim.ag/pod_6072) with author Richard A. Kerr.

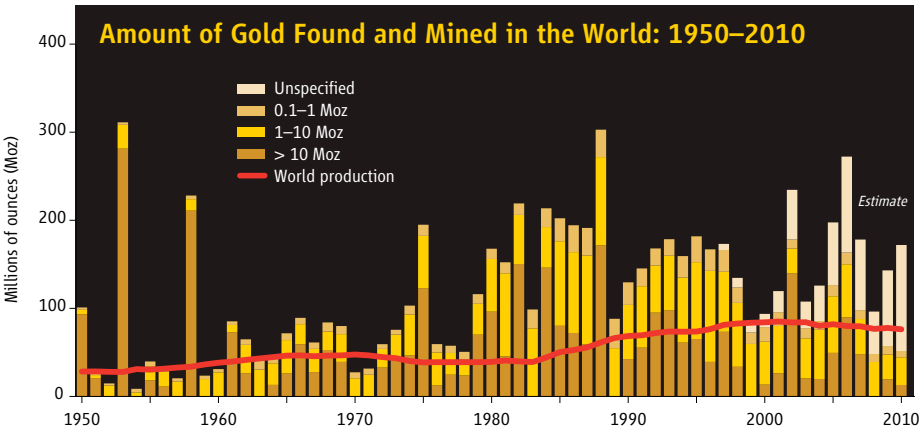

Up, up, and level. Record amounts of gold found in the 1980s let world production rise until 2001. Since then, production has been essentially flat. ("Unspecified" is an estimate.)

SOURCE CREDIT: © MINEX CONSULTING, NOVEMBER 2011

LETTERS

edited by Jennifer Sills

Editors' Note

WE THANK READERS FOR THE MORE THAN 120 COMMENTS IN RESPONSE TO THE NEWS FOCUS story "Saudi universities offer cash in exchange for academic prestige" (Y. Bhattacharjee, 9 December 2011, p. 1344). The comments cover a range of opinions, some of which are reflected in the letters printed below, on issues critical to the future of science in Saudi Arabia and the region. We encourage you to peruse the comments, available at http://comments.sciencemag.org/content/334/6061/1344. **COLIN NORMAN AND JENNIFER SILLS**

Saudi University Policy: King Saud Response

KING SAUD UNIVERSITY (KSU), THE PROGRAMS of which were discussed in the 9 December 2011 News Focus story by Y. Bhattacharjee (p. 1344), is the largest institution of higher education in the Kingdom of Saudi Arabia. Over decades, KSU has invested in scholarships, personnel, and infrastructure. In recent years, KSU has recruited over 700 faculty members, 345 researchers, and 323 foreign graduate students (bringing the total to 5626 faculty and 5851 graduate students). KSU has benefited from government research funds, including US$2.1 billion for science and technology, and has established a number of centers, institutes, research chairs, and satellite labs in Germany, France, and Canada. Since then, KSU has experienced a surge in research outcomes (1254 articles indexed in the Institute for Scientific Information in 2010) concurrent with a 50-fold increase in patents, the launch of four spin-off companies, investment of US$1.3 billion of endowments, and the creation of the 1.6-million-square-meter Science Park.

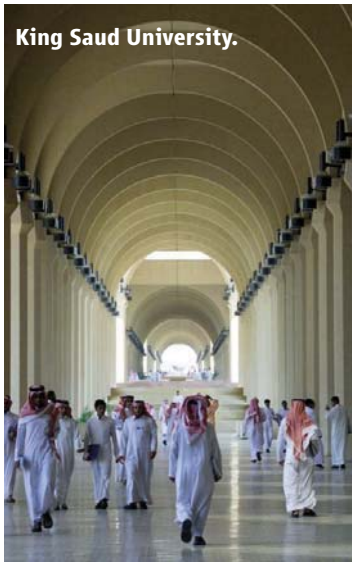

King Saud University.

KSU has been ranked among world-class universities since 2008. The increase in research papers published in 2010 was documented in all literature databases, not only those considered by rankings. Moreover, KSU faculty members, researchers, and students have contributed substantially to KSU research that has been published in databases that are not indexed by the Institute for Scientific Information (ISI).

KSU applies best practices for international collaborations through different programs, including the Distinguished Scientist Fellowship Program and the Visiting Professor Program. Both programs are common initiatives in top universities, set as KSU benchmarks according to KSU Strategy 2030.

KSU views international collaborations such as those described in the News Focus story as a means to share knowledge, accelerate development, and meet demand for academic scientists to serve new initiatives. These collaborations provide opportunities and high potential for research excellence. KSU has brilliant faculty and will expand international collaborations. Future expectations are very high, and the coming years will witness landmark achievements in knowledge production for the benefit of Saudi Arabia and the world.

ABDULAZIZ A. AL-KHEDHAIRY

Assistant Vice Rector, Graduate Studies and Research (Research Affairs), King Saud University, Riyadh 11451, Saudi Arabia. E-mail: kedhairy@ksu.edu.sa

Saudi University Policy: King Abdulaziz Response

KING ABDULAZIZ UNIVERSITY (KAU) IS FLATtered to receive international attention regarding its ambitious efforts to recruit scientific talents. Nevertheless, the title of the News Focus story "Saudi universities offer cash in exchange for academic prestige" (Y. Bhattacharjee, 9 December 2011, p. 1344) gave the wrong impression of a newly established program at KAU, which aims to further enhance its scientific research activities through the integration of visiting professors at the institution.

We appreciate the interviews with visiting professors Neil Robertson (Ohio State University) and Ray Carlberg (University of Toronto), in which they explained the real theme of our program.

KAU is clearly making a sound strategic business investment for the future of our country. Moreover, our program is not different from those in many elite universities around the world from which top scientists continue to receive attractive offers.

KAU had started a program in March 2010 in mathematics under which several top-notch mathematicians visited KAU and gave courses on topics of current research, collaborated in publishing research papers, began writing two books, and launched *Bulletin of Mathematical Sciences* (published by Springer). This program was extended to all disciplines by involving other distinguished visiting professors more intensively in research projects of mutual inter-

Amphibians under threat
1052

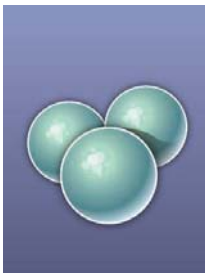

Selective signaling
1055

est to KAU faculty. The contracts made with highly cited scientists are on the basis of part-time or full-time work.

In this way, KAU is definitely not buying research publications for the sake of ranking. KAU would never sacrifice its reputation in order to obtain false rewards; neither would the elite scientists collaborating with the institution accept such an unethical proposition.

ADNAN ZAHED

Vice President for Graduate Studies and Scientific Research, King Abdulaziz University, Jeddah 21589, Saudi Arabia. E-mail: azahed@kau.edu.sa

Saudi University Policy: Meaningful Cooperation

THE NEW FOCUS STORY "SAUDI UNIVERSITIES offer cash in exchange for academic prestige" (Y. Bhattacharjee, 9 December 2011, p. 1344) gives the impression that King Abdulaziz University (KAU) and King Saud University (KSU) are paying researchers from prestigious institutions, most of them listed in the highly cited researcher list of the Institute for Scientific Information (ISI), for putting their name with their affiliation in Saudi Arabia into the ISI Web page and on their publications. The article claims that this is done regardless of whether the work involved any meaningful collaboration with KAU or KSU researchers. This impression is wrong.

I am a member of the Distinguished Scientist Fellowship Program (DSFP) at King Saud University. I received an e-mail 3 years ago offering me a part-time position including a real, research-oriented, joint project with a corresponding budget for personnel and equipment. I received this project granted by DSFP a year later and now I have another project granted by King Abdulaziz City for Science and Technology on the order of half a million euros. I am now a part-time professor at KSU. My KSU colleague, Omar Al-Dossary, has since participated in every experiment we have conducted at the Berlin Electron Storage Ring for Synchrotron Radiation (BESSY) of the Helmholtz-Zentrum Berlin, as well as the experiments at the Free-Electron Laser at the German Electron Synchrotron (DESY) in Hamburg. Next year, a female student of Al-Dossary's, Mashaal Al Khaldi, will join my group at the Fritz-Haber-Institute in Berlin. This is an effort to strengthen the still relatively weak scientific community in Saudi Arabia, a venture undertaken by many eminent scientists from around the world. I believe that my experience is true for many other scientists involved in cooperative activities with Saudi Arabia. We should appreciate these efforts, as they help the Arabic countries to survive.

UWE BECKER

Fritz-Haber-Institut der Max-Planck-Gesellschaft, 14195 Berlin, Germany. E-mail: becker_u@fhi-berlin.mpg.de

Saudi University Policy: Overvalued Rankings

I READ WITH GREAT INTEREST THE NEWS Focus Story "Saudi universities offer cash in exchange for academic prestige" (Y. Bhattacharjee, 9 December 2011, p. 1344) on the practices used by Saudi universities to boost their academic rankings. Just as with fellow astronomer Bob Kirschner, I received an e-mail out of the blue last June from someone I didn't know, offering me an adjunct professorship at King Abdulaziz University (KAU). Attached to the e-mail was a contract for a year, extendable for a second year.

Despite the strange way that the offer was made, I was enthusiastic initially. According to the e-mail, I was expected to visit Jeddah for 1 or 2 weeks in the year, "build up a research group (can be discussed later)," do 4 months of work for KAU, and add KAU as a second affiliation to my "ISIHighlyCited.com" Web page. The offer was extremely attractive financially. They would pay me $6000 per month for a year. In addition, they would provide me with a startup research grant of $80,000.

When I called the university to request more details, it became clear to me that the key reason for the offer was not a desire to strengthen my research field at KAU, but solely the fact that I happen to be included in ISIHighlyCited.com. This is a database that lists the 250 most-cited scientists for each of the 22 major subfields of science. Several Nobel prize–winning astronomers are not included, and I doubt whether Albert Einstein would ever have made it onto the list. Nevertheless, ISIHighlyCited.com is an important ingredient for the Shanghai Jiao Tong University rankings, regularly quoted by such publications as the Economist and Newsweek. The Shanghai rating is important reading for civil servants, ministers, philanthropists, and potential students throughout the world. It was clear to me that the new KAU adjunct professorship program is designed to boost the ranking of the university artificially by paying highly cited researchers to "sell" their affiliation.

I believe passionately that astronomy can be a unique tool for capacity building and global development. Hence, if I had thought that by accepting the KAU offer, I could have helped to build up astronomy in Jeddah or within Saudi Arabia, I would have welcomed the opportunity. Given the circumstances, I reluctantly felt compelled to decline the offer.

Three months later, in a quick browse through the astronomy/space sciences section of the ISI Highly Cited Web pages, I counted nine prominent astronomers newly affiliated to the KAU. This outnumbers ISI Highly Cited astronomers at the University of Cambridge in the UK by 50% and exceeds that of any European university.

I do not blame KAU or the Saudi authorities for setting up such a program. The problem is the ridiculous system of university rankings, which is exacerbated by the naivety of decision-makers who take these university rankings so seriously. The situation is extremely damaging for academia because the university ranking metrics are often used as the basis for policy-making and funding.

King Abdulaziz University.

University ranking tables can also be seen in a wider context—namely as part of the constant pressure to be accountable, to produce, and to be "the best in the world." The Saudi action illustrates the danger of fostering such a competitive, target-based approach in all walks of life. The distorting, sometimes counterproductive, effects of such a philosophy are obvious in areas as diverse as the targeted reduction of hospital waiting lists, published

CREDIT: AMMAR SHAKER/WIKIMEDIA COMMONS

rankings of schools, pressure on traffic wardens to dole out a specific number of parking tickets, and bonuses for bankers that sell large numbers of irresponsible mortgages.

We deceive ourselves by insisting that everything can be measured and quantified and that economic accountability should be the most important criterion driving society. How do you measure the cost-effectiveness of inspiring a young child with the excitement of the Universe? **GEORGE MILEY**

Department of Astronomy, Leiden Observatory, University of Leiden, Leiden, NL-2300 RA, Netherlands. E-mail: miley@strw.leidenuniv.nl

TECHNICAL COMMENT ABSTRACTS

Comment on "Phonemic Diversity Supports a Serial Founder Effect Model of Language Expansion from Africa"

T. Florian Jaeger, Daniel Pontillo, Peter Graff

Atkinson (Reports, 15 April 2011, p. 346) argues that the phonological complexity of languages reflects the loss of phonemic distinctions due to successive founder events during human migration (the serial founder hypothesis). Statistical simulations show that the type I error rate of Atkinson's analysis is hugely inflated. The data at best support only a weak interpretation of the serial founder hypothesis.

Full text at www.sciencemag.org/cgi/content/full/335/6072/1042-a

Response to Comment on "Phonemic Diversity Supports a Serial Founder Effect Model of Language Expansion from Africa"

Quentin D. Atkinson

Jaeger *et al.* use statistical simulations to show that the serial founder effect analysis I reported has an inflated type I error rate. Crucially, however, their simulations also reveal that the strength of the observed relationship between phonemic diversity and distance from Africa is unlikely to be due to chance, even accounting for multiple comparisons and geographic clustering of phonemic diversity.

Full text at www.sciencemag.org/cgi/content/full/335/6072/1042-b

CORRECTIONS AND CLARIFICATIONS

Reports: "Protein native-state stabilization by placing aromatic side chains in N-glycosylated reverse turns" by E. K. Culyba *et al.* (4 February 2011, p. 571). The authors inadvertently used the prejump equilibrium temperature to extract WW domain folding and unfolding rate information from the apparent rate constant data and in fitting the extracted folding rates as a function of temperature to Kramer's model. The postjump temperature differs by ~12°C. The corrected absolute folding and unfolding rates for each WW variant differ by less than twofold from those values reported originally. The corrected portion of Table 1 appears above. The beginning of the sixth sentence in the penultimate paragraph of the main text should read as follows: "Glycoprotein **g-WW-F**, **T** folds three times faster and unfolds at an indistinguishable rate relative to its nonglycosylated counterpart...." In the supporting online material, corrections have been made to table S3 and figs. S11 to S18. These changes do not affect the conclusions of the paper.

Protein	Sequence (30)	ΔG_f (kcal/mol)	$\Delta\Delta G_f$ (kcal/mol)	k_f (+glycan) / k_f (−glycan)	k_u (+glycan) / k_u (−glycan)
WW	–MSRSNGR–	−0.11 ± 0.05	0.26 ± 0.06	0.56 ± 0.05	0.8 ± 0.1
g-WW	–MSRS**N**GR–	0.15 ± 0.04			
WW-F	–MFRSNGR–	0.29 ± 0.04	0.07 ± 0.07	0.70 ± 0.07	0.8 ± 0.1
g-WW-F	–MFRS**N**GR–	0.36 ± 0.05			
WW-T	–MSRSNGT–	0.19 ± 0.06	0.08 ± 0.08	0.92 ± 0.07	1.0 ± 0.2
g-WW-T	–MSRS**N**GT–	0.28 ± 0.05			
WW-F,T	–MFRSNGT–	0.69 ± 0.05	−0.70 ± 0.08	3.0 ± 0.9	1.0 ± 0.3
g-WW-F,T	–MFRS**N**GT–	−0.01 ± 0.06			

Letters to the Editor

Letters (~300 words) discuss material published in *Science* in the past 3 months or matters of general interest. Letters are not acknowledged upon receipt. Whether published in full or in part, Letters are subject to editing for clarity and space. Letters submitted, published, or posted elsewhere, in print or online, will be disqualified. To submit a Letter, go to www.submit2science.org.

Comment on "Phonemic Diversity Supports a Serial Founder Effect Model of Language Expansion from Africa"

T. Florian Jaeger,[1,2]* Daniel Pontillo,[1] Peter Graff[3]

Atkinson (Reports, 15 April 2011, p. 346) argues that the phonological complexity of languages reflects the loss of phonemic distinctions due to successive founder events during human migration (the serial founder hypothesis). Statistical simulations show that the type I error rate of Atkinson's analysis is hugely inflated. The data at best support only a weak interpretation of the serial founder hypothesis.

Atkinson (*1*) presents evidence for the serial founder hypothesis that the sound structures of languages across the globe reflect a succession of founder events throughout human migration. Based on the hypothesis that "phoneme distinctions are more likely to be lost in small founder populations," Atkinson derives the prediction that the number of different sounds distinguished in a language (its phonemic diversity) should decrease with increasing migration distance to the geographical origin of language.

Because the point of origin of language is unknown, Atkinson pursues the search for the origin and the test of the serial founder hypothesis jointly. For 504 nonextinct languages from (*2*–*5*), he calculates the "total normalized phoneme diversity" as a standardized measure of each language's phonological complexity [see our supporting online material (SOM), section 1]. To test the serial founder hypothesis while simultaneously controlling for a previously documented population size effect (*6*), as well as nonindependence between languages due to genetic relations, he employs linear mixed models. Specifically, phonemic diversity is modeled as a linear combination of (log-transformed) population size, migration distance to the hypothesized point of origin, and the interaction of these two variables, while adjusting for genetic relations between languages (random intercepts for language family, subfamily, and genus) (SOM, section 2).

To determine the most probable point of origin, separate linear mixed regressions are fit for each of 2560 coordinates on the globe corresponding to known locations of extinct or nonextinct languages (*2*). Atkinson finds that the best model fits are obtained for coordinates in southwest Africa. His result is replicated in Fig. 1A, obtained using the same methods as in (*1*) but based on an updated database with 2677 language coordinates (*2*) [see figure 2A in (*1*)]. Atkinson then reports the best-fitting model, which exhibits the predicted negative correlation between phonemic diversity and migration distance to the origin ($P < 0.00003$). This highly significant effect in the predicted direction, together with the clustering of likely origins in southwest Africa, seems to lend strong support for the serial founder hypothesis.

However, as we show below, Atkinson's analysis suffers from a severely inflated type I error rate due to repeated tests on the same data. In three statistical simulations, we find that Atkinson's results only support a weak interpretation of the serial founder hypothesis.

Simulation 1 (SOM, section 4.1) randomly reassigned the 504 languages to language coordinates within language families (the top-level grouping structure reflecting genetic relationships between languages). For example, languages from the Niger-Congo family were randomly reassigned to coordinates of languages from the Niger-Congo family. For each of 10,000 simulation samples, we determined the best fit out of the 2677 possible origins, following the same procedure applied to the original data by Atkinson. The predicted significant negative effect of migration distance on phonemic diversity is found in 100% of the 10,000 random simulation samples. Even effects as strong as those observed by Atkinson are found in 9.8% of our simulation samples. As in the original analysis, all best-fit origins lie in southwest Africa (Fig. 1B). Moreover, for each individual fit, the same clustering of likely origins as in the original data is observed (fig. S3). This shows that, contrary to a literal interpretation of the serial founder hypothesis, the effect observed by Atkinson is independent of the distance of individual languages to the origin. As long as the centers of language families order geographically as in the original sample, the predicted effect is obtained. This result is, however, compatible with a weaker hypothesis: The effect of repeated founding events might only be detectable if aggregated over long periods of time. In that case, the effect is only expected to be visible at the family level (i.e., on data aggregated over language families), which is observed in simulation 1.

To assess how likely it is that the effect at the family level is due to chance, simulation 2 (SOM, section 4.2) employed a hierarchical sampling procedure: For each simulation sample, language families were randomly reassigned to coordinates around the globe, and languages were randomly reassigned conditionally on the geographical center of their language family (languages in the same family have a strong tendency to cluster geographically). We found the effect of migration distance in the predicted direction for 20.7% of 10,000 samples. This type I error rate is substantially higher than the conventionally accepted 5%. Unsurprisingly, the most probable origins in simulation 2 were more uniformly distributed around the globe than in simulation 1, although, interestingly, the highest proportion of likely origins was again found in Africa (Fig. 1C). This suggests that coordinates in Africa are a priori more likely to be associated with better fits, not because of the origin and direction of human migration but because of any or all of the following: (i) properties of the *World Atlas of Language Structures* data employed by Atkinson (*2*–*5*), such as the distribution of language coordinates across the globe; (ii) the fact that genetically related languages (which tend to share linguistic properties, including phonemic diversity) tend to cluster geographically; (iii) the geography of the globe; and (iv) the constraint that intercontinental migration routes have to pass through the five waypoints shown in Fig. 1A. Simulation 3 (SOM, section 4.3) further suggests that geographic clustering of most probable origins is obtained even in the absence of (ii), although not necessarily in Africa.

Despite the inflated type I error rates, simulation 2 finds support for the weak interpretation of the serial founder hypothesis: Effect sizes as large as or larger than those reported by Atkinson are observed in only 0.11% of all simulation samples. Although the resulting estimate for an adjusted significance level of the distance effect is two orders of magnitude larger (less significant) than the P value reported by Atkinson, it is still significant ($P < 0.002$). As detailed in the SOM (section 5), this estimate should be taken to be a lower bound (i.e., a best-case scenario for Atkinson).

In conclusion, the literal interpretation of Atkinson's serial founder hypothesis is not supported by Atkinson's data. The data are, however, compatible with a weaker interpretation of the serial founder hypothesis, although it is unclear whether the effect would remain significant under more realistic simulations. There is, nonetheless, reason to be optimistic about the prospect of future evaluations of the serial founder hypothesis: The approach taken here could be used to determine what type of data would be needed

[1]Brain and Cognitive Science, University of Rochester, Meliora Hall, Box 270268, Rochester, NY 14627–0268, USA. [2]Computer Science, University of Rochester, Box 270226, Rochester, NY 14627–0226, USA. [3]Department of Linguistics and Philosophy, Massachusetts Institute of Technology, 77 Massachusetts Avenue, Building 32-D808, Cambridge, MA 02139, USA.

*To whom correspondence should be addressed. E-mail: fjaeger@bcs.rochester.edu

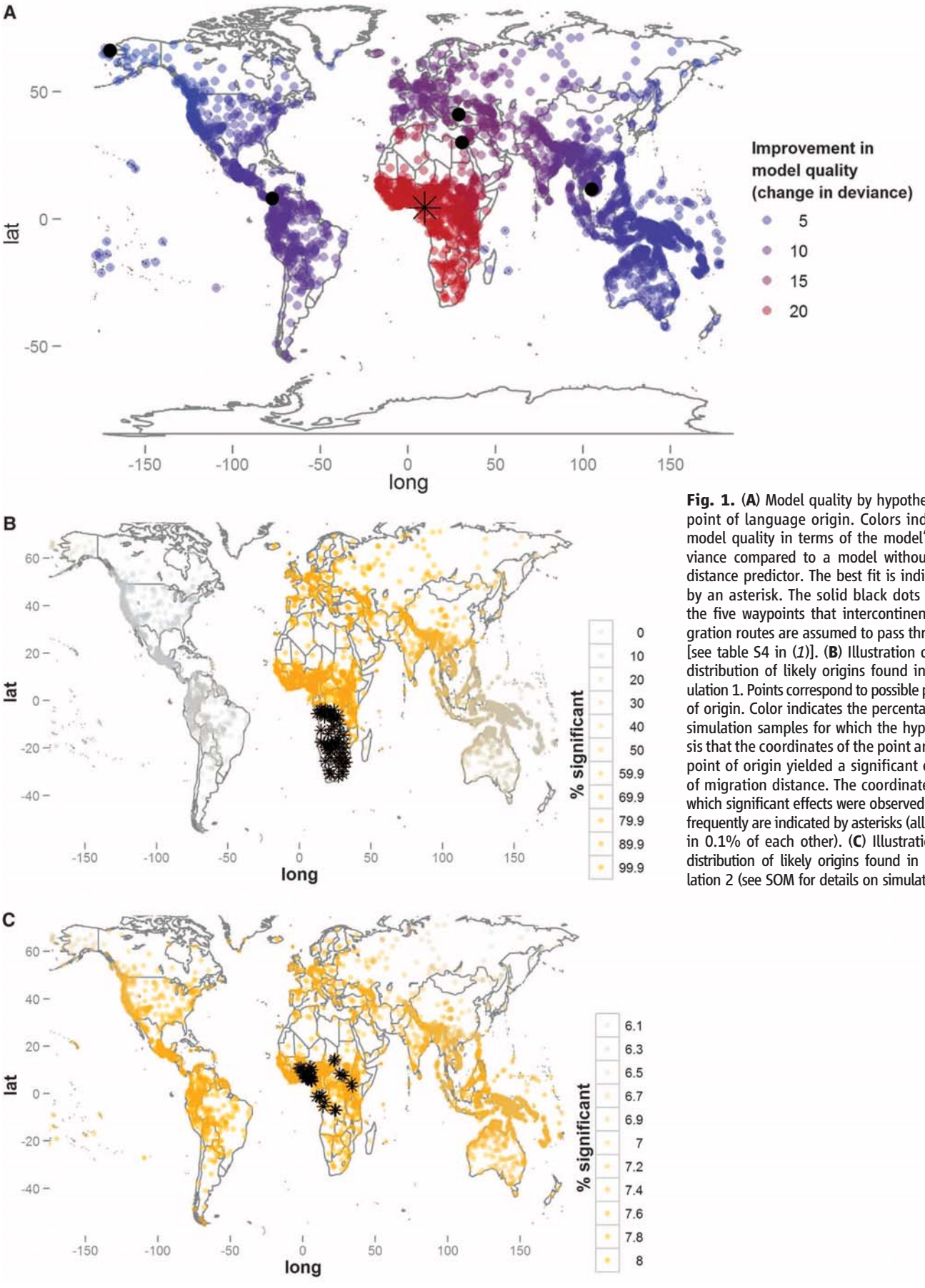

Fig. 1. (**A**) Model quality by hypothesized point of language origin. Colors indicate model quality in terms of the model's deviance compared to a model without the distance predictor. The best fit is indicated by an asterisk. The solid black dots mark the five waypoints that intercontinent migration routes are assumed to pass through [see table S4 in (*1*)]. (**B**) Illustration of the distribution of likely origins found in simulation 1. Points correspond to possible points of origin. Color indicates the percentage of simulation samples for which the hypothesis that the coordinates of the point are the point of origin yielded a significant effect of migration distance. The coordinates for which significant effects were observed most frequently are indicated by asterisks (all within 0.1% of each other). (**C**) Illustration of distribution of likely origins found in simulation 2 (see SOM for details on simulations).

to convincingly test the serial founder hypothesis. For example, simulations could determine how many language families with how many languages are required. Similarly, simulations could shed light on the question from which geographical regions more language data are most urgently needed to answer questions about the origin of language.

References and Notes

1. Q. D. Atkinson, *Science* **332**, 346 (2011).
2. M. Haspelmath, M. S. Dryer, D. Gil, B. Comrie, *The World Atlas of Language Structures Online* (Max Planck Digital Library, Munich, 2008).
3. I. Maddieson, in *The World Atlas of Language Structures Online*, M. Haspelmath, M. S. Dryer, D. Gil, B. Comrie, Eds. (Max Planck Digital Library, Munich, 2008), pp. 14–17.
4. I. Maddieson, in *The World Atlas of Language Structures Online*, M. Haspelmath, M. S. Dryer, D. Gil, B. Comrie, Eds. (Max Planck Digital Library, Munich, 2008), pp. 10–13.
5. I. Maddieson, in *The World Atlas of Language Structures Online*, M. Haspelmath, M. S. Dryer, D. Gil, B. Comrie, Eds. (Max Planck Digital Library, Munich, 2008), pp. 58–61.
6. J. Hay, L. Bauer, *Language* **83**, 388 (2007).

Acknowledgments: We are very grateful to Q. D. Atkinson for generously sharing his data with us and answering our questions about the analyses he conducted. The work presented here was partially supported by an Alfred P. Sloan Research Fellowship and the University of Rochester's Wilmot Award to T.F.J.

Supporting Online Material

www.sciencemag.org/cgi/content/full/335/6072/1042-a/DC1
Materials and Methods
SOM Text
Figs. S1 to S9
Table S1
References

11 October 2011; accepted 23 January 2012
10.1126/science.1215107

Response to Comment on "Phonemic Diversity Supports a Serial Founder Effect Model of Language Expansion from Africa"

Quentin D. Atkinson[1,2]*

Jaeger *et al.* use statistical simulations to show that the serial founder effect analysis I reported has an inflated type 1 error rate. Crucially, however, their simulations also reveal that the strength of the observed relationship between phonemic diversity and distance from Africa is unlikely to be due to chance, even accounting for multiple comparisons and geographic clustering of phonemic diversity.

I hypothesized that phoneme inventory size is subject to a serial founder effect like that observed in population genetics (*1*). I show that global variation in phonemic diversity is clinal and, like our genetic diversity, fits a serial founder effect model of expansion from Africa. Although there is reason for caution when interpreting any such correlational finding, I show in the paper that this result is robust in the face of alternative explanations, including the impact of geographic variation in modern demography (speaker population size, area, and density), language density, postglacial expansion, and statistical nonindependence due to relatedness between languages.

In their commentary, Jaeger *et al.* (*2*) raise a further concern. They use a range of statistical simulations to evaluate the type 1 error rate of a serial founder effect analysis like the one I report. Although they find an inflated type 1 error rate, Jaeger *et al.*'s simulations also elegantly demonstrate that a relationship between phonemic diversity and distance from Africa as strong as that observed in the real data is unlikely to be due to chance.

Jaeger *et al.* report the results of three simulations using different methods to randomly or semirandomly reassign languages to locations around the globe. The logic behind this approach is that if language locations are shuffled around the globe, a serial founder effect analysis should only infer a significant geographic cline in ~5% of samples (the standard type 1 error rate), because any global geographic patterning in the data should have been removed by the location reassignment.

Simulation 1 randomly assigns language locations within language families. This is an unusual approach to testing for type 1 error, because the test being conducted is on a global sample of languages and the simulated data preserves the global pattern of diversity between families. Detecting a global effect of distance from the origin in this case is not a type I error, and all such simulations still show the significant effect of distance from Africa preserved across language families.

Simulations 2 and 3 are more useful for assessing type 1 error rates. In simulation 3, languages are simply randomly shuffled around the globe, whereas simulation 2 shuffles language locations with the constraint that sets of related languages (the recognized language families) should cluster together in a manner similar to the clustering we observe in the real data (*2*). Using a random sample of 1000 of these simulated data sets (*3*), a serial founder effect analysis finds a significant global decline in phonemic diversity with distance from origin in between 15% (simulation 3) and 20% (simulation 2) of samples, suggesting an inflated type 1 error rate when searching for a clinal pattern from anywhere on the globe. Many of these cases would not, however, have constituted clear support for a serial founder effect, because for the simulated data the strongest relationship with distance from all putative origins often shows a positive slope, contrary to the predictions of the model. Removing these cases leaves 18% (simulation 2) and 12% (simulation 3) of the samples. Between 1.5% (simulation 3) and 2.5% (simulation 2) meet these criteria and show the strongest relationship with distance from a putative origin in Africa—that is, the simulations imply that between 1.5% and 2.5% of the time, we would find support for a significant cline from Africa by chance.

What we really want to know, however, is the probability of finding an effect of distance from any origin by chance that is at least as large as the effect we observe in the real data. The Dunn-Šidák correction for significance offered by Jaeger *et al.* is inappropriate because the tests being conducted are not independent. However, Jaeger *et al.*'s simulations allow us to answer the question. Among the sample data sets run under both simulation 2 and simulation 3 (and a further simulation with increased geographic clustering reported in their supporting online material), between 0.2% and 0.5% show a relationship with distance from any of the 2667 possible origins that is as strong as the relationship we observe between distance from Africa and the actual global distribution of phonemic diversity. Jaeger *et al.*'s simulations therefore demonstrate that despite inflated type 1 error rates, the pattern we observe in the data is unlikely to have occurred by chance ($P < 0.005$), even accounting for the multiple comparisons being made and the geographic clustering of families with similar phonemic inventories.

Jaeger *et al.*'s work shows the utility of simulation-based approaches to significance testing and suggests that caution is needed when interpreting the results of serial founder analyses. The type 1 error rates inferred here are specific to this data set and do not necessarily apply to other applications of a serial founder analysis, but it would be interesting to test their generality.

[1]Department of Psychology, University of Auckland, Private Bag 92019, Auckland 1142, New Zealand. [2]Institute of Cognitive and Evolutionary Anthropology, University of Oxford, 64 Banbury Road, Oxford OX2 6PN, UK.

*E-mail: q.atkinson@auckland.ac.nz

References and Notes

1. Q. D. Atkinson, *Science* **332**, 346 (2011).
2. T. F. Jaeger, D. Pontillo, P. Graff, *Science* **335**, 1042 (2012); www.sciencemag.org/cgi/content/full/335/6072/1042-a.
3. Data provided by Jaeger *et al*.

2 November 2011; accepted 23 January 2012
10.1126/science.1215788

EVOLUTION

Contemplating Some Big Shifts

Douglas H. Erwin

Early in John Maynard Smith and Eörs Szathmáry's 1995 book *The Major Transitions in Evolution* (*1*), the authors discuss why the origin of ecosystems is not included among their major evolutionary transitions: e.g., the origins of chromosomes, eukaryotes, sex, multicellular organisms, and social groups. Because ecosystems are not individuals, and hence cannot be units of selection, and moreover are essentially eternal rather than being "a final stage in a series," Maynard Smith and Szathmáry argue that they do not represent major evolutionary transitions. Despite the considerable and well-justified influence of the book, this emphasis on the evolution of information transmission has always made the authors' discussion seem incomplete. The enumerated transitions were doubtless critical events in the history of life, but without the evolution of various systems of metabolism (particularly oxygenic photosynthesis), none of the rest would have occurred. Similarly, while the origins of eukaryotes and sex involved the generation of new evolutionary entities—and may have required resolving conflicts between selection among, for example, symbionts within a eukaryotic cell and the cell itself—the eukaryotic cell also created new realms of adaptive space and evolutionary opportunities.

Maynard Smith and Szathmáry's book was very influential, shaping debates among biologists, philosophers, and others interested in the ongoing controversy over levels of selection and the nature of evolutionary individuals. Nonetheless, the debate has always seemed incomplete to those of us concerned about the ecological and environmental facets of these major evolutionary transitions: How did the changing redox of oceans and atmosphere during the Proterozoic influence the expansion of eukaryotes, for example, once they had evolved? What ecological and evolutionary factors account for the success of many social species? The origin of a new trait is one thing; its success in the evolutionary play is quite another.

The Major Transitions in Evolution Revisited

Brett Calcott and Kim Sterelny, Eds.

MIT Press, Cambridge, MA, 2011. 329 pp. $50, £34.95. ISBN 9780262015240. The Vienna Series in Theoretical Biology.

Many of the issues raised by Maynard Smith and Szathmáry have been the subject of considerable study, and controversy, since 1995. Brett Calcott and Kim Sterelny's *The Major Transitions in Evolution Revisited*, generated from a workshop at the Konrad Lorenz Institute for Evolution and Cognition Research in Vienna, summarizes and extends many of these debates, ably addressing evolutionary transitions in information as well as major evolutionary transitions in the broader sense. Thus the importance of mediating conflict between evolutionary individuals at different levels within a hierarchy has been a central issue in the debates, and Richard Michod discusses his considerable work using *Volvox* to study conflict, cooperation, and conflict mediation. A very different perspective is provided by Ellen Clarke as she brings plants into the discussion and argues that the emphasis on conflict may have been excessive. She suggests that at least theoretically, selection at different levels may be reinforcing rather than conflicting, although empirical evidence remains scant. This issue of conflict and individuality is a thread that ties together a number of both philosophical and more empirical contributions to this volume. There have clearly been considerable conceptual advances, sharpening, for example, the differences among the transitions that Maynard Smith and Szathmáry lumped together and clarifying the distinction between increases in complexity and levels of selection (see particularly the chapter by Daniel McShea and Carl Simpson). Still, many questions remain unresolved. Nor is it clear why the volume is restricted to Maynard Smith and Szathmáry's list of major transitions and does not also examine some others.

The ecological and environmental contexts of major evolutionary transitions are addressed primarily by Andrew Knoll and David Hewitt in their chapter, although they are acknowledged by several other authors. Focusing largely on the evolution of complex multicellularity during the Proterozoic, Knoll and Hewitt set aside issues of conflict and cooperation to consider the importance of active transport mechanisms for oxygen, nutrients, and other molecules. In their view, changes in the physical environment have constructed environments in which new evolutionary trends can prosper. But in some cases these changes in the physical environment were themselves the consequence of biotically driven change, creating interesting feedback loops that have yet to be fully explored.

By far the most interesting issue raised in the volume is the implications these major transitions have for understanding how evolutionary processes have themselves evolved. Regrettably, this topic is developed only by Calcott and Sterelny in their introduction and by Peter Godfrey-Smith and Sterelny in their chapters. As Sterelny observes, novelties that expand evolutionary possibility have arisen repeatedly throughout the history of life on Earth, but their success at surviving and spreading has differed considerably. More fully developing this line of research will be a fitting tribute to Maynard Smith and Szathmáry and the questions they initiated.

References

1. J. Maynard Smith, E. Szathmáry, *The Major Transitions in Evolution* (W. H. Freeman, Oxford, 1995).

10.1126/science.1217603

CREDIT: XVAZQUEZ/WIKIMEDIA COMMONS

After a major transition. *Grypania*, the earliest putative eukaryotic macrofossil, occurs in rocks around 2 billion years old.

The reviewer is at the Department of Paleobiology, National Museum of Natural History, Washington, DC 20013–7012, USA, and Santa Fe Institute, 1399 Hyde Park Road, Santa Fe, NM 87501, USA. E-mail: erwind@si.edu

Published by AAAS

HISTORY OF SCIENCE

Influenced by Caste and Gender

Asha Gopinathan

In *Dispersed Radiance*, Abha Sur examines the interactions among caste, gender, nationalism, and science in early-20th-century India. Sur (a historian of science at Massachusetts Institute of Technology) focuses on the contrasting lives of Nobel laureate C. V. Raman and the distinguished astrophysicist Meghnad Saha.

Saha, nominated for the Nobel Prize four times, was born in East Bengal (now Bangladesh) in 1893 to the family of a lower-caste village grocer. The first in his family to attain higher education, he proved a brilliant student and was soon appointed a lecturer. He published many papers integrating atomic physics and thermodynamics and was elected a Fellow of the Royal Society in 1927. He later turned his attention to nuclear physics and in 1950 set up the Institute of Nuclear Physics in Kolkata.

Groundbreakers. Meghnad Saha (sitting, left) was among the scientists of the early-20th-century Bengal Renaissance.

C. V. Raman was born in 1888 in a small village in Tamil Nadu to an upper-caste brahmin family. His father was a lecturer in physics and mathematics at Presidency College (Chennai, formerly Madras), which Raman entered at age 13. At 19, he earned a master's degree in physics and published a paper in *Philosophical Magazine*. Because research careers were at the time reserved mainly for the British, he wound up as an accountant in the Financial Civil Service based in Kolkata. However, working mornings and evenings in the laboratories of the Indian Association for the Cultivation of Science, he published extensively, including a few papers in *Nature*. A professorship in physics at the University of Calcutta followed. Elected to the Royal Society in 1924, he won the 1930 Nobel Prize in Physics for his work on the scattering of light. After a turbulent time as director of the Indian Institute of Science (IISc) in Bangalore (1933–1937), he continued as a professor there until 1948, when he established the Raman Research Institute.

Dispersed Radiance
Caste, Gender, and Modern Science in India
by Abha Sur
Navayana Press, New Delhi, 2011. 286 pp. Rs 495, $26.75. ISBN 9788189059323.

Forced out of the college hostel in Kolkata due to his caste background, Saha opposed separate housing for students from different communities. Sur argues that his social beliefs percolated into his scientific theories—for example, leading him to conclude that physical stimuli "do not act preferentially on atoms; rather, it is the atoms that interact selectively with the stimulus." In his scientific writings, he was cautious, attentive to experimental details, and always acknowledged the support of his students. Furthermore, he sought a level playing field for all castes and classes. Saha's engagement with these issues led him to edit *Science and Culture* and enter the Lok Sabha (the lower house of the Indian Parliament). He believed that massive industrialization and science would eventually solve all the problems of independent India. Nonetheless, he was systematically excluded from heading many important committees, including the Atomic Research Committee.

Although Raman also supported the nationalist cause, he did not participate in any protests or Gandhi's noncooperation movement; "he would not allow its more turbulent and chaotic manifestations to interfere with his science." Discussing Raman and his science, Sur examines the Born-Raman controversy in lattice dynamics. Whereas Born's theory predicted a quasi-continuous spectrum, results from Raman's experimental group emphasized a discrete structure. Raman reorganized his lab so that in the 1940s every member was working on validating his dynamic theory of lattice vibrations. Exhibiting a profound reluctance to engage with contrary evidence, Raman promoted his theories in increasingly repetitive papers in his own journal. Sur comments, "The interaction of brahminic culture, where privilege is ascribed by birth, with the precarious status accorded to indigenous scientists in British India created a culture of arrogant assertiveness." She highlights this controversy to bring forth Raman's control over science and scientific knowledge in his lab, the Indian Academy of Sciences, and its journals. All the same, as IISc director, Raman gave Born, a Jewish refugee scientist, a place to work in his institute.

When it came to issues of gender, both Saha and Raman were "quintessential patriarchs." While Saha's daughter felt that he became more open to ideas about gender as he grew more influenced by the politics of the left, the book doesn't reveal whether he ever had women students. Raman cautiously took a few, including Lalitha Chandrasekhar, Sunanda Bai, and Anna Mani. But, believing it scandalous for male and female students to even walk together, he maintained a strict separation of the sexes in his laboratory. As a result, the women students were very isolated from their peers. They were generally given work of a repetitive, descriptive nature. Despite publishing extensively, neither Mani nor Bai were awarded their Ph.D. Mani rose to deputy director general of the Indian Meteorological Department, later worked at the Raman Research Institute, and still later established a factory to manufacture instruments to measure wind speed and solar energy. Bai committed suicide in 1944, on the eve of her departure for postdoctoral studies in Sweden. Raman never again accepted women students. Sur concludes that women's survival in science demanded from them "social conformity and conservatism."

Although Sur bases *Dispersed Radiance* on primary sources wherever possible, she found access to personal papers and laboratory notebooks difficult (especially in the case of Raman). Hence she also turned to books, articles, and extensive interviews. From her sources she has woven a meticulous account of the subaltern history of physics in India during the first half of the 20th century.

The reviewer is at the Department of Neurology, Sree Chitra Tirunal Institute for Medical Sciences and Technology, Thiruvananthapuram 695011, Kerala, India. E-mail: dendron.15@gmail.com

10.1126/science.1218918

CONSERVATION

Reconsidering the Consequences of Selective Fisheries

Balanced fishing across a range of species, stocks, and sizes could mitigate adverse effects and address food security better than increased selectivity.

S. M. Garcia,[1*] J. Kolding,[1,2*] J. Rice,[1,3*] M.-J. Rochet,[4*†] S. Zhou,[5*] T. Arimoto,[6] J. E. Beyer,[7] L. Borges,[8] A. Bundy,[9] D. Dunn,[10] E. A. Fulton,[11] M. Hall,[12] M. Heino,[2,13,14] R. Law,[15] M. Makino,[1,16] A. D. Rijnsdorp,[17] F. Simard,[18] A. D. M. Smith[11]

Concern about the impact of fishing on ecosystems and fisheries production is increasing (*1*, *2*). Strategies to reduce these impacts while addressing the growing need for food security (*3*) include increasing selectivity (*1*, *2*): capturing species, sexes, and sizes in proportions that differ from their occurrence in the ecosystem. Increasing evidence suggests that more selective fishing neither maximizes production nor minimizes impacts (*4*–*7*). Balanced harvesting would more effectively mitigate adverse ecological effects of fishing while supporting sustainable fisheries. This strategy, which challenges present management paradigms, distributes a moderate mortality from fishing across the widest possible range of species, stocks, and sizes in an ecosystem, in proportion to their natural productivity (*8*), so that the relative size and species composition is maintained.

Selectivity: Rationale, Undesirable Effects

Fishers select species and sizes for various practical, economic, and regulatory reasons. The idea of increasing size-selectivity to increase yields is centuries old (*9*). The concept of growth overfishing (loss of yield when small fish are caught) has been a cornerstone of modern fisheries management since the 1950s (*10*). Avoiding juveniles has been justified to let fish reproduce at least once before they are harvested (*11*). Protecting rare and charismatic species has also gained currency (*12*). New guidelines from the United Nations Food and Agriculture Organization (FAO) reiterate the objective of "minimizing the capture and mortality of species and sizes which are not going to be used," i.e., by-catch (*13*). Fisheries worldwide have used species and size limits (*9*, *14*), gear technology (*5*, *15*), and spatial and temporal fishing restrictions (*16*) to reduce fishing impacts while pursuing human benefits.

But selective removals will inevitably alter the composition of a population or community and, consequently, ecosystem structure and biodiversity. Old individuals contribute the most to reproduction (*17*). Even moderate fishing reduces the proportion of large and old fish in a population. Selectively fishing large individuals amplifies this effect, and although it does not provide the expected yield benefits (*9*), it results in ecological and evolutionary side effects. Removal of older age classes can increase fluctuations in population abundance (*18*), which, in turn, increase the risks associated with low abundance. Increased and selective fishing has been predicted to drive stocks toward earlier maturation and smaller adult body size (*19*). Such changes appear common (*20*), although their environmental and genetic causes are not fully disentangled (*21*).

Community effects of heavy, selective exploitation include alteration of trophic structure on the Eastern Scotian Shelf (*6*), and a shift from large- to smaller-sized species and individuals in the North Sea (*22*) (fig. S1). By contrast, in several African small-scale inland fisheries, the fish size spectrum (*23*) has been maintained under intense and diverse fishing activities that cause high mortality with low selectivity (*5*, *24*) (fig. S1).

Results from models suggest that moderating fishing mortality across a wide range of species and sizes maximizes overall catch summed across species while better conserving biodiversity. Multispecies fishery models show that increased mesh sizes may reduce total yield, owing to increased predation by large fish (*25*), and that targeting a limited range of species or sizes will not maximize diversity at most fishing mortalities (*26*). In size-based models, depletion of particular sizes by fishing affects smaller-size groups because their predation mortality is reduced and impinges on larger-size groups by both reduced food for predators of the harvested sizes and faster growth rates of the survivors of the selective fishing. This causes destabilizing fluctuations in biomass that are wider when the size range fished is narrower and/or the sizes fished are large (*27*). When models allow for some diversity in properties other than size within size classes, fluctuations persist but are dampened (*28*).

Balanced harvesting … distributes a moderate mortality from fishing across the widest possible range of species, stocks, and sizes in an ecosystem.

Synthesizing across ecosystem models from 30 systems [see supporting online material (SOM) for details] suggests that the biodiversity benefits from selective fishing occur only at fishing mortalities so low that yield is not economically sustainable (see the graph). With fishing spread over more groups and sizes, yields are higher and impacts of fishing—such as population extirpations (local extinctions) and biomass depletion—are lower across a broad range of fishing mortalities.

[1]Commission on Ecosystem Management, International Union for Conservation of Nature (IUCN-CEM), Fisheries Expert Group, 1000 Brussels, Belgium. [2]Department of Biology, University of Bergen, 5020 Bergen, Norway. [3]Fisheries and Oceans, Ottawa, Ontario K1A OE6, Canada. [4]L'Institut Francais de Recherche pour l'Exploitation de la Mer (IFREMER), 44300 Nantes, France. [5]CSIRO Marine and Atmospheric Research, Brisbane, Queensland 4001, Australia. [6]Tokyo University of Marine Science and Technology, Tokyo 108-8477, Japan. [7]Danish National Institute of Aquatic Resources (DTU Aqua), Charlottenlund Castle, 2920, Denmark. [8]FishFix, Brussels, Belgium. [9]Bedford Institute of Oceanography, Dartmouth, Nova Scotia B3B 1A5, Canada. [10]Duke University Marine Geospatial Ecology Lab, Beaufort, NC 28516, USA. [11]CSIRO Marine and Atmospheric Research, Hobart, Tasmania 7000, Australia. [12]Inter-American Tropical Tuna Commission, La Jolla, CA 92037, USA. [13]Institute of Marine Research, 5005 Bergen, Norway. [14]International Institute for Applied Systems Analysis, 2361 Laxenburg, Austria. [15]Biology Department, University of York, York YO10 5DD, UK. [16]Fisheries Research Agency, Yokohama, 220-6115, Japan. [17]Institute for Marine Resources and Ecosystem Studies (IMARES), 1976 IJmuiden, Netherlands. [18]Global Marine Programme, IUCN, 1196 Gland, Switzerland.

*These authors contributed equally to this work. †Author for correspondence. E-mail: Marie.Joelle.Rochet@ifremer.fr

Published by AAAS

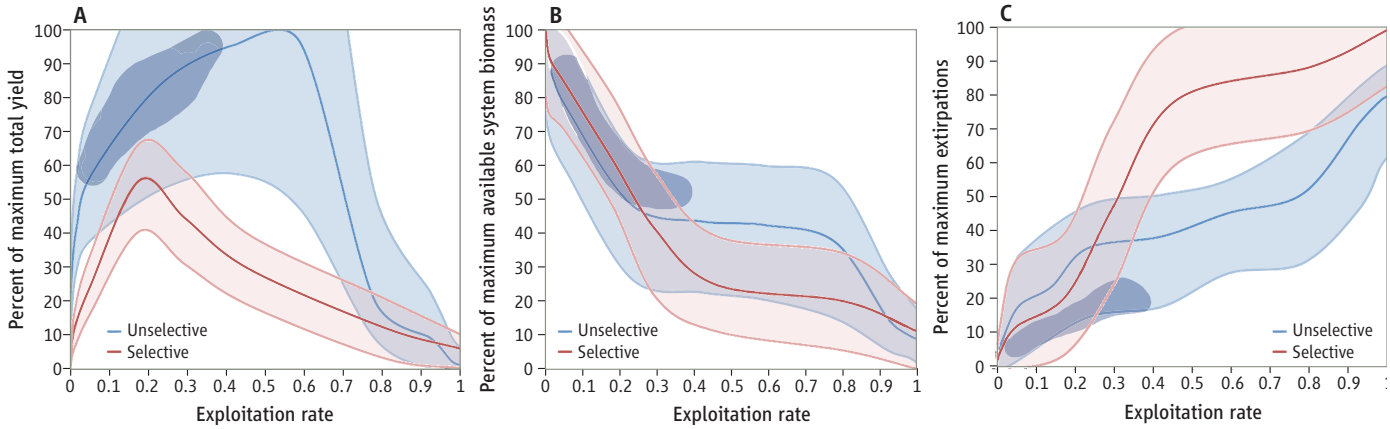

Effects of conventionally selective (red), unselective (blue), and balanced (dark blue) fishing. Unselective fishing harvests all exploitable nonmicrofauna and nonlarval ecosystem components. Balanced fishing mortality rates are set in proportion to productivity per biomass for each group. (**Left**) Results for total catch weight (as a percentage of the maximum total yield for a system across all fishing scenarios), (**middle**) total available biomass (i.e., biomass that could be harvested), and (**right**) extirpations (number of groups that have dropped below 10% of their unfished levels). All values are plotted against the maximum system level exploitation rate (i.e., roughly total catch as a proportion of total available biomass). For each fishing type (conventionally selective or unselective), the solid line is the average across 36 ecosystem models, and the lower and upper bounds of the lightly shaded areas represent the 5th and 95th percentiles across models. The darker blue shaded areas encompass >90% of the balanced harvest scenarios across the ecosystems. See SOM for details; the selective fishing results were part of supplementary fig. S1 in (*2*).

Toward Balanced Harvesting

The conventional "increased selectivity" paradigm may be inconsistent with objectives of an approach that considers all ecosystem consequences while managing fisheries. Balanced harvest is selective, but it broadens the selectivity perspective from scales of fishing operations and stocks to the integrated scale of ecosystem productivity and impacts.

Conventionally selective removal of parts of the ecosystem leads to unintended consequences that are inconsistent with a range of international conventions and agreements, including the international commitment to rebuild world fish stocks to their maximum sustainable yield (MSY) (*29*, *30*). It is increasingly recognized that all stocks within an ecosystem cannot be rebuilt to biomasses consistent with their single-species MSY levels (*31*). If the focus is on how much to fish as calculated from reducing fishing mortality (*1*, *2*), MSY's dependence on what type of fishing is done—size-selectivity within stocks and species-selectivity at the community level (*32*)—is overlooked. Balanced harvesting requires adjusting selectivity regulations to balance the impact of all fisheries in an area with the relative productivities of the species and sizes of fish in the ecosystem; MSYs are subject to that constraint.

Regulations in many jurisdictions promote selectivity as an intended outcome, e.g., by using mesh-size limits. Our results suggest that such regulations often will be inconsistent with goals to maintain biodiversity as well as fish yield. Implementing balanced harvesting requires coordinated management across multiple fisheries with consideration of ecosystem structure, consequences of current fishing selectivity, and implications for future yields. This involves quantifying patterns of fishing activities and ecological consequences aggregated at the fish-community and ecosystem levels.

We propose that fisheries management should address community properties such as the size-spectrum slope, for which acceptable levels would be agreed (*33*, *34*). Ecosystem modeling could help in determining appropriate patterns of fishing mortality and selectivity to conserve these properties, and constraints on removals (including discards), not just landings. Perhaps the greatest changes required for a balanced harvesting approach concern by-catch and markets. As each ecosystem component is to be caught in appropriate amounts, by-catch ceases to be an operational nuisance to be minimized and becomes part of the management strategy. Markets and the processing sector will need incentives to accommodate a wider range of catch components, including many not currently utilized in Western countries but commonly used in multispecies, multigear fisheries (*5*, *35*) in the Mediterranean, Asia, and the Southern Hemisphere: for example, (i) enhancing industrial processing for animal feed or human consumption (*36*), (ii) status change from by-catch to target (*14*), and (iii) consuming less-utilized fish species (*37*).

Issues regarding the potential benefits and implementation of balanced harvesting remain. However, consideration of food security and minimizing ecosystem impacts suggest that the time has come to take action.

References and Notes

1. E. K. Pikitch *et al.*, *Science* **305**, 346 (2004).
2. B. Worm *et al.*, *Science* **325**, 578 (2009).
3. S. M. Garcia, A. A. Rosenberg, *Philos. Trans. R. Soc. London Ser. B* **365**, 2869 (2010).
4. S. M. Garcia *et al.*, Selective fishing and balanced harvest in relation to fisheries and ecosystem sustainability: Report of a scientific workshop in Nagoya, Japan, 14 to 16 October 2010 (IUCN and European Bureau for Conservation and Development, Gland, Switzerland, and Brussels, 2011); http://data.iucn.org/dbtw-wpd/edocs/2011-001.pdf.
5. O. A. Misund, J. Kolding, P. Fréon, in *Handbook of Fish Biology and Fisheries*, vol. 2, *Fisheries* P. J. B. Hart, J. D. Reynolds, Eds. (Blackwell, Malden, MA, 2002), pp. 13–36.
6. A. Bundy, P. Fanning, K. C. T. Zwanenburg, *ICES J. Mar. Sci.* **62**, 503 (2005).
7. S. Zhou *et al.*, *Proc. Natl. Acad. Sci. U.S.A.* **107**, 9485 (2010).
8. Biological productivity is the amount of new organic matter produced per biomass unit during a given period of time.
9. R. G. Halliday, A. T. Pinhorn, *Fish. Res.* **57**, 211 (2002).
10. R. J. H. Beverton, S. J. Holt, On the dynamics of exploited fish populations, Fishery Investigations, Series 2 (Her Majesty's Stationery Office, London, 1957).
11. M. P. Sissenwine, J. G. Shepherd, *Can. J. Fish. Aquat. Sci.* **44**, 913 (1987).
12. R. L. Lewison, L. B. Crowder, A. J. Read, S. A. Freeman, *Trends Ecol. Evol.* **19**, 598 (2004).
13. FAO, Report of the technical consultation to develop international guidelines on by-catch management and reduction of discards, Rome, 6 to 10 December 2010 (FAO Fisheries and Aquaculture Report no. 957, FAO, Rome, 2011).
14. S. J. Hall, B. M. Mainprize, *Fish Fish.* **6**, 134 (2005).
15. S. J. Kennelly, M. K. Broadhurst, *Fish Fish.* **3**, 340 (2002).
16. D. C. Dunn, A. M. Boustany, P. N. Halpin, *Fish Fish.* **12**, 110 (2011).
17. C. Birkeland, P. K. Dayton, *Trends Ecol. Evol.* **20**, 356 (2005).
18. C. N. Anderson *et al.*, *Nature* **452**, 835 (2008).
19. R. Law, *ICES J. Mar. Sci.* **57**, 659 (2000).
20. C. Jørgensen *et al.*, *Science* **318**, 1247 (2007).
21. A. Kuparinen, J. Merilä, *Trends Ecol. Evol.* **22**, 652 (2007).
22. N. Daan, H. Gislason, J. G. Pope, J. C. Rice, *ICES J. Mar. Sci.* **62**, 177 (2005).
23. The size spectrum is the relative proportion of biomass per size-class in the fish community (see fig. S1). Increased spectrum slope reflects relative increase in biomass in

Published by AAAS

smaller-size classes compared with larger classes.
24. E. Jul-Larsen, J. Kolding, J. R. Nielsen, R. Overa, P. A. M. van Zwieten, Management, co-management or no management? Major dilemmas in southern African freshwater fisheries (Tech. Rep. 426/1–2, FAO, Rome, 2003).
25. J. G. Pope, *ICES Mar. Sci. Symp.* **193**, 22 (1991).
26. M.-J. Rochet, J. S. Collie, S. Jennings, S. J. Hall, *Can. J. Fish. Aquat. Sci.* **68**, 469 (2011).
27. M.-J. Rochet, E. Benoît, *Proc. Biol. Sci.* **279**, 284 (2012).
28. K. H. Andersen, M. Pedersen, *Proc. Biol. Sci.* **277**, 795 (2010).
29. United Nations, Report of the World Summit on Sustainable Development, Johannesburg, South Africa, 26 August to 4 September 2002 (Tech. Report No.A/CONF.199/20*, United Nations, New York, 2002).
30. MSY calculations assume that, by applying a constant fishing mortality with a given selectivity (externally determined by fisheries), a constant yield can be taken from a stock over an indefinite period. There is one given fishing mortality rate that maximizes this yield, providing MSY.
31. M. N. Maunder, *Fish Fish.* **3**, 251 (2002).
32. J. Link *et al.*, *Fish Fish.* **12**, 152 (2011).
33. Ecosystem level constraints on target species catch limits have been agreed, e.g., in the Antarctic ecosystem (*34*).
34. A. J. Constable *et al.*, *ICES J. Mar. Sci.* **57**, 778 (2000).
35. B. Gobert, *Fish. Res.* **19**, 87 (1994).
36. I. Clucas, A study of the options for utilization of bycatch and discards from marine capture fisheries (FAO Fish. Circ., FAO, Rome, 1997).
37. Sainsbury's launches 'Switch the Fish' campaign, www.fishnewseu.com/latest-news/uk/5973-sainburys-launches-switch-thefish-campaign.html.
38. This work results from a workshop sponsored by the International Union for the Conservation of Nature, the Convention on Biological Diversity, the Census of Marine Life, the Ministries of Fisheries and Coastal Affairs and of Foreign Affairs of Norway, the Global Guardian Trust of Japan, the Ocean Alliance of the University of Tokyo, the Japan National Association for the Conservation of Fishing Ground, the Japan Fisheries Association, and the Technical University of Denmark. M.-J.R. received support from the Pew Charitable Trusts. The opinions expressed are those of the authors and do not necessarily reflect the views of the supporting organizations.

Supporting Online Material
www.sciencemag.org/cgi/content/full/335/6072/1045/DC1

10.1126/science.1214594

PUBLIC HEALTH AND BIOSECURITY

The Limits of Government Regulation of Science

A transparent institutional review process will balance scientific freedom and national security better than publication restrictions.

John D. Kraemer[1,2] and Lawrence O. Gostin[2]*

Last summer, two research teams funded by the National Institutes of Health genetically modified H5N1 avian influenza viruses, making them capable of efficient respiratory transmission between ferrets. Ferrets are thought to be a good animal model for influenza in humans. A small number of genetic changes might be able to convert the presently zoonotic H5N1 virus into a pathogen with dangerous pandemic potential—transmissible from human-to-human, with a >50% case-fatality rate. The National Science Advisory Board for Biosecurity (NSABB), which advises the U.S. Department of Health and Human Services (HHS), recommended that two journals, *Science* and *Nature*, redact key information before publication. The NSABB and HHS expressed concerns that published details about the papers' methodology and results could become a blueprint for bioterrorism (*1*).

The U.S. government's request not to publish key scientific findings sparked considerable controversy. To many researchers, knowledge about what mutations enable respiratory transmission is essential to surveillance of and early action against variants of H5N1. They worry that government intrusion into scientific innovation would discourage vital research. However, security advocates believe the greater risk is that the mutated virus could escape or that knowledge about these mutations could get into the wrong hands. They suggest that research of this kind should not be funded or undertaken in the first place. Where, as here, the research has already been conducted, they urge scientific journals not to publish any sensitive methods or results (*1*).

The court ruled that federally funded scientific research, especially at universities, should be free from prior restraint—calling into question the validity of CUI conditions on research grants.

The HHS request reveals a troubled relationship between security and science. This is not the first time a government has requested that a journal not publish information. In 1979, the U.S. Department of Energy secured an injunction against the magazine *The Progressive* to prevent the publication of an article about building a hydrogen bomb, even though the information was in the public domain; the injunction was later vacated when the article was published elsewhere (*2*). In 2005, the *Proceedings of the National Academy of Sciences* refused to comply with an HHS request to decline publishing a mathematical model of botulism in the milk supply (*3*). The H5N1 case, however, is the first time government has sought to redact information after an institutionalized HHS review process.

Constitutional Limits on Government Restrictions of Scientific Publications

The First Amendment to the U.S. Constitution affords considerable protection to political, artistic, and scientific expression, that could trigger "strict scrutiny" by the Supreme Court (*4*). The court is most vigorous in reviewing government restraints on speech in advance of publication, which it calls "prior restraints." Prior restraints are uniquely threatening to First Amendment values because they prevent ideas from ever being heard (*5*).

Had the government compelled the H5N1 researchers to cease research or the journals to withhold publication—whether through the force of law or by creating adverse consequences such as loss of funding—it could have violated the First Amendment. Even informal systems of restraint can be unconstitutional, such as a government threat to prosecute publishers (5). In this case, however, HHS' request, by its own terms, was nonbinding, and the journals had discre-

[1]Department of Health Systems Administration, Georgetown University School of Nursing and Health Studies, Washington, DC 20057, USA. [2]O'Neill Institute for National and Global Health Law, Georgetown University Law Center, Washington, DC 20001, USA.

*Author for correspondence. E-mail: gostin@law.georgetown.edu

tion whether or not to comply (*6*). Given the absence of legal force or undue inducements or penalties, the government's request to withhold information does not violate the First Amendment.

There are situations in which a government has the authority to block scientific communications. The clearest case is when research has been properly classified under federal law and the person seeking to communicate findings obtained it under the terms of a security clearance—whether they are still working for the government or not, so long as procedural requirements are met (*7*). Although a researcher is obliged to keep classified information confidential, publishers who obtain that information lawfully have a right to publish. In the *Pentagon Papers* case, the Supreme Court held that President Nixon did not overcome the "heavy presumption" against prior restraint when he sought to prohibit publication of classified materials. The court found that an undefined concept of "security" did not "abrogate the fundamental law embodied in the First Amendment" (*8*).

It is far less clear whether government may suppress the publication of research conducted with government funding when the results are "controlled unclassified information" (CUI) [sometimes referred to as "sensitive but unclassified" (SBU)] under conditions set by government grants or contracts. Traditionally, the federal government restricted communication about basic science research only through classification. However, CUI restrictions have become more common, and no court has directly addressed their constitutionality. Although it is unclear how often CUI clauses include a prepublication review requirement, research suggests that they occur with some regularity (*9*).

Board of Trustees of Leland Stanford Jr. University v. *Sullivan* is the most pertinent case for evaluating CUI restrictions. Stanford University challenged an NIH confidentiality clause that required the university to seek prior approval before publishing preliminary findings about artificial heart research to protect the public from unvalidated research findings. The court ruled that federally funded scientific research, especially at universities, should be free from prior restraint—calling into question the validity of CUI conditions on research grants. The wider the scope of CUI conditions, the more likely that courts will invalidate them (*4*).

The Supreme Court's "unconstitutional conditions" doctrine holds that government may not place conditions on public funding that require the recipient to surrender First Amendment rights. Thus, government has no obligation to provide research funding, but if it chooses to, it cannot restrain the free expression of researchers without a compelling state interest. For example, a federal appellate court recently struck down HHS guidelines requiring recipients of AIDS prevention funding to pledge their opposition to prostitution, reasoning that it was an unconstitutional condition (*10*).

The unconstitutional conditions doctrine, however, is hard to decipher. For example, the Supreme Court upheld HHS prohibitions on the use of family planning funds to counsel women regarding abortion, reasoning that government is entitled to subsidize one protected right (family planning), while refusing to subsidize analogous rights (abortion counseling) (*11*). The court similarly upheld the government's right to withhold funding to any public university that denied access to military recruiters, even though the universities claimed it violated their freedom to disapprove of the military's "don't ask, don't tell" rule. The court said the law neither denied the institutions the right to speak nor required them to say anything (*12*).

Could the public obtain sensitive data that have been redacted from publications through a FOIA request? If so, governmental requests to redact sensitive information would be fruitless.

Scientific Publication from Countries Subjected to U.S. Economic Sanctions

In the past, the federal government has impeded scientific publication processes, not because of articles' content but rather because the authors were from countries against which the United States had imposed economic sanctions. The Department of Treasury's Office of Foreign Assets Control (OFAC) enforces these economic sanctions. For a brief period in 2003, OFAC restricted the review process for scientific papers submitted from countries sanctioned by the United States (*13*). In particular, OFAC informed the Institute of Electrical and Electronics Engineers (IEEE) that, although its journals could subject papers from sanctioned countries to peer review, they could not make prepublication edits without a specific license. In essence, OFAC argued that editing a paper was providing a service to foreign authors in violation of trade embargoes. In 2004, OFAC reversed that decision and allowed normal scientific editing to occur (*14*). Had OFAC not reversed itself, First Amendment challenges against the policy likely would have prevailed (*15*).

Access to Sensitive Data Under the Freedom of Information Act

A functioning democracy requires that citizens be able to access information in the government's possession, but not if access poses an unacceptable security risk. The Freedom of Information Act (FOIA) balances these concerns by affording access to federal agency records unless the records fall within a statutory exemption. Federal agencies support much of the research in the United States, including both of the recent H5N1 studies. Could the public obtain sensitive data that have been redacted from publications through a FOIA request? If so, governmental requests to redact sensitive information would be fruitless.

FOIA applies only to "agency records," so a threshold issue is whether university research data acquired under a grant constitute an agency record. In 1980, the Supreme Court ruled that research data produced under an NIH grant and used in regulatory proceedings by the U.S. Food and Drug Administration did not constitute an agency record subject to FOIA because it was retained by the nongovernmental grantee. The court found that FOIA required the agency to either produce or obtain permanent custody of the data (*16*).

The "Shelby amendment," enacted in 1999, expanded public access to data produced at universities and other nonprofit research entities under federal grants. The public can request the data if they were produced under a federal grant and "cited publically and officially by the Federal Government in support of an agency action that has the force and effect of law" (*17*). Federal agencies could take care not to officially cite highly sensitive data, thereby avoiding a successful FOIA request. However, it is not always simple or easy to refrain from referencing sensitive research. The NIH, for example, might reasonably refer to the H5N1 research as justification for revising biosecurity policies.

Even if sensitive data do become part of an agency record, FOIA provides the federal government with ample authority to refuse a request on security grounds. FOIA provides nine exemptions under which records that would otherwise have to be disclosed

Published by AAAS

may be withheld, one of which is for "matters that are specifically authorized under criteria established by an executive order to be kept secret in the interest of national defense or foreign policy and are in fact properly classified pursuant to such an executive order" (*18*). Through this exception, Congress has acknowledged broad executive authority to classify records so long as it is done lawfully pursuant to an executive order.

President Obama's 2009 Executive Order 13526 revises existing classification standards (*19*). Although it was designed to reduce the amount of classified materials, the executive order affords agencies considerable discretion to classify on security grounds. Consistent with prior policy, the executive order mandates that "basic scientific research information not clearly related to the national interest shall not be classified." However, the order permits the classification of "scientific, technical, or economic matters relating to the national security," provided that disclosure is reasonably expected "to cause identifiable or describable damage to the national security." Furthermore, agencies may classify data that meet the executive order's standards even if the data were not classified at the time of the FOIA request (*19*). Thus, federal agencies have wide authority to prevent the release of research information through a FOIA request simply by classifying it, provided that there are legitimate national security justifications.

In 2010, President Obama issued a further executive order stating that CUI is not automatically exempt from FOIA (*20*). Thus, to ensure that sensitive biological research information is not disclosed, agencies would have to classify it. [Certain nonbiological research, such as nuclear energy, is automatically exempt from FOIA, as are the locations where select biological agents are held (*21*).] Some research data also might be protected under FOIA exemptions for trade secrets or predecisional deliberative memoranda within the government, but these options are limited (*22*).

The law, then, draws a distinction between classified and controlled unclassified information. However, from a constitutional perspective, it would be troubling if the result turned solely on the label the government placed on the data. If the result did turn on the label, the government could simply relabel research from CUI to classified and thus prohibit its dissemination. Although decisions to classify can be challenged, prevailing is difficult, and unnecessary classification is common (*23*). This appears to place too much discretion in the hands of public officials.

The problem of government discretion is compounded by highly inconsistent practices among federal agencies in the classification systems they use. There is inconsistency of structure (the labels attached, such as classified, CUI, SBU, or other terminology), as well as in the application of that structure to individual documents (no clear standard exists for deciding whether to classify particular information). In short, the line between classified and CUI remains unclear, as agencies struggle to apply President Obama's executive orders (*24*).

Balancing Scientific Freedom, Constitutional Values, and Biosecurity

The federal government has the power to prevent the dissemination of sensitive life-sciences research, but there are good reasons to exercise that power sparingly. The current system of deliberation by a federal expert advisory board and HHS-issued voluntary recommendations is preferable to formal government mandates. Although we do not have all the data, the NSABB process in the H5N1 cases appears reasonable, given that unredacted publication could enable bad actors with scientific skill to replicate the studies, with profoundly harmful effects. The federal government has promised to share the researchers' methods and conclusions with scientists with a need to know, which substantially advances scientific objectives.

Can the review process for high-risk biologic research be improved further? The NSABB's origins can be traced to the so-called Fink report issued in 2004 by the National Research Council (*21*). However, vital aspects of the Fink report have not been implemented. In particular, the Fink report proposed an institutional review process for biological "experiments of concern"—those falling into seven research classes, making the pathogen considerably more attractive as a bioterrorism agent (e.g., by enhancing virulence or transmissibility or by rendering vaccines ineffective). This approach was patterned on the Institutional Biosafety Committees (IBCs) required by NIH for recombinant DNA research at institutions receiving federal funding, which generally have been considered to be successful (*21*).

HHS, in partnership with institutions, will have to ensure that the IBC model works effectively: (i) institutions must develop the requisite expertise to review dual-use research of concern; (ii) HHS must specify the categories of research requiring institutional review—minimally including the seven types of high-risk experiments; and (iii) HHS must set clear and consistent standards for institutional review. If IBCs are formally designated to conduct the institutional review function, HHS will have to clarify whether NSABB will guide and oversee the process (*21*). In addition, because IBCs may recommend that researchers voluntarily restrict access to methods or results in some instances, it will be important for HHS to develop a system for managing access to sensitive data and for disseminating it to those with a need to know in a fair manner.

If HHS improves its functioning, the institutional review process can ensure a sound balance between scientific freedom and national security. A fair, transparent process undertaken by research institutions, with a balanced approach to scientific benefits and public safety, together with HHS guidance and oversight of high-risk research, is preferable to government constraints on scientific information by force of law.

References and Notes

1. D. Grady, W. J. Broad, *New York Times*, 21 December 2011, p. A1.
2. *United States* v. *Progressive, Inc.*, 467 F. Supp. 990 (1979).
3. Letter from Stewart Simonson to Bruce Alberts, 27 May 2005; www.fas.org/sgp/bush/hhs052705.pdf.
4. *Board of Trustees of Leland Stanford Jr. University* v. *Sullivan*, 773 F. Supp. 472 (1991).
5. *Bantam Books* v. *Sullivan*, 372 U.S. 58 (1963).
6. NIH, Press statement on NSABB review of H5N1 Research (20 December 2011); www.nih.gov/news/health/dec2011/od-20.htm.
7. *Snepp* v. *United States*, 444 U.S. 507 (1980).
8. *N.Y. Times* v. *United States*, 403 U.S. 713 (1971).
9. A. Chamberlain, Science and Security in the Post-9/11 Environment—Export Controls: Grants, Contracts, and Publishing (American Association for the Advancement of Science, Washington, DC, 2004); www.aaas.org/spp/post911/grants.
10. *Alliance for Open Society International* v. *USAID* (2nd Cir. 2011).
11. *Rust* v. *Sullivan*, 500 U.S. 173 (1991).
12. *Rumsfeld* v. *Forum for Academic and Institutional Rights, Inc.*, 547 U.S. 47 (2006).
13. Letter from R. Richard Newcomb (OCAF) to Nelson G. Dong, 2 April 2004; www.ieee.org/documents/OFAC_40204_Letter.pdf.
14. IEEE, OFAC Background; www.ieee.org/about/corporate/compliance/regulatory/ofac/background.html.
15. T. J. Chin, *New York Univ. Law Rev.* **83**, 1883 (2008).
16. *Forsham* v. *Harris*, 445 U.S. 169 (1980).
17. Office of Management and Budget, Revised circular 110A; www.whitehouse.gov/omb/circulars_a110.
18. Freedom of Information Act, 5 U.S.C. §552.
19. Executive Order 13526, Classified National Security Information (2009).
20. Executive Order 13556, Controlled Unclassified Information (2010).
21. National Research Council, *Biotechnology Research in an Age of Terrorism* (National Academies Press, Washington, DC, 2004).
22. D. G. Goldenson, *Boston Coll. Environ. Aff. Law Rev.* **29**, 311 (2001–2002).
23. M. Steffan, The high cost of keeping a secret, *Washington Post*, ideas@innovation [blog], 13 October 2011.
24. J. P. Fitzpatrick, M. A. Pustay, Guidance regarding Controlled Unclassified Information and the Freedom of Information Act [memorandum], 22 November 2011; www.fas.org/sgp/cui/foia112211.pdf.

10.1126/science.1219215

CELL BIOLOGY

Reconfiguring Regulation

Guilhem Chalancon, Kai Kruse, M. Madan Babu

Cells adapt to changes in their environment by regulating the expression of multiple genes, but a deeper understanding of this phenomenon requires quantitative, genome-wide measurements of the abundance of different cellular components at high temporal resolution and under a large number of conditions. Technological advances have made it possible to monitor how this takes place from a systems biology perspective (*1*–*5*). Two papers in this issue—by Nicolas *et al*. on page 1103 (*6*) and Buescher *et al*. on page 1099 (*7*)—describe how the bacterium *Bacillus subtilis* achieves adaptation at an unprecedented level of detail and breadth.

Studies on *Mycoplasma pneumoniae* (*1*–*3*) individually documented the bacterium's cellular transcripts (transcriptome), proteins (proteome), and metabolites (metabolome). A more comprehensive understanding of cellular adaptation was achieved in a study of the bacterium *Escherichia coli* (*4*), where a large-scale and integrated collection of "omics" data sets was obtained from a single experimental setup. However, it did not provide time-resolved dynamic data or examine a wide range of environmental conditions. These limitations were partly addressed by a system-wide temporal integration of the transcriptome, proteome, and metabolome of *B. subtilis* to monitor the changes during adaptation to nutrient starvation (*5*).

Nicolas *et al*. and Buescher *et al*. take another important step toward the integrative characterization of an entire organism. Nicolas *et al*. analyzed the genome-wide transcriptional activity of *B. subtilis* across 104 different nutritional and environmental conditions, reflecting the bacterium's natural habitat. Buescher *et al*. combined multiple time-resolved omics data in a mathematical framework to compare *B. subtilis* adaptation to glucose-rich and malate-rich nutrient conditions. Together, their results provide broad (in terms of the number of environmental conditions) and detailed (in terms of temporal resolution) views of the *B. subtilis* response to environmental changes.

Nicolas *et al*. observed considerable complexity in the promoter architecture of protein-coding genes. Their findings triple the number of mapped promoter regions and reveal that ~50% of the characterized genes can be transcribed from more than one promoter. This is accomplished by alternative sigma factors, which form an essential but variable subunit of the RNA polymerase complex, and confer promoter sequence binding specificity. In particular, 85% of protein-coding genes were highly expressed in at least one condition, but <3% of them remained constitutively expressed in all conditions, indicating an unexpectedly high transcriptional plasticity.

Buescher *et al*. reveal that shifts to malate-rich and glucose-rich nutrient conditions introduced substantial global reconfigurations at all levels of regulation. Most genes were differentially expressed, and 127 out of 154 transcription factors changed their activity during one or both shifts. Changes in carbon metabolism during both shifts were mediated largely by altering the abundance of a small number of proteins. Although both nutrients are preferred carbon sources for *B. subtilis*, adaptation to glucose availability was slow and largely controlled transcriptionally, whereas adaptation to malate was fast and primarily regulated posttranscriptionally (see the figure).

To achieve adaptation, *B. subtilis* makes some compromises. The observations of Nicolas *et al*. suggest that transcriptional plasticity is often associated with imperfect control, leading to the generation of antisense RNAs. This may arise due to aberrant termination of transcription, or spurious transcription initiation while using alternative sigma factors. Similarly, the results from Buescher *et al*. suggest that, depending on the prevailing environmental condition, the preferential uptake of one carbon source over the other might confer condition-specific evolutionary advantages in growth. This is achieved by active regulation or constitutive expression of several genes—two distinct strategies, nei-

Cell adaptation to changing environments requires a trade-off between complex regulation and imperfect control.

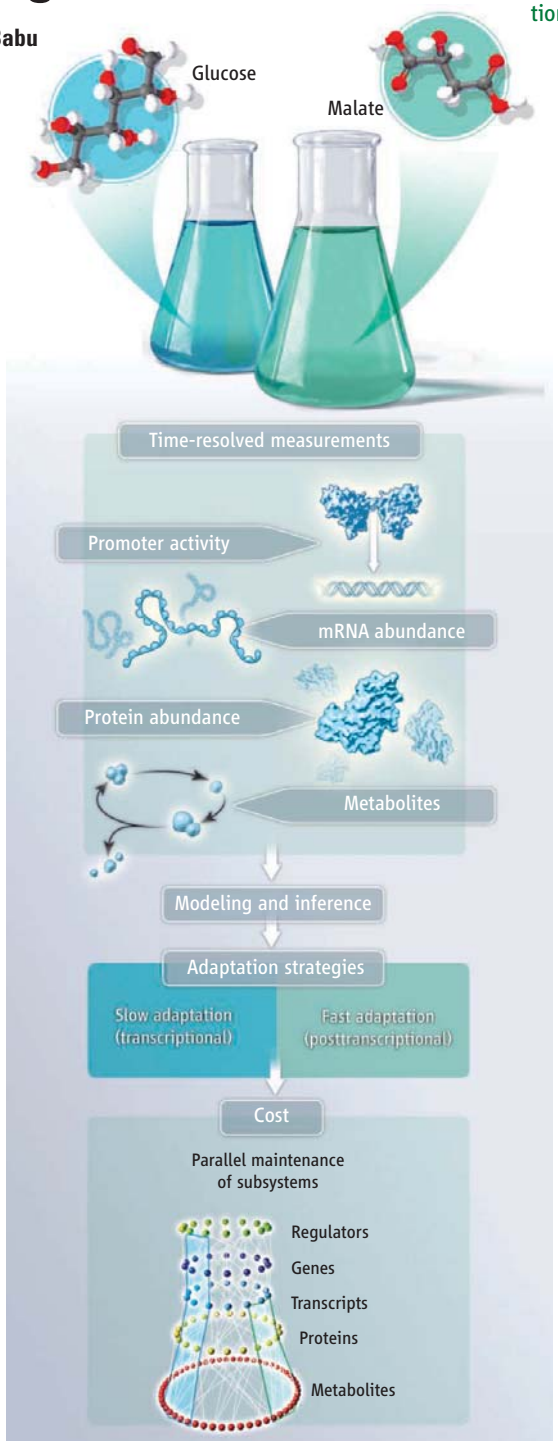

An integrated view of adaption. Adaptation of *B. subtilis* to changing environments (such as nutrients) requires a balance between complex regulation (adaptation strategy) and imperfect control (cost).

CREDIT: Y. HAMMOND/*SCIENCE*

MRC Laboratory of Molecular Biology, Hills Road, Cambridge CB2 0QH, UK. E-mail: madanm@mrc-lmb.cam.ac.uk

Published by AAAS

ther of which is advantageous per se. Thus, to adapt to changing environments, *B. subtilis* makes a trade-off between the implementation of complex regulatory programs and imprecise regulation.

However, when seen in a different light, those apparent compromises may be advantageous. Spurious transcription of antisense RNAs might provide an additional means of regulation (*8*). In addition to silencing gene expression, antisense transcription increases gene expression variability among individual cells in a population (*9*). Such variation in the expression of key adaptation-conferring genes could increase the chance that some cells will successfully adapt when environmental conditions fluctuate (*10*). Likewise, active regulation or constitutive expression of enzymes need not be detrimental but may even be beneficial. For instance, constitutive malate uptake combined with delayed glucose consumption is a successful strategy in environments where *B. subtilis* primarily encounters malate (*7*).

The studies by Nicolas *et al*. and Buescher *et al*. jointly demonstrate that adaptation to changing conditions involves a global reorganization of the gene expression process. Many directions remain to be explored in light of these findings. Other factors may influence cellular adaptation: the impact of post-translational modifications and decay rates of cellular components (*11*), the influence of three-dimensional organization of genomes on transcriptional plasticity (*12*), and protein and mRNA localization within a cell (*13*). Moreover, single-cell measurements on individual cells, rather than on entire cell populations, are beginning to reveal the importance of stochastic variation in expression levels of genes as an important strategy for adaptation (*14*). Thus, these factors and approaches need to be explicitly considered in future investigations aimed at characterizing cellular changes to environmental adaptation. Similar studies in other organisms will become imperative to understanding long-standing fundamental questions in biology.

References and Notes

1. M. Güell *et al*., *Science* **326**, 1268 (2009).
2. S. Kühner *et al*., *Science* **326**, 1235 (2009).
3. E. Yus *et al*., *Science* **326**, 1263 (2009).
4. N. Ishii *et al*., *Science* **316**, 593 (2007).
5. A. Otto *et al*., *Nat. Commun.* **1**, 137 (2010).
6. P. Nicolas *et al*., *Science* **335**, 1103 (2012).
7. J. M. Buescher *et al*, *Science* **335**, 1099 (2012).
8. L. S. Waters, G. Storz, *Cell* **136**, 615 (2009).
9. Z. Xu *et al*., *Mol. Syst. Biol.* **7**, 468 (2011).
10. L. López-Maury *et al*., *Nat. Rev. Genet.* **9**, 583 (2008).
11. T. Maier *et al*., *Mol. Syst. Biol.* **7**, 511 (2011).
12. M. A. Umbarger *et al*., *Mol. Cell* **44**, 252 (2011).
13. P. Bork, L. Serrano, *Cell* **121**, 507 (2005).
14. A. Eldar, M. B. Elowitz, *Nature* **467**, 167 (2010).
15. G.C. and K.K. contributed equally. We thank the Medical Research Council and Gates Scholarship (G.C.) for funding.

10.1126/science.1219303

GEOPHYSICS

Probing the Mantle Past

Precision isotope analysis can reveal details of the dynamic processes involved in the formation of Earth's mantle.

Vickie C. Bennett

Until recently, geologists generally believed that all evidence of the first few hundred million years of Earth's 4.56-billion-year history had been erased by mantle convection and plate tectonics. Although planetary analogs with Mars and the Moon suggest that Earth likely experienced large-scale melting soon after accretion, vigorous convection in the early mantle due to higher heat production from radioactive decay, core formation, and large impacts followed by 4 billion years of crustal recycling at plate boundaries was thought to have efficiently mixed and homogenized the mantle, obliterating all signs of Earth's youthful exuberance. That all changed with the discovery of zircon grains more than 4.0 billion years old from the Jack Hills in western Australia in 1983 (*1*), followed by the demonstration in 2003 that geochemical signals linked to decay of short-lived radioactive isotopes are preserved in some ancient crustal terrains. The recognition of ^{142}Nd isotopic variations, produced by decay of ^{146}Sm with a half-life of 103 million years, in 3.8-billion-year-old terrestrial rocks (*2*) proved that traces of Earth's earliest history are still legible in the rock record. On page 1065 of this issue, Touboul *et al*. (*3*) report highly precise measurements of the isotopic composition of tungsten (W) in 2.8-billion-year-old "komatiites," a type of basaltic rock known to be derived from source regions deep within the mantle. The results help to produce a clearer picture of the dynamic processes involved in the formation of Earth's early mantle.

As ^{182}W forms from the decay of an isotope of hafnium (^{182}Hf), which has a half-life of only 9 million years, any anomalous variations in ^{182}W must have been created while the parent isotope ^{182}Hf was still alive and actively decaying, that is, within the first ~60 million years of the origin of the solar system. Touboul *et al*. found that these komatiites, from the Baltic Shield in Russia, have appreciable enrichments in ^{182}W to the level of about 13 parts per million higher and are thus "anomalous" compared with modern terrestrial rocks. This is only the second report of such an anomaly in the Earth, following last year's discovery by Willbold *et al*. (*4*) of similar-sized ^{182}W isotopic anom-

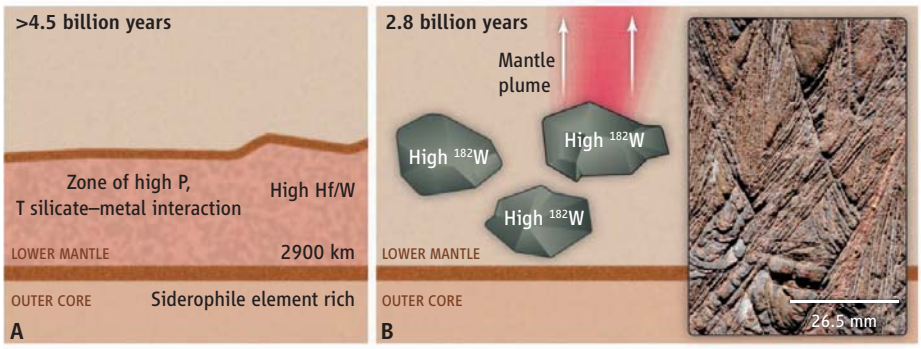

Mantle dynamics. (**A**) Under conditions of high-temperature and pressure metal-silicate partitioning, regions of the deep mantle near the core-mantle boundary of Earth may have formed with high Hf/W ratios. If this occurred in the first 60 million years of Earth's history, while ^{182}Hf (half-life of 9 million years) was actively decaying, then regions with enriched amounts of the daughter isotope ^{182}W would form. (**B**) Preservation of some of this ancient material in Earth's mantle over extended time periods could result in the unusual isotopic signatures measured in some 2.8-billion-year-old rocks, known as komatiites, derived from the deep mantle (*3*).

Research School of Earth Sciences, Australian National University, Canberra, ACT 0200, Australia. E-mail: vickie.bennett@anu.au.edu

PHOTO CREDIT: (RIGHT INSET) NICOLAS ARNDT

Published by AAAS

alies in older (3.8 billion years old) crustal rocks from Greenland.

The results obtained by Willbold *et al*. (*4*) and Touboul *et al*. add to a growing body of work that is revolutionizing our understanding of the deep Earth and early Earth processes through the use of highly precise (to better than ±5 parts per million) measurements of the daughter products of "extinct" (that is, no longer actively decaying) isotopic systems in carefully selected terrestrial samples. These measurements are at the limit of current analytical capabilities and are far from routine. The ^{142}Nd isotopic variations in ancient terrestrial rocks revealed a record of chemical processing on Earth that started >4.4 billion years ago. The new ^{182}W data push that record back even farther.

As with many new discoveries, the interpretation of the data are contentious. Willbold *et al*. (*4*) proposed that the anomalous tungsten reflects the composition of Earth's primordial mantle that predates a "late veneer" addition of siderophile elements (iron-associated elements such as W) to Earth by meteorite influx associated with the Late Heavy Bombardment at ~3.9 billion years ago. In that scenario, core formation stripped the mantle of siderophile elements such as W, while ^{182}Hf was still alive, allowing the mantle to accumulate an excess of radiogenic ^{182}W, with late accretion of meteoritic material adding a new supply of siderophile elements (*5*) and overprinting the early formed signatures.

In contrast, the results of Touboul *et al*. are not in accord with this simple explanation. For example, the Russian komatiites have siderophile element abundances similar to those in the modern mantle source and so cannot be the products of a W-depleted early mantle. This is consistent with previous siderophile element studies of ancient mantle samples showing that by 3.8 billion years ago, Earth's mantle already had its full complement of siderophile elements and in the relative abundances found in the modern mantle (*6*).

Touboul *et al*. consider two possibilities to explain the ^{182}W anomalies in the Kostomuksha komatiites. One is that the siderophile element characteristics of their mantle source region were set by metal-silicate partitioning at high temperature and pressure under redox conditions that were more reducing than the modern mantle (see the figure). Under these conditions, the siderophile element partitioning relationships would create a high Hf/W reservoir that could mix with more normal mantle to produce the komatiite source. Alternatively, the early W-Hf fractionation may be due to crystallization of a magma ocean or formation of an early basaltic crust. These scenarios are difficult to test, but additional integrated studies of short-lived and longer-lived isotopic systems in early terrestrial rocks would provide useful constraints on the timing and importance of core formation, early mantle differentiation, and late accretion.

Regardless of the exact mechanism by which they formed, one question for understanding deep mantle dynamics is how these early isotopic anomalies can be preserved in the mantle for at least 1 to 2 billion years, despite convective mixing and possible overprints from meteorite bombardment. The preservation of anomalies produced during the first 60 million years of solar system history may imply that Earth was never totally molten early in its history and that mixing times were much longer than have been considered to date (*7*), allowing isotopic signatures to be preserved, perhaps to the present day (*8*), if we can figure out where to look for them. Sophisticated dynamical models of mantle mixing, coupled with a broader understanding of late accretion and how the interiors of terrestrial planets respond to energetic events such as large impacts, core formation, and magma ocean crystallization, will be necessary to explain the preservation of such ancient domains.

The studies of Touboul *et al*. and Willbold *et al*. (*4*) show that we now have the ability to examine processes and events that shaped the deep Earth in the first few tens of millions of years of geologic time. Amazingly, that record still exists if we can learn how to read it. The answers will certainly reveal new aspects of the history, composition, and structure of the early mantle as a key part of understanding the Earth system.

References

1. D. O. Froude *et al*., *Nature* **304**, 616 (1983).
2. G. Caro, B. Bourdon, J.-L. Birck, S. Moorbath, *Nature* **423**, 428 (2003).
3. M. Touboul, I. S. Puchtel, R. J. Walker, *Science* **335**, 1065 (2012).
4. M. Willbold, T. Elliott, S. Moorbath, *Nature* **477**, 195 (2011).
5. W. Maier *et al*., *Nature* **460**, 620 (2009).
6. V. C. Bennett, A. Nutman, C. Friend, *Geochim. Cosmochim. Acta* **66**, 2615 (2002).
7. V. Solomatov, C. C. Reece, *J. Geophys. Res.* **113**, B07408 (2008).
8. M. G. Jackson *et al*., *Nature* **466**, 853 (2010).

10.1126/science.1219126

ECOLOGY

Facing Extinction in Real Time

David B. Wake

Amphibian populations worldwide are under threat as a result of additive effects of multiple stressors.

A sense of impending doom has enveloped the community of amphibian biologists for more than two decades, as evidence has built that the subjects of their research are in severe difficulty. What at first was a puzzle based mainly on anecdotes (*1*) became an evident fact when intensive studies were completed: Throughout the world, amphibians are in decline, and many species—perhaps 40%—face imminent extinction (*2*). Recent studies have elucidated some agents for amphibian losses and projected the likely prospects for amphibian survival across the globe. The picture that emerges is disturbing.

The amphibian decline is generally acknowledged to be a multifarious problem, connected to factors such as habitat destruction, climate change, and pesticide use, among others. The discovery in 1998 (*3*) of a previously unknown infectious agent—a chytrid fungus that kills amphibians—established a new focus of research on amphibian declines. Chytridiomycosis is having a devastating impact on frog populations in Australia (*4*) and Central America (*5*). A southeastward wave of chytrid infection in lower Central America (*6*) has been traced back to the northwest to Monteverde, Costa Rica, at the time of perhaps the best-documented early amphibian disappearance in 1987, and even further north to Veracruz, Mexico, as early as 1972 (*7*). Despite its recent discovery, the chytrid probably has been adversely affecting amphibian populations for decades.

Hof *et al*. (*8*) remind us that there are other major factors besides chytridiomycosis in the general decline and paint a gloomy picture for the future of amphibians. The authors project that multiple drivers of extinction

Museum of Vertebrate Zoology, University of California, Berkeley, CA 94720–3160, USA. E-mail: wakelab@berkeley.edu

Published by AAAS

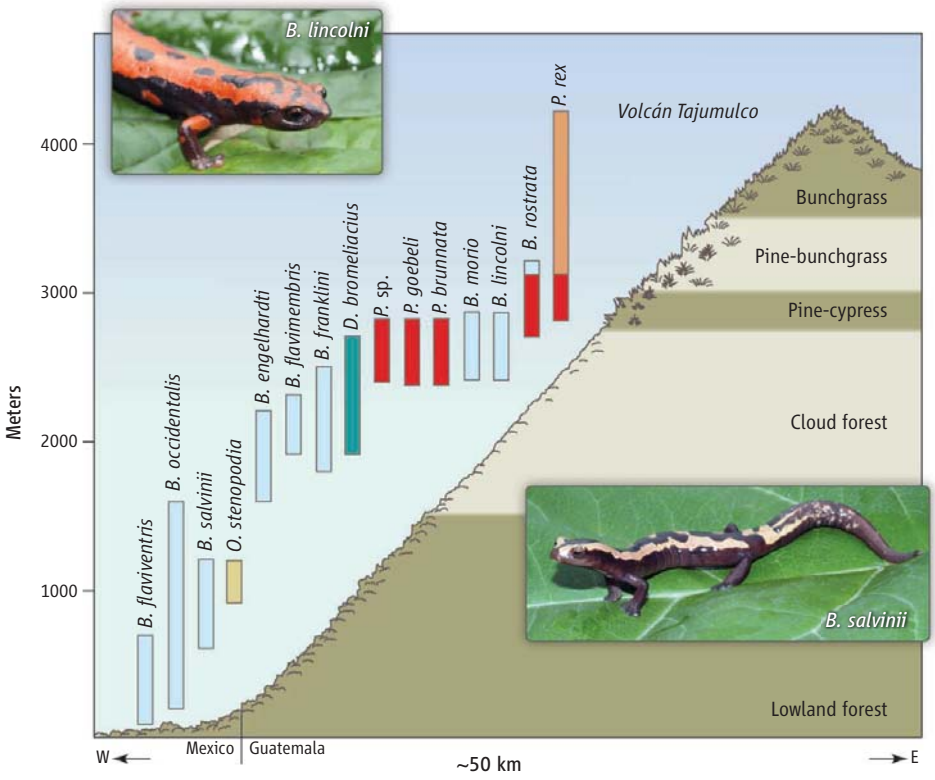

Nowhere to go. Elevational distributions of salamanders on Volcán Tajumulco, Guatemala, show that between 1978 and 2005 to 2007, three once common upland species disappeared; two others experienced upward range restrictions. Each genus is shown in a different color: *Bolitoglossa*, light blue; *Dendrotriton*, turquoise; *Oedipina*, yellow; *Pseudoeurycea*, orange. Species losses at specific elevations are shown in red.

will become increasingly important, with more intense impacts than previous assessments have found (*2*). Some regions with high species richness face the greatest risk. Climate change alone is projected to negatively affect as many as 73% of the frog species in the northern Andes and 66% of the local salamander fauna in one part of Central America; taking into account the other variables makes matters worse. The substantial overlap of threats in areas of high species richness is troubling.

The authors project a relatively small role for chytridiomycosis, in sharp contrast with much recent thought. However, it remains to be seen how accurate the models used for chytrid will prove to be. Knowledge of the basic biology of fungus is increasing rapidly, ranging from its genetics (*9*) and ecology (*4*, *10*, *11*), to the development of mitigation strategies to maintain wild populations afflicted by chytridiomycosis (*12*). Chytridiomycosis may be a greater threat, especially in the short term, than the findings of Hof *et al*. suggest.

Over the past decade, the number of known amphibian species has increased by ~25% to nearly 7000. Most of these species are new discoveries with very restricted geographic ranges and are thus likely to be vulnerable to all factors currently threatening amphibians. Land-use changes are critical, based on my own field experience with Mesoamerican salamanders. Other important factors, such as pollutants and the impact of invasive species, are likely to make matters even worse.

With their moist and seemingly delicate skins, amphibians might be highly susceptible to climate change (*13*), but they are long-term survivors, having gotten through the end-Cretaceous extinctions and Pleistocene climate changes (*14*). Although geographic ranges of amphibians might adjust in response to climate change, just how is unclear. Many amphibians have narrow elevational ranges along altitudinal gradients, with essentially no latitudinal or longitudinal ranges at all; those restricted to near the tops of mountains may experience range collapse under a climatic warming scenario, because suitable environmental conditions no longer exist locally (see the figure) (*15*).

Early and Sax (*13*) have projected climate paths, determined by the location of places with suitable climatic conditions during a sequence of time steps in the history of a species, for 15 species of salamanders in western North America between 1990 and 2100 C.E. They argue that processes related to range shifts—dispersal and population persistence—can have dramatic effects on range shift forecasts, which result from short-term climatic and population characteristics. The authors show that persistence in the face of climate change, even for as short a time as two decades, would contribute importantly to survival, but they think that persistence under unfavorable conditions for so long is unlikely. They conclude that some of the species studied face increased endangerment, while others face probable extinction.

Yet, amphibians may have greater ability to persist than is generally assumed. Phylogeographic studies of widespread amphibians south of the borders of Pleistocene glaciation have consistently found geographically structured genetic variation, which is clear evidence that populations have persisted for tens to hundreds of thousands of years through cycles of climate change (*16*). Hence, effects of climate change on amphibians may be less predictable than projected in recent research (*8*, *13*).

The main message of the new research on amphibians is that there are additive threats from multiple forcers. This has serious implications. Whether we are studying long-term climatic trends, changes in populations, patterns in human behavior, interactions among diverse factors in infectious disease ecology, or mitigation of stressors, integrative approaches in conservation biology, ecology, and ultimately evolution are essential for understanding and countering the threat to amphibians.

References

1. D. B. Wake, *Science* **253**, 860 (1991).
2. S. N. Stuart *et al*., *Science* **306**, 1783 (2004).
3. L. Berger *et al*., *Proc. Natl. Acad. Sci. U.S.A.* **95**, 9031 (1998).
4. J. Voyles, E. B. Rosenblum, L. Berger, *Microbes Infect.* **13**, 25 (2011).
5. A. J. Crawford, K. R. Lips, E. Bermingham, *Proc. Natl. Acad. Sci. U.S.A.* **107**, 13777 (2010).
6. K. R. Lips, J. Diffendorfer, J. R. Mendelson, M. W. Sears, *PLoS Biol.* **6**, e72 (2008).
7. T. L. Cheng, S. M. Rovito, D. B. Wake, V. T. Vredenburg, *Proc. Natl. Acad. Sci. U.S.A.* **108**, 9502 (2011).
8. C. Hof, M. B. Araújo, W. Jetz, C. Rahbek, *Nature* **480**, 516 (2011).
9. R. A. Farrer *et al*., *Proc. Natl. Acad. Sci. U.S.A.* **108**, 18732 (2011).
10. C. J. Briggs, R. A. Knapp, V. T. Vredenburg, *Proc. Natl. Acad. Sci. U.S.A.* **107**, 9695 (2010).
11. V. T. Vredenburg, R. A. Knapp, T. S. Tunstall, C. J. Briggs, *Proc. Natl. Acad. Sci. U.S.A.* **107**, 9689 (2010).
12. D. C. Woodhams *et al*., *Front. Zool.* **8**, 8 (2011).
13. R. Early, D. F. Sax, *Ecol. Lett.* **14**, 1125 (2011).
14. D. B. Wake, V. T. Vredenburg, *Proc. Natl. Acad. Sci. U.S.A.* **105** (suppl. 1), 11466 (2008).
15. S. M. Rovito, G. Parra-Olea, C. R. Vásquez-Almazán, T. J. Papenfuss, D. B. Wake, *Proc. Natl. Acad. Sci. U.S.A.* **106**, 3231 (2009).
16. I. Martínez-Solano, E. L. Jockusch, D. B. Wake, *Mol. Ecol.* **16**, 4335 (2007).

10.1126/science.1218364

CHEMISTRY

Roaming Reaction Pathways Along Excited States

The photodissociation of NO_3 into NO and O_2, an important atmospheric reaction, has no transition state but proceeds via an O atom roaming around the NO_2 core.

Meredith J. T. Jordan and Scott H. Kable

Transition state theory (TST) describes chemical reactions in terms of "reaction coordinates," usually the coordinates of atoms involved in breaking and forming bonds. Typically, there is an energetic barrier, the transition state (TS), between reactants and products. In 2004, a reaction mechanism was reported that seemingly defied the tenets of TST (*1*). In the photodissociation of H_2CO, one of the hydrogen (H) atoms "roamed" around the periphery of the HCO core, with no apparent reaction coordinate, and abstracted the other H atom to form H_2 and CO. The roaming products showed characteristic product-state distributions, distinct from those arising from a standard TS mechanism. On page 1075 of this issue, Grubb *et al*. (*2*) use detailed state-selective correlated experiments, together with theoretical calculations, to show that the photodissociation of NO_3 into NO and O_2, an important reaction in the atmosphere, occurs via roaming reactions on both the electronic excited state and the ground state of NO_3.

Roaming reactions are at odds with the simple TST picture of chemical reactivity. Since 2004, roaming has been implicated in dozens of photochemical reactions, in thermal reactions, and in shock tube studies (*3*). Indeed, a consensus is emerging that any barrierless bond-cleavage process might have a roaming mechanism alongside.

The NO_3 radical studied by Grubb *et al*. is an important oxidant in atmospheric chemical cycles. During the day, NO_3 is rapidly photolyzed, forming either NO_2 and O (reaction 1) or NO and O_2 (reaction 2):

$$NO_3 \rightarrow NO_2 + O \quad (1)$$
$$\rightarrow O_2 + NO \text{ (low rotation)} \quad (2a)$$
$$\rightarrow O_2 + NO \text{ (high rotation)} \quad (2b)$$

Reaction 1 is a straightforward barrierless N–O bond cleavage (*4*). The mechanism for reactional 2, however, has remained a mystery. No TS has been found at photon energies of relevance in the atmosphere. To add to the mystery, reaction 2 shows two distinct product state distributions, suggesting two distinct pathways (*5*). In reaction 2a, the NO is in a low rotational state, and the excess energy is carried by a highly vibrationally excited O_2. In reaction 2b, the excess energy is carried by a highly rotationally excited NO, and the O_2 is vibrationally cold. The product-state distributions from reaction 2a have the same characteristics as the roaming reaction in H_2CO photolysis (*1*, *5*), which suggests that a similar roaming mechanism on the ground (X) state of NO_3 is responsible. Reaction 2b had been thought to arise from an undiscovered TS. Recently, however, it was proposed that roaming in the first excited (A) electronic state of NO_3 might be responsible (*6*).

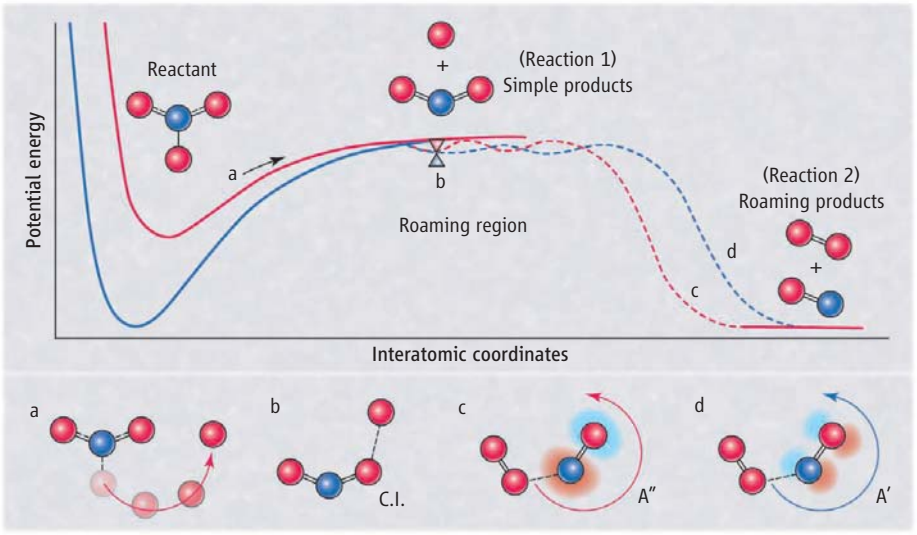

Where the O atoms roam. The schematic shows the energetics of the formation of products of NO_3 photodissociation from roaming on two electronic states. The structures corresponding to various points along the reaction (a to d) are shown below. (a) An O atom almost dissociating to NO_2 + O, but instead roaming around the core on the excited state in the van der Waals region. There is a conical intersection (C.I.) in the roaming region, which extensively mixes the ground and excited states (b). From here, the system can return to reactant in either state or produce products on either state. The A″ and A′ Λ-doublet states of the NO product (c and d) reveal which electronic state is responsible for the molecular products.

The pathways from the X and A states to products formed by reaction 1 and the roaming products formed by reaction 2a and reaction 2b are shown in the figure (the ground state in blue and the excited state in red). Photoexcitation results in rapid production of NO_3 in the A state (*6*). Slightly below the NO_2 + O asymptote is the roaming region, shown as dashed lines.

If the incipient O + NO_2 products have insufficient relative translational energy, the O atom roams around the NO_2 core in the region of van der Waals contact (see a in the figure). Morokuma and co-workers have identified several local minima and transition states in this region on both X and A states (*6*), illustrated by the wavy lines. They also identified a conical intersection (C.I.) in the roaming region that facilitates efficient internal conversion between the two electronic states (see b in the figure). Roaming pathways on both states lead to the same products, so the experimental challenge was to distinguish the two mechanisms.

Fortunately, NO_3 is a radical with an unpaired electron, and Grubb *et al*. used the alignment of this electron (in the pπ orbital of the NO fragment of NO_3) as a fingerprint of roaming on the X and A states (*5*). When the departing NO fragment spins away from its O_2 partner, the lobe of the pπ orbital may lie in, or out of, the NO plane of rotation (see c and d in the figure). These are manifest as spectroscopically distinct Λ-doublet states of the free NO radical. Grubb *et al*. found that reaction 2b (rotationally excited

School of Chemistry, University of Sydney, Sydney, NSW, 2006 Australia. E-mail: scott.kable@sydney.edu.au; m.jordan@chem.usyd.edu.au

Published by AAAS

NO) was associated almost exclusively with the A″ Λ-doublet state (see d in the figure), which is consistent only with reaction on the excited electronic state. NO formed via reaction 2a (rotationally cold) had a larger contribution from the A′ Λ-doublet component (d), in agreement with theoretical predictions for reaction on the ground state. Thus, all atmospheric production of NO + O_2 from NO_3 is mediated by roaming O atoms.

Grubb *et al*. not only solve a long-standing puzzle in atmospheric chemistry but also demonstrate roaming on an excited electronic state, which may be observed in other reactions. We can reflect on what properties of the A state of NO_3 might be important in supporting roaming. First, because of symmetry restrictions, the A state cannot radiate back to the ground state. Second, the only energetically accessible conical intersections between the A and X states are in the roaming region of configuration space. (*6*). Third, the A state is nested inside the X state and correlates with the same asymptotic products; no repulsive states cross the A state. These three factors together mean that the A state is metastable, and this long lifetime is likely to be crucial for roaming.

Roaming on the X and A states involves very large excursions on the potential energy surfaces in regions where the difference in electronic energy is very small. These dynamics are ripe for the breakdown of the Born-Oppenheimer approximation. Recently, roaming was also implicated in photoisomerization (*7*). If roaming contributes to dissociation, isomerization, and nonradiative curve crossings, and is as ubiquitous as it appears, then the challenge to incorporate roaming into reaction schemes and kinetic models is considerable indeed.

References

1. D. Townsend *et al*., *Science* **306**, 1158 (2004).
2. M. P. Grubb *et al*., *Science* **335**, 1075 (2012).
3. J. M. Bowman, B. C. Shepler, *Annu. Rev. Phys. Chem.* **62**, 531 (2011).
4. H. F. Davis *et al*., *J. Phys. Chem.* **97**, 2172 (1993).
5. M. P. Grubb *et al*., *J. Phys. Chem. A* **115**, 3218 (2011).
6. H. Xiao *et al*., *J. Phys. Chem. Lett.* **2**, 934 (2011).
7. M. L. Hause *et al*., *Nat. Chem.* **3**, 932 (2011).

10.1126/science.1218767

CELL SIGNALING

Structural Origins of Receptor Bias

Agonists can elicit pathway-specific conformational changes in a G protein–coupled receptor.

Stephen R. Sprang and Jackson Chief Elk

Humans express more than 800 G protein–coupled receptors (GPCRs), through which myriad physiological, immune, and neurophysiological processes are regulated (*1*). These receptors are embedded in the cell's plasma membrane and bind to extracellular chemical stimuli (agonists). This interaction induces conformational changes in the receptor that converge at intracellular sites that bind to either heterotrimeric guanine nucleotide–binding proteins (G proteins) or to β-arrestin proteins that block G protein binding and lead to receptor desensitization and internalization, as well as provide a scaffold for protein regulatory complexes that control gene expression (*2*). Many agonists induce functionally selective or biased states of the receptor, wherein one pathway is activated with greater efficacy than another (*3*). Thus, GPCRs are not simple on-off switches, but can adopt multiple conformational states to control diverse processes. On page 1106 of this issue, Liu *et al*. (*4*) provide clues as to how a GPCR called the β_2-adrenergic receptor (β_2AR) can tune its conformation to achieve a balance of functional outcomes, as directed by the chemical structure of the receptor agonist.

Like all GPCRs, the polypeptide chain of the β_2AR traverses back and forth across the membrane, forming a series of seven-transmembrane (TM) α helices (see the figure). Ligands occupy a site that is deep within the receptor but accessible to the extracellular environment. Adrenergic receptor agonists are typically composed of a cyclic aromatic "head" group and an alkyl-amine "tail." Crystal structure analyses of the β_1AR and β_2AR reveal that the head group reinforces contacts between TM5 and TM6, whereas the amine substituent stabilizes interactions between TM3 and TM7 (*5*, *6*). Conformational changes upon ligand binding follow a common theme in the three activated GPCRs, including the β_2AR, that have so far been crystallized (*7*–*9*). Local structural perturbations induced by agonist binding are transduced into a concerted outward displacement of TM5 and TM6, which opens a pocket on the intracellular surface of the receptor that accepts the G protein. Binding of β-arrestin to GPCRs requires the addition of phosphate groups at specific sites on the intracellular surface of the receptor by GPCR protein kinases. This phosphorylation occurs at a separate site, beyond TM7, toward the C terminus of the receptor. Structural changes

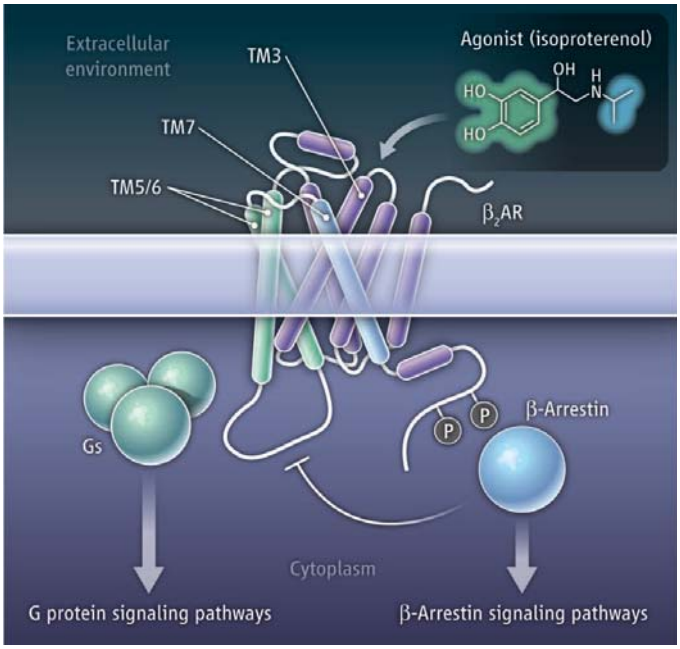

Functionally selective. Binding of agonists to the β_2AR results in conformational changes that displace TM5 and TM6 (green) and/or TM7 (blue). The conformational changes permit G protein (Gs) binding or receptor phosphorylation (P) and β-arrestin binding. β-arrestin binding blocks G protein signaling. The aromatic moiety of the agonist (isoproterenol shown) contacts TM5 and TM6, whereas the hydroxylamine substituent interacts with TM3 and TM7.

CREDIT: C. BICKEL/*SCIENCE*

Center for Biomolecular Structure and Dynamics, University of Montana, Missoula, MT 59812, USA. E-mail: stephen.sprang@umontana.edu

Published by AAAS

at the intracellular side of TM6 and TM7 would therefore be diagnostic of ligands that show selective agonism toward G protein or β-arrestin signaling pathways.

To monitor the structural consequences of agonist binding, Liu *et al*. attached fluorine-19 (^{19}F) probes to cysteine residues at the intracellular ends of TM6 and TM7. The nuclear magnetic resonance (NMR) spectrum of ^{19}F is sensitive to its chemical environment and to the dynamic behavior of the site to which it is attached. The spectra revealed that TM6 and TM7 are each in equilibrium between two distinct conformations in the basal, ligand-free state of the receptor. By correlating the relative population in each state with agonist potency, the authors could assign each spectral component to either the active or inactive state for G protein and for β-arrestin pathway activation.

Most ligands induced roughly equivalent shifts toward activating TM6 or TM7 according to their relative potency. A particularly informative antagonist, carvedilol, induced a strong shift toward the TM7 active state but had little effect on the conformational equilibrium at TM6. This antagonist not only blocks G protein signaling but also induces receptor desensitization and internalization (*10*). Drugs such as carvedilol are prototypes for biased agonists that focus signaling along a specific pathway. Site-specific NMR probes like those used by Liu *et al*. provide direct structural assays to guide the design of such functionally specific ligands.

Fluorescence studies performed in the past decade had already revealed a hierarchy of discrete structural states that can be induced by agonists of varying potency (partial agonists) (*11*–*13*). The weakest agonists loosen interactions (the "ionic lock" and "toggle") that hold TM3 and TM6 in the inactive state—sufficient for coupling the receptor to a G protein. Receptor interactions with the polar substituents of the aromatic "head" group of the ligand are critical for this transduction pathway. More potent agonists also perturb the Asn-Pro-x-x-Tyr (NPxxY, where "x" is any amino acid) sequence of TM7 that permits phosphorylation of the receptor and subsequent β-arrestin binding. Substituents appended to the hydroxylamine "tail" of the ligand influence its ability to activate this pathway, large nonpolar groups being particularly effective. Supercomputers "hardwired" for molecular dynamics calculations have been used to simulate multimicrosecond trajectories of the β_2AR in the membrane (*14*). These calculations provide structural insight into spectroscopically observed intermediate agonist-bound states in which the ionic lock is broken while the transition in the NPxxY motif has not yet occurred. That certain agonists can stimulate β-arrestin, but not G protein signaling, suggests parallel rather than hierarchical modes of activation. Nevertheless, how any particular mode of agonist-receptor interaction stabilizes a unique conformational ensemble of the receptor is, for the most part, a mystery.

Agonist-induced receptor bias for G protein versus β-arrestin signaling is one of many instances of the plastic and multistate behavior characteristic of GPCRs (*15*). Many receptors couple to more than one class of G protein, and hence can drive alternative signaling pathways, depending on the chemical structure of the agonist. Dimerization between the same or different classes of receptor signaling, and allosteric modulators that bind at loci other than the agonist site, also affect GPCR function. The challenge is to construct computational models that account for the specific effects of ligands—and of other protein partners in the membrane—on the energetic landscape of receptor conformational states, to predict how these will translate into specific biological outcomes.

References

1. D. M. Rosenbaum *et al*., *Nature* **459**, 356 (2009).
2. S. K. Shenoy, R. J. Lefkowitz, *Trends Pharmacol. Sci.* **32**, 521 (2011).
3. J. D. Urban *et al*., *J. Pharmacol. Exp. Ther.* **320**, 1 (2007).
4. J. J. Liu *et al*., *Science* **335**, 1106 (2012).
5. T. Warne *et al*., *Nature* **469**, 241 (2011).
6. D. Wacker *et al*., *J. Am. Chem. Soc.* **132**, 11443 (2010).
7. P. Scheerer *et al*., *Nature* **455**, 497 (2008).
8. F. Xu *et al*., *Science* **332**, 322 (2011).
9. S. G. F. Rasmussen *et al*., *Nature* **477**, 549 (2011).
10. J. W. Wisler *et al*., *Proc. Natl. Acad. Sci. U.S.A.* **104**, 16657 (2007).
11. P. Ghanouni *et al*., *J. Biol. Chem.* **276**, 24433 (2001).
12. G. Swaminath *et al*., *J. Biol. Chem.* **280**, 22165 (2005).
13. X. Yao *et al*., *Nat. Chem. Biol.* **2**, 417 (2006).
14. R. O. Dror *et al*., *Proc. Natl. Acad. Sci. U.S.A.* **108**, 18684 (2011).
15. T. Kenakin, L. J. Miller, *Pharmacol. Rev.* **62**, 265 (2010).

10.1126/science.1219302

BEHAVIOR

Origins of Cumulative Culture

Why does human culture accumulate, but that of other species do not?

Robert Kurzban[1] and H. Clark Barrett[2]

Representations in the minds of 21st-century Londoners include concepts—derivatives trading, personal computer, suicide bomber—that could not have been entertained by their 11th-century counterparts; in contrast, we can reasonably guess that the concepts in the minds of chimpanzees and capuchins separated by centuries, or even millennia, are not very different from one another. What is it about our species that allows for the gradual accumulation of knowledge (see the figure)? On page 1114 of this issue, Dean *et al*. (*1*) take an important step toward understanding the psychological underpinnings of human cumulative culture.

A plausible answer to the above question lies in the mechanisms that humans possess—but other species lack—for acquiring information from conspecifics. For instance, humans, but not other species, imitate what others are doing from a very young age in a strikingly sophisticated way, not merely mimicking another person's particular body movements, but performing actions to accomplish the goal that the other person can be inferred to have in mind (*2*). This behavior requires complex computational machinery, including mechanisms that can make inferences about invisible intentions and goals based only on visible patterns of motion (*3*).

Researchers have made progress in understanding some of the computational mechanisms that underlie the transmission of information from one human brain to another—that is, social learning. Language acquisition is an obvious example (*4*). Advances have similarly been made in understanding aspects of the mechanisms that guide acquisition of knowledge in other domains, such as supernatural beliefs (*5*) and food choice (*6*).

One approach to such questions is to consider the relationship between form and function. A hypothesis that a given psychological mechanism has a particular function can be tested with behavioral experiments. In a classic study, Garcia and Koelling (*7*) showed that

[1]Department of Psychology University of Pennsylvania, Philadelphia, PA 19104, USA. [2]Department of Anthropology, University of California, Los Angeles, CA 90095, USA. E-mail: kurzban@psych.upenn.edu

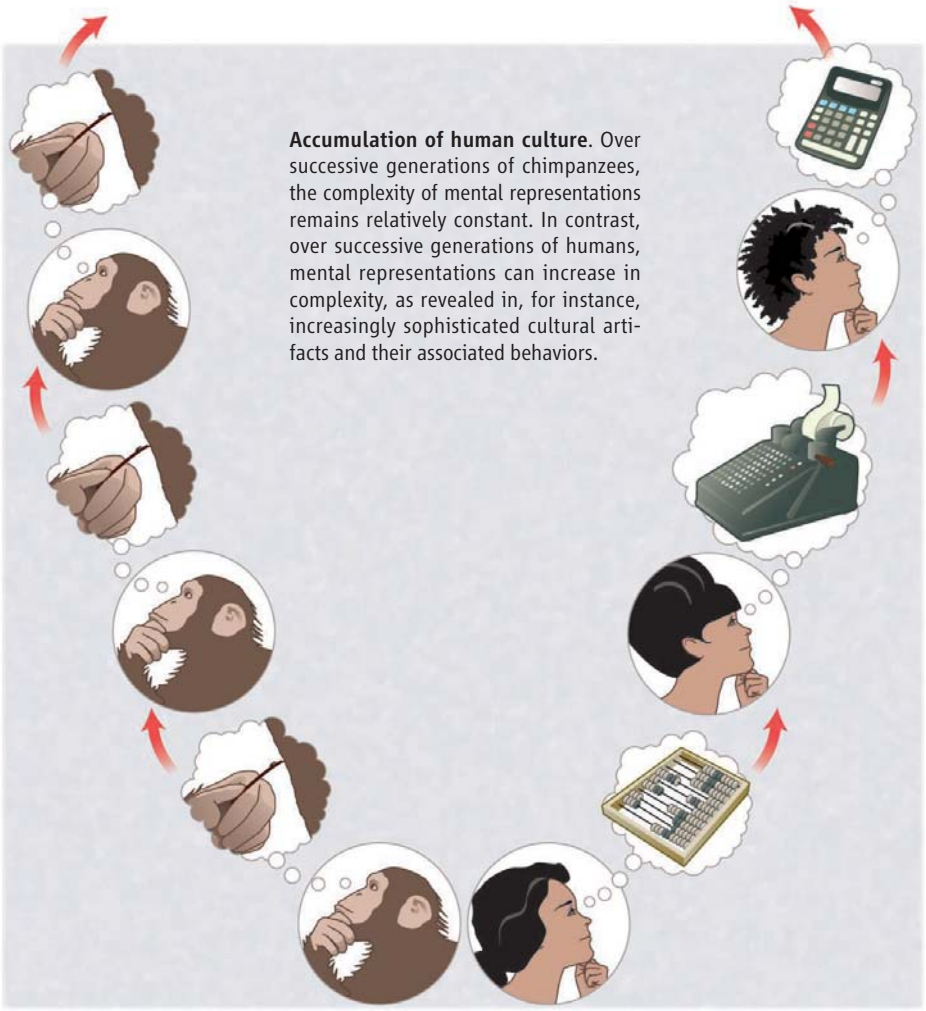

Accumulation of human culture. Over successive generations of chimpanzees, the complexity of mental representations remains relatively constant. In contrast, over successive generations of humans, mental representations can increase in complexity, as revealed in, for instance, increasingly sophisticated cultural artifacts and their associated behaviors.

CREDIT: P. HUEY/*SCIENCE*

rats more readily learn to associate a flavor with nausea than they do a visual stimulus; this observation suggests that the underlying learning mechanism was designed specifically to learn about dangerous foods rather than to form more general associations between experiences and outcomes. In humans, specialized social learning mechanisms that enable the accumulation of locally relevant knowledge might have evolved in part to facilitate survival across very different ecological conditions (*8*). Various design features have been proposed, including learning biases such as a tendency to imitate locally prestigious individuals (*6*).

Dean *et al*. took a comparative approach to identifying the mechanisms responsible for cumulative cultural evolution in humans. They used a standard method for examining social learning of a complex procedure—a puzzlebox with multiple stages—and tested human children, chimpanzees, and capuchins on the task. The authors reasoned that if a particular factor, such as imitation, is a cause of cumulative culture, then two results should be observed. First, species that imitate should perform better on the task. Second, when imitation does occur in a given species, it should be positively correlated with task performance. On the basis of their data, the authors suggest that the hypotheses that fare best are the ones that assign a key role to social cognition: pedagogy, communication, imitation, and prosociality.

This work provides many valuable new insights into the question of cumulative culture. However, the human species is unique, with its own particular package of psychological elements, and assigning subjects randomly to species is, of course, impossible. It is thus difficult to draw strong causal conclusions based on differences between humans and other primates, and the usual difficulties for inferring causality from correlational data apply. Unmeasured third variables might be responsible for both between-species differences and within-species effects.

For example, the products of the gradual accumulation of culture in humans include elaborate, hierarchically organized representations such as formal mathematics and the rules of language. Thus, a capacity to form complex concepts or other unmeasured cognitive abilities, such as skills of causal inference (*9*) or the ability to make inferences about the mental states of others (*3*), might influence both performance on the puzzlebox and the degree of imitation and pedagogy.

As an analogy, suppose that we want to know why certain birds can recall the locations of thousands of seeds while humans lack this ability (*10*). We hypothesize that the reason has to do with flying ability. We present humans and Clark's nutcrackers with a caching task, measuring how many seeds were recovered in a minute, and find that the humans do poorly while the birds excel. We also observe a positive correlation between flying ability and performance among the nutcracker group. Would we conclude that these data support the hypothesis that flying is necessary for the evolution of excellent spatial memory capacity?

Moreover, it seems likely that gradual accumulation of knowledge requires a number of computational mechanisms, and that these mechanisms evolved in some complex sequence over time, each system influencing the evolution of other systems. In that case, adaptations currently part of the set of human mental capacities may or may not be responsible for the initial evolutionary divergence of human cultural capacities. In short, finding psychological differences between species in the present does not in itself afford the inference that these differences led to divergence in the domain in question.

Ratcheting cultural evolution is a milestone of human evolution, setting us apart from all other species. In a few tens of thousands of years, humans have gone from a relatively small population of Pleistocene hominins to a globally dominant species, aided mightily by our abilities of cultural transmission and the increasingly elaborate cultural products to which these abilities give rise. These abilities explain, in part, the cultural evolution of scientific methods that allow us to test hypotheses about our own evolution, such as those explored by Dean *et al*.

References

1. L. G. Dean, R. L. Kendal, S. J. Schapiro, B. Thierry, K. N. Laland, *Science* **335**, 1114 (2012).
2. G. Gergely, H. Bekkering, I. Király, *Nature* **415**, 755 (2002).
3. R. Saxe, *Curr. Opin. Neurobiol.* **16**, 235 (2006).
4. P. Bloom, *How Children Learn the Meanings of Words* (MIT Press, Cambridge, MA, 2000).
5. P. Boyer, *Am. Anthropol.* **100**, 876 (1998).
6. M. Chudek, S. Heller, S. Birch, J. Henrich, *Evol. Hum. Behav.* **33**, 46 (2012).
7. J. Garcia, R. A. Koelling, *Psychon. Sci.* **4**, 123 (1966).
8. P. Richerson, R. Boyd, *Not by Genes Alone: How Culture Transformed Human Evolution* (Univ. of Chicago Press, Chicago, 2005).
9. A. Gopnik *et al*., *Psychol. Rev.* **111**, 3 (2004).
10. R. P. Balda, A. C. Kamil, *Anim. Behav.* **44**, 761 (1992).

10.1126/science.1219232

The Geological Record of Ocean Acidification

Bärbel Hönisch,[1]* Andy Ridgwell,[2] Daniela N. Schmidt,[3] Ellen Thomas,[4,5] Samantha J. Gibbs,[6] Appy Sluijs,[7] Richard Zeebe,[8] Lee Kump,[9] Rowan C. Martindale,[10] Sarah E. Greene,[2,10] Wolfgang Kiessling,[11] Justin Ries,[12] James C. Zachos,[13] Dana L. Royer,[5] Stephen Barker,[14] Thomas M. Marchitto Jr.,[15] Ryan Moyer,[16] Carles Pelejero,[17] Patrizia Ziveri,[18,19] Gavin L. Foster,[6] Branwen Williams[20]

Ocean acidification may have severe consequences for marine ecosystems; however, assessing its future impact is difficult because laboratory experiments and field observations are limited by their reduced ecologic complexity and sample period, respectively. In contrast, the geological record contains long-term evidence for a variety of global environmental perturbations, including ocean acidification plus their associated biotic responses. We review events exhibiting evidence for elevated atmospheric CO_2, global warming, and ocean acidification over the past ~300 million years of Earth's history, some with contemporaneous extinction or evolutionary turnover among marine calcifiers. Although similarities exist, no past event perfectly parallels future projections in terms of disrupting the balance of ocean carbonate chemistry—a consequence of the unprecedented rapidity of CO_2 release currently taking place.

The geological record is imprinted with numerous examples of biotic responses to natural perturbations in global carbon cycling and climate change (Fig. 1), some of which could have been caused by large-scale ocean acidification. By reconstructing past changes in marine environmental conditions, we can test hypotheses for the causes and effects of future-relevant stressors such as ocean acidification on ecosystems (*1*). However, for the fossil record to be of direct utility in assessing future ecosystem impacts, the occurrence and extent of past ocean acidification must be unambiguously identified. In recent years, a variety of trace-element and isotopic tools have become available that can be applied to infer past seawater carbonate chemistry. For instance, the boron isotopic composition ($\delta^{11}B$) of marine carbonates reflects changes in seawater pH, the trace element (such as B, U, and Zn)–to-calcium ratio of benthic and planktic foraminifer shells records ambient [CO_3^{2-}], and the stable carbon isotopic composition ($\delta^{13}C$) of organic molecules (alkenones) can be used to estimate surface ocean aqueous [CO_2] (*2*).

Because direct ocean geochemical proxy observations are still relatively scarce, past ocean acidification is often inferred from a decrease in the accumulation and preservation of $CaCO_3$ in marine sediments, potentially indicated by an increased degree of fragmentation of foraminiferal shells (*3*). However, it is difficult to distinguish between the original calcification responses to chemical changes in the surface ocean and post-mortem conditions at the sea floor. For instance, planktic calcifiers may secrete heavier or lighter shells (*4*), but that signal may be modified at the sea floor through dissolution or overgrowth after deposition (*5*, *6*). This duality can introduce controversy over the identification of causes and effects, the drivers of biological change, and

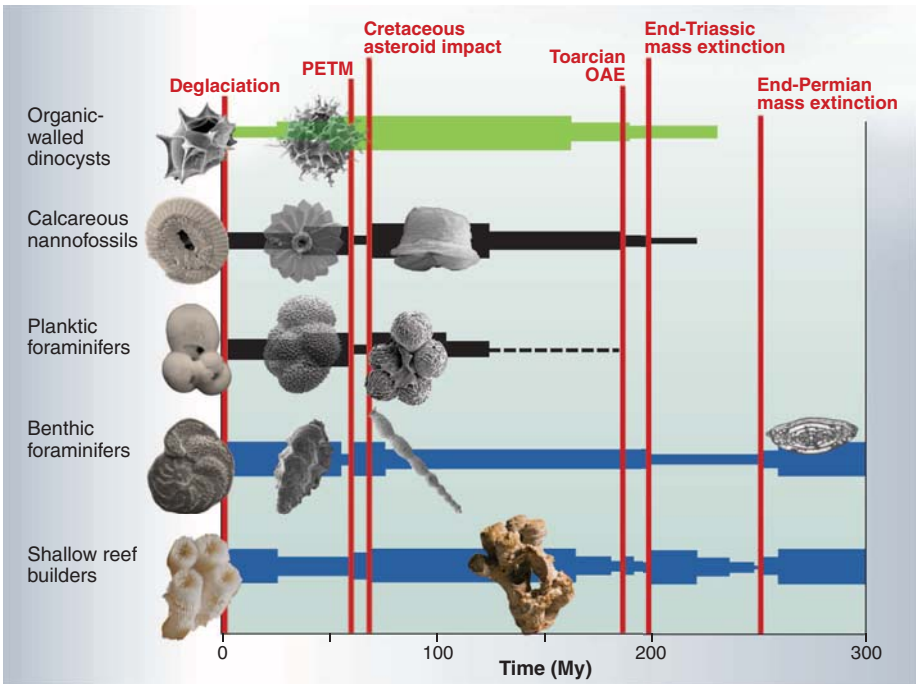

Fig. 1. Idealized diversity trajectories of the calcareous and organic fossil lineages discussed in the text. Extinction and radiation suggest events of major environmental change throughout the past 300 My. Calcareous plankton is shown in black, calcareous benthos in blue, and organic fossils in green, and the line thickness indicates relative and smoothed species richness. Highlighted events (vertical red lines) have been associated with potential ocean acidification events (Fig. 4). Calcareous organisms were not uniformly affected at all times, suggesting the importance of synergistic environmental factors to extinction, adaptation, and evolution as well as different sensitivity due to physiological factors. Identification of a paleo-ocean acidification event therefore requires independent geochemical evidence for ocean chemistry changes. Images of organisms are exemplary. References and further information on the displayed organisms are available in the supporting online material.

[1]Lamont-Doherty Earth Observatory of Columbia University, Palisades, NY 10964, USA. [2]School of Geographical Sciences, University of Bristol, Bristol BS8 1SS, UK. [3]School of Earth Sciences, University of Bristol, Bristol, BS8 1RJ, UK. [4]Department of Geology and Geophysics, Yale University, New Haven, CT 06520, USA. [5]Department of Earth and Environmental Sciences, Wesleyan University, Middletown, CT 06459, USA. [6]Ocean and Earth Science, National Oceanography Centre Southampton, University of Southampton, Southampton SO14 3ZH, UK. [7]Department of Earth Sciences, Utrecht University, 3584 CD Utrecht, Netherlands. [8]School of Ocean and Earth Science and Technology, Department of Oceanography, University of Hawaii at Manoa, Honolulu, HI 96822, USA. [9]Department of Geosciences, Pennsylvania State University, University Park, PA 16802, USA. [10]Department of Earth Sciences, University of Southern California (USC), Los Angeles, CA 90089, USA. [11]Museum für Naturkunde at Humboldt University, 10115 Berlin, Germany. [12]Department of Marine Sciences, University of North Carolina–Chapel Hill, NC 27599, USA. [13]Earth and Planetary Sciences Department, University of California Santa Cruz, CA 95064, USA. [14]School of Earth and Ocean Sciences, Cardiff University, Cardiff CF10 3AT, UK. [15]Department of Geological Sciences and Institute of Arctic and Alpine Research, University of Colorado, Boulder, CO 80309, USA. [16]University of South Florida St. Petersburg, Department of Environmental Science, Policy, and Geography, St. Petersburg, FL 33701, USA. [17]Institució Catalana de Recerca i Estudis Avançats and Department of Marine Biology and Oceanography, Consejo Superior de Investigaciones Científicas, 08003 Barcelona, Catalonia, Spain. [18]Institute of Environmental Science and Technology, Universitat Autònoma de Barcelona, 01893 Barcelona, Spain. [19]Department of Earth Sciences, Vrije Universiteit, 1081HV Amsterdam, Netherlands. [20]W. M. Keck Science Department of Claremont McKenna College, Pitzer College, and Scripps College, Claremont, CA 91711, USA.

*To whom correspondence should be addressed. E-mail: hoenisch@ldeo.columbia.edu

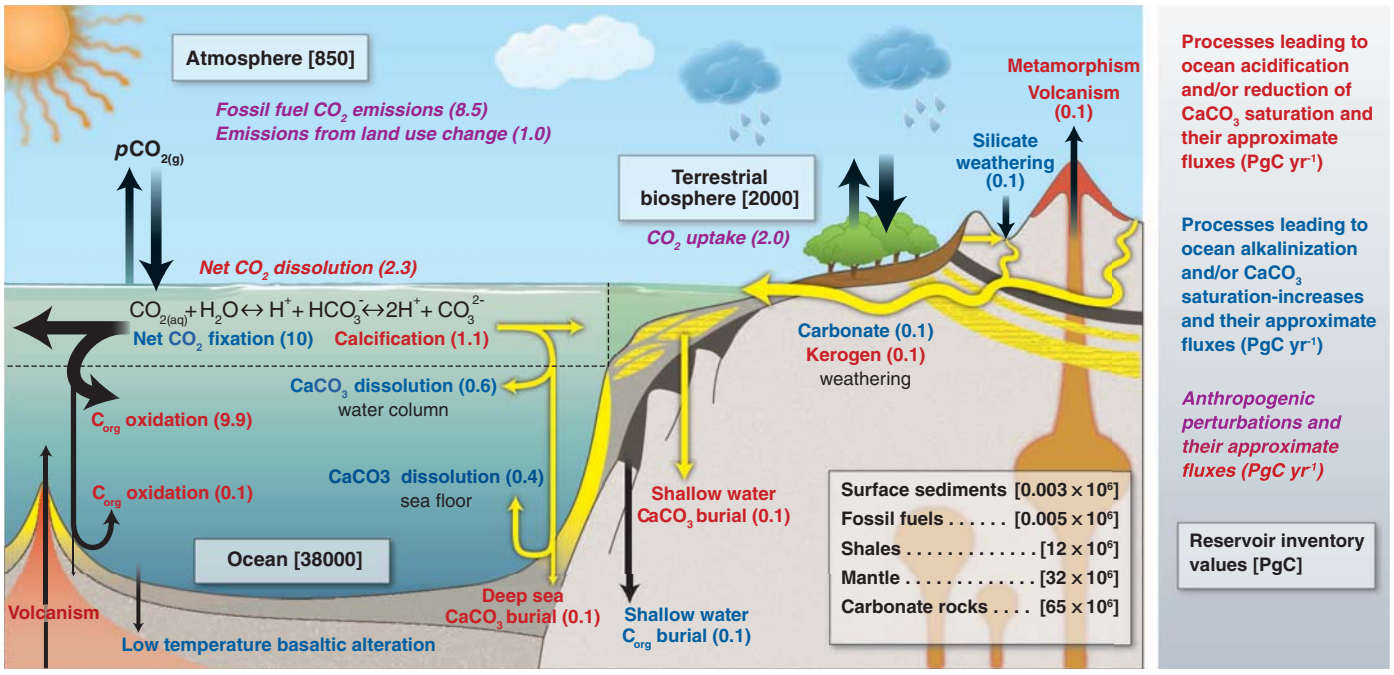

Fig. 2. When CO_2 dissolves in seawater, it reacts with water to form carbonic acid, which then dissociates to bicarbonate, carbonate, and hydrogen ions. The higher concentration of hydrogen ions makes seawater acidic, but this process is buffered on long time scales by the interplay of seawater, seafloor carbonate sediments, and weathering on land. Shown are the major pathways of reduced carbon (black) and of alkalinity (yellow). Processes leading to ocean acidification and/or reduction of $CaCO_3$ saturation are indicated in red, and processes leading to ocean alkalinization and/or $CaCO_3$ saturation increases are indicated in blue. Anthropogenic perturbations are marked in italics. Approximate fluxes are printed in parentheses (PgC year^{-1}), whereas reservoir inventory values are shown in brackets [PgC]. Natural carbon cycle fluxes are from (*70*); anthropogenic fluxes for 2008 are from (*57*), which for the land sink is significantly above its 1990–2000 average of 2.6 PgC year^{-1} due to the 2008 La Niña state (*8*).

whether past intervals of ocean acidification are characterized by environmental conditions relevant for the near future. Coeval changes in ocean circulation will also introduce regional biases in proxy records and hence affect global interpretations.

Here, we review the factors controlling ocean acidification, describe evidence for the occurrence of ocean acidification events in the past, and discuss the potential as well as weaknesses of the geological record in helping us predict future ecosystem changes.

Is Ocean Acidification Primarily a pH-Decline Phenomenon?

The current rate of anthropogenic CO_2 release leads to a surface ocean environment characterized not only by elevated dissolved CO_2 and decreased pH (*7*) but, critically, decreased saturation with respect to calcium carbonate ($CaCO_3$), a compound widely used by marine organisms for the construction of their shells and skeletons (*8*). In contrast, slower rates of CO_2 release lead to a different balance of carbonate chemistry changes and a smaller seawater $CaCO_3$ saturation response, which may induce differential biotic response or even no response at all, invalidating a direct analog. The reason for a smaller saturation response to slow CO_2 release is that the alkalinity released by rock weathering on land must ultimately be balanced by the preservation and burial of $CaCO_3$ in marine sediments (Fig. 2), which itself is controlled by the calcium carbonate saturation state of the ocean (*9*). Hence, $CaCO_3$ saturation is ultimately regulated primarily by weathering on long time scales, not atmospheric partial pressure of CO_2 (P_{CO_2}). While weathering itself is related to atmospheric P_{CO_2} (*10*), it is related much more weakly than ocean pH, which allows pH and $CaCO_3$ saturation to be almost completely decoupled for slowly increasing atmospheric P_{CO_2}.

Using a global carbon cycle model (*2*), we show the progressive coupling between $CaCO_3$ saturation and pH as the rate of CO_2 emissions increases and sources (weathering) and sinks ($CaCO_3$ burial) of alkalinity are no longer balanced. For rapid century-scale and thus future-relevant increases in atmospheric P_{CO_2}, both surface ocean pH and saturation state decline in tandem (Fig. 3). The projected decrease in ocean surface saturation state—here, with respect to aragonite ($\Omega_{aragonite}$)—is an order of magnitude larger for a rapid CO_2 increase than for a slow [100 thousand years (ky)] CO_2 increase. Ultimately, saturation recovers while the pH remains suppressed, reflecting how changes in the oceanic concentrations of dissolved inorganic carbon (DIC) and alkalinity make it possible to have simultaneously both high CO_2 and high carbonate ion concentration saturation ($[CO_3^{2-}]$, which controls saturation), but with the relatively greater increase in $[CO_2]$ causing lower pH. The key to unlocking the geological record of ocean acidification is hence to distinguish between long-term steady states and transient changes. We use the term "ocean acidification event" for time intervals in Earth's history that involve both a reduction in ocean pH and a substantial lowering of $CaCO_3$ saturation, implying a time scale on the order of 10,000 years and shorter (Fig. 3).

Indications of Paleo-Ocean Acidification

With these criteria in mind, we review (in reverse chronological order) the intervals in Earth's history for which ocean acidification has been hypothesized, along with the evidence for independent geochemical and biotic changes. We confine this review to the past ~300 million years (My) because the earlier Phanerozoic (and beyond) lacks the pelagic calcifiers that not only provide key proxy information but also create the strong deep-sea carbonate (and hence atmospheric P_{CO_2}) buffer that characterizes the modern Earth system (*9*). Our criteria for identifying potentially future-relevant past ocean acidification are (i) massive CO_2 release, (ii) pH decline, and (iii) saturation decline. We also discuss evidence for the time scale of CO_2 release, as well as for global warming. Events are given a similarity index that is based on available geochemical data (table S1) and are indicated in Fig. 4A.

Late Pleistocene deglacial transitions. The last deglaciation is the best documented past event associated with a substantive (30%) CO_2 rise: 189 to 265 μatm between 17.8 to 11.6 ky before

the present (B.P.) (*11*). Boron isotope estimates from planktic foraminifers show a 0.15 ± 0.05 unit decrease in sea surface pH (*12*) across the deglacial transition—an average rate of decline of ~0.002 units per 100 years compared with the current rate of more than 0.1 units per 100 years (table S1). Planktic foraminiferal shell weights decreased by 40 to 50% (*4*), and coccolith mass decreased by ~25% (*13*). In the deep ocean, changes in carbonate preservation (*14*), pH [from foraminiferal $\delta^{11}B$ (*15*)] and [CO_3^{2-}] [from foraminiferal B/Ca and Zn/Ca (*16*, *17*)] differed between ocean basins, reflecting covarying changes in deep-water circulation and an internal carbon shift within the ocean. The regional nature of these variations highlights the general need for careful evaluation of regional versus global effects in paleo-studies.

Oligocene–Pliocene. The climate of the Oligocene to Pliocene [34 to 2.6 million years ago (Ma)] contains intervals of elevated temperature and modest deviations of atmospheric P_{CO_2} from modern values (Fig. 4). Of particular interest has been the Pliocene warm period [3.29 to 2.97 Ma (*18*, *19*)], which is characterized by global surface temperatures estimated to be ~2.5°C higher than today (*19*), atmospheric P_{CO_2} between 330 to 400 µatm (Fig. 4C) (*18*, *20*), and sea surface $pH_{(T)}$ ~0.06 to 0.11 units lower (*18*) than the preindustrial. Ecological responses to the warming include migration of tropical foraminifer species toward the poles (*21*), but there are no documented calcification responses or increased nannoplankton extinction rates (*22*). The early to middle Miocene (23 to 11 Ma) and Oligocene (34 to 23 Ma) were also characterized periods of elevated temperatures and slightly higher P_{CO_2} compared with preindustrial values (Fig. 4C) but, because of their long duration, were not associated with changes in $CaCO_3$ saturation (Fig. 3C).

Paleocene–Eocene. Evidence for rapid carbon injection associated with the Paleocene–Eocene Thermal Maximum (PETM, 56 Ma) as well as a number of smaller transient global warming events (hyperthermals) during the late Paleocene and early Eocene (58 to 51 Ma) comes primarily from observations of large [up to –4 per mil (‰)] negative $\delta^{13}C$ excursions (*23*) associated with pronounced decreases in calcium carbonate preservation (*24*). Depending on the assumed source, rate, and magnitude of CO_2 release (*25*), a 0.25 to 0.45 unit decline in surface seawater pH is possible, with a reduction in mean surface ocean aragonite saturation from $\Omega = 3$ down to 1.5 to 2 (*1*). The calcite compensation depth (CCD) (*8*) rose by ~2 km to shallower than 1.5 km in places (*24*) (compared with >4 km today). Although a pH decrease or P_{CO_2} increase remains to be confirmed by geochemical proxies for any of the hyperthermal events, the amount of carbon injected can be modeled on the basis of consistent carbonate $\delta^{13}C$ and CCD changes, yielding between ~2000 and 6000 PgC for the onset of the PETM (*26*, *27*). However, as with the last glacial transition, deep sea geochemistry appears strongly modulated by regional ocean circulation changes (*28*), which adds an additional layer of complexity to global extrapolation and highlights the importance of adequate spatial coverage of the data.

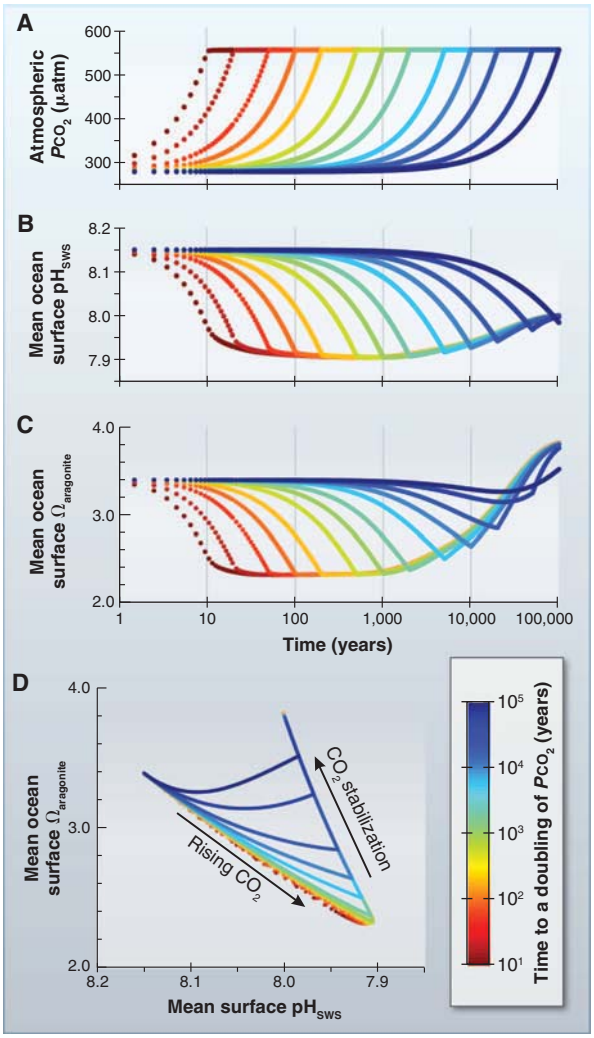

Fig. 3. The trajectories of mean ocean surface pH and aragonite saturation ($\Omega_{aragonite}$) become progressively decoupled as the rate of atmospheric P_{CO_2} change increases. The four panels show the results of a series of experiments in an Earth system model (*2*). (**A**) Prescribed linear increases of atmospheric P_{CO_2} (on a $\log_{10}$ scale) from ×1 to ×2 preindustrial CO_2, with the different model experiments spanning a range of time scales (but experiencing the same ultimate CO_2 change). (**B**) Evolution of mean surface pH in response to rising CO_2. (**C**) Evolution of mean surface $\Omega_{aragonite}$. (**D**) A cross-plot illustrating how $\Omega_{aragonite}$ is progressively decoupled from pH as the rate of P_{CO_2} increase slows, with future-relevant rate of P_{CO_2} increase showing a diagonal trajectory from top left to bottom right, whereas slow P_{CO_2} increases result in an almost horizontal trajectory toward lower pH with very little saturation change. All plots are color-coded from red ("fast") to blue ("slow"). These model results include both climate and long-term (silicate) weathering feedback. See (*2*) and fig. S1 for the role of these and other feedbacks.

PETM sediments record the largest extinction among deep-sea benthic foraminifers of the past 75 My (*29*), and a major change in trace fossils indicates a disruption of the macrobenthic community (*30*). However, the covariation of ocean acidification, warming, and corresponding oxygen depletion (fig. S2) (*23*) precludes the attribution of this extinction to a single cause (*1*, *29*). In shallow water environments, a gradual shift from calcareous red algae and corals to larger benthic foraminifers as dominant calcifiers started in the Paleocene and was completed at the PETM with the collapse of coralgal reefs and larger benthic foraminiferal turnover (*31*). This event is recognized as one of the four major metazoan reef crises of the past 300 My (Fig. 1) (*32*). In marginal marine settings, coccolithophore (*33*) and dinoflagellate cyst (*34*) assemblages display changes in species composition, but these are interpreted to reflect sensitivity to temperature, salinity stratification, and/or nutrient availability (*34*, *35*), not necessarily acidification (fig. S2). In the open ocean, the occurrence of deformities in some species of calcareous nannoplankton has been described (*36*), but despite a strong change in assemblages, there is no bias in extinction or diversification in favor of or against less or more calcified planktic species (*37*).

Cretaceous and Cretaceous-Paleogene. The well-known mass extinction at 65 Ma is generally accepted to have been triggered by a large asteroid impact (*38*). In addition to potential terrestrial biomass or fossil carbon burning, the impact may have caused the emission of SO_2 from vaporized gypsum deposits at the impact site and/or nitric acid aerosols produced by shock heating of the atmosphere, which could have led to acid rain and hence potentially to rapid acidification of the surface ocean (*38*). Although planktic calcifiers exhibited elevated rates of extinction and reduced production (*22*, *39*), reef corals did not experience a major extinction (*32*), and benthic foraminifers were not affected in either shallow or deep waters (*29*). Because multiple environmental changes covaried and proxy data for marine carbonate chemistry are not yet available, unambiguous attribution of the planktic extinctions to any one driver such as ocean acidification is currently not possible.

The earlier Cretaceous (K) (Fig. 4A) is generally a time of massive chalk deposition (mainly

in the form of nannofossil calcite), as well as one of elevated P_{CO_2} (Fig. 4B) and lower pH (Fig. 4D). This association can be misconceived as evidence that marine calcification will not be impaired under conditions of low pH in the future. However, this reasoning is invalid because extended periods of high P_{CO_2} (Fig. 4B) do not necessarily result in a suppressed seawater calcite saturation state (Fig. 3) (*1*, *40*), which exerts an important control on organisms' calcification (*41*).

Cretaceous and Jurassic oceanic anoxic events. The Mesozoic oceanic anoxic events (OAEs) (in particular, OAE 2 ~93 Ma, OAE1a ~120 Ma, and Toarcian OAE ~183 Ma) were intervals during which the ocean's oxygen minimum and deep anoxic zones expanded markedly (*42*). The onsets of these OAEs have been linked to the emplacement of large igneous provinces, degassing large amounts of CO_2 and associated environmental consequences of warming, lower oxygen solubility, and possibly ocean acidification (*42*). Some of the Cretaceous OAEs were associated with turnover in plankton communities (*43*). Deformities and some minor size reduction in coccoliths, as well as a massive increase in the abundance of heavily calcified nannoconids, have been observed (*44*, *45*). However, similar to more recent events, there is difficulty in unequivocally attributing observations to surface water acidification given the covariation of environmental changes (*46*).

Because most old sea floor (~180 Ma or older) is subducted, the sedimentary record of the Toarcian OAE is now restricted to former continental margins. Sedimentary organic and inorganic carbon deposits display initially negative, followed by positive $\delta^{13}C$ excursions, which is consistent with an influx of CO_2 into the atmosphere followed by organic carbon burial (*42*). The negative isotopic transition occurs in distinct negative $\delta^{13}C$ shifts, each estimated to occur in less than 20 ky (*47*) and possibly in as little as 650 years (*48*). The Toarcian OAE is associated with a reef crisis that was particularly selective against corals and hypercalcifying sponges (animals with a large skeletal-to–organic biomass ratio) (Fig. 4B) (*32*) and with a decrease in nannoplankton flux (*49*). Again, these observations could have been a response to any one or combination of a number of different contemporaneous environmental changes.

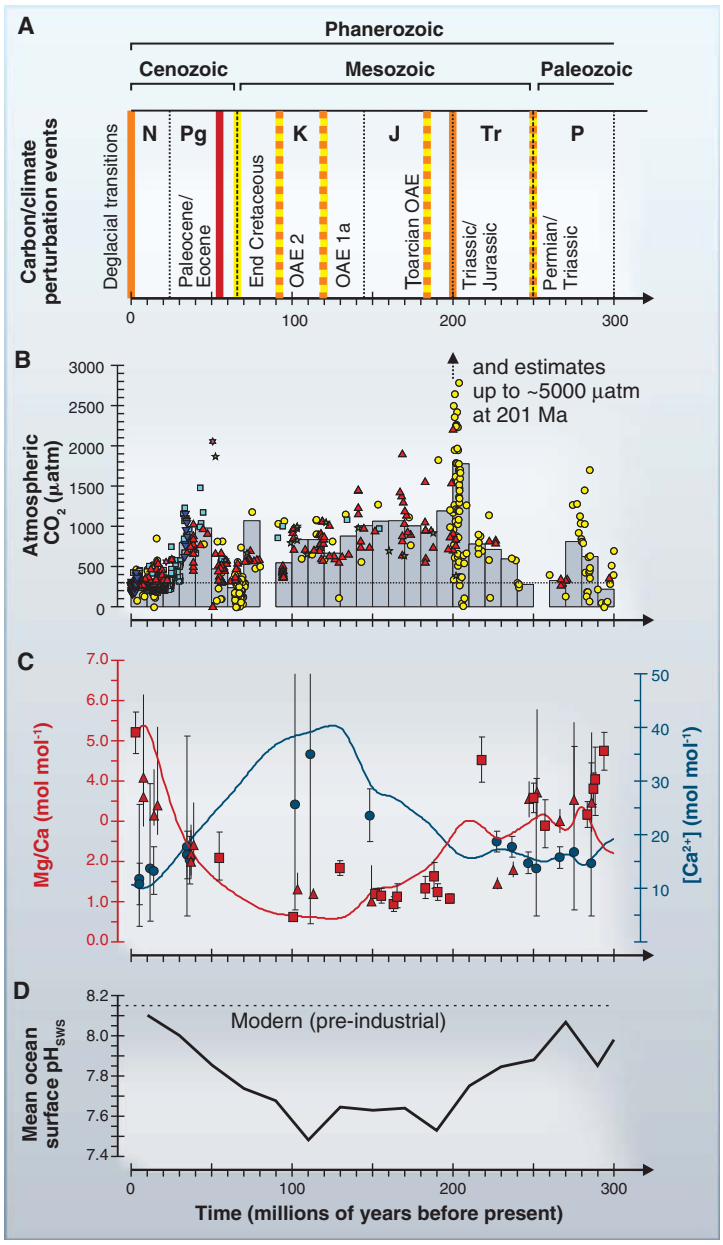

Fig. 4. Compilation of data-based [(B) and (C)] and model-reconstructed [(C) and (D)] indicators of global carbon cycle evolution over the past 300 My together with candidate ocean acidification events (A). (**A**) Summarization of the degree to which events (table S1) have some similarity to modern ocean acidification. The similarity index (table S1) is color-coded, where red indicates 3/most similar, orange indicates 2/partly similar, and yellow indicates 1/unlike. (**B**) Proxy-reconstructed atmospheric P_{CO_2} (*2*) grouped by proxy: yellow circles indicate paleosol $\delta^{13}C$, light blue squares indicate marine phytoplankton $\delta^{13}C$, red triangles indicate stomatal indices/ratios, dark blue inverted triangles indicate planktic foraminiferal $\delta^{11}B$, green five-pointed stars indicate liverwort $\delta^{13}C$, purple six-pointed stars indicate sodium carbonates, with 10-My averages shown by gray bars. For plotting convenience, estimates exceeding 3000 µatm are not shown [primarily paleosol $\delta^{13}C$ from the uppermost Triassic/lowermost Jurassic (*2*)]. (**C**) Ocean Mg/Ca ratios (red triangles, left axis), reconstructed from fluid inclusions (*2*) and echinoderm fossil carbonate [red squares (*71*)] together with the Phanerozoic seawater model of (*72*) (red line). Also shown (blue circles, right axis) is $[Ca^{2+}]$ from fluid inclusions (*2*) and models [blue line (*72*)]. (**D**) Model-reconstructed changes in mean ocean surface pH at 20-My intervals [black line (*73*)].

Triassic–Jurassic. The Triassic–Jurassic (T/J) mass extinction is linked to the coeval emplacement of the Central Atlantic Magmatic Province (*50*). Proxy records across the T/J boundary (~200 Ma) suggest a doubling of atmospheric P_{CO_2} over as little as 20 ky (*51*, *52*), although the absolute P_{CO_2} estimates differ greatly between proxies, with leaf stomata suggesting an increase from 700 to 2000 µatm, whereas pedogenic carbonates indicate an increase from 2000 to 4400 µatm (Fig. 4C) (*2*). Decreased carbonate saturation is inferred from reduced pelagic carbonate accumulation in shelf sediments (*53*), although shallow water carbonate deposition can vary in response to many parameters, not only acidification. A calcification crisis amongst hypercalcifying taxa is inferred for this period (Fig. 4B), with reefs and scleractinian corals experiencing a near-total collapse (*32*). However, the observation that tropical species were more affected than extratropical species suggests that global warming may have been an important contributor or even dominant cause of this extinction (*32*).

Permian–Triassic. The Permo–Triassic (P/T) mass extinction (252.3 Ma) was the most severe of the Phanerozoic Era and coincided, at least in part, with one of the largest known continental eruptions, the Siberian trap basalts. Recent estimates for the total CO_2 release put it at ~13,000 to 43,000 PgC in 20 to 400 ky (*54*–*56*)—an annual carbon release of ~0.1 to 1 PgC [compared with 9.9 PgC in 2008 (*57*)]. There is some observational evidence for carbonate dissolution in shelf settings (*54*), but its interpretation is again debated (*58*). There is abundant evidence for ocean anoxia, photic zone euxinia (enrichment in

hydrogen sulfide) (*59*), and strong warming (*54*), but no direct proxy evidence for pH or carbonate ion changes. Knoll *et al*. (*59*) inferred the preferential survival of taxa with anatomical and physiological features that should confer resilience to reduced carbonate saturation state and hypercapnia (high CO_2 in blood) and preferential extinction of taxa that lacked these traits, such as reef builders (*32*).

Is There a Geologic Analog for the Future?

A number of past ocean carbon-cycle perturbation events share many of the characteristics of anthropogenic ocean acidification (Fig. 4 and table S1), with the notable exception of the estimated rates of CO_2 release. In the general absence of direct proxy evidence for lower pH and reduced saturation before the Pliocene, global carbon cycle models can be used to infer the magnitude of carbon release by fitting observed changes in the $\delta^{13}C$ of calcium carbonates and organic remnants (*60*). However, as well as needing information on the source and isotopic composition of the added carbon, the time scale of $\delta^{13}C$ change is critically important to the estimation of CO_2 fluxes (*25*). Because of the lack of open-ocean sediments and increasingly poor temporal and spatial resolution of the geological record further back in time, it is difficult to place adequate constraints on the duration and rate of CO_2 release. Radiometric dating techniques are not accurate enough to identify Mesozoic intervals of 10-ky duration, although orbital spectral analysis of highly resolved isotope and/or sedimentological records can help to partly overcome this—for example, if a $\delta^{13}C$ excursion is shorter or longer than one precession cycle [21 ky (*51*)]. Even for the well-studied PETM, the duration of the main phase of this carbon injection is still debated (*35*, *61*), and model-inferred peak rates of ≤1 PgC per year (*26*, *61*) could potentially be an underestimate.

Additional complications arise because carbon may not have been released at a uniform rate and, in the extreme, may have occurred in the form of rapid pulses. In such cases, the assumption of an average emissions rate throughout the entire duration of the pulsed release will fail to capture the potential for episodes of intense acidification. For instance, although the total duration of the CO_2 release from the T/J–age Central Atlantic Magmatic Province was estimated to be ~600 ky, pulses as short as ~20 ky have been suggested (*51*, *62*). Similarly, the main phase of OAE1a (excluding the recovery interval) was ~150 ky (*45*) and hence too slow for carbonate saturation to be significantly affected (Fig. 3), but major volcanic eruptions and thus rapid CO_2 release could potentially have produced future-relevant perturbations in the carbon cycle. Substantially improved chronologies and higher-resolution records are needed to refine estimates of rate.

Given current knowledge of the past 300 My of Earth's history (Fig. 4 and table S1), the PETM and associated hyperthermal events, the T/J, and potentially the P/T all stand out as having excellent potential as analog events, although the T/J and P/T are much more poorly constrained because of the absence of deep-sea carbonate deposits. OAEs may also be relevant but were associated with less severe volcanism (CO_2 release) than were the older events (P/T and T/J). The last deglacial transition, although characterized by temperature and CO_2-increase, is two orders of magnitude slower than current anthropogenic change. It is also thought to largely represent a redistribution of carbon within the ocean and to the atmosphere and terrestrial biosphere and hence did not have as potent and globally uniform an acidification effect as an input from geological reserves. Because of the decoupling between pH and saturation on long time scales (Fig. 3), extended intervals of elevated P_{CO_2} such as the middle Miocene, Oligocene, and Cretaceous can be firmly ruled out as future-relevant analogs.

What Are the Perspectives for Using the Geological Record to Project Global Change?

Only rapid or pulsed CO_2 release events can provide direct future-relevant information. Assessment of such events critically depends on independent geochemical quantification of the associated changes in the carbonate system, specifically seawater-pH and $CaCO_3$ saturation. Geochemical proxy estimates are not yet available for the Cretaceous and beyond and need to be obtained to verify whether ocean acidification did indeed happen. This is challenging, because in addition to the potential for increasing post-depositional alteration and reduced stratigraphic exposure, uncertainty over the chemical and isotopic composition of seawater increases and limits our interpretation of these proxies (*63*, *64*). Future studies will have to improve and expand geochemical estimates and their uncertainties of surface and deep-ocean carbonate chemistry associated with carbonate dissolution and ecological changes. This includes finding new archives to study the secular evolution of seawater chemistry but also the laboratory study of living proxy carriers under conditions mimicking past seawater chemistry. An unfortunate aspect of the geological record, however, is the lack of deep-sea carbonates in the Early Jurassic and beyond, which further reduces our ability to reconstruct the carbonate chemistry of those older events.

The sensitivity of ocean chemistry to CO_2 release, and the relationship between induced pH and P_{CO_2} changes, vary through time and further complicate the picture. For instance, seawater calcium and magnesium ion concentrations were different in the past (Fig. 4C). This alters the ocean's carbonate ion buffering capacity and hence sensitivity of the Earth system to carbon perturbation (*65*) because all other things being equal, higher ambient Ca^{2+} concentrations means that a lower carbonate ion concentration is required to achieve the same saturation and hence balance weathering. Varying seawater Mg/Ca ratios may potentially also affect the mineralogy of marine calcifiers, where the more soluble high-Mg calcite predominated Neogene reefs and reefs during the Permian through Early Jurassic, and more resistant low-Mg calcite predominated during the Late Jurassic through Paleogene (*66*). Thus, on this mineralogical basis the response of marine calcifiers to ocean acidification and seawater geochemistry during the P/T and T/J would arguably be closer to the modern than, for example, during the PETM (*67*). Improved estimates of past seawater–Mg/Ca composition are necessary to better evaluate all of this.

Although we have concentrated on the prospects for extracting information from the geological record concerning the impact of ocean acidification, we must question whether it really is necessary to isolate its effect on marine organisms from other covarying factors (*68*). In particular, consequences of increasing atmospheric CO_2 will also be associated with warming in the surface ocean and a decrease in dissolved oxygen concentration (*69*). Massive carbon release, whether future or past, will hence share the same combination and sign of environmental changes. The strength of the geological record therefore lies in revealing past coupled warming and ocean acidification (and deoxygenation) events as an "integrated" analog, with future and past events sharing the same combination and sign of environmental changes. However, in additionally driving a strong decline in calcium carbonate saturation alongside pH, the current rate of (mainly fossil fuel) CO_2 release stands out as capable of driving a combination and magnitude of ocean geochemical changes potentially unparalleled in at least the last ~300 My of Earth history, raising the possibility that we are entering an unknown territory of marine ecosystem change.

References and Notes

1. A. Ridgwell, D. N. Schmidt, *Nat. Geosci.* **3**, 196 (2010).
2. Materials and methods are available as supporting material on *Science* Online.
3. W. H. Berger, *Deep-Sea Res.* **15**, 31 (1968).
4. S. Barker, H. Elderfield, *Science* **297**, 833 (2002).
5. S. Barker *et al*., *Paleoceanography* **19**, PA3008 (2004).
6. S. J. Gibbs, H. M. Stoll, P. R. Bown, T. J. Bralower, *Earth Planet. Sci. Lett.* **295**, 583 (2010).
7. K. Caldeira, M. E. Wickett, *Nature* **425**, 365 (2003).
8. An online associated carbonate chemistry tutorial is available as supporting material on *Science* Online.
9. A. Ridgwell, R. E. Zeebe, *Earth Planet. Sci. Lett.* **234**, 299 (2005).
10. D. Archer, H. Kheshgi, E. Maier-Reimer, *Geophys. Res. Lett.* **24**, 405 (1997).
11. E. Monnin *et al*., *Science* **291**, 112 (2001).
12. B. Hönisch, N. G. Hemming, *Earth Planet. Sci. Lett.* **236**, 305 (2005).
13. L. Beaufort *et al*., *Nature* **476**, 80 (2011).
14. J. W. Farrell, W. Prell, *Paleoceanography* **4**, 447 (1989).
15. B. Hönisch, T. Bickert, N. G. Hemming, *Earth Planet. Sci. Lett.* **272**, 309 (2008).
16. J. Yu *et al*., *Science* **330**, 1084 (2010).
17. T. M. Marchitto, J. Lynch-Stieglitz, S. R. Hemming, *Earth Planet. Sci. Lett.* **231**, 317 (2005).
18. O. Seki *et al*., *Earth Planet. Sci. Lett.* **292**, 201 (2010).
19. A. M. Haywood *et al*., *Global Planet. Change* **66**, 208 (2009).
20. M. Pagani, Z. Liu, J. LaRiviere, A. C. Ravelo, *Nat. Geosci.* **3**, 27 (2010).

21. H. J. Dowsett, M. M. Robinson, *Micropaleontology* **53**, 105 (2007).
22. P. R. Bown *et al*., in *Coccolithophores—From Molecular Processes to Global Impacts,* H. R. Thierstein, J. R. Young, Eds. (Springer, Berlin, 2004), pp. 481–508.
23. J. P. Kennett, L. D. Stott, *Nature* **353**, 225 (1991).
24. J. C. Zachos *et al*., *Science* **308**, 1611 (2005).
25. J. C. Zachos, H. McCarren, B. Murphy, U. Röhl, T. Westerhold, *Earth Planet. Sci. Lett.* **299**, 242 (2010).
26. R. E. Zeebe, J. C. Zachos, G. R. Dickens, *Nat. Geosci.* **2**, 576 (2009).
27. K. Panchuk, A. Ridgwell, L. R. Kump, *Geology* **36**, 315 (2008).
28. R. E. Zeebe, J. C. Zachos, *Paleoceanography* **22**, PA3201 (2007).
29. E. Thomas, in *Geological Society of America Special Paper,* S. Monechi, R. Coccioni, M. R. Rampino, Eds. (Geological Society of America, Boulder, CO, 2007), pp. 1–23.
30. F. J. Rodríguez-Tovar, A. Uchman, L. Alegret, E. Molina, *Mar. Geol.* **282**, 178 (2011).
31. C. Scheibner, R. P. Speijer, *Earth Sci. Rev.* **90**, 71 (2008).
32. W. Kiessling, C. Simpson, *Glob. Change Biol.* **17**, 56 (2011).
33. S. J. Gibbs, T. J. Bralower, P. R. Bown, J. C. Zachos, L. M. Bybell, *Geology* **34**, 233 (2006).
34. A. Sluijs, H. Brinkhuis, *Biogeosciences* **6**, 1755 (2009).
35. A. Sluijs *et al*., *Nat. Geosci.* **2**, 777 (2009).
36. I. Raffi, B. De Bernardi, *Mar. Micropaleontol.* **69**, 119 (2008).
37. S. J. Gibbs, P. R. Bown, J. A. Sessa, T. J. Bralower, P. A. Wilson, *Science* **314**, 1770 (2006).
38. P. Schulte *et al*., *Science* **327**, 1214 (2010).
39. S. D'Hondt, M. E. Q. Pilson, H. Sigurdsson, A. K. Hanson Jr., S. Carey, *Geology* **22**, 983 (1994).
40. R. E. Zeebe, P. Westbroek, *Geochem. Geophys. Geosyst.* **4**, 1104 (2003).
41. C. Langdon *et al*., *Global Biogeochem. Cycles* **14**, 639 (2000).
42. H. C. Jenkyns, *Geochem. Geophys. Geosyst.* **11**, Q03004 (2010).
43. R. M. Leckie *et al*., *Paleoceanography* **17**, 1041 (2002).
44. E. Erba, F. Tremolada, *Paleoceanography* **19**, PA1008 (2004).
45. E. Erba, C. Bottini, H. J. Weissert, C. E. Keller, *Science* **329**, 428 (2010).
46. S. J. Gibbs, S. A. Robinson, P. R. Bown, T. D. Jones, J. Henderiks, *Science* **332**, 175; author reply, 175 (2011).
47. G. Suan *et al*., *Earth Planet. Sci. Lett.* **267**, 666 (2008).
48. A. S. Cohen, A. L. Coe, D. B. Kemp, *J. Geol. Soc. London* **164**, 1093 (2007).
49. E. Mattioli, B. Pittet, L. Petitpierre, S. Mailliot, *Global Planet. Change* **65**, 134 (2009).
50. J. H. Whiteside, P. E. Olsen, D. V. Kent, S. J. Fowell, M. Et-Touhami, *Palaeogeogr. Palaeoclimatol. Palaeoecol.* **244**, 345 (2007).
51. D. B. Kemp, A. L. Coe, A. S. Cohen, L. Schwark, *Nature* **437**, 396 (2005).
52. M. Ruhl, N. R. Bonis, G. J. Reichart, J. S. Sinninghe Damsté, W. M. Kürschner, *Science* **333**, 430 (2011).
53. A. E. Crne, H. Weissert, S. Gorican, S. M. Bernasconi, *Geol. Soc. Am. Bull.* **123**, 40 (2011).
54. J. L. Payne *et al*., *Proc. Natl. Acad. Sci. U.S.A.* **107**, 8543 (2010).
55. S. V. Sobolev *et al*., *Nature* **477**, 312 (2011).
56. S. Z. Shen *et al*., *Science* **334**, 1367 (2011).
57. C. Le Quéré *et al*., *Nat. Geosci.* **2**, 831 (2009).
58. P. B. Wignall, S. Kershaw, P.-Y. Collin, S. Crasquin-Soleau, *Geol. Soc. Am. Bull.* **121**, 954 (2009).
59. A. H. Knoll, R. K. Bambach, J. L. Payne, S. Pruss, W. W. Fischer, *Earth Planet. Sci. Lett.* **256**, 295 (2007).
60. J. Zachos, M. Pagani, L. Sloan, E. Thomas, K. Billups, *Science* **292**, 686 (2001).
61. Y. Cui *et al*., *Nat. Geosci.* **4**, 481 (2011).
62. M. Ruhl *et al*., *Earth Planet. Sci. Lett.* **295**, 262 (2010).
63. D. Lemarchand, J. Gaillardet, E. Lewin, C. J. Allègre, *Nature* **408**, 951 (2000).
64. R. M. Coggon, D. A. Teagle, C. E. Smith-Duque, J. C. Alt, M. J. Cooper, *Science* **327**, 1114 (2010).
65. R. E. Zeebe, A. Ridgwell, in *Ocean Acidification*, J.-P. Gattuso, L. Hansson, Eds. (Oxford Univ. Press, Oxford, 2011), pp. 21–40.
66. S. M. Stanley, L. A. Hardie, *Palaeogeogr. Palaeoclimatol. Palaeoecol.* **144**, 3 (1998).
67. J. B. Ries, *Biogeosciences* **7**, 2795 (2010).
68. C. Turley *et al*., *Mar. Pollut. Bull.* **60**, 787 (2010).
69. N. Gruber, *Philos. Trans. R. Soc. A-Math. Phys. Eng. Sci.* **369**, 1980 (2011).
70. E. T. Sundquist, K. Visser, Elsevier, in *Treatise on Geochemistry: Biogeochemistry*, W. H. Schlesinger, Ed. (Elsevier, Pergamon, Oxford, 2004), chap. 9.
71. J. A. D. Dickson, *Science* **298**, 1222 (2002).
72. R. V. Demicco, T. K. Lowenstein, L. A. Hardie, R. J. Spencer, *Geology* **33**, 877 (2005).
73. A. Ridgwell, *Mar. Geol.* **217**, 339 (2005).

Acknowledgments: Funding for the "Workshop on Paleocean Acidification and Carbon Cycle Perturbation Events" was provided by NSF OCE 10-32374 and Past Global Changes (PAGES). We thank the workshop participants for stimulating discussions and contributions to this manuscript, and the USC Wrigley Institute on Catalina Island for hosting the workshop. Particular thanks are owed to Thorsten Kiefer of PAGES, who initiated the workshop and supported it at all stages. This work is a contribution to the "European Project on Ocean Acidification" (EPOCA). Data presented in Fig. 4 are presented in tables S2 and S3 (*2*).

Supporting Online Material

www.sciencemag.org/cgi/content/full/335/6072/1058/DC1
SOM Text
Figs. S1 to S3
Tables S1 to S3
References (*74*–*217*)

10.1126/science.1208277

Turbulence, Cleavage, and the Naked Embryo: A Case for Coral Clones

A. J. Heyward[1]* and A. P. Negri[2]

The successful settlement of coral larvae is critical to the persistence of fully functional coral reef ecosystems (*1*, *2*). An almost universal aspect of metazoan sexual reproduction is the presence of a protective capsule or membrane around the fertilized egg and early embryo. However, reef-building corals provide a notable exception, and coral spawning events result in billions of naked embryos floating at the sea surface (*2*). Fertilized coral eggs cleave within the first 2 hours after spawning and continue to divide throughout the night to produce early-stage larvae the next day. During this early developmental phase, they are not motile, behaving as passive, buoyant particles moved about by waves and surface currents. We have observed that mixing or aeration in the laboratory can result in embryos of 2, 4, 8, and 16 cells disintegrating into irregular groups of cells or individual blastomeres. At sea, even gentle to moderate sea breezes above 11 knots produce small breaking waves, including white caps, 30 cm or greater in height (*3*). The strong shear forces and turbulence associated with bubble formation in white caps (*4*) at the sea surface are likely to easily exceed laboratory conditions known to fragment coral embryos. The most recent decade of wind data for four Australian inner, mid-, and outer shelf reefs on the central Great Barrier Reef (*5*) show that, on the predicted nights of major coral spawning (*2*), wind speed averaged or exceeded 11 knots during 52% of spawning events, with a third of those events representing higher-category winds capable of generating surface waves over a meter. We set out to investigate this apparent threat to reproductive success during the annual mass spawning periods by exposing naturally spawned coral embryos to modest experimentally generated turbulence, mimicking small white caps. Laboratory experiments confirmed the fragmentation of 45.4% ± 13.1% (SE) of embryos in a coral larval cohort after turbulence caused by deliberately pouring embryos floating in seawater over a vertical distance of 30 cm to mimic the minimum wave height associated with white cap formation (*6*). We followed the fate of these fragments and, in contrast to expectations, noted that it was common for individual blastomeres or partial embryos to reorganize and continue cleaving. Blastomeres produced from two-, four-, and eight-cell embryos (Fig. 1A) resulted in individual larvae of proportionately smaller sizes as embryo stage advanced, disaggregating yet remaining viable. These clone blastomeres developed into larvae (Fig. 1B), then settled and metamorphosed normally (*6*) into juvenile corals (Fig. 1, C and D).

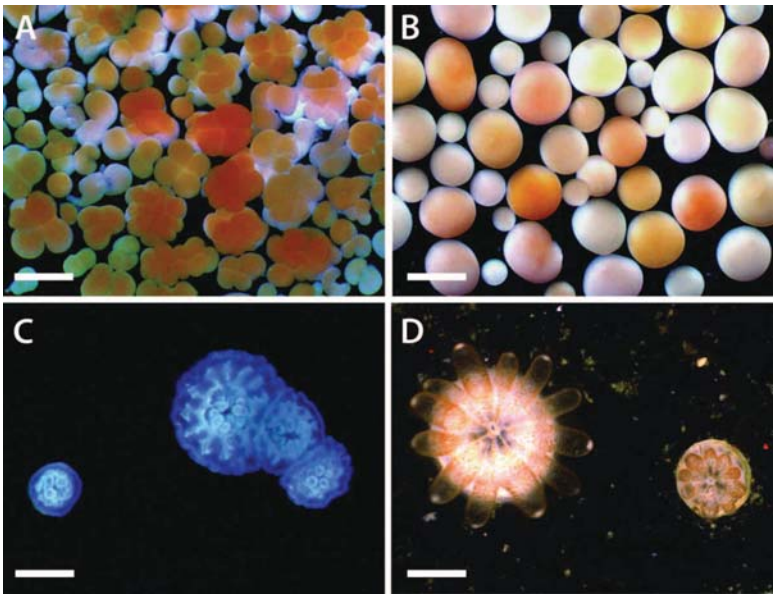

Fig. 1. Development of the hard coral *A. millepora* after fragmentation. Scale bars indicate 0.5 mm. (**A**) Mix of fragmented and intact embryos 3 hours postfertilization. (**B**) Early-stage larvae at 12 hours in three classes corresponding to the blastomere sizes of one- , two-, and four-cell embryos. (**C**) Juveniles of three size classes after 4 days of development. (**D**) Juveniles of different size classes with symbionts after 6 weeks.

Totipotency of cells within the early embryonic stages of corals and the subsequent development of fragments mirrors the early European observations on echinoderms (*7*). However, the echinoderms have a protective embryonic envelope, and skilled surgical intervention was used in those classical studies to generate clones from cells of early-stage embryos. In contrast, coral embryos across disparate families lack fertilization envelopes, so disruption of the embryo and subsequent adjustment of the pieces toward normal development require only natural forces. We have observed vulnerability to fragmentation when culturing coral embryos from the families Acroporidae, Faviidae, Mussidae, Fungidae, and Occulinidae. We have also noted the continuing cleavage postfragmentation in *Favites chinensis*, various fungid species, *Acropora digitifera*, and *A. tenuis*. This intriguing ability of naked coral embryos to fragment easily in the wild provides a mechanism for development of planktonic clones on coral reefs worldwide. Sexual reproduction producing dispersive planktonic larvae is the most common reproductive strategy in marine organisms but has not previously been associated with propagation of genetic clones. Clonal propagation in corals has been a process associated with colony fragmentation or the production of asexual planulae by brooding species (*8*). Our observations indicate that clonal propagation of drifting coral embryos may be commonplace, requiring only moderate wind strength. The ability to easily generate clones in the laboratory also offers new research opportunities where control over larval size and replication are required.

These findings add another mode of reproduction to the diverse repertoire already displayed by corals and a novel capability among the majority of species for the dispersal of genetic coral clones both within and between reefs. For corals, this mixed breeding system, combining elements of outcrossed sexual recombination and asexual propagation, may provide additional reproductive assurance in unpredictable environments, where selection will act differentially on multiple copies of the genotype.

References and Notes

1. O. Hoegh-Guldberg *et al.*, *Science* **318**, 1737 (2007).
2. P. L. Harrison *et al.*, *Science* **223**, 1186 (1984).
3. National Oceanic and Atmospheric Administration, Beaufort Scale of Wind Speed, www.spc.noaa.gov/faq/tornado/beaufort.html (2011).
4. G. B. Deane, M. D. Stokes, *Nature* **418**, 839 (2002).
5. AIMS, http://data.aims.gov.au/aimsrtds/ (2011).
6. Materials and methods are available as supporting material on *Science* Online.
7. S. Hörstadius, *Experimental Embryology of Echinoderms* (Clarendon, Oxford, 1973).
8. A. Baird, J. Guest, B. Willis, *Annu. Rev. Ecol. Evol. Syst.* **40**, 551 (2009).

Acknowledgments: We thank V. Beltran-Ramirez, A. Baird, R. Brinkman, J. Kerry, G. Jones, N. Webster, J. Gilmour, and M. van Oppen for assistance and AIMS, Monbusho (Japan), Sesoko Station, Palau International Coral Reef Center, and Global Environmental Facility/World Bank for funding and field support.

Supporting Online Material

www.sciencemag.org/cgi/content/full/335/6072/1064/DC1
Materials and Methods
Reference (*9*)

1 November 2011; accepted 25 January 2012
10.1126/science.1216055

[1]Australian Institute of Marine Science (AIMS), The University of Western Australia Oceans Institute, 35 Stirling Highway, WA 6009, Australia. [2]AIMS, PMB 3, Townsville, QLD 4810, Australia.

*To whom correspondence should be addressed. E-mail: a.heyward@aims.gov.au

^{182}W Evidence for Long-Term Preservation of Early Mantle Differentiation Products

Mathieu Touboul,* Igor S. Puchtel, Richard J. Walker

Late accretion, early mantle differentiation, and core-mantle interaction are processes that could have created subtle ^{182}W isotopic heterogeneities within Earth's mantle. Tungsten isotopic data for Kostomuksha komatiites dated at 2.8 billion years ago show a well-resolved ^{182}W excess relative to modern terrestrial samples, whereas data for Komati komatiites dated at 3.5 billion years ago show no such excess. Combined ^{182}W, ^{186,187}Os, and ^{142,143}Nd isotopic data indicate that the mantle source of the Kostomuksha komatiites included material from a primordial reservoir that represents either a deep mantle region that underwent metal-silicate equilibration or a product of large-scale magmatic differentiation of the mantle. The preservation, until at least 2.8 billion years ago, of this reservoir—which likely formed within the first 30 million years of solar system history—indicates that the mantle may have never been well mixed.

Over the past two decades, the short-lived ^{182}Hf-^{182}W isotopic system (^{182}Hf → ^{182}W + β^-, half-life = 8.9 million years) has been widely used for dating early solar system processes because of the unique geochemical properties of the system (*1*–*3*). As a moderately siderophile element (MSE), W is largely, but not completely, extracted from the silicate portions of planetary bodies during segregation of metallic cores [e.g., (*4*–*6*)]. Hafnium, in contrast, is lithophile and is essentially retained in silicate portions of planetary bodies. Therefore, determination of the abundance of the daughter nuclide ^{182}W, relative to other stable, nonradiogenic isotopes (e.g., ^{184}W), is of special interest for constraining the timing of planetary core formation. For example, although Hf and W are both refractory elements and are presumed to occur in chondritic relative abundances in bulk planetary objects, most terrestrial rocks have ^{182}W/^{184}W ratios that are approximately 200 parts per million (ppm) higher than bulk chondrites (*7*–*9*). The higher than chondritic ^{182}W/^{184}W ratio of the terrestrial mantle has been interpreted to reflect core segregation and generation of suprachondritic Hf/W in the mantle during the first ~30 million years of solar system history, while ^{182}Hf was still extant (*9*). The isotopic difference between the mantle and chondritic meteorites, together with mass balance constraints, also implies that Earth's core is a W-rich reservoir characterized by a ^{182}W/^{184}W ratio that is ~220 ppm lower than the terrestrial mantle.

After the cessation of substantial core segregation, the Hf/W ratio of Earth's mantle would likely have been further modified by post–core formation events, such as the crystallization of transient magma oceans, partial melting of the mantle, or subsequent crystal-liquid fractionation processes (*10*). If such events occurred before ^{182}Hf became extinct, additional ^{182}W isotopic variations would have been generated in the mantle. It is even likely that ^{182}W isotopic heterogeneities were created in the mantle after ^{182}Hf was no longer extant—for example, as a result of late accretion. The term "late accretion" is used to describe the process of addition of ~0.3 to 0.8% of the total mass of the mantle (*11*) to Earth by continued accretion of materials with bulk chondritic compositions, subsequent to cessation of core formation. It is a process that has been commonly invoked to account for the relatively high absolute and chondritic relative abundances of the highly siderophile elements (HSEs: including Re, Os, Ir, Ru, Rh, Pt, Pd, and Au) present in the mantle (*12*–*15*). Late accretion would have lowered the ^{182}W/^{184}W ratio of the mantle by 10 to 30 ppm, as materials with comparatively ^{182}W-depleted compositions, such as planetesimals with bulk chondritic compositions, were accreted to Earth. Tungsten isotopic anomalies in mantle domains could also have been generated throughout Earth's history as a result of interactions with the core.

Given these possibilities for heterogeneity, the isotopic composition of W in the mantle may complement data from other radiogenic isotope systems, such as the short-lived ^{146}Sm-^{142}Nd isotope system [e.g., (*16*–*18*)], for use in discerning the timing and nature of early Earth differentiation processes, as well as the detection of core-mantle exchange. The possibility of identifying these important processes has led to intensive W isotopic analysis of diverse terrestrial materials (*19*–*21*). Until recently, these studies have reported no resolved ^{182}W isotopic heterogeneities among terrestrial rocks. Willbold *et al*. (*22*), however, reported 13 ± 4 ppm ^{182}W enrichments, relative to younger terrestrial rocks and standards, in rocks dated at 3.8 billion years ago (Ga) from the Isua greenstone belt, Greenland. This study provided the first evidence for W isotopic heterogeneity in terrestrial materials. The rocks analyzed were also characterized by enrichments in ^{142}Nd.

Tungsten isotope heterogeneities in the Archean komatiites. We recently developed a technique to measure ^{182}W/^{184}W to a 2σ (SD) precision of ±4.6 ppm by means of negative thermal ionization mass spectrometry (*23*). This technique has enabled us to begin a high-resolution search for W isotopic anomalies in diverse terrestrial rocks. Here, we present W concentration and isotope composition data for 3.47 Ga komatiites from the Komati Formation of the Barberton greenstone belt, South Africa, and 2.82 Ga komatiites from the Kostomuksha greenstone belt, Baltic Shield, Russia (Table 1) (*24*).

For the Komati and Kostomuksha komatiites, W concentrations vary from 28 to 102 ppb and from 45 to 106 ppb, respectively. In neither suite do W concentrations correlate well with chemical indicators of crystal-liquid fractionation typical of komatiitic systems, such as the MgO content (fig. S2). This may indicate complex behavior of W within crystallizing flows and/or minor mobility of W within the flows at some point after lava solidification.

The μ^{182}W values (where μ is the deviation, in ppm, from terrestrial reference standards) for four Komati samples average +2.7 ± 4.1 (2σ SD) and are indistinguishable from the average for the terrestrial standards and the modern La Palma basalt (Canary Islands) that we repeatedly analyzed during the analytical campaign (μ^{182}W = +0.2 ± 2.49) (Fig. 1). In contrast, the 18 Kostomuksha komatiite samples analyzed (including one to five replicate digestions of the same samples) have an average μ^{182}W of +15.0 ± 4.8 (2σ SD), which is well resolved from the terrestrial standard average (Fig. 1). In addition to differences in location, age, and W isotopic composition, the mantle sources of these two komatiite suites were also characterized by widely differing HSE concentration and Os isotopic systematics. The mantle source of the Komati komatiites has been estimated (*25*) to have had ~50% of the total HSE abundances of the modern primitive mantle (*26*). This is consistent with the observations of Maier *et al*. (*27*), who reported Pt and Ru contents in komatiites ranging in age between 3.5 and 2.9 Ga and discovered what appears to be a progressive increase in Pt concentrations in lavas from the early to late Archean. They attributed this increase to be the result of sluggish downward mixing of a HSE-rich veneer of late-accreted

Department of Geology, University of Maryland, College Park, MD 20742, USA.

*To whom correspondence should be addressed. E-mail: mtouboul@umd.edu

materials to Earth. The Komati source was also characterized by an essentially chondritic initial γ^{187}Os of +0.23 ± 0.12 (*24*) (where γ denotes the percent deviation of the initial Os isotopic composition of the source of the lava from that of a chondritic reference at that time), consistent with common chemical evolution models for Os in the early upper mantle [e.g., (*28*)]. The initial ε^{143}Nd of +1.9 ± 0.7 [compiled from (*29*)] for the Komati rocks (where ε denotes the deviation in parts per 10,000 of the isotopic composition of the source of the lava from that of a chondritic reference at that time) suggests a source characterized by long-term depletion in Nd relative to Sm. This isotopic composition is generally consistent with standard models of the evolution of ^{143}Nd in the early Earth [e.g., (*30*, *31*)]. No ^{142}Nd data are currently available for the Komati komatiites.

In contrast to the Komati source, the mantle source of the Kostomuksha komatiites has been estimated to have had total HSE abundances that are ~80% of those present in the modern primitive mantle (*32*). Puchtel *et al*. (*33*) reported coupled enrichments in both ^{187}Os (initial γ^{187}Os = +2.55 ± 0.13) and ^{186}Os (initial μ^{186}Os = +22 ± 6). Thus, in comparison to the Komati komatiites, the Kostomuksha komatiites were derived from a mantle source characterized by long-term suprachondritic Hf/W, Re/Os, and Pt/Os ratios. The Os isotopic characteristics were interpreted by Puchtel *et al*. to reflect an early onset of Earth's inner-core crystallization. This resulted in suprachondritic Pt/Os and Re/Os in the liquid outer core, creation of coupled ^{186,187}Os enrichments over time, and transfer of this outer-core Os isotopic signature to the mantle source subsequently tapped by the Kostomuksha plume. The Sm-Nd isotopic systematics of the Kostomuksha komatiites, however, are not anomalous, with initial ε^{143}Nd of +2.8 ± 0.2 (*34*) and initial μ^{142}Nd of −0.5 ± 4.0 (*17*). Such values are generally consistent with common chemical evolution models for the early upper mantle [e.g., (*17*)].

The combined W and HSE abundance data, as well as W, Os, and Nd isotopic systematics of the Komati and Kostomuksha komatiites, can be used to place some important constraints on the origin of the MSE and HSE in the deep sources of the two komatiite suites. First, given the consistency of the W isotopic data and W concentrations in the analyzed multiple lava flows from the Kostomuksha suite, it is unlikely that the enrichment in ^{182}W is the result of contamination of parental magmas with the crust or secondary alteration of the lavas, even if we assume that ^{182}W-enriched crust could somehow have been formed. Further, the lithophile trace element data and Nd- and Pb-isotope systematics indicate no detectable crustal contribution to either komatiite system (*29*, *34*). Hence, we interpret both the Komati and Kostomuksha komatiites to have W isotope compositions representative of their respective, deep mantle sources.

Second, the positive μ^{182}W anomaly in the mantle source of the Kostomuksha komatiites cannot be due to the contribution of an outer-core component, as was initially suggested to explain the coupled ^{186,187}Os enrichments present in the system (*33*). The observed W anomaly in the Kostomuksha komatiites is in the opposite direction (μ^{182}W = +15.0 ± 4.8) to that of a core component (μ^{182}W ≈ –220).

Third, Willbold *et al*. (*22*) concluded that the ^{182}W-enriched isotopic composition of the Isua suite preserves the composition of the mantle prior to a final stage of late accretion to Earth and the Moon, termed the terminal cataclysm, or late heavy bombardment (*35*). This event has been previously hypothesized to have occurred between ~3.9 and 3.8 Ga, as assessed from ages of lunar impact melt rocks associated with the major impact basins [e.g., (*36*)]. Willbold *et al*. noted that the addition of materials of chondritic bulk composition (μ^{182}W = –200) that were rich in W, as well as HSE, would have lowered the W isotopic composition of the bulk mantle from an older, more radiogenic composition. Although the 13 ppm enrichment in ^{182}W in rocks from Isua is similar in magnitude to that in the source of the Kostomuksha komatiites, the interpretation that Willbold *et al*. proposed for the Isua rocks is problematic for the Kostomuksha rocks, and below we show why this is the case.

Coupled late accretion and mantle mixing model. In order to explain the observed W, Os, and Nd isotopic systematics for the Komati and Kostomuksha sources, we model mixing between modern mantle and a primordial, ^{182}W-enriched, yet HSE-depleted, reservoir (Fig. 2). Total HSE content is expressed as the deviation of content in the mantle source, relative to the concentration in the modern mantle. The effects of contributions of late-accreted materials ranging from 0.3 to 0.8% of the total mass of the mantle are calculated, assuming that the HSE present in the silicate Earth today were derived entirely from late-accreted materials. Beginning with a radiogenic μ^{182}W value and zero total HSE content prior to late accretion, this model shows that Earth's mantle would have evolved toward its present W isotopic composition, as increasingly more chondritic materials were accreted and the total HSE content increased to the present-day values. This

Table 1. Tungsten concentrations (in ppb) and isotopic compositions of 3.47 Ga Komati (South Africa) and 2.82 Ga Kostomuksha (Russia) komatiites, and the modern La Palma basalt LP15 (Canary Islands). ol spx, olivine spinifex; ol cum, olivine cumulate.

Sample	Lithology	Lava flow	Depth (m)	W (ppb)	μ^{182}W
Kostomuksha					
KGB 9495	ol spx	17	250	44	16.6 ± 5.8
					19.0 ± 6.9
KGB 9496	ol spx	17	251	103	7.5 ± 4.6
					13.5 ± 2.3
					13.4 ± 9.3
					16.1 ± 11.6
					15.8 ± 3.5
					15.7 ± 4.6
KGB 9497	ol spx	17	252	53	15.5 ± 5.8
					15.4 ± 5.8
					14.9 ± 8.1
					17.3 ± 3.5
KGB 94100	ol cum	17	255	78	15.1 ± 3.5
KGB 94114	ol spx	19	263	47	13.6 ± 4.6
KGB 94123	ol spx	26	292	43	14.0 ± 10.4
					14.0 ± 4.6
					17.5 ± 5.8
KGB 94126	ol cum	26	296	71	15.0 ± 11.6
Average (2σ SD, *n* = 18)					15.0 ± 4.8
Komati					
BV 02	ol spx	1	112	30	2.6 ± 5.8
BV 09	ol spx	2	71	27	2.9 ± 7.3
BV 14A	ol cum	11	30	99	5.2 ± 3.9
BV 14B	ol cum	11	30	32	0.2 ± 7.1
Average (2σ SD, *n* = 4)					2.7 ± 4.1
La Palma basalt					
LP 15				844	−0.5 ± 4.7
					1.9 ± 3.7
					−0.7 ± 5.4
Average (2σ SD, *n* = 3)					0.2 ± 2.9
Alfa Aesar W standard (2σ SD, *n* = 40)					0.0 ± 4.6

scenario is broadly similar to those advocated by Willbold *et al.* (*22*) and Maier *et al.* (*27*). Given the estimates that the Komati and Kostomuksha komatiite sources contained ~50 and ~80%, respectively, of the late accretionary component present in the modern mantle (*25*, *32*), the older Komati komatiites should show more radiogenic $\mu^{182}W$ than the Kostomuksha komatiites (Fig. 2). This is not observed, which suggests that the Kostomuksha source cannot simply be primordial mantle that had been largely stripped of HSE by core formation.

Early metal-silicate equilibration model. We next present two approaches for explaining the ^{182}W enrichments, as well as other isotopic and elemental characteristics, of the Kostomuksha komatiites. For the first approach, we assume that ^{182}W, ^{186}Os, and ^{187}Os excesses were generated by the same process. This would mean that the Kostomuksha source included an early-formed component that was characterized by high Hf/W, as well as high Re/Os and Pt/Os, relative to the present-day mantle. One possible mechanism for the attainment of these chemical characteristics would be metal-silicate partitioning at high temperatures and pressures, such as might be found at the base of a primordial transient magma ocean or in a partially molten zone at or near the core-mantle boundary. Transient magma oceans, as well as more limited molten regions at the core-mantle boundary, have been proposed to explain both geochemical and geophysical observations [e.g., (*37*)]. Here, we envision a very early, deep mantle location where silicate melt could potentially equilibrate with metal that is either the growing core, or metal that is passing through the molten region on its way to the core. This approach (*24*) is based on experimental observations of substantially reduced metal-silicate partitioning for Re and Pt, relative to Os, at high temperatures and pressures, compared to relatively low temperatures and pressures of the upper mantle or crust. It is also based on the more siderophilic behavior of W under moderately reducing conditions with respect to the present upper mantle.

In contrast to simple downward mixing of late-accreted materials proposed by Maier *et al.* (*27*), our model requires the long-term survival of some portion of the mantle whose HSE and MSE were set by metal-silicate partitioning under reducing conditions at high temperature and pressure. In order to achieve the isotopic and elemental characteristics of the Kostomuksha source, we envision a plume tapping this liquid or solid reservoir and mixing material from this reservoir with overlying mantle characterized by HSE concentrations and Os isotopic characteristics similar to those in estimates for primitive mantle. The HSE characteristics of the dominant mantle reservoir would be best explained by late accretion. This reservoir would also serve as an appropriate source for the Komati komatiites. A good fit to the $^{187,186}Os$ and ^{182}W isotopic characteristics of the Kostomuksha komatiites can be achieved by mixing ~53% material of the early-formed reservoir with 47% material of the overlying mantle (Fig. 3 and table S6). Because the major fractionations that occur in this model result from metal-silicate interaction, the processes envisioned would have had no predictable effect on the lithophile element isotopic systems, including the Sm-Nd system.

Early magmatic differentiation model. A second approach to account for the ^{182}W enrichment in the mantle is to focus entirely on mantle differentiation processes, such as magma ocean crystallization or partial melting (*24*). Silicate crystal-liquid fractionation processes can induce Hf/W fractionation, and hence potentially could have resulted in the production of mantle reservoirs with ^{182}W excesses or deficits. In general, both Hf and W behave as incompatible elements and concentrate into silicate melts. In the upper mantle, Hf and W abundances are largely controlled by the presence of clinopyroxene and garnet, both of which preferentially incorporate Hf relative to W (*10*). Therefore, fractional crystallization of silicate melts and partial melting of

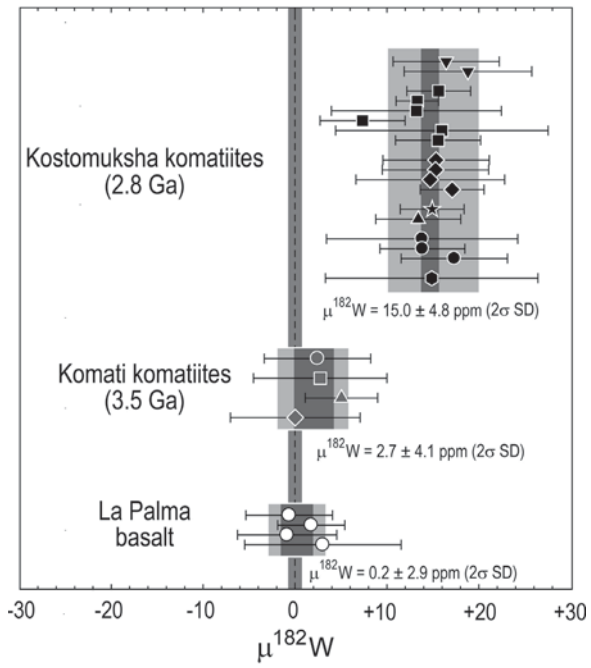

Fig. 1. Tungsten isotopic compositions of the Komati and Kostomuksha komatiites, and of the modern La Palma basalt LP15. Each unique symbol corresponds to a distinct sample. Identical symbols show replicate measurements of the same sample via processing additional aliquots of rock powder. The light gray bands represent 2σ SD uncertainties for the average $\mu^{182}W$ values, and the dark gray bands represent 2σ SE. The dark gray band at $\mu^{182}W = 0$ corresponds to the 2σ SE uncertainty (±0.7 ppm) for repeated analyses of the Alfa Aesar W standard ($n = 40$).

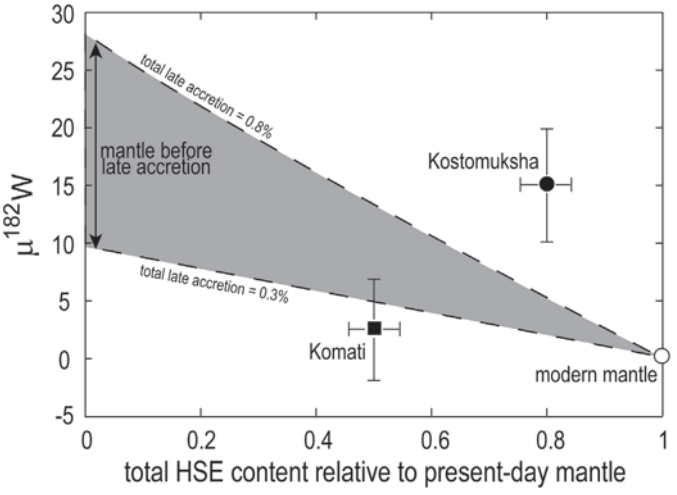

Fig. 2. Plot of $\mu^{182}W$ versus total estimated HSE contents in the Komati (solid square) and Kostomuksha (solid circle) mantle sources relative to those in the present-day mantle. This corresponds to the fraction of mass added by late accretion relative to the modern mantle, assuming an HSE-free mantle prior to late accretion. The W isotopic composition of Earth's mantle prior to late accretion is estimated assuming the total contributions of late accretion to be between 0.3 to 0.8% of mass of the mantle, as determined from HSE abundances in Earth's mantle (*11*), and W contents of 200 and 13 ppb for chondrites (*41*) and modern mantle (*42*), respectively. Evolution of the mantle composition during late accretion, or mixing between a preserved mantle reservoir and current accessible mantle (open circle), are represented by the gray segment. Estimates for the total HSE content in the mantle sources of the Kostomuksha and Komati komatiites are from (*32*) and (*25*).

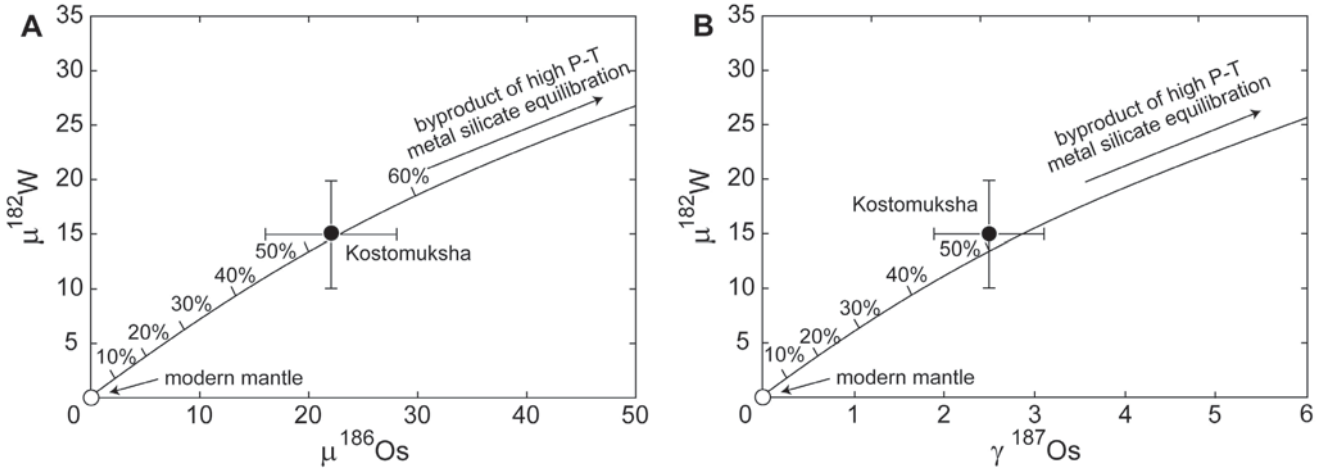

Fig. 3. (**A** and **B**) Plot of $\mu^{182}W$ versus (A) $\mu^{186}Os$ and (B) $\gamma^{187}Os$, illustrating mixing between the modern primitive mantle and a mantle reservoir preserved from an early magma ocean, where Re/Os, Pt/Os, and Hf/W ratios were established by metal-silicate equilibration at high pressure and temperature, resulting in extreme $^{187,186}Os$ and ^{182}W enrichments at 2.82 Ga. For this model, the coupled ^{186}Os and ^{182}W excesses in the source of the Kostomuksha komatiites (solid circle) can be explained by a 53% contribution from the isotopically enriched reservoir to the ambient mantle source (open circle).

silicate rocks at upper-mantle conditions produce solids with high Hf/W ratios relative to melts. Strong Hf-W fractionation is also expected in the lower mantle, as Hf is less incompatible than W in Mg-perovskite, a lower-mantle phase (*38*). Thus, Mg-perovskite would be characterized by higher Hf/W relative to equilibrium melts. Hence, any cumulate reservoir formed as a result of magma ocean crystallization, or any mantle depleted by melting and crustal extraction, would be characterized by high Hf/W ratios—and would develop positive ^{182}W anomalies—if isolated from the convecting portion of the mantle while ^{182}Hf was still extant.

Clinopyroxene, garnet, and Mg-perovskite are also phases that control rare earth element (REE) fractionation in Earth's mantle (table S7) (*24*). All of these mineral phases are typically depleted in Nd relative to Sm, such that, in addition to their higher Hf/W ratio, solids in equilibrium with melts at lower- and upper-mantle conditions would also have had a higher Sm/Nd ratio. Therefore, it might be expected that if the Kostomuksha W isotopic anomaly is related to early silicate differentiation, the enriched ^{182}W should also be accompanied by an excess in ^{142}Nd. Yet, although Kostomuksha komatiites have $\mu^{142}Nd$ values that are identical to Earth's modern mantle within analytical uncertainty (*17*), a contribution from an early differentiated mantle component cannot be summarily excluded. This is because the magnitude of Hf-W fractionation induced by partial melting and crystallization is likely much larger than the magnitude of Sm-Nd fractionation. Hence, early igneous processes could potentially result in substantial ^{182}W anomalies without a resolvable effect on ^{142}Nd.

To model this type of scenario, we consider two early differentiation end members. The first, similar to the differentiation model considered in Willbold *et al*. (*22*) to account for the Isua data, assumes that Hf-W fractionation is coupled to the global differentiation event advocated by Boyet and Carlson (*17*) for explaining the 20 ppm enrichment in ^{142}Nd of the accessible silicate Earth relative to chondrites. At ~4.53 Ga, bulk mantle characterized by chondritic Sm/Nd and suprachondritic Hf/W would have differentiated into two complementary reservoirs: an early enriched reservoir (EER), characterized by lower Sm/Nd and Hf/W ratios, and an early depleted reservoir (EDR) with higher ratios. Partial remixing of the EER back into the EDR could have resulted in the generation of the modern accessible mantle with appropriate Sm/Nd and Hf/W ratios that translate into the observed present-day $\mu^{142}Nd$ and $\mu^{182}W$ values of 0. Consistent with this model, positive ^{142}Nd anomalies in early Archean samples from Isua [7 to 15 ppm (*16*, *18*)] are accompanied by a ^{182}W anomaly of +13 ± 4 ppm (*22*). Hence, if both isotopic anomalies reflect the involvement of remnants of the EDR, a ^{182}W anomaly that is considerably smaller than 15 ppm would be expected when there is no resolvable ^{142}Nd enrichment. Within analytical uncertainties, Kostomuksha komatiites have identical $\mu^{182}W$ to the Isua samples, so if this interpretation is correct for the Isua samples, this global mantle differentiation model is difficult to reconcile with the combined data for the Kostomuksha komatiites.

A second mantle differentiation model explores the effects of early partial melting of the mantle with a present-day $\mu^{182}W = 0$ and $\mu^{142}Nd = 0$, as opposed to the parental reservoir with chondritic $\mu^{142}Nd = -20$, considered in the early global differentiation model. This parental reservoir, with current $^{142,143}Nd$ isotope compositions that are identical to the modern upper mantle, corresponds to bulk mantle, assuming an initial Earth with suprachondritic Sm/Nd (*16*), or to an already depleted mantle, if Earth was instead characterized by chondritic Sm/Nd and experienced early global mantle differentiation, as proposed by Boyet and Carlson (*17*). The Hf-W and Sm-Nd fractionations induced by partial melting are estimated using a batch melting model and published partition coefficients for these elements between constituent mantle phases and silicate melt (table S7) (*24*). For this model, the $\mu^{182}W$ and $\mu^{142}Nd$ values of the Kostomuksha komatiites are most consistent with a mantle source that was residual to partial melting of the lower mantle earlier than ~4.52 Ga, assuming that the degree of melting remained lower than ~4% (Fig. 4) (*24*).

A current problem with any mantle differentiation model is that it is impossible to meaningfully predict the effects that such differentiation events would have had on the absolute and relative abundances of the HSE. The total HSE abundances calculated for the mantle source of the Kostomuksha komatiites of 80% relative to those in the modern primitive mantle estimate (*32*) would require that late accretion largely occurred prior to the differentiation event that fractionated Hf-W. If the putative giant impact that generated the Moon resulted in a final clearing of HSE from the mantle prior to late accretion, this model would be inconsistent with formation of the Moon later than 4.50 Ga (*39*). Alternatively, an early differentiated mantle component may have been mixed with convecting mantle in which the HSE budget had been previously established by late accretion. The +15 ppm ^{182}W anomaly would represent the diluted isotopic signature of such an early differentiated mantle component, which had initially higher $\mu^{182}W$. Mixing with current mantle defines a straight line passing through the origin in Fig. 4. Therefore, the formation of such a reservoir would still be constrained to have occurred earlier than ~4.52 Ga, although the upper limit of the degree of partial melting for the model is increased to as much as ~10%. Taking into account a

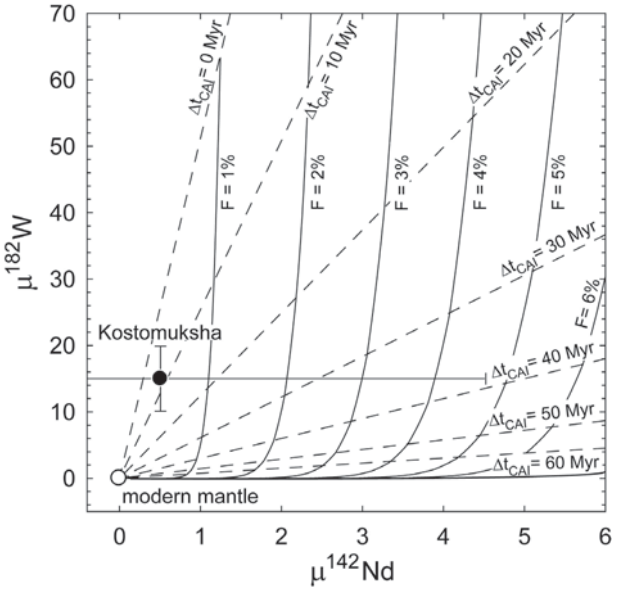

Fig. 4. Coupled ^{142}Nd-^{182}W evolution model of depleted reservoirs formed from a parental reservoir with μ^{182}W and μ^{142}Nd values of 0, corresponding to the isotopic compositions of the modern upper mantle (open circle). Dashed lines are loci of equal differentiation time after the formation of calcium and aluminum–rich inclusions (CAI), Δt_{CAI} [in millions of years (Myr)], marking the beginning of the solar system. Solid curves are the loci of depletion with identical degrees of partial melting, *F* (in percent). This model assumes partial melting of a lower mantle with 80% Mg-perovskite, 15% magnesiowüstite, and 5% Ca-perovskite. Partition coefficients for Hf, W, Sm, and Nd in Mg- and Ca-perovskite used are reported in table S7. Note that mantle depletion earlier than 4.52 Ga can result in the generation of a resolvable ^{182}W anomaly without a detectable ^{142}Nd anomaly.

dilution factor of ~5, as necessary for explaining the high HSE abundances in the source of the Kostomuksha komatiites, the most consistent mantle differentiation model involves ~2% partial melting of the lower mantle at ~4.55 Ga, which then produced a reservoir with μ^{182}W of ~60 and μ^{142}Nd of ~2.

For Isua rocks, the model favored by Willbold *et al*. (*22*), whereby the mantle source corresponds to a portion of the mantle preserved from late accretion, cannot be excluded at present because the HSE concentrations in the source of these rocks are not yet determined. We note, however, that our models of metal-silicate equilibration and magmatic differentiation could also successfully account for the apparent coupling of the positive ^{182}W anomaly of Isua rocks with, respectively, the ^{187}Os [initial γ^{187}Os = +4.2 ± 1.2 (*40*)] and ^{142}Nd excess [μ^{142}Nd = +7 to +15 (*16*, *18*)] also present in the Isua rocks. Although the mantle sources of the Isua rocks and Kostomuksha komatiites could have experienced similar early processes, they must sample distinct mantle reservoirs, which formed under different conditions (as they are characterized by different ^{187}Os and ^{142}Nd excesses), despite having similar ^{182}W anomalies.

Implications for early mantle dynamics. We conclude that the positive ^{182}W anomaly of the Kostomuksha komatiite source does not correspond to the composition of the dominant Hadean mantle prior to the addition of extraterrestrial materials via late accretion. Instead, it must record a very early differentiation event, which could be related to either metal-silicate equilibration or mantle differentiation processes. Combined investigations of HSE abundances and ^{186,187}Os, ^{182}W, and ^{142}Nd systematics of other komatiites derived from mantle sources with variable Sm/Nd ratios may ultimately permit discrimination between the different models presented here.

Regardless of the true cause of the W anomaly, the generation of these komatiites at 2.8 Ga attests to the long-lived nature of an early ^{182}W-enriched mantle reservoir, and highlights the evident sluggish mixing of at least some portions of the mantle throughout the Hadean and Archean. Dense cumulate piles, crystallized from a basal magma ocean [e.g., (*37*)], may constitute good candidates for storage and preservation of ^{182}W heterogeneities over at least 1.7 billion years. If generation of this primordial component predated the formation of the Moon [>60 million years after formation of the solar system (*39*)], it can be concluded that the putative Moon-forming giant impact, although highly energetic, did not induce complete homogenization of Earth's mantle. This would most likely mean that Earth was not completely melted by the event.

References and Notes

1. C. L. Harper Jr., S. B. Jacobsen, *Geochim. Cosmochim. Acta* **60**, 1131 (1996).
2. M. F. Horan, M. I. Smoliar, R. J. Walker, *Geochim. Cosmochim. Acta* **62**, 545 (1998).
3. D.-C. Lee, A. N. Halliday, *Science* **288**, 1629 (2000).
4. H. Palme, W. Rammensee, *Proc. Lunar Planet. Sci.* **12B**, 949 (1981).
5. M. J. Walter, Y. Thibault, *Science* **270**, 1186 (1995).
6. M. J. Walter *et al*., in *Origin of the Earth and Moon*, R. M. Canup, K. Righter, Eds. (Lunar and Planetary Institute, Houston, 2000), pp. 265–289.
7. R. Schoenberg, B. S. Kamber, K. D. Collerson, S. Moorbath, *Nature* **418**, 403 (2002).
8. T. Kleine, C. Münker, K. Mezger, H. Palme, *Nature* **418**, 952 (2002).
9. Q.-Z. Yin *et al*., *Nature* **418**, 949 (2002).
10. K. Righter, C. K. Shearer, *Geochim. Cosmochim. Acta* **67**, 2497 (2003).
11. R. J. Walker, *Chem. Erde* **69**, 101 (2009).
12. A. E. Ringwood, *Geochim. Cosmochim. Acta* **30**, 41 (1966).
13. J. W. Morgan, J. F. Lovering, *Earth Planet. Sci. Lett.* **3**, 219 (1967).
14. R. H. Mitchell, R. R. Keays, *Geochim. Cosmochim. Acta* **45**, 2425 (1981).
15. J. W. Morgan, G. A. Wandless, R. K. Petrie, A. J. Irving, *Tectonophysics* **75**, 47 (1981).
16. G. Caro, B. Bourdon, J. L. Birck, S. Moorbath, *Nature* **423**, 428 (2003).
17. M. Boyet, R. W. Carlson, *Science* **309**, 576 (2005).
18. V. C. Bennett, A. D. Brandon, A. P. Nutman, *Science* **318**, 1907 (2007).
19. A. Scherstén, T. Elliott, C. Hawkesworth, M. Norman, *Nature* **427**, 234 (2004).
20. F. Moynier *et al*., *Proc. Natl. Acad. Sci. U.S.A.* **107**, 10810 (2010).
21. T. Iizuka *et al*., *Earth Planet. Sci. Lett.* **291**, 189 (2010).
22. M. Willbold, T. Elliott, S. Moorbath, *Nature* **477**, 195 (2011).
23. M. Touboul, R. J. Walker, *Int. J. Mass Spectrom.* **309**, 109 (2011).
24. See supporting material on *Science* Online.
25. I. S. Puchtel *et al*., *Geochim. Cosmochim. Acta* **74**, A834 (2010).
26. H. Becker *et al*., *Geochim. Cosmochim. Acta* **70**, 4528 (2006).
27. W. D. Maier *et al*., *Nature* **460**, 620 (2009).
28. S. B. Shirey, R. J. Walker, *Annu. Rev. Earth Planet. Sci.* **26**, 423 (1998).
29. V. Chavagnac, *Lithos* **75**, 253 (2004).
30. D. J. DePaolo, in *Evolution of the Earth*, R. J. O'Connell, W. S. Fyfe, Eds. (American Geophysical Union/Geological Society of America, Washington, DC, 1981), pp. 59–68.
31. S. J. Goldstein, R. K. O'Nions, P. J. Hamilton, *Earth Planet. Sci. Lett.* **70**, 221 (1984).
32. I. S. Puchtel, M. Humayun, *Geochim. Cosmochim. Acta* **69**, 1607 (2005).
33. I. S. Puchtel *et al*., *Earth Planet. Sci. Lett.* **206**, 411 (2005).
34. I. S. Puchtel *et al*., *Earth Planet. Sci. Lett.* **155**, 57 (1998).
35. F. Tera, D. A. Papanastassiou, G. J. Wasserburg, *Earth Planet. Sci.* **22**, 1 (1974).
36. G. B. Dalrymple, G. Ryder, *Lunar Planet. Sci.* **27**, 285 (1996).
37. S. Labrosse, J. W. Hernlund, N. Coltice, *Nature* **450**, 866 (2007).
38. A. Corgne, C. Liebske, B. J. Wood, D. C. Rubie, D. J. Frost, *Geochim. Cosmochim. Acta* **69**, 485 (2005).
39. M. Touboul, T. Kleine, B. Bourdon, H. Palme, R. Wieler, *Nature* **450**, 1206 (2007).
40. R. Frei, A. Polat, A. Meibom, *Geochim. Cosmochim. Acta* **68**, 1645 (2003).
41. T. Kleine, K. Mezger, C. Munker, H. Palme, A. Bischoff, *Geochim. Cosmochim. Acta* **68**, 2935 (2004).
42. R. J. Arevalo Jr., W. F. McDonough, *Earth Planet. Sci. Lett.* **272**, 656 (2008).

Acknowledgments: Supported by NSF Cooperative Studies of Earth's Deep Interior grant 0757808. We thank J. Day for providing the La Palma basalt, and T. Kleine and one anonymous reviewer for their thorough and constructive reviews. Methods and detailed data are presented in the supporting online material.

Supporting Online Material

www.sciencemag.org/cgi/content/full/science.1216351/DC1
Materials and Methods
SOM Text
Figs. S1 to S4
Tables S1 to S7
References (*43*–*57*)

8 November 2011; accepted 26 January 2012
Published online 16 February 2012;
10.1126/science.1216351

Observation of Quantum Criticality with Ultracold Atoms in Optical Lattices

Xibo Zhang,* Chen-Lung Hung, Shih-Kuang Tung, Cheng Chin*

Quantum criticality emerges when a many-body system is in the proximity of a continuous phase transition that is driven by quantum fluctuations. In the quantum critical regime, exotic, yet universal properties are anticipated; ultracold atoms provide a clean system to test these predictions. We report the observation of quantum criticality with two-dimensional Bose gases in optical lattices. On the basis of in situ density measurements, we observe scaling behavior of the equation of state at low temperatures, locate the quantum critical point, and constrain the critical exponents. We observe a finite critical entropy per particle that carries a weak dependence on the atomic interaction strength. Our experiment provides a prototypical method to study quantum criticality with ultracold atoms.

In the vicinity of a continuous quantum phase transition, a many-body system enters the quantum critical regime, where quantum fluctuations lead to nonclassical universal behavior (*1*, *2*). Quantum criticality not only provides novel routes to new material design and discovery (*1*, *3*–*6*), but also provides a common framework for problems in condensed matter, nuclear physics (*7*, *8*), and cosmology (*1*, *9*). Quantum criticality plays a central role in strongly correlated systems such as heavy-fermion materials (*5*), spin dimer systems (*10*), Ising ferromagnets (*11*), and chromium at high pressure (*12*).

Ultracold atoms offer a clean setting for quantitative and precise investigation of quantum phase transitions (*13*–*16*) and critical phenomena (*17*). For example, the superfluid-to-Mott insulator quantum phase transition can be realized by loading atomic Bose-Einstein condensates into optical lattices (*13*). In recent experiments, scaling behavior of physical observables was reported in interacting Bose gases in three (*17*) and two dimensions (*18*), and in Rydberg gases (*19*), where collective behavior is insensitive to microscopic details. In addition, suppression of the superfluid critical temperature near the Mott transition was observed in three-dimensional (3D) optical lattices (*20*). Studying quantum criticality in cold atoms on the basis of finite-temperature thermodynamic measurements, however, remains challenging and has attracted increasing theoretical interest in recent years (*21*–*24*).

We report the observation of quantum critical behavior of ultracold cesium atoms in a two-dimensional (2D) optical lattice across the vacuum-to-superfluid transition. This phase transition can be viewed as a transition between a Mott insulator with zero occupation number and a superfluid, and can be described by the Bose-Hubbard model (*25*). Our measurements are performed on atomic samples near the normal-to-superfluid transition, connecting to the vacuum-to-superfluid quantum phase transition in the zero-temperature limit.

The quantum phase transition and quantum critical regime in this study are illustrated in Fig. 1. The zero-temperature vacuum-to-superfluid transition occurs when the chemical potential μ approaches its critical value μ_0. Sufficiently close to the quantum critical point, the critical temperature T_c for the normal-to-superfluid transition is expected to decrease according to the following scaling (*25*)

$$\frac{k_B T_c}{t} = c\left(\frac{\mu - \mu_0}{t}\right)^{z\nu} \quad (1)$$

where k_B is the Boltzmann constant, t is the tunneling energy, z is the dynamical critical exponent, ν is the correlation length exponent, and c is a constant. In the quantum critical regime (shaded area in Fig. 1), the temperature T provides the sole energy scale, and all thermodynamic observables are expected to scale with T (*25*). Thus, the equation of state is predicted to obey the following scaling (*21*)

$$\tilde{N} = F(\tilde{\mu}) \quad (2)$$

in which $F(x)$ is a generic function, and

$$\tilde{N} = \frac{N - N_r}{\left(\frac{k_B T}{t}\right)^{\frac{D}{z}+1-\frac{1}{z\nu}}} \text{ and } \tilde{\mu} = \frac{\frac{\mu-\mu_0}{t}}{\left(\frac{k_B T}{t}\right)^{\frac{1}{z\nu}}} \quad (3)$$

are the scaled occupation number and scaled chemical potential, respectively. Here, N is the occupation number, D is the dimensionality, and N_r is the nonuniversal part of the occupation number. For the vacuum-to-superfluid transition in the 2D Bose-Hubbard model, we have $N_r = 0$ and $D = 2$, and the predicted critical exponents are $z = 2$ and $\nu = 1/2$, characteristics of the dilute Bose gas universality class (*2*, *22*, *23*, *25*). We note that in a 2D system, there can be logarithmic corrections to scaling functions, including those in this study, near the quantum critical point (*2*). Within the temperature range of our experiment, however, the measurement is consistent with the above scaling laws in the absence of logarithmic corrections. Scaling behavior of T_c in the quantum critical regime was also observed in 2D condensates of spin triplets (*10*).

Our experiment is based on 2D atomic gases of cesium-133 in 2D square optical lattices (*26*, *27*). The 2D trap geometry is provided by the weak horizontal (r-) confinement and strong vertical (z-) confinement (*27*), with envelope trap frequencies f_r = 9.6 Hz and f_z = 1940 Hz, respectively. Typically, 4000 to 20,000 atoms are loaded into the lattice. The lattice constant is $d = \lambda/2 = 0.532$ μm and the depth is $V_L = 6.8\ E_R$, where $E_R = k_B \times 63.6$ nK is the recoil energy, $\lambda = 1064$ nm is the lattice laser wavelength, and h is the Planck constant. In the lattice, the tunneling energy is $t = k_B \times 2.7$ nK, the on-site interaction is $U = k_B \times 17$ nK, and the scattering length is $a = 15.9$ nm. The sample temperature is controlled in the range of 5.8 to 31 nK.

We determine the equation of state $n(\mu,T)$ of the sample from the measured in situ density distribution $n(x,y)$ (*18*, *26*). The chemical potential $\mu(x,y)$ and the temperature T are obtained by fitting the low-density tail of the sample where the atoms are normal. The fit is based on a mean-field model that accounts for interaction (*28*–*30*).

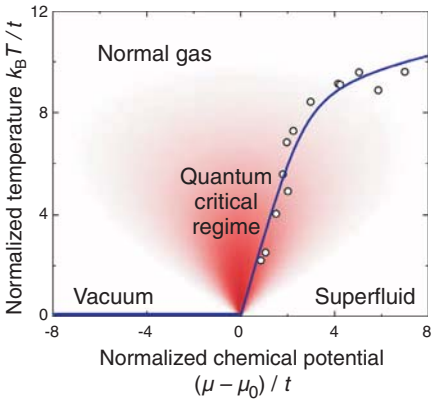

Fig. 1. The vacuum-to-superfluid quantum phase transition in 2D optical lattices. At zero temperature, a quantum phase transition from vacuum (horizontal thick blue line) to superfluid occurs when the chemical potential μ reaches the critical value μ_0. Sufficiently close to the transition point μ_0, quantum criticality prevails (red shaded area), and the normal-to-superfluid transition temperature T_c [measurements (*30*) shown as empty circles] is expected to vanish as $T_c \sim (\mu - \mu_0)^{z\nu}$; the blue line is a guide to the eye. From the prediction $z\nu = 1$ (*22*, *23*, *25*), the linearly extrapolated critical chemical potential is $\mu_0 = -3.6(6)t$, consistent with the theoretical value $-4t$ (*28*). Both the thermal energy scale $k_B T$ and the chemical potential μ are normalized by the tunneling t.

The James Franck Institute and Department of Physics, The University of Chicago, Chicago, IL 60637, USA.

*To whom correspondence should be addressed. E-mail: xibo@uchicago.edu (X.Z.); cchin@uchicago.edu (C.C.)

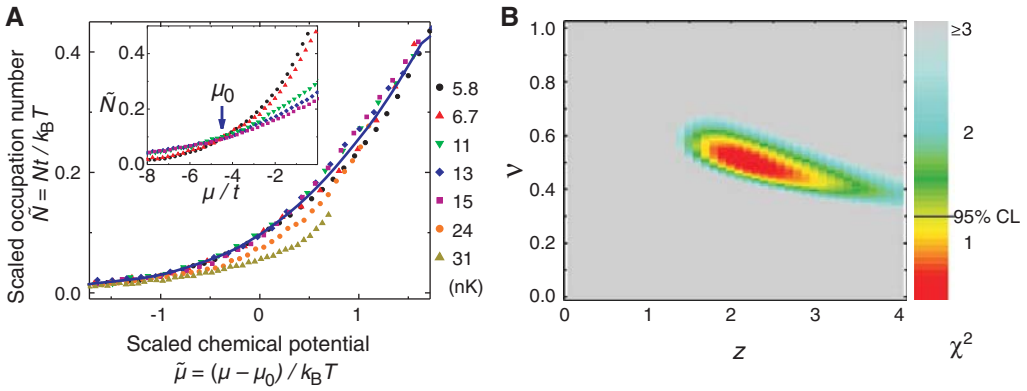

Fig. 2. Evidence of a quantum critical regime. (**A**) Scaled occupation number $\tilde{N} = Nt/k_BT$ as a function of the scaled chemical potential $\tilde{\mu} = (\mu - \mu_0)/k_BT$; the blue solid line shows the average curve for the lowest four temperatures. Inset shows the low-temperature data in the range of $T = 5.8$ to 15 nK, and the critical chemical potential μ_0 is identified as the crossing point; see text. The result, $\mu_0 = -4.5(6)\,t$, agrees with the prediction $\mu_0 = -4t$ (*28*). (**B**) Determination of the dynamical critical exponent z and the correlation length exponent ν based on $\mu_0 = -4.5t$. The color represents the reduced chi-squared (χ^2), and indicates how well the scaled equation of state can collapse into one single curve. The exponents are determined as $z = 2.2^{+1.0}_{-0.5}$ and $\nu = 0.52^{+0.09}_{-0.10}$, and the uncertainties correspond to a 95% confidence level. The predicted values are $z = 2$ and $\nu = 1/2$.

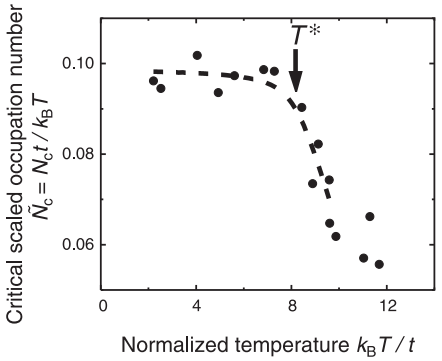

Fig. 3. Finite-temperature effect on quantum critical scaling. Scaled occupation number $\tilde{N}_c = N_c t/k_BT$ at the critical chemical potential $\mu = \mu_0$ as a function of the normalized temperature k_BT/t. The black dashed line is an empirical fit, giving a temperature scale $T^* \approx 8t/k_B$. For $T < T^*$, $\tilde{N}_c \approx 0.097$ is independent of the temperature; for $T > T^*$, $\tilde{N}_c$ deviates from the low-temperature value.

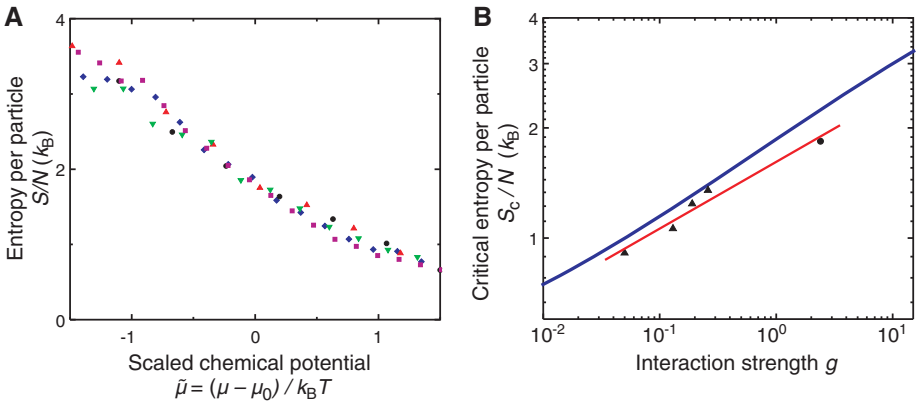

Fig. 4. Entropy per particle in the critical regime. (**A**) Entropy per particle S/N as a function of the scaled chemical potential $\tilde{\mu}$, measured in the temperature range of 5.8 to 15 nK (same symbol and color scheme as in Fig. 2A). (**B**) Critical entropy per particle S_c/N as a function of the effective interaction strength g: measurements for Bose gases with 2D optical lattices (black circle) and without lattice [black triangles, extracted from data in (*18*)], mean-field calculations (blue line), and a power-law fit to the measurements, $S_c/Nk_B = 1.6(1)g^{0.18(2)}$ (red line).

Equation of state measured near the quantum critical point can reveal essential information on quantum criticality, as proposed in (*28*).

We locate the quantum critical point by noting that at the critical chemical potential $\mu = \mu_0$, the scaled occupation number $\tilde{N} = Nt/k_BT = nd^2t/k_BT$ is temperature-independent, as indicated by Eq. 2. Here, we have applied a predicted exponent $\nu = 1/2$. We plot $\tilde{N}$ as a function of μ in the low-temperature range of 5.8 to 15 nK, and indeed observe a crossing point at $\mu_0 = -4.5(6)t$ (Fig. 2A, inset). We identify this point as the critical point for the vacuum-to-superfluid transition, and our result agrees with the prediction $-4t$ (*28*).

To test the critical scaling law, we compare the equation of state at different temperatures. On the basis of the expected exponents $z = 2$ and $\nu = 1/2$, we plot the scaled occupation number $\tilde{N}$ as a function of the scaled chemical potential $\tilde{\mu} = (\mu - \mu_0)/k_BT$ (Fig. 2A). Below 15 nK, all the measurements collapse into a single curve, confirming the emergence of the quantum critical scaling law (Eq. 2) at low temperatures. Note that we observe scaling behavior at temperatures from 5.8 to 15 nK, which are high compared to the tunneling scale $t/k_B = 2.7$ nK. Deviations become obvious at higher temperatures.

We examine the range of critical exponents z and ν that allow the scaled equation of state at low temperatures to overlap within experimental uncertainties. Taking $\mu_0 = -4.5t$ and various values of z and ν in the range of $0 < z < 4$ and $0 < \nu < 1$, we compute the corresponding scaled occupation numbers $\tilde{N}$ and scaled chemical potentials $\tilde{\mu}$ based on Eq. 3. We then evaluate how well the scaled equation of state in the range of $T = 5.8$ to 15 nK can collapse to a single curve by computing the reduced chi-squared (*30*). The best-fit exponents (Fig. 2B) are determined as $z = 2.2^{+1.0}_{-0.5}$ and $\nu = 0.52^{+0.09}_{-0.10}$, and the uncertainties correspond to a 95% confidence level. On the basis of the theoretical value of $\mu_0 = -4t$, we find the exponents to be $z = 2.6^{+1.2}_{-0.6}$ and $\nu = 0.44(8)$. In the following analyses, we adopt $z = 2$, $\nu = 1/2$, and $\mu_0 = -4.5t$.

Our measurements at different temperatures allow us to investigate the breakdown of quantum criticality at high temperatures. To quantify the deviations, we focus on the temperature dependence of the scaled occupation number $\tilde{N}$ at the critical chemical potential $\mu = \mu_0$ (Fig. 3). Deviations from the low-temperature value are clear when the temperature exceeds $T^* = 22$ nK $\approx 8t/k_B$. From this, we conclude that at $\mu = \mu_0$, the upper bound of thermal energy for the quantum critical behavior in our system is $k_BT^* \approx 8t$. Our result is in fair agreement with the prediction of $6t$ based on quantum Monte Carlo calculations (*23*).

From the equation of state, one can derive other thermodynamic quantities in the critical regime. We derive the entropy per particle S/N based on measurements in the temperature range of 5.8 to 15 nK, using a procedure similar to (*31*). The measured entropy per particle depends only on the scaled chemical potential $\tilde{\mu}$ and monotonically decreases (Fig. 4A), indicating a positive specific heat. Near the critical point $\tilde{\mu} = 0$, the entropy per particle has an approximate linear dependence on the scaled chemical potential: $S/Nk_B = a - b\tilde{\mu}$, with $a = 1.8(1)$, $b = 1.1(1)$. From this linear dependence, we derive an em-

pirical equation of state analogous to the ideal gas law (*30*)

$$P = Cn^{x}(k_{B}T)^{y} \quad (4)$$

where P is the pressure of the 2D gas, $x = 2/(1+b) = 0.95(5)$, $y = 2b/(1+b) = 1.05(5)$, $C = 0.8(2)(td^2)^{w}$ is a constant, and $w = (1-b)/(1+b) = -0.05(5)$.

Finally, we observe a weak dependence of the critical entropy per particle on the atomic interaction. Noting that a weakly interacting 2D Bose gas follows similar scaling laws near $\mu = 0$ (*18*) because it belongs to the same underlying dilute Bose gas universality class (*2*, *32*), we apply similar analysis and extract the critical entropy per particle S_c/N at four interaction strengths $g \approx 0.05, 0.13, 0.19, 0.26$, shown together with the lattice data ($g \approx 2.4$) in Fig. 4B. We observe a slow growing of S_c/N with g, and compare the measurements with mean-field calculations. The measured S_c/N is systematically lower than the mean-field predictions, potentially as a consequence of quantum critical physics. The weak dependence on the interaction strength can be captured by a power-law fit to the data as $S_c/Nk_B = 1.6(1)g^{0.18(2)}$.

In summary, on the basis of in situ density measurements of Bose gases in 2D optical lattices, we confirm the quantum criticality near the vacuum-to-superfluid quantum phase transition. Our experimental methods hold promise for identifying general quantum phase transitions, and prepare the tools for investigating quantum critical dynamics.

References and Notes

1. P. Coleman, A. J. Schofield, *Nature* **433**, 226 (2005).
2. S. Sachdev, *Quantum Phase Transitions* (Cambridge Univ. Press, Cambridge, 1999).
3. D. van der Marel *et al.*, *Nature* **425**, 271 (2003).
4. H. v. Löhneysen, A. Rosch, M. Vojta, P. Wölfle, *Rev. Mod. Phys.* **79**, 1015 (2007).
5. P. Gegenwart, Q. Si, F. Steglich, *Nat. Phys.* **4**, 186 (2008).
6. S. Sachdev, *Nat. Phys.* **4**, 173 (2008).
7. U. Al Khawaja, H. Stoof, *Nature* **411**, 918 (2001).
8. T. Senthil, A. Vishwanath, L. Balents, S. Sachdev, M. P. A. Fisher, *Science* **303**, 1490 (2004).
9. S. Sachdev, M. Müller, *J. Phys. Condens. Matter* **21**, 164216 (2009).
10. S. E. Sebastian *et al.*, *Nature* **441**, 617 (2006).
11. R. Coldea *et al.*, *Science* **327**, 177 (2010).
12. R. Jaramillo, Y. Feng, J. Wang, T. F. Rosenbaum, *Proc. Natl. Acad. Sci. U.S.A.* **107**, 13631 (2010).
13. M. Greiner, O. Mandel, T. Esslinger, T. W. Hänsch, I. Bloch, *Nature* **415**, 39 (2002).
14. K. Baumann, C. Guerlin, F. Brennecke, T. Esslinger, *Nature* **464**, 1301 (2010).
15. E. Haller *et al.*, *Nature* **466**, 597 (2010).
16. J. Simon *et al.*, *Nature* **472**, 307 (2011).
17. T. Donner *et al.*, *Science* **315**, 1556 (2007).
18. C.-L. Hung, X. Zhang, N. Gemelke, C. Chin, *Nature* **470**, 236 (2011).
19. R. Löw *et al.*, *Phys. Rev. A* **80**, 033422 (2009).
20. S. Trotzky *et al.*, *Nat. Phys.* **6**, 998 (2010).
21. Q. Zhou, T.-L. Ho, *Phys. Rev. Lett.* **105**, 245702 (2010).
22. K. R. A. Hazzard, E. J. Mueller, *Phys. Rev. A* **84**, 013604 (2011).
23. S. Fang, C.-M. Chung, P.-N. Ma, P. Chen, D.-W. Wang, *Phys. Rev. A* **83**, 031605(R) (2011).
24. Y. Kato, Q. Zhou, N. Kawashima, N. Trivedi, *Nat. Phys.* **4**, 617 (2008).
25. M. P. A. Fisher, P. B. Weichman, G. Grinstein, D. S. Fisher, *Phys. Rev. B* **40**, 546 (1989).
26. N. Gemelke, X. Zhang, C.-L. Hung, C. Chin, *Nature* **460**, 995 (2009).
27. C.-L. Hung, X. Zhang, N. Gemelke, C. Chin, *Phys. Rev. Lett.* **104**, 160403 (2010).
28. X. Zhang, C.-L. Hung, S.-K. Tung, N. Gemelke, C. Chin, *New J. Phys.* **13**, 045011 (2011).
29. B. Capogrosso-Sansone *et al.*, *New J. Phys.* **12**, 043010 (2010).
30. Materials and methods are available as supporting online material on *Science* Online.
31. T. Yefsah, R. Desbuquois, L. Chomaz, K. J. Günter, J. Dalibard, *Phys. Rev. Lett.* **107**, 130401 (2011).
32. S. Sachdev, E. R. Dunkel, *Phys. Rev. B* **73**, 085116 (2006).

Acknowledgments: We thank N. Prokof'ev and D.-W. Wang for discussions and numerical data; Q. Zhou, K. Hazzard, and N. Trivedi for discussions; and N. Gemelke and C. Parker for discussions and reading of the manuscript. The work was supported by NSF (grants PHY-0747907 and NSF-MRSEC DMR-0213745), the Packard foundation, and a grant from the Army Research Office with funding from the Defense Advanced Research Projects Agency Optical Lattice Emulator program. The data presented in this paper are available upon request sent to cchin@uchicago.edu.

Supporting Online Material

www.sciencemag.org/cgi/content/full/science.1217990/DC1
Materials and Methods
Fig. S1
References (*33*, *34*)

15 December 2011; accepted 30 January 2012
Published online 16 February 2012;
10.1126/science.1217990

Reactions of Solvated Electrons Initiated by Sodium Atom Ionization at the Vacuum-Liquid Interface

William A. Alexander,[1] Justin P. Wiens,[2] Timothy K. Minton,[1]* Gilbert M. Nathanson[2]*

Solvated electrons are powerful reagents in the liquid phase that break chemical bonds and thereby create additional reactive species, including hydrogen atoms. We explored the distinct chemistry that ensues when electrons are liberated near the liquid surface rather than within the bulk. Specifically, we detected the products resulting from exposure of liquid glycerol to a beam of sodium atoms. The Na atoms ionized in the surface region, generating electrons that reacted with deuterated glycerol, $C_3D_5(OD)_3$, to produce D atoms, D_2, D_2O, and glycerol fragments. Surprisingly, 43 ± 4% of the D atoms traversed the interfacial region and desorbed into vacuum before attacking C-D bonds to produce D_2.

Radiolysis experiments provide fundamental insights into electron reactivity in protic liquids such as water and alcohols through the use of ionizing reagents, including gamma rays and high-energy electrons, which penetrate deeply into solution. These reagents energize and ionize solvent molecules, creating hydrogen atoms and other free radicals, as well as solvated electrons, e_s^-, often in high enough concentrations to react with each other (*1*, *2*). Electrons and radicals created at the vacuum-liquid interface may behave differently from those in the bulk because of their partial solvation (*3*–*6*) and because transient neutral intermediates may evaporate before reacting further. Recent photoionization experiments show that partially to fully solvated electrons persist for $\geq 10^{-10}$ s at the surface of water, potentially leading to enhanced destruction of organic molecules in contact with these electrons (*6*–*8*). Molecular beam methods, using gas-phase sodium atoms as neutral precursors, provide a previously unexplored alternative for generating interfacial electrons in protic liquids. These electrons initiate a wide range of chemical events, including the production of atomic and molecular radicals that react at and near the surface or escape by evaporating from solution.

We performed the experiments by directing a weak effusive beam of sodium atoms at the surface of a liquid glycerol (1,2,3-propanetriol) film in vacuum. These Na atoms rapidly ionize into Na_s^+ and e_s^- in the interfacial region. We chose glycerol because of its low vapor pressure (10^{-4} torr) and water-like ability to solvate ions and electrons (*9*, *10*). Solvated electrons react in more diverse ways with alcohols than with water. In the latter case, the primary pathways are slow dissociation, $e_s^- + H_2O \rightarrow H + OH^-$, and fast recombination, $2e_s^- + 2H_2O \rightarrow H_2 + 2OH^-$ (*2*, *11*). The low flux of our effusive Na beam ensures that similar electron-electron recombination and additional radical-radical reactions do not compete with electron-solvent and radical-solvent reactions, whereas the soft landing and gentle ionization of Na generates elec-

[1]Department of Chemistry and Biochemistry, Montana State University, Bozeman, MT 59717, USA. [2]Department of Chemistry, University of Wisconsin, Madison, WI 53706, USA.

*To whom correspondence should be addressed. E-mail: tminton@montana.edu (T.K.M.); gmnathan@wisc.edu (G.M.N.)

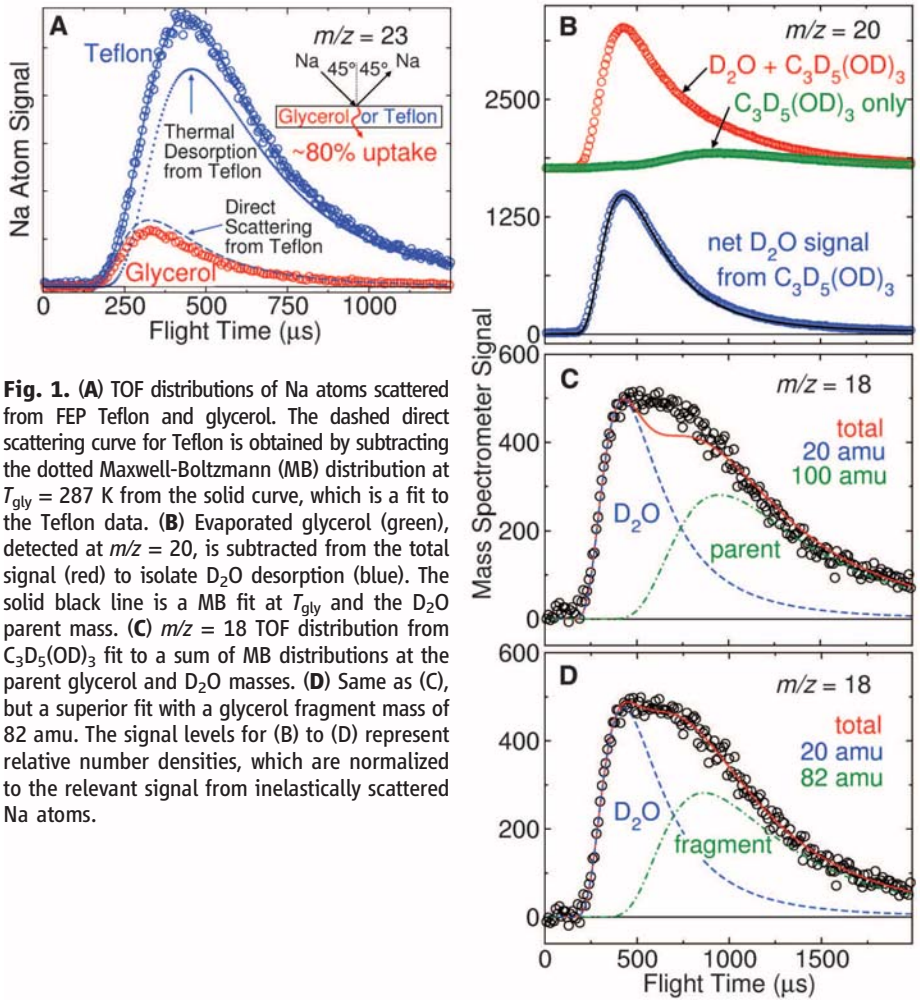

Fig. 1. (**A**) TOF distributions of Na atoms scattered from FEP Teflon and glycerol. The dashed direct scattering curve for Teflon is obtained by subtracting the dotted Maxwell-Boltzmann (MB) distribution at T_{gly} = 287 K from the solid curve, which is a fit to the Teflon data. (**B**) Evaporated glycerol (green), detected at m/z = 20, is subtracted from the total signal (red) to isolate D_2O desorption (blue). The solid black line is a MB fit at T_{gly} and the D_2O parent mass. (**C**) m/z = 18 TOF distribution from $C_3D_5(OD)_3$ fit to a sum of MB distributions at the parent glycerol and D_2O masses. (**D**) Same as (C), but a superior fit with a glycerol fragment mass of 82 amu. The signal levels for (B) to (D) represent relative number densities, which are normalized to the relevant signal from inelastically scattered Na atoms.

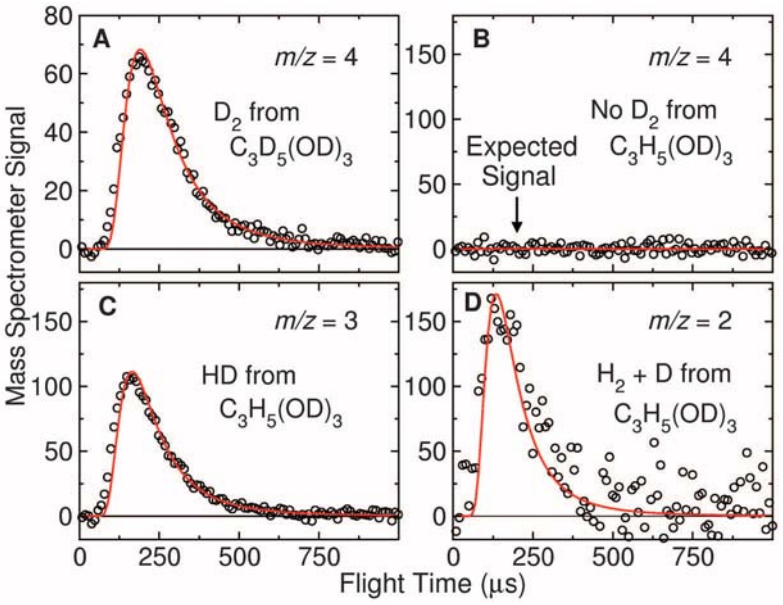

Fig. 2. TOF distributions of molecular hydrogen isotopologues: (**A**) D_2 from $C_3D_5(OD)_3$, (**B**) D_2 from $C_3H_5(OD)_3$, (**C**) HD from $C_3H_5(OD)_3$, and (**D**) H_2 + D from $C_3H_5(OD)_3$. The contribution from evaporated glycerol has been subtracted from each distribution. The solid red curves are MB fits at T_{gly} = 287 K.

trons in the absence of high-energy excitations. As shown below, reactions between these electrons and glycerol generate atomic and molecular hydrogen, water, and glycerol fragments within an estimated depth of 50 Å.

The continuously refreshed glycerol film, 0.1 mm thick, was held at 287 K during Na-atom exposure (fig. S1) (*12*, *13*). To delineate the reaction pathways, we used both $C_3H_5(OD)_3$ and $C_3D_5(OD)_3$ isotopologues. The velocity and angular distributions of the scattered Na atoms and desorbed reaction products were monitored by a rotatable mass spectrometer (*14*). Product signals were recorded as time-of-flight (TOF) distributions after the stream of molecules exiting the liquid surface was divided into pulses by a spinning slotted wheel. The Na oven (held at 670 K) produced a nearly effusive beam that deposited ~1 monolayer of Na atoms on the glycerol film during its 0.2-s exposure time.

Na-atom uptake into glycerol is explored in Fig. 1A, which compares the Na-atom signal after collision with the glycerol film to that obtained from FEP (fluorinated ethylene propylene) Teflon, presumed to be much less reactive than glycerol. The strength of the integrated flux from Teflon is ~4 times that from glycerol, implying that at least ~80% of the impinging Na atoms dissolve into glycerol and do not escape. The recorded distribution of Na atoms scattered from Teflon was decomposed into two components corresponding to (i) Na atoms that scatter directly (higher velocities and shorter arrival times; dashed line) and (ii) those that fully dissipate their energy at the surface and then thermally desorb in a Maxwell-Boltzmann (MB) distribution at the glycerol temperature of T_{gly} = 287 K (lower velocities and longer arrival times; dotted line). The glycerol distribution mimics direct scattering from Teflon and is entirely missing the thermal desorption component. Thus, Na atoms that thermally equilibrate on the glycerol film do not desorb into vacuum but instead remain in contact with glycerol molecules. The absence of thermally desorbed Na atoms implies that they ionize into Na_s^+ and e_s^- before motions of the surface glycerol molecules can propel the atoms back into the gas phase. Ab initio molecular dynamics simulations of Na-atom collisions with H_2O clusters corroborate this rapid interfacial ionization and show that surface water molecules reorient to point their OH groups toward the evolving Na_s^+ and e_s^- (*15*). The high density of OH groups in glycerol likely promotes both the immediate Na ionization inferred here and the subnanosecond solvation of electrons in the bulk (*10*). Reactions of these ionizing Na atoms with solvent glycerol may occur through direct electron transfer from Na to glycerol (*16*) or after partial or full electron solvation to form contact Na^+/e^- ion pairs or solvent-separated ions and electrons (*17*, *18*).

Analysis of the observed product signals revealed that electrons from Na atoms react with $C_3D_5(OD)_3$ to generate four volatile species: D

atoms, D_2, D_2O, and glycerol fragments. The D atoms are created close enough to the surface that nearly half of them escape into the vacuum before reacting with the solvent or with each other.

We observed copious water production from both glycerol isotopologues upon Na-atom exposure. Figure 1B shows D_2O desorption from $C_3D_5(OD)_3$ detected at a mass-to-charge ratio m/z = 20 (D_2O^+). This desorption is accompanied by the natural evaporation of intact glycerol molecules, which appear at m/z = 20 through dissociative ionization in the mass spectrometer. The D_2O product molecules desorb with a MB velocity distribution at T_{gly} (blue curve fit to the net D_2O signal) and a cosine angular distribution (fig. S2). These good fits demonstrate that reactions of e_s^- create D_2O molecules that thermally equilibrate before desorbing into vacuum. D_2O may be produced by ionic and neutral routes, as established in previous radiolysis studies of bulk liquid ethanol (*19*) and ethylene glycol (*20*). In the ionic pathway, an electron attacks solvent glycerol to make hydroxide, $e_s^- + C_3D_5(OD)_3 \rightarrow {\bullet}C_3D_5(OD)_2 + OD^-$, followed by an acid-base reaction, $C_3D_5(OD)_3 + OD^- \rightarrow D_2O + C_3D_5(OD)_2O^-$ (*19*). A second, neutral pathway involves D-atom attack on solvent glycerol to make D_2 and ${\bullet}C_3D_4(OD)_3$, which subsequently decomposes into D_2O and the open-shell ketone ${\bullet}CD_2COCD_2OD$ (*20*).

Figure 1, C and D, provides evidence for one or both D_2O channels through identification of the matching glycerol fragments. The TOF distribution, monitored at m/z = 18 (OD^+), is much broader than expected for pure D_2O desorption even after subtracting the parent glycerol signal. Figure 1C shows an attempt to fit this long–arrival time component with evaporation of parent glycerol (100 amu): The poor fit indicates that this component cannot be explained by glycerol desorption created by Na-atom sputtering or the local heat of reaction. Instead, the extra signal in Fig. 1D can be well fit by a MB distribution in the mass range of 78 to 84 amu. This range is consistent with evaporation of the ${\bullet}C_3D_5(OD)_2$ and ${\bullet}CD_2COCD_2OD$ radicals and their closed-shell products after abstracting a D atom from a neighboring glycerol molecule (*13*). To the extent that it occurs, the desorption of the radical species provides a means to halt their decomposition and the associated chain reactions that occur in the bulk (*20*).

Na ionization also initiates reactions that generate molecular hydrogen, as shown in Fig. 2. As with D_2O, the D_2 molecules arising from reactions with $C_3D_5(OD)_3$ in Fig. 2A are fit well by MB velocity (solid lines) and cosine angular distributions (fig. S2). This D_2 production implies that D atoms are created by electron-induced dissociation of O-D and C-D bonds, after which the D atom abstracts a second D atom from the solvent. We found that D_2 is not produced from the mixed isotopologue, $C_3H_5(OD)_3$, as shown in Fig. 2B. The absence of D_2 in this case has two implications. First, D atoms created by e_s^- near the surface are not energetic enough to overcome the high activation energy for D-atom abstraction from O-D bonds (*21*). In the case of $C_3D_5(OD)_3$ in Fig. 2A, D_2 must instead arise from D-atom abstraction from a C-D bond. Second, D atoms react with solvent glycerol faster than they can react with each other ($D + D \rightarrow D_2$) at our low Na beam flux. The missing D_2 signal from $C_3H_5(OD)_3$ instead appears as HD at m/z = 3 (Fig. 2C), which arises from D-atom attack on glycerol C-H rather than O-D bonds. The signal at m/z = 2 in Fig. 2D reflects the evaporation of both H_2 and D, which have the same mass, where H_2 is created from H-atom attack on glycerol C-H. Although D atoms almost exclusively break C-H bonds over the stronger O-D bonds, we find that e_s^- preferentially breaks O-D bonds, generating D and $C_3H_5(OD)_2O^-$ (*2*, *13*, *19*, *22*). A detailed analysis of the H_2 and HD signals from $C_3H_5(OD)_3$ indicates that e_s^- generates D and H from glycerol O-D and C-H bonds in the ratio of 3:1 (*13*). This ratio of electron-induced O-D to C-D bond breaking for $C_3D_5(OD)_3$ is expected to be even higher because of the lower zero-point energy and weaker reactivity of C-D bonds relative to C-H bonds.

The most striking distinction between our gas-liquid experiments and bulk liquid studies is shown in Fig. 3. The data provide direct evidence for the creation of D atoms near the surface of glycerol and their evaporation into vacuum. We monitored these D atoms at m/z = 2 from the $C_3D_5(OD)_3$ isotopologue, where there is no interference from desorbing H_2. The TOF distribution shown in Fig. 3A includes dissociative ionization components from parent glycerol or glycerol fragments, D_2O, and D_2, in addition to D atoms themselves. These extra components were subtracted from the distribution after fitting each component with a MB distribution at its parent mass with relative intensities consistent with established mass spectral patterns (table S1). The remaining signal in the distribution at early arrival times was fit by a MB distribution at the D-atom mass in Fig. 3B. Analysis of the D and D_2 signal intensities (table S2) indicates that 43 ± 4% of the D atoms desorb before they react to form D_2, implying that D atoms are created close enough to the surface that desorption and reaction occur simultaneously.

The similar time scales for D-atom desorption and reaction may be used to gauge where these atoms are created by Na-atom ionization in glycerol. D-atom reaction times can be estimated from the 1.0×10^7 M^{-1} s^{-1} rate constant for the analogous $D + (CD_3)_2CDOD \rightarrow D_2 + (CD_3)_2\dot{C}OD$ reaction in D_2O at 287 K (*22*). Using this rate constant and taking into account the 14 M density of glycerol, the half-life ($t_{1/2}$)

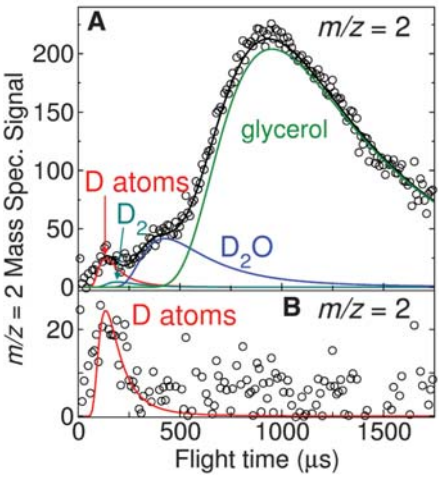

Fig. 3. (**A**) Deconvolution of the m/z = 2 TOF distribution after collisions of Na with $C_3D_5(OD)_3$. The distribution is fit by a sum of D, D_2, D_2O, and glycerol MB distributions at T_{gly}. (**B**) D-atom signal after subtraction.

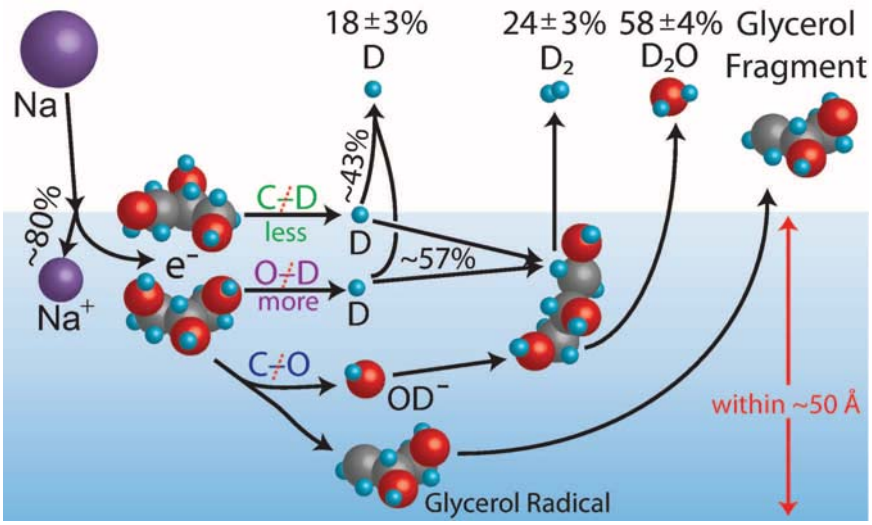

Fig. 4. First steps in the Na atom–initiated electron reactions with deuterated glycerol, $C_3D_5(OD)_3$. Only the OD^- pathway for D_2O production is shown.

for D atoms in pure glycerol is calculated to be 5 ns. D-atom desorption competes nearly equally with D-atom reaction; these atoms desorb on average over a depth of $(Dt_{1/2})^{1/2} \approx 50$ Å, or ~10 glycerol layers, using a diffusion coefficient $D \approx 4 \times 10^{-5}$ cm^2 s^{-1} for D atoms in D_2O (*23*, *24*). This reaction depth may even be shallower if the D atoms diffuse more slowly in pure glycerol because of its viscosity, 2800 cP, at 287 K (*13*). D atoms are therefore created by e_s^- close to, but not necessarily within, the outermost region where Na atoms ionize (*15*).

Figure 4 summarizes the production of D, D_2, D_2O, and glycerol fragments initiated by surface Na-atom ionization, along with possible scenarios for their creation. Each species desorbs only after thermal equilibration. This observation is complementary to the nonthermal ejection of D and O atoms after bombardment of D_2O ice by electrons carrying 5 to 50 eV of energy (*25*), which is substantially greater than the –0.8 eV ionization enthalpy of Na in bulk water (*26*, *27*). Analysis of the TOF signals (table S2) indicates that D, D_2, and D_2O desorb in the flux ratio 1:1.3:3.2. We thus find that nearly half of the D atoms produced by electron-stimulated dissociation of O-D and C-D bonds escape into the vacuum before they abstract a second D atom from the solvent to produce D_2. This high desorption rate implies that near-surface reactions of even this energetic species must compete with its escape into the vacuum—a route that is not available deep within glycerol or other solvents, potentially including aqueous solutions. Because of the proximity of surface molecules to the gas phase, the observed competition between evaporation and reaction should be a universal feature of the interfacial chemistry of neutral energetic species created by interfacial electrons. Alkali-atom collisions provide a promising approach to prepare these electrons and the radicals they create, and to explore their reactions with both solvent and solute molecules at or near the surfaces of liquids.

References and Notes

1. B. C. Garrett *et al.*, *Chem. Rev.* **105**, 355 (2005).
2. G. V. Buxton, C. L. Greenstock, W. P. Helman, A. B. Ross, W. Tsang, *J. Phys. Chem. Ref. Data* **17**, 513 (1988).
3. N. I. Hammer *et al.*, *Science* **306**, 675 (2004).
4. J. R. R. Verlet, A. E. Bragg, A. Kammrath, O. Cheshnovsky, D. M. Neumark, *Science* **307**, 93 (2005).
5. Á. Madarász, P. J. Rossky, L. Turi, *J. Chem. Phys.* **126**, 234707 (2007).
6. D. M. Sagar, C. D. Bain, J. R. R. Verlet, *J. Am. Chem. Soc.* **132**, 6917 (2010).
7. K. R. Siefermann *et al.*, *Nat. Chem.* **2**, 274 (2010).
8. B. Abel, U. Buck, A. L. Sobolewski, W. Domcke, *Phys. Chem. Chem. Phys.* **14**, 22 (2012).
9. A. H. Muenter, J. L. DeZwaan, G. M. Nathanson, *J. Phys. Chem. B* **110**, 4881 (2006).
10. J. Bonin, I. Lampre, P. Pernot, M. Mostafavi, *J. Phys. Chem. A* **112**, 1880 (2008).
11. R. N. Barnett, R. Giniger, O. Cheshnovsky, U. Landman, *J. Phys. Chem. A* **115**, 7378 (2011).
12. M. E. Saecker, G. M. Nathanson, *J. Chem. Phys.* **99**, 7056 (1993).
13. See supporting material on *Science* Online.
14. J. Zhang, D. J. Garton, T. K. Minton, *J. Chem. Phys.* **117**, 6239 (2002).
15. L. Cwiklik, U. Buck, W. Kulig, P. Kubisiak, P. Jungwirth, *J. Chem. Phys.* **128**, 154306 (2008).
16. Y. Ferro, A. Allouche, V. Kempter, *J. Chem. Phys.* **120**, 8683 (2004).
17. R. M. Forck *et al.*, *J. Chem. Phys.* **132**, 221102 (2010).
18. D. H. Paik, I.-R. Lee, D.-S. Yang, J. S. Baskin, A. H. Zewail, *Science* **306**, 672 (2004).
19. J. J. J. Myron, G. R. Freeman, *Can. J. Chem.* **43**, 381 (1965).
20. C. E. Burchill, K. M. Perron, *Can. J. Chem.* **49**, 2382 (1971).
21. J. Park, Z. F. Xu, M. C. Lin, *J. Chem. Phys.* **118**, 9990 (2003).
22. A. M. Lossack, E. Roduner, D. M. Bartels, *J. Phys. Chem. A* **102**, 7462 (1998).
23. E. Roduner, *Radiat. Phys. Chem.* **72**, 201 (2005).
24. V. A. Benderskii, A. G. Krivenko, *Russ. J. Electrochem.* **32**, 663 (1996).
25. T. M. Orlando, G. A. Kimmel, *Surf. Sci.* **390**, 79 (1997).
26. J. O. M. Bockris, A. K. N. Reddy, *Modern Electrochemistry I: Ionics* (Plenum, New York, ed. 2, 1998).
27. H. Shiraishi, G. R. Sunaryo, K. Ishigure, *J. Phys. Chem.* **98**, 5164 (1994).

Acknowledgments: This work was supported by NSF grant CHE-0943639 as part of the Center for Energetic Non-Equilibrium Chemistry at Interfaces. We thank L. Sankaran, G. Schatz, I. Benjamin, and a reviewer for invaluable advice. The data described in this work can be obtained from the corresponding authors upon request.

Supporting Online Material

www.sciencemag.org/cgi/content/full/335/6072/1072/DC1
Materials and Methods
SOM Text
Figs. S1 and S2
Tables S1 and S2
References (*28*–*36*)

31 October 2011; accepted 25 January 2012
10.1126/science.1215956

No Straight Path: Roaming in Both Ground- and Excited-State Photolytic Channels of $NO_3 \rightarrow NO + O_2$

Michael P. Grubb,[1] Michelle L. Warter,[1] Hongyan Xiao,[2] Satoshi Maeda,[2,3] Keiji Morokuma,[2,4] Simon W. North[1]*

Roaming mechanisms have recently been observed in several chemical reactions alongside trajectories that pass through a traditional transition state. Here, we demonstrate that the visible light–induced reaction $NO_3 \rightarrow NO + O_2$ proceeds exclusively by roaming. High-level ab initio calculations predict specific NO Λ doublet propensities (orientations of the unpaired electron with respect to the molecular rotation plane) for this mechanism, which we discern experimentally by ion imaging. The data provide direct evidence for roaming pathways in two different electronic states, corresponding to both previously documented photolysis channels that produce $NO + O_2$. More broadly, the results raise intriguing questions about the overall prevalence of this unusual reaction mechanism.

Traditionally, chemical reaction mechanisms involving multiple bond breaking and formation steps are characterized by a transition state in the form of a well-defined saddle point on the potential energy surface. Recently, however, a second type of mechanism termed "roaming" has come to light, which bypasses this saddle point entirely (*1*–*3*). Instead, a frustrated bond cleavage leaves part of the molecule without sufficient energy to escape, and it orbits the remaining fragment until encountering a reactive site to form the products via intramolecular abstraction. This mechanism has received considerable attention in the past 8 years, having been first identified in formaldehyde dissociation as a minor channel (*4*, *5*) and then later in acetaldehyde as the dominant pathway to $CH_4 + CO$ products (albeit still a minor fraction of the overall quantum yield) (*6*, *7*). Evidence of roaming dynamics has since been observed in a handful of other systems, but in all cases has been observed alongside a traditional tight transition state channel (*2*, *8*).

Recently, we reported that roaming may be the dominant of the two observed pathways that produce molecular products in NO_3 photodissociation (*9*), a reaction of considerable atmospheric importance. Additionally, theoretical calculations implicated roaming on the excited-state potential surface; previous observations of roaming were restricted to the electronic ground state (*10*, *11*). Here, we report direct experimental and theoretical evidence confirming the role of excited-state roaming in NO_3 photodissociation. Thus, roaming is not only the dominant mechanism for forming the molecular products of NO_3 but the exclusive mechanism, with no evidence of a competing traditional transition state.

[1]Department of Chemistry, Texas A&M University, College Station, TX 77842, USA. [2]Fukui Institute for Fundamental Chemistry, Kyoto University, 34-4 Takano Nishihiraki-cho, Sakyo, Kyoto 606-8103, Japan. [3]The Hakubi Center, Kyoto University, Yoshida-Ushinomiya-cho, Sakyo-ku, Kyoto 606-8302, Japan. [4]Cherry L. Emerson Center for Scientific Computation and Department of Chemistry, Emory University, Atlanta, GA 30322, USA.

*To whom correspondence should be addressed. E-mail: swnorth@tamu.edu

The two dissociative pathways of NO_3 to yield NO and O_2 products were recently resolved via high-resolution ion imaging experiments (*9*, *12*). In those experiments, a molecular beam of dilute NO_3 (<1%) in helium was photolyzed by a 588-nm laser pulse. A single rovibronic quantum state of the NO photofragment was selectively ionized by a second laser, and the resulting NO cations were focused by electrostatic lenses onto a two-dimensional microchannel plate–phosphor ion detector. The radial displacement of each ion impact is a measure of the recoil velocity resulting from the photolysis. By simultaneously measuring the NO quantum state and velocity, the quantum state of the coincident O_2 fragment could be determined through the conservation of energy and linear momentum. State-selective correlated measurements are ideal for uncovering multiple reaction pathways and revealed two separate pathways for the $NO_3 \rightarrow NO + O_2$ reaction. Pathway 1 (Pwy 1), the dominant pathway, resulted in highly vibrationally excited O_2 fragments in coincidence with lower NO rotational quantum numbers (Fig. 1, inset). This pathway bears many similarities to the roaming pathway observed in formaldehyde dissociation. The excited O_2 vibrational distribution originates from the extended O-O bond distance at the roaming saddle point (ONO-O). Vibrationally excited O_2 products ($v > 6$) have also been observed in the intermolecular abstraction reaction $NO_2 + O \rightarrow NO + O_2$ (*13*), reinforcing the description of roaming as an intramolecular abstraction (*14*, *15*).

The nature of pathway 2 (Pwy 2), which results in fragments with large rotational angular momentum in both products and a colder O_2 vibrational distribution (Fig. 1, inset), has proven more elusive. Although it was speculated that the pathway originated from a traditional three-center transition state (*12*, *16*), which is present in all other systems where roaming has been identified, no transition state of relevant energy has yet been calculated by theory. Recent theoretical calculations mapping the potential energy surfaces of the first several electronic states of NO_3 have shown that the lowest-lying excited state, which is optically dark, is accessible through a series of conical intersections after photoexcitation to a higher-energy "bright" state (Fig. 1) (*10*). Maeda and co-workers proposed that roaming actually occurs on this first excited dark state and may later access the ground state at long (O_2N-O) bond distances through another conical intersection. The two experimentally observed pathways could therefore be explained by dissociation on two different electronic potential surfaces (*10*, *11*). Furthermore, the ONO-O saddle point on each potential surface (SP1 and SP2) has a different O-O bond length leading to different vibrational distributions in the O_2 product fragment, consistent with experimental observations. The critical role of the optically dark state in the photochemistry of NO_3 was unexpected and warranted further experimental exploration.

An experimental test of this two-state roaming theory requires that a signature of the dissociative electronic state be retained in the photofragments. Electronic symmetry must be conserved for chemical processes, and thus the electronic orbital symmetry in NO_3 should be maintained in the product fragments. The orbital symmetry of a diatomic molecule in a $^2\Pi$ electronic configuration such as the ground state of NO can be expressed by the Λ doublet propensity. An A" Λ doublet propensity indicates that the singly occupied pπ-orbital lobe is pointed out of the fragment rotational plane, whereas an A' Λ doublet propensity indicates that the lobe is oriented in the rotational plane. The photodissociation of water is a classic example of this electronic symmetry conservation. The absorption of a photon leads to an excited electronic state of water characterized by an unpaired electron in an out-of-plane pπ-orbital lobe. This symmetry is conserved during dissociation, resulting

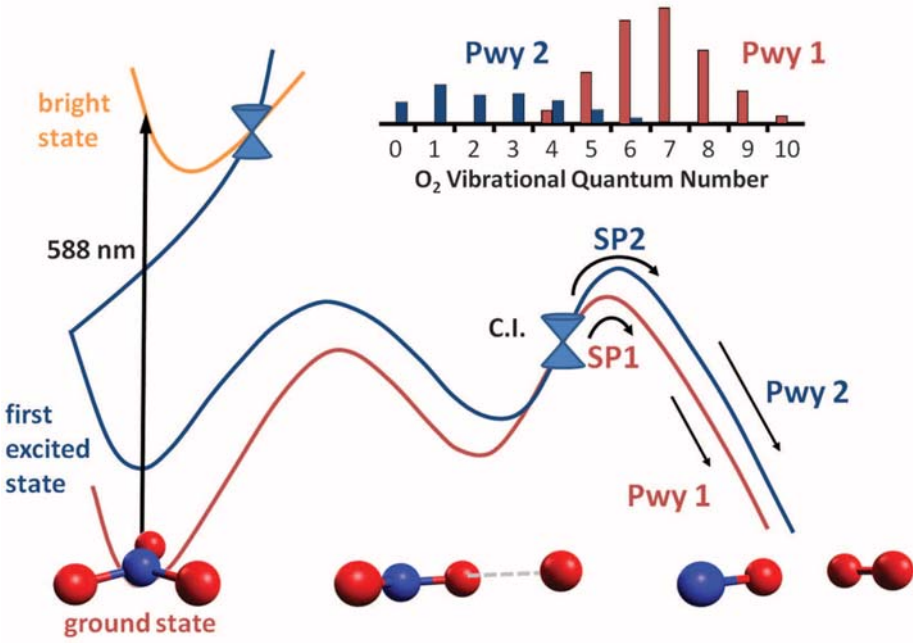

Fig. 1. Schematic diagram of the lowest-lying electronic state surfaces proposed to give rise to the two experimentally observed pathways (Pwy 1 and 2) via C.I. (conical intersection) resulting from NO_3 photolysis at 588 nm. The experimental vibrational distributions of the O_2 fragments produced from the two pathways are also provided, with the difference ascribed to different ONO-O bond lengths at the saddle points on the two surfaces (SP1 and SP2).

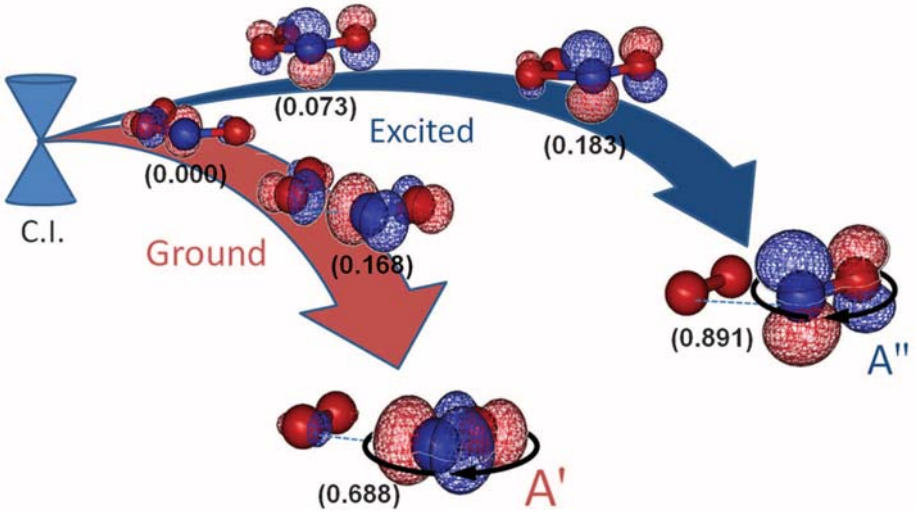

Fig. 2. Evolution of the key electronic orbital in the NO_3 exit channel derived from the CASSCF calculations (*18*) of some representative structures along the post-C.I. reaction pathways determined by our previous study (*10*). The occupancy of the orbital is shown at each step in parentheses. In-plane dissociation results in opposite NO Λ doublet propensities for the two pathways.

in a strong preference for producing OH fragments in the upper A" Λ doublet state, from which stimulated emission has been proposed as a source for interstellar masers (*17*). The correlation between Λ doublet propensities and electronic origin provides a convenient means of distinguishing pathways on different electronic potential surfaces, provided the electronic states possess different electronic symmetries.

We performed ab initio calculations to determine the evolution of the electronic orbitals in the NO_3 exit channel, in order to predict the preferred Λ doublet state arising from each electronic state potential surface. These orbitals were obtained by CASSCF calculations (*18*) and calculated for some representative structures along the reaction pathways determined in our previous study (*10*). The results shown in Fig. 2 support in-plane dissociation on both surfaces (*19*) and conveniently predict opposite Λ doublet propensities for each pathway. The pπ-orbital lobe in the NO fragment containing the unpaired electron lies in the NO rotational plane (A' Λ doublet state) for trajectories evolving on the ground state of NO_3, whereas the lobe is perpendicular to the NO rotational plane (A" Λ doublet state) for trajectories evolving on the dark state of NO_3. Thus, experimental measurements of the NO Λ doublet propensities should show an A' preference for pathway 1 and an A" preference for pathway 2, if the two-state dissociation model is correct (*20*).

The unpaired pπ-orbital lobe in NO defines the spectroscopic transition dipole moment **μ** for the $A(^2\Sigma) \leftarrow X(^2\Pi)$ transition, which is the resonant step of the two-photon detection scheme previously used in the ion imaging experiments of (*9*, *12*). The Λ doublet propensity of the NO fragment can therefore be determined by comparing the relative intensities of the P, Q, and R branches of this transition (*21*). For a classical Q branch transition, **μ** is parallel to the rotational axis **j**. Therefore, a Q branch transition will primarily excite the A" Λ doublet state, where the unpaired pπ-orbital lobe and hence **μ** is pointing out of the rotational plane along **j**. For a P or R branch transition, **μ** is perpendicular to **j** and thus the A' Λ doublet state is preferred. In the case of our ion imaging experiments, the two dissociation pathways result in NO fragments with two different translational energy distributions (observed as different radii in the ion images). Relative Λ doublet propensities for the two pathways can therefore be determined by observing how the relative intensity of the two energy distributions changes when the NO is detected via Q and P (or R) branch transitions. Previous measurements of rotationally excited NO fragments focused on Q branch transitions, as the lines of this branch are more isolated in the excitation spectrum. Here, we present measurements of a particular NO rotational state probed via multiple rotational branches (*18*).

Figure 3 shows velocity map images of the NO ($^2\Pi_{3/2}$ $v = 0$, $N = 22$) photoproducts after resonance-enhanced multiphoton ionization, as well as the corresponding NO total translational energy distributions, probed via the Q_{22} branch (right) and the P_{22} branch (left). The lower–translational energy NO fragments originate from pathway 1 (because most of the available energy is in the vibration of the O_2 cofragment), whereas the higher–translational energy NO originates from pathway 2. The results are dramatic, showing highly suppressed pathway 2 signal in the P_{22} branch ion image. This implies a strong preference in pathway 2 for producing NO in the A" Λ doublet state, in agreement with the theoretical prediction shown in Fig. 2. The magnitude of the difference in the relative intensities also suggests that NO derived from pathway 1 must possess the opposite Λ doublet propensity, in agreement with the ab initio calculations, although this result is not necessarily of dynamical origin because a 2:1 ratio favoring the A' state is statistically predicted if the dissociation is not constrained to the molecular plane (*22*).

The results of these measurements and the corresponding theory strongly support in-plane two-state roaming dynamics for NO_3 photodissociation, without competition from a traditional transition state mechanism. Additionally, the NO_3 system differs from previous documented roaming dissociations in that its roaming dynamics access multiple electronic potential surfaces. Near the product asymptotes the electronic potentials converge, and because roaming trajectories explore a large area of these asymptotic surfaces, it is not surprising that the trajectories may involve multiple electronic states. What effect does the slow, broadly sampling dynamics of roaming have on a system's ability to access additional potential energy surfaces? Do roaming dynamics lead to an even more complicated reaction than a simple intramolecular abstraction? The low vibrational states of the oxygen fragment associated with the dark state pathway could not be measured due to diminishing Franck-Condon factors in previous laser-induced fluorescence experiments. It is therefore unclear whether the excited state is accessed in the bimolecular NO_2 + O abstraction reaction or the thermal dissociation of NO_3, or is confined to the photochemistry. However, the conical intersection at extended NO_3 geometries between the ground- and excited-state potential energy surfaces, which has been proposed to lead to the observed multistate dynamics, should be equally accessible by bimolecular and thermal reactions. Whether excited-state roaming is widespread, or constitutes a unique feature of the NO_3 system, remains to be seen.

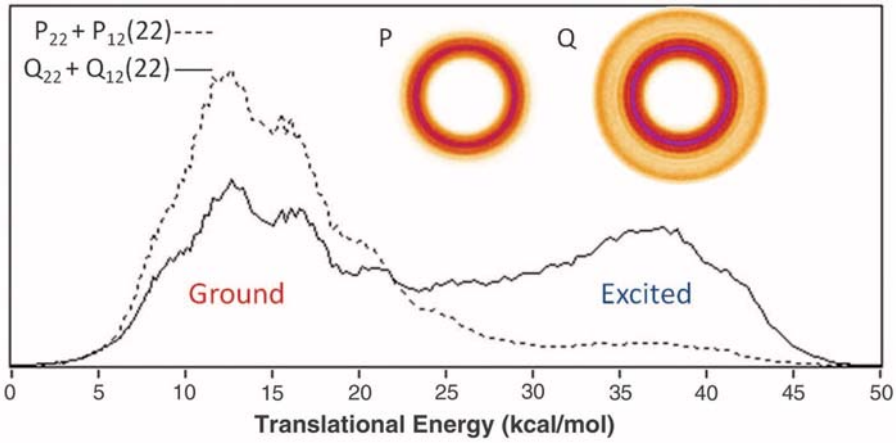

Fig. 3. Total translational energy distributions obtained from ion images of the NO photoproduct ($^2\Pi_{3/2}$, $v = 0$, $N = 22$) probing the $P_{22} + P_{12}(22)$ (dashed) and $Q_{22} + Q_{12}(22)$ (solid) transitions, demonstrating the relative Λ doublet propensities of the two reaction channels (*23*).

References and Notes

1. J. M. Bowman, B. C. Shepler, *Annu. Rev. Phys. Chem.* **62**, 531 (2011).
2. N. Herath, A. G. Suits, *J. Phys. Chem. Lett.* **2**, 642 (2011).
3. J. Mikosch *et al.*, *Science* **319**, 183 (2008).
4. R. D. van Zee, M. F. Foltz, C. B. Moore, *J. Chem. Phys.* **99**, 1664 (1993).
5. D. Townsend *et al.*, *Science* **306**, 1158 (2004).
6. P. L. Houston, S. H. Kable, *Proc. Natl. Acad. Sci. U.S.A.* **103**, 16079 (2006).
7. B. R. Heazlewood *et al.*, *Proc. Natl. Acad. Sci. U.S.A.* **105**, 12719 (2008).
8. L. B. Harding, S. J. Klippenstein, *J. Phys. Chem. Lett.* **1**, 3016 (2010).
9. M. P. Grubb, M. L. Warter, A. G. Suits, S. W. North, *J. Phys. Chem. Lett.* **1**, 2455 (2010).
10. H. Y. Xiao, S. Maeda, K. Morokuma, *J. Phys. Chem. Lett.* **2**, 934 (2011).
11. S. W. North, *Nat. Chem.* **3**, 504 (2011).
12. M. P. Grubb, M. L. Warter, K. M. Johnson, S. W. North, *J. Phys. Chem. A* **115**, 3218 (2011).
13. I. W. M. Smith, R. P. Tuckett, C. J. Whitham, *Chem. Phys. Lett.* **200**, 615 (1992).
14. K. M. Christoffel, J. M. Bowman, *J. Phys. Chem. A* **113**, 4138 (2009).
15. A. G. Suits, *Acc. Chem. Res.* **41**, 873 (2008).
16. K. Mikhaylichenko, C. Riehn, L. Valachovic, A. Sanov, C. Wittig, *J. Chem. Phys.* **105**, 6807 (1996).
17. P. Andresen, G. S. Ondrey, B. Titze, *Phys. Rev. Lett.* **50**, 486 (1983).
18. Materials and methods are detailed in the supporting online material at *Science* Online.
19. Recent vector correlation measurements of the NO fragment show strong perpendicular correlations between the NO velocity and its rotation, consistent with in-plane dissociation.

20. Although the predicted in-plane abstraction of the oxygen atom may at first seem at odds with the geometrically unconstrained abstraction observed in previous roaming systems, we contend that forces acting as the products separate are governed by the exit channel of the corresponding bimolecular abstraction reaction. Any constraints on the bimolecular reaction should therefore also apply to roaming and will vary for different molecular systems.
21. F. Lahmani, C. Lardeux, D. Solgadi, *Chem. Phys. Lett.* **129**, 24 (1986).
22. M. J. Bronikowski, R. N. Zare, *Chem. Phys. Lett.* **166**, 5 (1990).
23. The two translational distributions have been area normalized for comparison purposes. Absolute propensities are difficult to obtain from our experiment, but maximum propensity calculations necessitate that these normalizations are coincidently approximately correct.

Acknowledgments: We acknowledge G. Hall and P. Dagdigian for helpful discussions on Λ doublets and their dynamical implications. Support for this project was provided by the Robert A. Welch Foundation (A-1405), by a grant from the Japan Science and Technology Agency with Core Research for Evolutional Science and Technology (CREST) in the Area of High Performance Computing for Multiscale and Multiphysics Phenomena at Kyoto University, and by a grant from the U.S. Air Force Office of Scientific Research (grant FA9550-10-1-0304) at Emory University.

Supporting Online Material

www.sciencemag.org/cgi/content/full/335/6072/1075/DC1
Materials and Methods
Fig. S1
Reference (*24*)

21 November 2011; accepted 6 January 2012
10.1126/science.1216911

High-Latitude Dust Over the North Atlantic: Inputs from Icelandic Proglacial Dust Storms

Joseph M. Prospero,[1] Joanna E. Bullard,[2]* Richard Hodgkins[2]

Mineral aerosols play an important role in the atmosphere-ocean climate system. Research has focused almost exclusively on sources in low-latitude arid regions, but here we show that there are substantial sources in cold, higher latitudes. A 6-year record of measurements made on Heimaey, an island south of Iceland, reveals frequent dust events with concentrations exceeding 20 micrograms per cubic meter. Much of this potentially iron-rich dust is transported southward and deposited in the North Atlantic. Emissions are highest in spring and spatially and temporally associated with active glacial outwash plains; large dust events appear to be associated with glacial outburst floods. In response to global warming, ice retreat on Iceland and in other glacierized areas is likely to increase dust emissions from these regions.

Mineral dust aerosols affect climate directly by scattering and absorbing solar and terrestrial radiation and indirectly by affecting cloud properties and, in turn, the hydrological cycle (*1*, *2*). Moreover, dust is an important source of iron (Fe), which in soluble form is an essential micronutrient in marine biota; consequently, dust inputs to the oceans can affect primary productivity and, in turn, the global carbon cycle (*3*, *4*). This is not only a contemporary phenomenon; evidence from terrestrial (loess) and ice core records shows increased dust activity associated with glacial periods that has been linked to the carbon cycle and long-term climate change (*5*–*7*). Accordingly, there is considerable interest in the global distribution of dust sources (*8*), factors affecting dust emissions, and the properties of emitted particles; there are major efforts to model these processes on a global scale (*4*–*9*).

Thus far, research efforts have focused almost exclusively on tropical and mid-latitude arid regions that clearly are major global dust sources (*8*). However, substantial dust events also occur in higher latitudes, particularly in proglacial and paraglacial regions (*10*–*12*). Dust emissions in high latitudes are not confined to arid regions and can occur in humid areas such as Alaska, New Zealand, Patagonia, and Iceland (*10*–*14*). In ice-proximal areas, this is due to limited vegetation cover, high meltwater sediment supply, and strong katabatic or density-driven downglacier winds (*11*, *12*, *15*). Near ice sheets winds driven by steep regional or continental pressure gradients are important. To date, most measurements of high-latitude dust emissions have been confined to individual dust events (storms) or single seasons. Here we report a 6-year data set of aerosol emissions from Iceland.

Daily dust aerosol measurements were made at Stórhöfði, located on the southern tip of the island Heimaey, 17 km off the south coast of Iceland (Fig. 1). A detailed description of the site and sampling protocols are available as supporting online material (SOM) on *Science* Online. Data for February 1997 to December 2002 are shown in Fig. 2, along with data from October to November 2004, when intense dust activity was reported on Iceland.

Dust is present year-round at concentrations of a few micrograms per cubic meter, but occasionally, concentrations increase sharply (Fig. 2). Concentrations exceeded 20 μg m^{-3} in 53 filter samples exposed over a total of 150 days and exceeded 50 μg m^{-3} in 26 filters exposed over 71 days. The highest concentration in our entire record occurred on 19–20 October 2004 and was 1400 μg m^{-3}; the daily average concentration over the period 15 to 22 October was 555 μg m^{-3}. The original objective was to study pollution from the low latitudes; consequently, the sampler is controlled by wind direction to a 180° sector centered on due south. It therefore does not collect aerosols transported directly to the site by northerly winds; dust is sampled only after winds subsequently shift into sector, a frequent occurrence under typical weather conditions in the region. Thus, the concentrations reported here are minimum estimates of the actual values in plumes crossing the coast.

Dust activity is greatest in spring and early summer (Fig. 2C and table S1); concentrations >20 μg m^{-3} occurred most frequently in April (19 filter samples over 43 days) and May (14 samples over 41 days). The dust events in Fig. 2 are not associated with peaks in nonseasalt $SO_4^=$ or NO_3^-, which might have suggested that the dust was transported from Europe in pollution events or dust events from Africa (*16*), but they are instead linked to dust storms on Iceland. Forward air parcel trajectories from Stórhöfði calculated by use of the Hybrid Single-Particle Lagrangian Integrated Trajectory (HYSPLIT) Model (*17*) indicate that much of this dust is transported over the Atlantic Ocean. Trajectories for days when dust concentration exceeded 50 μg m^{-3} reveal that after 120 hours, 14 (39%) of the air masses associated with dust events remained over the North Atlantic, and consequently, the dust was most likely deposited in the marine system. Of the remainder, 13 (36%) made landfall within 120 hours on the west coast of Ireland or the UK; the remaining trajectories reached Norway, France, southern Greenland, or elsewhere in southern Iceland.

To set Icelandic contributions of dust to the Atlantic in context, mineral dust concentrations measured at seven other North Atlantic locations are shown in Fig. 3. The highest concentrations are measured at Cape Verde and Izaña (Tenerife, Canary Islands), reflecting their proximity to Saharan dust sources (*8*, *18*). Dust is transported westward across the North Atlantic and subsequently recorded at samplers in Cayenne, Barbados, Miami, and Bermuda. Dust concentrations recorded at Mace Head, Ireland are generally low (maximum monthly mean, 1.4 μg m^{-3} from 1989 to 1994) with the highest concentrations in the winter and spring (*18*), some of which may be attributable to Icelandic sources. Dust concentrations measured at Stórhöfði are comparable with those reported from Miami and Bermuda; however,

[1]Division of Marine and Atmospheric Chemistry and Cooperative Institute for Marine and Atmospheric Studies, Rosenstiel School of Marine and Atmospheric Science, University of Miami, 4600 Rickenbacker Causeway, Miami, FL 33149, USA. [2]Polar and Alpine Research Centre, Department of Geography, Loughborough University, Leicestershire LE11 3TU, UK.

*To whom correspondence should be addressed. E-mail: j.e.bullard@lboro.ac.uk

given the different nature of the marine ecosystems in the North Atlantic compared with the Caribbean, the biophysical impacts of dust in the two regions will not necessarily be the same.

The magnitude, frequency, and timing of dust events are determined by aeolian transport capacity and sediment supply and availability in source regions (*19*). Using satellite imagery and HYSPLIT back trajectories, we can attribute all the dust concentrations recorded at Stórhöfði to dust storms occurring on glacial outwash plains (sandar) in southern Iceland. A particularly intense source is Landeyjarsandur and is associated with sediments from the Markarfljót river (fed by meltwater from the Mýrdalsjökull and Eyjafjallajökull ice caps), which are deposited on the sandar plains near Þórsmörk and form a wide coastal outwash plain. Another major source is the floodplain of the Ölfusá River near Þorlakshöfn. Deposits associated with these rivers have previously been identified as sources of dust that contribute material to soils in southern Iceland (*20*) and that can affect air quality in Reykjavík (*21*). On the southeast coast, the most active sandar sources are Meðallandssandur and Skeiðarársandur, located between the Mýrdalsjökull and Vatnajökull ice caps. All of these dust sources are active in Fig. 4, a Moderate Resolution Imaging Spectroradiometer (MODIS) (Aqua) image for 5 October 2004. The plumes off the southeast coast are particularly dense and extend more than 500 km over the Atlantic Ocean.

Studies of proglacial dust emissions indicate that the relative timing of meltwater events and dust emissions depends on wind velocities, fluvial suspended sediment concentration, rate of desiccation of deposits, and the absence of snow cover (*11*, *12*, *22*). With unlimited sediment supply, stronger winds will result in higher dust emissions, but if all winds are above the sediment transport threshold, the temporal variability of sediment supply and availability may control dust concentrations (*19*). Meteorological data from Stórhöfði, Kirkjubæjarklaustur, and Hæll (Fig. 1) indicate that the highest dust concentrations occur when temperatures and rainfall are low in the spring, but there are no clear relationships with mean monthly or mean daily wind speed, or with the maximum gust recorded on the days of dust events (SOM). This is probably due to sediment supply controls; however, the locations of the meteorological stations are likely to underestimate the strength of ice-sheet–driven katabatic winds (*23*). Extraglacial snow cover is low and variable in southern Iceland (accounting for 5 to 10% precipitation over December–March) and has generally thawed by early April (*24*). Rivers feeding the sandar receive direct runoff, but most are also glacier-, lake-, or spring-fed. Peak discharge is typically in spring, and highest suspended sediment loads are in April; there is a second weaker peak in September (*25*, *26*). It is likely that early spring

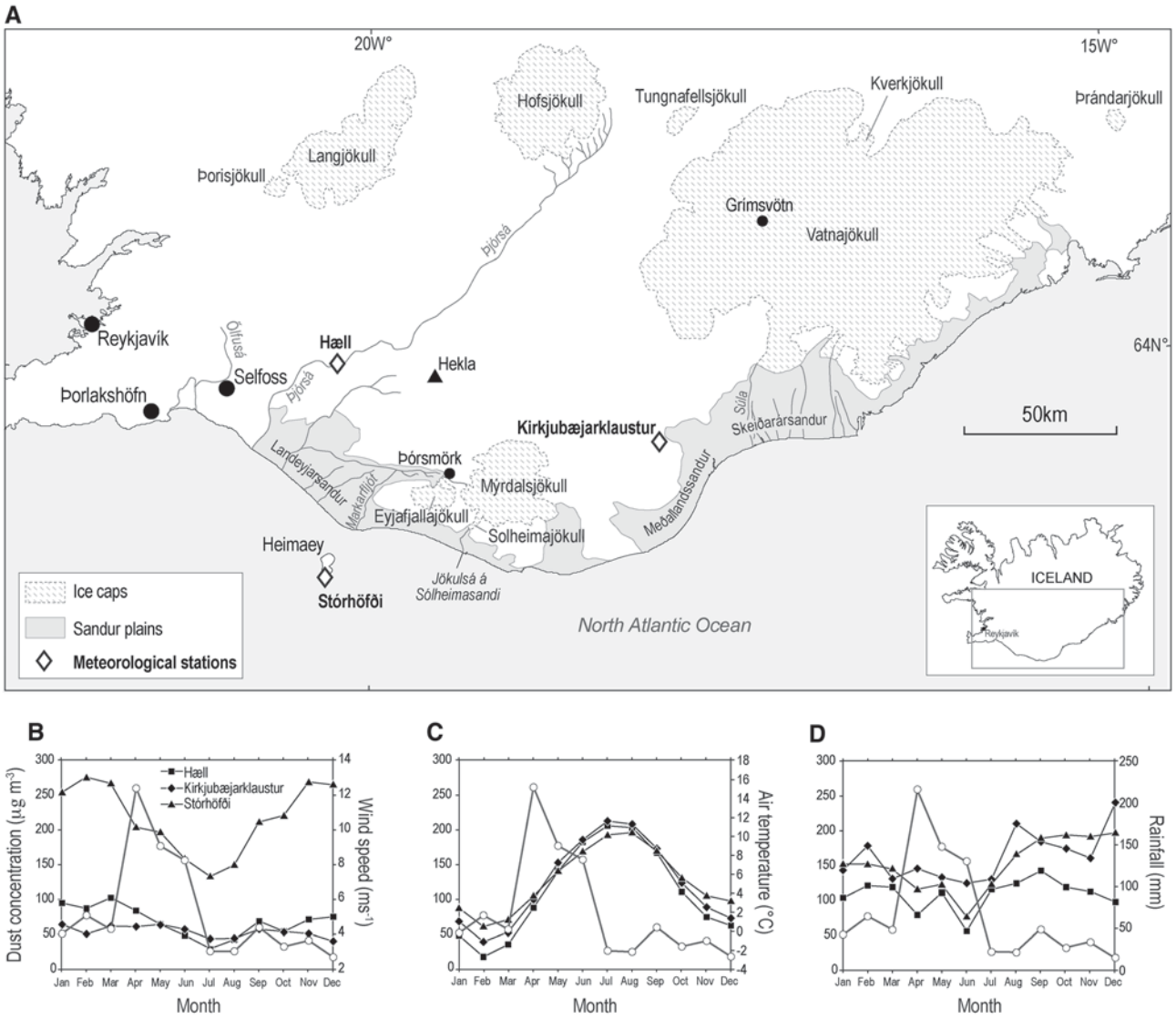

Fig. 1. (**A**) Southern Iceland indicating locations mentioned in the text. Data are from meteorological stations at Stórhöfði, Kirkjubæjarklaustur, and Hæll, showing the relationship between mean monthly dust concentration measured at Stórhöfði (open circles) and mean monthly (**B**) wind speed, (**C**) air temperature, and (**D**) rainfall, all for the period 1997–2002.

floods flush out subglacial sediment, which is subsequently deposited on the floodplain; once floods have receded and sediments have dried, these deposits can be easily deflated. Depending on the quantity and nature of sediments delivered to the floodplain, fluvial sediments may be rapidly deflated, or as has been observed on floodplains in Greenland, a lag deposit may develop, limiting further aeolian entrainment (*11*). Late summer or autumn floods carry low sediment loads, which along with weaker winds might explain the low dust emissions in these seasons. The timing of dust events in Iceland contrasts with that observed in Alaska, where snow cover persists until early summer, and the coincidence of maximum sediment exposure and strong winds does not take place until the autumn (*12*).

In Iceland, a clear seasonal variation in dust concentrations can be linked to meltwater hydrological regime; however, there are also occasional major, multiday dust events that can occur throughout the year. These large events may be associated with catastrophic glacial outburst floods (jökulhlaups) that deliver high-magnitude pulses of sediment to the sandar and rework existing deposits. For example, the 2 to 5 June 1997 dust event followed an increase in proglacial sediment supply resulting from a jökulhlaup in November 1996. On 29 September 1996, a magnitude 5 Richter scale earthquake occurred under Vatnajökull, followed by a volcanic eruption on 2 October. Meltwater accumulated under the ice cap until 5 November, when a large jökulhlaup was triggered (*27*); 3.2 km^3 of water drained from the subglacial lake in 40 hours (*28*). The suspended sediment load was 1.8×10^{11} kg (*29*); although much of this was derived from reworking of preexisting fluvioglacial sediments (*30*), large quantities of silt and clay were also deposited on the floodplain surface. These sediments remained on the floodplain after the event and during the winter of 1996 to 1997 until the following spring, when they were deflated from Skeiðarársandur by northeasterly winds in June and subsequently detected at Stórhöfði. A smaller jökulhlaup occurred in the same region in mid-August 1997, apparently related to earthquake activity under Vatnajökull (*26*). This event might account for the high dust concentrations measured in September 1997.

The intense dust period in April 2000 is associated with deflation from the Markarfljót area. In July 1999, subglacial volcanic activity within the Mýrdalsjökull caldera generated a flood in the river Jökulsá á Sólheimasandi (*31*). This caused major reworking and deposition of sediments over extensive areas of the proglacial floodplain. The jökulhlaup deposits fined downstream, laying down silt drapes across the floodplain surface (*31*). Deflation from these deposits was limited by high rainfall and low wind speeds in Autumn 1999 and February to March 2000 and by episodic snow cover and frozen surfaces in December 1999 and January 2000. However, in April 2000 rainfall was low, and wind speeds were high, causing desiccation and deflation of the jökulhlaup silts and leading to the high dust emissions observed (Fig. 2A).

Last, we focused on October to November 2004 (Fig. 2B) and the MODIS image from 5 October 2004 (Fig. 4). The mean dust concentration on Heimaey from 3 to 6 October was rather low, only 47 μg m^{-3}. The peak concentration of 1400 μg m^{-3} occurred on 19 to 20 October. This period of dust emissions may be associated with seismic activity before the eruption of the volcano Grímsvötn on 1 to 4 November 2004. The Icelandic Meteorological Service (*32*) reported

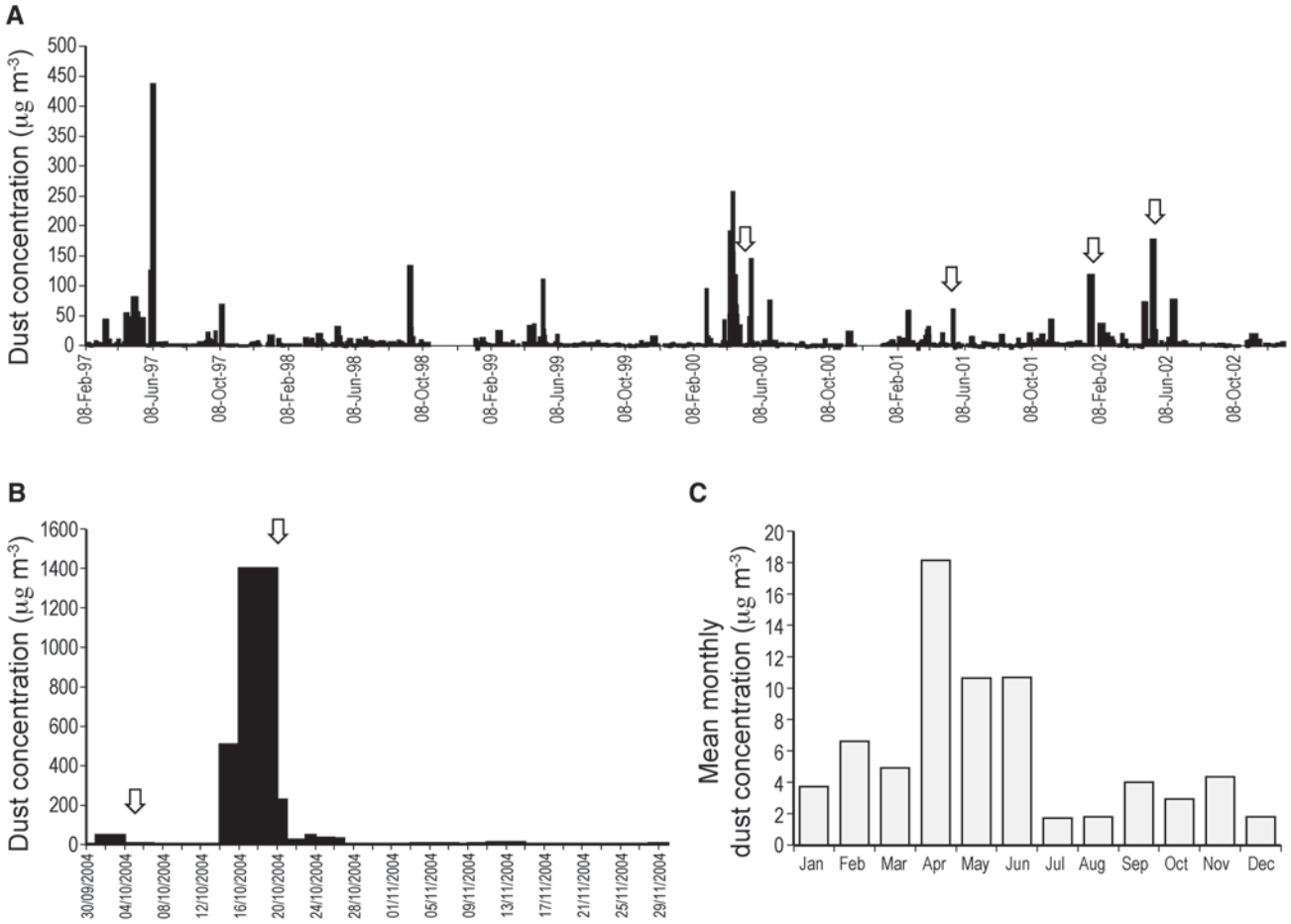

Fig. 2. Mineral dust aerosol concentration time series recorded at Stórhöfði, Heimaey, Iceland (**A**) 1997 to 2002 and (**B**) October to November 2004 [scale change from (A)]. Arrows indicate dust events captured by MODIS (M) or SeaWiFS (SW) satellite imagery: 14 April 2000 (SW); 18 May 2000 (SW); 15 May 2001 (M and SW); 28 January 2002 (M and SW); 15 May 2002 (SW); and 5 October 2004 (M and SW). (**C**) The annual cycle of monthly mean dust concentrations measured at Stórhöfði, Heimaey (1997 to 2002 only).

tremor bursts beginning in mid-August, suggesting an increased seismic activity. On 11 October, icequakes were recorded within the subglacial catchment of the Súla River, possibly triggered by a small jökulhlaup. Although the occurrence of a dust peak in our records in this time frame may be coincidental, the magnitude and timing suggests that it might be related to the volcanic-glacial activity. However, the main eruption in early November did not result in increased aerosol in our measurements, presumably because of wind conditions. In contrast, the eruption of Hekla on 26 February, ending 8 March 2000, yielded a dust concentration of 94 μg m^{-3} in our record.

Recent studies of glacial dust sources suggest that they are potentially important contributors of iron to marine systems (*12*, *33*). We do not have detailed information about the chemical composition of the dust being transported, but Icelandic soils are primarily of volcanic origin, with reworking by physical weathering and glaciers. They comprise brown andosols, gleyic andosols, and vitrisols, with levels of ferrihydrite measured as 1 to 8%, 1 to 7%, and 0.4 to 3%, respectively (*34*). The analysis (*35*) of six aerosol samples collected at Stórhöfði during dust events (two from June 1997 and four from April 2000) yielded an average Fe content of 2.6% (ranging from 1.3 to 4.4%), which is similar to average upper-crustal abundance, 3.5% (*36*), and to concentrations in trade-wind African dust (*35*). This suggests that Icelandic dust emissions could contribute a substantial amount of iron to the North Atlantic. Maximum dust transport occurs in spring, when productivity in the Iceland Basin is at a maximum because of the upwelling of nutrient-rich waters (*37*). Dust-iron could conceivably play a role at this time, and possibly later, after the bloom ends in summer, when productivity is known to be Fe-limited (*37*) but when dust levels are low (Fig. 2C).

Here, we have linked large dust events to proglacial sediment sources in southern Iceland. There is widespread aeolian activity across the remainder of Iceland, which could also contribute dust to atmospheric and marine systems (*20*). Our data show year-round dust emissions, but there is a seasonal (spring maximum) pattern that is associated with meltwater sediment supply hysteresis. This seasonality can be overprinted by influxes of dust from sediment deposits after catastrophic glacial flood events. In response to climate change, glaciers and ice caps on Iceland, as in many other regions, are predicted to recede, accompanied by an increase in meltwater runoff (*38*) and an increase in sediment flux during the initial stages of retreat (*39*). The topography underlying the south coast ice caps has a low gradient to the north and a steep topography on the southern side; ice retreat from the northern edge will expose more outwash plain (*38*), from which northerly winds may entrain sediments. Although some of these sediments will be lofted to high altitudes and transported out to sea, other material will be deposited on the snow and ice, decreasing the albedo and hence increasing the

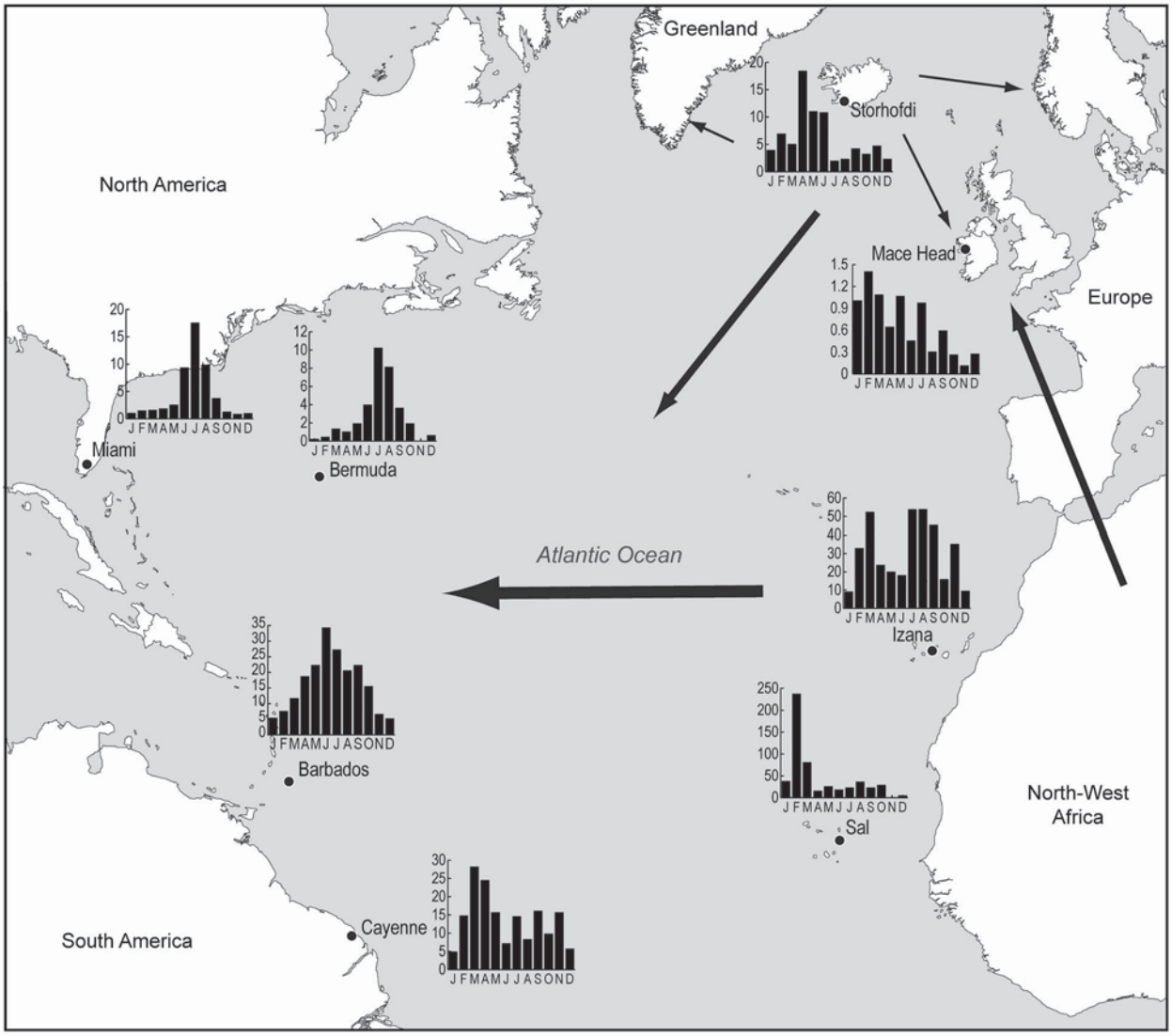

Fig. 3. Mean monthly dust concentrations recorded at eight stations around the Atlantic Ocean. Arrows (not to scale) indicate main directions and relative magnitude of dust transported over the North Atlantic. Individual graphs are derived from data collected over time periods that are not necessarily concurrent with that from Heimaey.

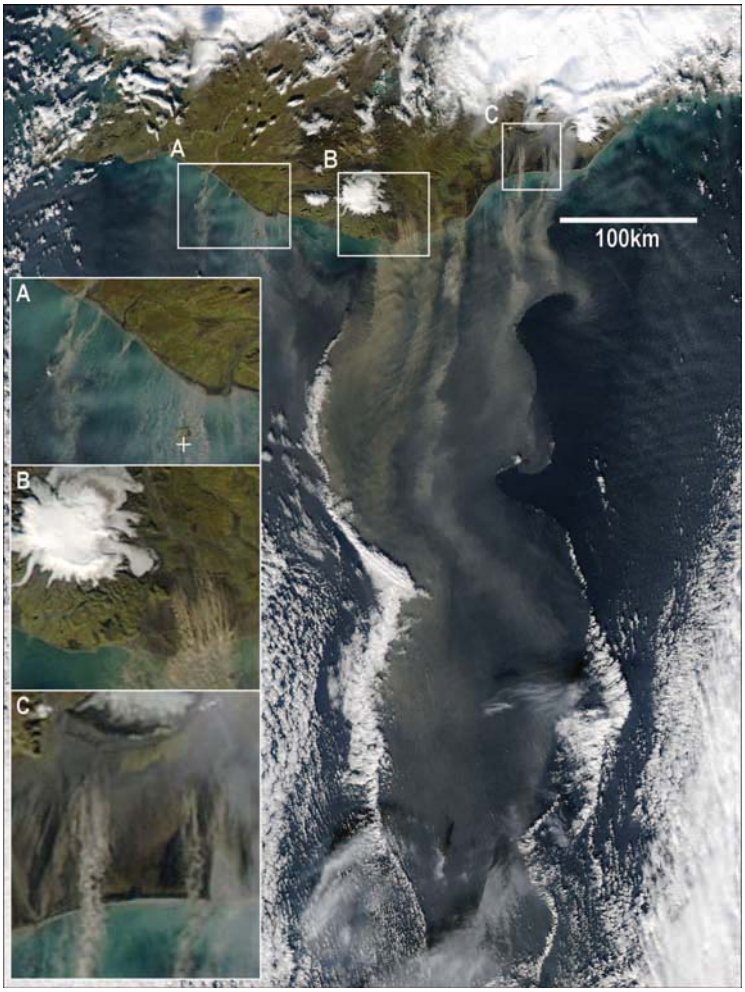

Fig. 4. MODIS image, 5 October 2004, showing dust plumes emanating from sources in southern Iceland. Insets show dust plumes (**A**) along the coast of Landeyjarsandur; plus symbol indicates sampling sites at Stórhöfði, (**B**) Mýrdalssandur, and (**C**) Skeiðarársandur.

rate of melting and recession (*40*, *41*). The strength of katabatic winds may also decrease, increasing the probability of upslope dust transport onto the ice (*42*). It is likely therefore that the frequency of dust storms on Iceland and their intensity will increase in coming decades. This would have implications for a number of climate-forcing processes. It also raises issues of air quality and human health impacts (*21*) in Iceland and will increase the quantities of dust being transported to the Atlantic and to Europe.

We would expect that the dust-related processes observed on Iceland are also occurring in other high-latitude glacierized regions and that proglacial dust activity will become more widespread and intense as climate change continues. Global-scale modeling of changes in atmospheric dust loading under different climate conditions has shown that the inclusion of inferred glacigenic dust sources improves the simulation for the Last Glacial Maximum (*4*), but there have been very few process-based studies or systematic measurements of contemporary high-latitude dust emissions that can be used to better constrain these models. The results reported here represent a step toward a better understanding of high-latitude dust sources.

References and Notes

1. D. Rosenfeld, Y. Rudich, R. Lahav, *Proc. Natl. Acad. Sci. U.S.A.* **98**, 5975 (2001).
2. M. Yoshioka *et al.*, *J. Clim.* **20**, 1445 (2007).
3. T. D. Jickells *et al.*, *Science* **308**, 67 (2005).
4. N. M. Mahowald *et al.*, *J. Geophys. Res.* **111**, (D10), D10202 (2006).
5. K. E. Kohfeld, S. P. Harrison, *Quat. Sci. Rev.* **22**, 1859 (2003).
6. F. Lambert *et al.*, *Nature* **452**, 616 (2008).
7. T. Hughes, *Arct. Alp. Res.* **28**, 448 (1996).
8. J. M. Prospero, P. Ginoux, O. Torres, S. E. Nicholson, T. E. Gill, *Rev. Geophys.* **40**, 1002 (2002).
9. N. Huneeus *et al.*, *Atmos. Chem. Phys.* **11**, 7781 (2010).
10. Ó. Arnalds, F. O. Gísladóttir, H. Sigurjónsson, *J. Arid Environ.* **47**, 359 (2001).
11. J. E. Bullard, M. J. Austin, *Aeolian Res.* **3**, 43 (2011).
12. J. Crucius *et al.*, *Geophys. Res. Lett.* **38**, L06602 (2011).
13. M. S. Johnson, N. Meskhidze, V. P. Kiliyanpilakkil, S. Gassó, *Atmos. Chem. Phys.* **11**, 2487 (2011).
14. S. Gassó *et al.*, *Atmos. Chem. Phys.* **10**, 8287 (2010).
15. J. F. Orwin, S. F. Lamoureux, J. Warburton, A. Beylich, *Geogr. Ann.* **92A**, 155 (2010).
16. J. M. Prospero, D. L. Savoie, R. Arimoto, H. Olafsson, H. Hjartarson, *Sci. Total Environ.* **160-161**, 181 (1995).
17. R. R. Draxler, G. D. Rolph, HYSPLIT (HYbrid Single-Particle Lagrangian Integrated Trajectory) Model access via NOAA ARL READY Web site (http://ready.arl.noaa.gov/HYSPLIT.php). NOAA Air Resources Laboratory, Silver Spring, MD (2011).
18. R. Arimoto *et al.*, *J. Geophys. Res.* **100**, (D1), 1199 (1995).
19. J. E. Bullard *et al.*, *J. Geophys. Res.* 10.1029/2011JF002061 (2011).
20. Ó. Arnalds, *Icelandic Agric. Sci.* **23**, 3 (2010).
21. T. Thorsteinsson, G. Gísladóttir, J. E. Bullard, G. McTainsh, *Atmos. Environ.* **45**, 5924 (2011).
22. C. McKenna-Neuman, R. Gilbert, in *Aeolian Geomorphology* W. G. Nickling, Ed. (Allen & Unwin, Boston, 1986), pp. 213–235.
23. H. Ágústsson, H. Olafsson, *Meteorol. Atmos. Phys.* **103**, 173 (2009).
24. M. A. Einarsson, in *World Survey of Climatology: 15: Climates of the Oceans*, H. Van Loon, Ed. (Elsevier, Amsterdam, 1984), pp. 673–697.
25. S. R. Gislason, J. O. Olafsson, A. Snorrason, *Science Institute Progress Report* RH-25-97 (1997).
26. G. H. Old, D. M. Lawler, Á. Snorrason, *Earth Surf. Process. Landf.* **30**, 1441 (2005).
27. F. J. Magilligan *et al.*, *Geomorphology* **44**, 95 (2002).
28. H. Björnsson, *Global Planet. Change* **35**, 255 (2002).
29. A. Snorrason *et al.*, in *Floods and Megaflood Deposits: Recent and Ancient Examples*, I. P. Martini *et al.*, Eds. (Blackwell Science, Oxford, 2002), pp. 55–65.
30. A. S. Maria, S. Carey, H. Sigurdsson, C. Kincaid, G. Helgadóttir, *Geol. Soc. Am. Bull.* **112**, 1507 (2000).
31. A. J. Russell *et al.*, *Quat. Sci. Rev.* **29**, 1363 (2010).
32. Icelandic Meteorological Service, *Eruption in Grimsvotn in November 2004*; available at http://hraun.vedur.is/ja/englishweb/eruption_grimsvotn.html (accessed 27 June 2011).
33. A. W. Schroth, J. Crusius, E. R. Scholkovitz, B. C. Bostick, *Nat. Geosci.* **2**, 337 (2009).
34. Ó. Arnalds, *Catena* **56**, 3 (2004).
35. J. M. Trapp, F. J. Millero, J. M. Prospero, *Mar. Chem.* **120**, 71 (2010).
36. S. R. Taylor, S. M. McLennan, *The Continental Crust: Its Composition and Evolution* (Blackwell, Oxford, 1985).
37. M. C. Nielsdóttir, C. M. Moore, R. Sanders, D. J. Hinz, E. P. Achterberg, *Global Biogeochem. Cycles* **23**, GB3001 (2009).
38. H. Björnsson, F. Pálsson, *Jökull* **58**, 365 (2008).
39. P. Jansson, G. Rosqvist, T. Schneider, *Geogr. Ann.* **87A**, 37 (2005).
40. T. H. Painter *et al.*, *Geophys. Res. Lett.* **34**, L12502 (2007).
41. G. Krinner, O. Boucher, Y. Balkanski, *Clim. Dyn.* **27**, 613 (2006).
42. C. M. Zdanowicz, G. A. Zielinski, C. P. Wake, D. A. Fisher, R. M. Koerner, *Quat. Res.* **53**, 62 (2000).

Acknowledgments: We thank the Iceland Meteorological Service for their assistance in establishing our study and, specifically, E. Astradsson, who oversees operations on Heimaey. Sampling at Stórhöfði has been carried out by the lighthouse keeper, Ó. J. Sigurðsson, and more recently by his son, P. Freyr. In Miami, technical assistance was provided by T. Snowdon and chemical analyses by L. Custals. We thank Ó. Arnalds (Agricultural Research Institute, Iceland) for discussions on Iceland soils and geomorphic processes, H. Ólafsson (University of Iceland, Geophysical Institute) for discussions on meteorology, and G. Gísladóttir (Veðurstofa Íslands) for providing the meteorological data. The authors gratefully acknowledge the NOAA Air Resources Laboratory (ARL) for the provision of the HYSPLIT transport and dispersion model. This work was supported by the National Oceanic and Atmospheric Administration under cooperative agreement NA90-RAH0075 and by grants by the U.S. National Science Foundation OCE-0623189 and AGS-0962256. J.E.B. and R.H. were supported by Royal Society grant RG062190 and Loughborough University.

Supporting Online Material

www.sciencemag.org/cgi/content/full/335/6072/1078/DC1
Materials and Methods
Table S1
References

5 December 2011; accepted 2 February 2012
10.1126/science.1217447

Glacial Survival of Boreal Trees in Northern Scandinavia

Laura Parducci,[1,2*] Tina Jørgensen,[2*] Mari Mette Tollefsrud,[3*] Ellen Elverland,[4*] Torbjørn Alm,[4] Sonia L. Fontana,[1,5,6] K. D. Bennett,[7,8] James Haile,[2,9] Irina Matetovici,[1,10] Yoshihisa Suyama,[11] Mary E. Edwards,[12] Kenneth Andersen,[2] Morten Rasmussen,[2,13] Sanne Boessenkool,[14] Eric Coissac,[15] Christian Brochmann,[14] Pierre Taberlet,[15] Michael Houmark-Nielsen,[2] Nicolaj Krog Larsen,[16] Ludovic Orlando,[2] M. Thomas P. Gilbert,[2] Kurt H. Kjær,[2] Inger Greve Alsos,[4] Eske Willerslev[2]†

It is commonly believed that trees were absent in Scandinavia during the last glaciation and first recolonized the Scandinavian Peninsula with the retreat of its ice sheet some 9000 years ago. Here, we show the presence of a rare mitochondrial DNA haplotype of spruce that appears unique to Scandinavia and with its highest frequency to the west—an area believed to sustain ice-free refugia during most of the last ice age. We further show the survival of DNA from this haplotype in lake sediments and pollen of Trøndelag in central Norway dating back ~10,300 years and chloroplast DNA of pine and spruce in lake sediments adjacent to the ice-free Andøya refugium in northwestern Norway as early as ~22,000 and 17,700 years ago, respectively. Our findings imply that conifer trees survived in ice-free refugia of Scandinavia during the last glaciation, challenging current views on survival and spread of trees as a response to climate changes.

Understanding rates of tree migration and resilience to climate change is important for explaining both the distribution of single species and anticipating how ecosystems may respond to ongoing climate changes. Although trees are among the plants best able to disperse widely, and thus able to track their niches as climate changes (*1*), their rate of spread is debated (*2*–*4*). Strong paleoecological and genetic evidence supports the observation that most temperate and boreal plant species survived the glacial periods in south and east European ice-free macrorefugia and recolonized northern areas when the ice retreated at the end of the Late Weichselian (Wisconsian) and the beginning of the Holocene (*5*).

Several recent studies using fossil and genetic data indicate the presence of populations of boreal trees in the tundra of recent cold stages in Alaska (*6*), Yukon (*7*), Siberia (*8*), and Estonia (*9*). However, it remains controversial whether finds of spruce (*Picea*) and pine (*Pinus*) megafossils in the mountains of central Scandinavia dated to ~13,500 calibrated years before the present (cal. yr B.P.) (11,700 ^{14}C yr B.P.) (*10*) indicate the presence of these tree taxa within the limits of the Scandinavian Ice Sheet (SIS) (Fig. 1A). If they did survive here, glacial tree locations were much farther north than generally accepted (*11*, *12*). Previous estimates of potential Last Glacial Maximum (LGM) tree distributions using species distribution modeling have shown that boreal trees were much more widespread on the exposed North Sea continental shelf than thought (*13*). However, analyses of sedimentary pollen from central Scandinavia yield limited evidence to support the refugia hypothesis in this region (*14*), but near the tree limit there may be little or no pollen production (*15*).

Here, we extend traditional paleoecological methods with analyses of modern and ancient DNA (aDNA) to examine whether trees existed in Scandinavia at the LGM. We used mitochondrial DNA (mtDNA) analyses (*16*) to investigate whether modern Scandinavian Norway spruce (*Picea abies*) might be descended from ancient populations deriving from putative northern glacial locations. We sampled more than 100 forest stands across the contemporary European range of the species (the majority coming from the northern range) (Fig. 1B and table S1) and tested 11 variable noncoding regions. In spruce, mtDNA is maternally inherited (*17*) and shows a slow mutation rate in plants compared to the nuclear and chloroplast genomes (*18*). This may result in strong genetic differentiation among modern populations underlined by the genetic signature of the glacial locations.

Sequencing analysis showed a deletion of 21 base pairs (bp) in the 141 bp constitutive of the mh05 fragment, yielding two haplotypes (Fig. 1B and table S4). Haplotype A was found only in populations within Scandinavia, with the highest frequency in the western regions and a decreasing frequency toward the east. A second haplotype B was also observed in Scandinavia. Haplotype B can be considered ancestral to A because of its complete sequence similarity with the two sister species, Siberian spruce (*Picea obovata*) and white spruce (*Picea glauca*), and with the outgroup species Scots pine (*Pinus sylvestris*) (*16*). Haplotype B is fixed in all populations outside Scandinavia—including trees sampled from the southern European range of spruce in Germany, Switzerland, Serbia, Italy, and Austria (table S1).

The distinct geographic distribution of haplotypes A and B is in agreement with classical patterns of population expansion out of at least two different locations after the LGM. As haplotype B is fixed outside Scandinavia, it appears to have dispersed after deglaciation from areas east or south of the Late Weichselian ice sheet, most likely from the Russian refugial areas, as indicated by earlier fossil (*19*) and molecular data (*20*). In contrast, haplotype A appears to have dispersed from western Scandinavia, as it is absent from the rest of the European range. Reconstructions of the distribution and flow patterns of the SIS suggest the presence of ice-free corridors along the Atlantic coastal areas of north Scandinavia and the Kola Peninsula during most of the Middle and Late Weichselian, except for relatively short intervals during the LGM between 22,000 and 20,000 cal. yr B.P. and 18,000 and 16,000 cal. yr B.P. (Fig. 1A). The origin of haplotype A must, however, predate the LGM, as simple models with constant population size and exponential growth show that the fixation of a mitochondrial mutation requires a minimum number of 200,000 years in spruce populations [~5000 generations; (*16*)], excluding, therefore, a Holocene founder event from the east followed by subsequent expansion across northern Scandinavia. Alleles can also surf to high frequency at the edge of a colonization process, although in such circumstances we would expect to see a decreasing level of nuclear genetic diversity with increasing genetic distance from the Russian glacial origin. Instead, nuclear genetic diversity in Norway spruce is largely maintained from the Russian refugial areas to Scandinavia (*21*). A western origin of haplotype A is supported also by modern molecular analysis based on nuclear microsatellites that identified in the northern European range of Norway spruce a cluster of populations from central Scandinavia (*21*). Such differentiation had not previously been found in the *nad*1 region of the slower-evolving mtDNA genome,

[1]Department of Ecology and Genetics, Evolutionary Biology Centre, Uppsala University, Norbyvägen 18D, 75236 Uppsala, Sweden. [2]Centre for GeoGenetics, Natural History Museum of Denmark, University of Copenhagen, Øster Voldgade 5-7, DK-1350 Copenhagen, Denmark. [3]Norwegian Forest and Landscape Institute, Høgskoleveien 8, 1430 Ås, Norway. [4]Tromsø University Museum, NO-9037 Tromsø, Norway. [5]Department of Palynology and Climate Dynamics, University of Göttingen, Untere Karspüle 2, 37073 Göttingen, Germany. [6]Department of Geology, University of Helsinki, Post Office Box 64, FI-00014, Finland. [7]Department of Earth Sciences, Uppsala University, Villavägen 16, 75236 Uppsala, Sweden. [8]School of Geography, Archaeology and Palaeoecology, Queen's University Belfast, University Road, Belfast BT7 1NN, Northern Ireland. [9]Ancient DNA Research Laboratory, Murdoch University, South Street, Perth 6150, Australia. [10]Molecular Biology Center, Interdisciplinary Research Institute on Bio-Nano-Sciences, Babes-Bolyai-University Cluj Napoca, 42 Treboniu Laurian Street, RO-400271 Cluj-Napoca, Romania. [11]Graduate School of Agricultural Science, Tohoku University, 232-3 Yomogida, Naruko-onsen, Osaki, Miyagi 989-6711, Japan. [12]Geography and Environment, University of Southampton, Highfield, Southampton SO17 1BJ, UK. [13]The Danish National High-Throughput DNA Sequencing Facility, Øster Farimagsgade 2D entrance E, 2nd floor, DK-1353 Copenhagen, Denmark. [14]National Centre for Biosystematics, Natural History Museum, University of Oslo, Post Office Box 1172 Blindern, NO-0318 Oslo, Norway. [15]Laboratoire d'Ecologie Alpine, CNRS UMR 5553, Universite de Grenoble, BP 53, F-38041 Grenoble Cedex 9, France. [16]Department of Geoscience, Aarhus University, Høegh-Guldbergs Gade 2, DK-8000 Aarhus C, Denmark.

*These authors contributed equally to this work.
†To whom correspondence should be addressed. E-mail: ewillerslev@snm.ku.dk

but all populations from the northern European range share a similar old and ancestral *nad*1 mtDNA variant (*20*).

A likely explanation for the distribution patterns of haplotypes A and B is that scattered populations carrying A survived the LGM in microenvironmentally favorable pockets in western Norway, where proximity to the relatively temperate conditions of the Atlantic Ocean may have favored survival during glacial times. After climate warming, colonization of Scandinavia started first from local western stands that initially expanded slowly and eventually mixed with populations arriving from the east. Rapidly rising sea levels and complex glaciated terrain probably contributed to the scattered populations on the Atlantic coast remaining isolated and becoming fixed for haplotype A. As spruce can persist for hundreds of years by vegetative propagation under unfavorable conditions (*22*), it is possible that these trees produced no pollen, leaving no trace in the palynological record.

To test whether spruce trees carrying haplotype A are indeed early Scandinavian survivors, we used aDNA extracted from lake sediments (*23*, *24*) from the Trøndelag region (63°N; central Norway) and on the island of Andøya (69°N; northern Norway). Such environmental aDNA (*25*) is shown to be local in origin and provides a proxy for plant paleo-community reconstruction that exhibits more similarity to macrofossils than to pollen records (*26*, *27*). We also extracted and analyzed aDNA from the oldest spruce pollen found in the Trøndelag core [6300 cal. yr B.P.; (*16*)]. We could not recover mtDNA from the deepest Andøya samples, likely due to the relatively low–copy number of mtDNA compared to chloroplast DNA (cpDNA) in plant tissues (see below). In contrast, we detected the spruce mtDNA haplotype A from the deepest samples at Trøndelag dating to 10,300 and 6500 cal. yr B.P. and from spruce pollen 6300 years old (Fig. 2 and table S5A).

These early occurrences of haplotype A in Trøndelag indicate that spruce was already present in the region during the early Holocene, much earlier than the first wave of colonization inferred from pollen analyses (~3000 cal. yr B.P.) (*19*). Our data are reinforced by a recent report of late-glacial and early-Holocene pollen and stomata of *Pinus* and *Picea* in the Dovre mountains in central Norway, which also indicate local presence of the two taxa (*28*).

To further test where, and for how long, spruce trees might have survived in Scandinavia, we focused our studies at Andøya (Fig. 1A). This island is particular with regards to Late Weichselian and Holocene paleoenvironments, due to its long, continuous lacustrine sedimentary records, its early deglaciation at ~26,000 cal. yr B.P. (*29*), and its location only a few hundred kilometers north of the modern northern limit of spruce haplotype A. Thus, at a time when almost the whole of Scandinavia was covered by ice, Andøya's northern tip harbored a nunatak ecosystem [see (*29*–*31*)]. Previous work on the early vegetation history of Andøya is based on pollen records, and to a lesser extent on macrofossils (*32*). Here, we combined macrofossil and aDNA analyses of lake sediments to assess past local vegetation (*16*, *33*) to amplify short fragments of cpDNA [generally <100 bp; thus, shorter than the mtDNA mh05 fragment (*16*)]. Chloroplast DNA is also more common than mtDNA in many plant tissues (*34*, *35*), increasing the chances of DNA survival and detection in older sediments.

Results from both macrofossil and cpDNA analyses indicate the presence of a polar desert or open pioneer vegetation community from ~ 22,000 cal. yr B.P. (fig. S3). Tundra herb diversity increased with a climatic warming around 15,000 cal. yr B.P., and there were further increases and changes in diversity in the Holocene, including the establishment of boreal species such as rowan (*Sorbus aucuparia*), generally reflecting previous vegetation reconstructions [see (*29*–*31*)]. The most notable result was the finding of DNA of pine (*Pinus* sp.) in sediments dating to ~22,000 and ~19,200 cal. yr B.P., and spruce (*Picea* sp.) in sediments dating to ~17,700 cal. yr B.P. (Fig. 2 and fig. S3).

There is little knowledge about aDNA taphonomy and the processes that may deliver plant DNA to lake sediments. However, it is likely that tree aDNA at Andøya and Trøndelag reflects contemporaneous plant biomass derived

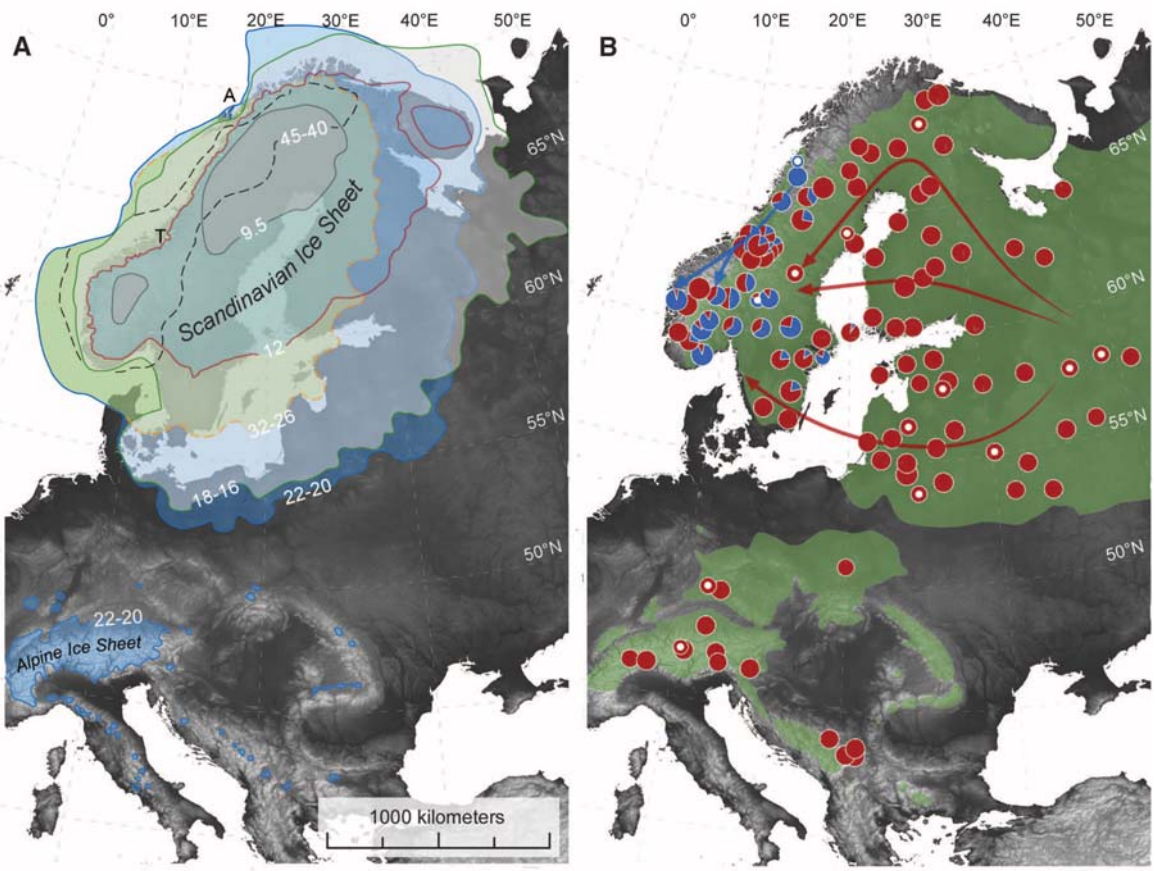

Fig. 1. (**A**) Reconstructions of stages in the development of the Scandinavian Ice Sheet 45,000 to 9500 cal. yr B.P. compiled from a range of sources (*16*) A, Andøya; T, Trøndelag. (**B**) Geographical distribution of mitochondrial mh05 haplotypes A (dark blue circles) and B (red circles) in Norway spruce populations. Size of the circles is proportional to population size (centered white dots indicate populations with $N < 10$; table S1). Arrows suggest postglacial movements of the two haplotypes after the LGM. The olive shading shows the natural range of Norway spruce.

from the lake catchment. Seeds, needles, and bud scales can indeed be blown or washed over substantial distances, especially in open ice-covered landscapes, but the long-distance proportion deposited into an Arctic lake appears very small compared to that of any local component. Additionally, during the early Holocene, the shortest distance to any known pine or spruce locality from Andøya makes any long-distance transportation of macrofossils highly unlikely. The degree of vertical migration or leaching of DNA through the sediments is also of concern, as periodic downward percolation of water can move DNA in porous, granular sediments of cave profiles (*36*). Lake sediments, however, are permanently saturated, and vertical percolation of liquids does not occur while organic compounds are immobilized in the sediment matrix (*23*). Other processes must be also considered, such as DNA derived from nonlocal pollen (i.e., from long-distance transport) and reworking of older organic material. However, no pollen grains of spruce or pine were found in the Andøya samples in question [investigated explicitly microscopically (*16*)]. Additionally, the possibility of a pollen source for our amplifications is unlikely as pollen grains contain small amounts of DNA, which are difficult to amplify (*37*). Also, at Trøndelag in an attempt to use the generic *trn*L primers, we failed to recover pine and spruce DNA from horizons where such pollen was present (*16*). For Andøya, reworking (e.g., of interglacial or interstadial material) is also unlikely even though ice-free conditions prevailed before LGM. Although Quaternary terrestrial deposits containing Eemian material have been reported 120 km farther north (*16*), none are known from Andøya itself, and pollen stratigraphies do not indicate that reworking is prevalent (*29*–*31*).

Coupling our findings with the results of previous megafossil-based analyses (*10*), the overall evidence for presence of conifer trees in Scandinavia during the last glaciation seems the only explanation for our observations. Although we cannot yet resolve whether this evidence reflects local survival of trees from previous warm periods, or an early spread of trees as land became ice-free, these findings have considerable conservation implications, particularly in relation with the ability of spruce to survive under changing climates. Although long-term survival does not exclude long-distance dispersal, such northerly spruce distributions provide a case study of a species capacity to persist locally in a marginal environment during the LGM and expand rapidly under more favorable conditions to develop dispersed populations over a broad area, and expand yet again under even more favorable conditions to form dense and widespread populations. The identification of these genetic resources is also of great importance to breeding programs interested in identifying spruce provenances with traits related to flexibility to survive under changing climatic conditions.

Northern glacial distributions of trees also indicate that tree populations can be undetected in pollen assemblages for millennia, which has cascading implications for pollen-based inference of species invasion and migration patterns and rates. The latter may well have been lower for conifer trees than estimated from classical palynological studies. This should be taken into account when modeling future vegetational changes due to global warming. Finally, if tree populations survived one of the most severe glacial periods (LGM), and by inference even previous ones, this extends the history of trees in these locations back to before the last glacial–interglacial period. Such persistence highlights the importance of extending ecological and genetic studies in forest trees to longer time scales, in order to properly explain the evolutionary processes that shaped the modern distribution and genetic patterns of tree taxa.

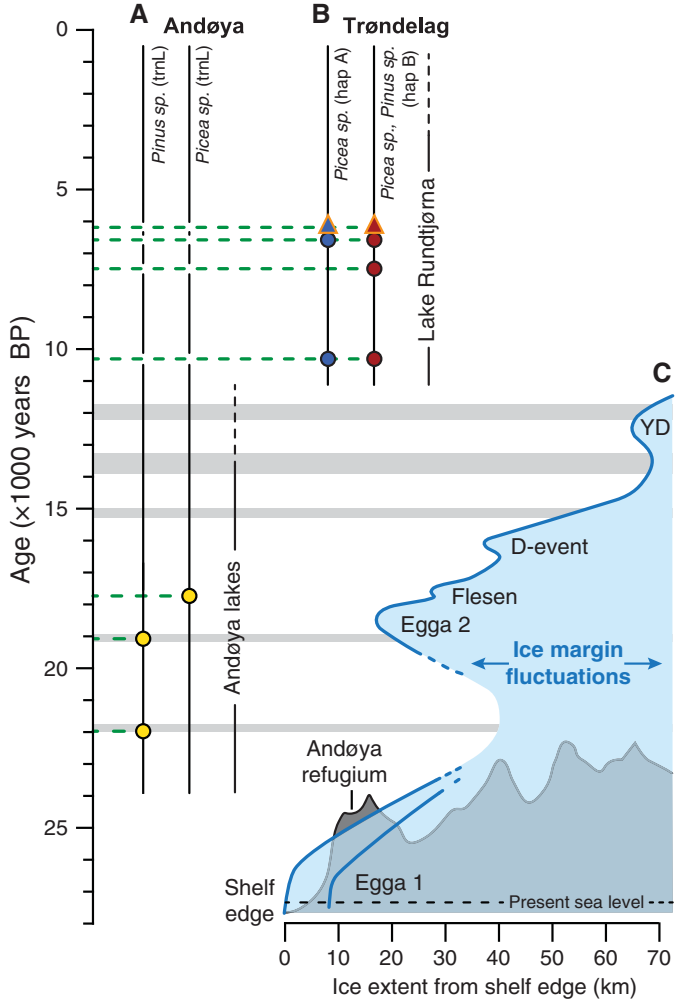

Fig. 2. Temporal occurrence of boreal trees at Andøya (**A**) and Trøndelag (**B**) based on fossils, aDNA from sediments (circles), and aDNA from pollen (triangles) data. (**C**) Ice sheet fluctuations across northwestern Norway 27,000 to 10,000 years ago. LGM (Egga 1) glacier extent went beyond the examined Andøya lakes, reaching the west coast of the island (*38*) or alternatively 10 km farther west at the shelf edge (*39*). Readvances (Egga 2, Flesen D-event, Younger Dryas) left lakes unglaciated. Possible location for the Andøya refugium is indicated. Horizontal gray scaled lines indicate +10°C, as reconstructed by Alm (*29*).

References and Notes

1. J. Hamrick, *For. Ecol. Manage.* **197**, 323 (2004).
2. J. C. Svenning, F. Skov, *Ecol. Lett.* **7**, 565 (2004).
3. E. Welk, H. Bruelheid, *J. Biogeogr.* **33**, 2013 (2006).
4. B. Huntley, H. J. B. Birks, *An Atlas of Past and Present Pollen Maps of Europe: 0-13,000 years ago* (Cambridge Univ. Press, Cambridge, 1983).
5. J. R. Stewart, A. M. Lister, I. Barnes, L. Dalén, *Proc. Biol. Sci.* **277**, 661 (2010).
6. L. L. Anderson, F. S. Hu, D. M. Nelson, R. J. Petit, K. N. Paige, *Proc. Natl. Acad. Sci. U.S.A.* **103**, 12447 (2006).
7. G. D. Zazula, A. M. Telka, C. R. Harington, C. E. Schweger, R. W. Mathewes, *Arctic* **59**, 391 (2006).
8. P. Tarasov, *PAGES News* **17**, 122 (2009).
9. M. Heikkilä, S. Fontana, H. Seppä, *J. Quat. Sci.* **24**, 802 (2009).
10. L. Kullman, *J. Biogeogr.* **29**, 1117 (2002).
11. H. Birks, E. Larsen, H. Birks, *J. Biogeogr.* **32**, 1461 (2005).
12. L. Kullman, *J. Biogeogr.* **33**, 377 (2006).
13. J. C. Svenning, S. Normand, M. Kageyama, *J. Ecol.* **96**, 1117 (2008).
14. U. Segerström, H. von Stedingk, *Holocene* **13**, 897 (2003).
15. S. Hicks, *Veg. Hist. Archaeobot.* **15**, 253 (2006).
16. Materials and methods are available as supporting material on *Science* Online.
17. D. Grivet, S. Jeandroz, J. Favre, *Theor. Appl. Genet.* **99**, 346 (1999).
18. K. H. Wolfe, W. H. Li, P. M. Sharp, *Proc. Natl. Acad. Sci. U.S.A.* **84**, 9054 (1987).
19. T. Giesecke, K. Bennett, *J. Biogeogr.* **31**, 1523 (2004).
20. M. M. Tollefsrud *et al.*, *Mol. Ecol.* **17**, 4134 (2008).
21. M. M. Tollefsrud *et al.*, *Heredity* **102**, 549 (2009).
22. L. Kullman, *Ecology* **76**, 2490 (1995).
23. L. L. Anderson-Carpenter *et al.*, *BMC Evol. Biol.* **11**, 30 (2011).
24. E. K. Magyari *et al.*, *BMC Evol. Biol.* **11**, 66 (2011).
25. E. Willerslev *et al.*, *Science* **300**, 791 (2003).
26. T. Jørgensen *et al.*, *Mol. Ecol.* 10.1111/j.1365-.2011.05287.x (2011).

27. K. Andersen *et al.*, *Mol. Ecol.* 10.1111/j.1365-.2011.05261.x (2011).
28. A. Paus, G. Velle, J. Berge, *Quat. Sci. Rev.* **30**, 1780 (2011).
29. T. Alm, *Boreas* **22**, 171 (1993).
30. T. O. Vorren, K.-D. Vorren, T. Alm, S. Gulliksen, R. Løvlie, *Boreas* **17**, 41 (1988).
31. K. D. Vorren, *Boreas* **7**, 19 (1978).
32. T. Alm, H. H. Birks, *Nord. J. Bot.* **11**, 465 (1991).
33. P. Taberlet *et al.*, *Nucleic Acids Res.* **35**, e14 (2007).
34. T. Preuten *et al.*, *Plant J.* **64**, 948 (2010).
35. U. Rauwolf, H. Golczyk, S. Greiner, R. G. Herrmann, *Mol. Genet. Genomics* **283**, 35 (2010).
36. J. Haile *et al.*, *Mol. Biol. Evol.* **24**, 982 (2007).
37. L. Parducci, Y. Suyama, M. Lascoux, K. D. Bennett, *Mol. Ecol.* **14**, 2873 (2005).
38. T. O. Vorren, L. Plassen, *Boreas* **31**, 97 (2002).
39. J. Mangerud, in *Quaternary Glaciations—Extent and Chronology, Part 1—Europe* (Elsevier, Amsterdam, 2004), pp. 271–294.

Acknowledgments: We thank T. Giesecke and M. Lascoux for helpful comments; J. Chen, T. Geburek, and C. Sperisen for providing modern samples; and L. Yuan for initial spruce genotyping. We also thank T. Vorren and K.-D. Vorren for providing Andøya core samples with lithostratigraphy and radiocarbon dates. This study was supported by the Swedish Research Council (grant 2007-4490 to L.P.) and the Carl Trygger's Foundation (grant 08:303 to L.P.); KAKENHI (22658046); a Royal Society–Wolfson Merit Award to K.D.B.; the Danish National Research Foundation; the Norwegian Forest and Landscape Institute, University of Tromsø; and the Tromsø University Museum, the Roald Amundsen Centre for Arctic Research, and the European Commission under the Sixth Framework 378 Programme (EcoChange project, contract no. FP6-036866). L.P., T.J., M.M.T., and E.E. should be considered joint first authors. I.G.A. and E.W. should be considered joint senior authors. The authors declare no competing financial interests. P.T. is coinventor of patents related to the g/h primers and the use of the P6 loop of the chloroplast *trn*L (UAA) intron for plant identification using degraded template DNA. These patents only restrict commercial applications and have no impact on the use of this locus by academic researchers. The *trn*L DNA sequences can be found at the European Nucleotide Archive with the study accession no. ERP001153. The mtDNA sequences can be found at the European Molecular Biology Laboratory database with the accession no. HE652882-HE653002.

Supporting Online Material

www.sciencemag.org/cgi/content/full/335/6072/1083/DC1
Materials and Methods
SOM Text
Figs. S1 to S5
Tables S1 to S5
References (*40*–*92*)

1 November 2011; accepted 26 January 2012
10.1126/science.1216043

Founder Effects Persist Despite Adaptive Differentiation: A Field Experiment with Lizards

Jason J. Kolbe,[1]*† Manuel Leal,[2] Thomas W. Schoener,[3] David A. Spiller,[3] Jonathan B. Losos[1]

The extent to which random processes such as founder events contribute to evolutionary divergence is a long-standing controversy in evolutionary biology. To determine the respective contributions of founder effects and natural selection, we conducted an experiment in which brown anole (*Anolis sagrei*) lizard populations were established on seven small islands in the Bahamas, from male-female pairs randomly drawn from the same large-island source. These founding events generated significant among-island genetic and morphological differences that persisted throughout the course of the experiment despite all populations adapting in the predicted direction—shorter hindlimbs—in response to the narrower vegetation on the small islands. Thus, using a replicated experiment in nature, we showed that both founder effects and natural selection jointly determine trait values in these populations.

Island populations are renowned for their extent of divergence from each other and from mainland source populations (*1*, *2*). Mayr (*3*, *4*) argued that these differences are often triggered by random sampling when island populations are founded by a few colonizing individuals. The resultant founder effects—changes in the genetic and phenotypic composition of a population due to founding by a small number of individuals—have been proposed as an important cause of evolutionary divergence and even speciation for the past half-century (*3*–*6*). However, an alternative explanation is that island environments differ from each other and from the source locality, and these ecological differences result in divergent natural selection (*7*–*9*). The evolutionary significance of founder effects also has been questioned because their imprint may be short-lived if populations perish because of a lack of genetic variation or because of demographic stochasticity, or if natural selection overwhelms their effects (*10*, *11*). Data from nature are lacking because founder events are rarely observed [but see (*12*)], and thus their effects must be inferred post hoc; yet laboratory studies indicate that even in the presence of natural selection, genetic drift induced by founder effects or population bottlenecks can contribute to patterns of phenotypic divergence [e.g., (*13*, *14*)]. We report an experimental study of founder effects in a natural system of a Caribbean lizard, demonstrating that morphological divergence caused by the founder effect persists even as populations adapt to their new environments.

Some have argued that marked phenotypic change from a single founder event is very unlikely (*11*) and that genetic drift in general plays little part in morphological evolution (*15*). Moreover, others note that evidence from recent introductions suggests that adaptation is a more common cause of trait evolution than drift (*16*–*18*). Yet most concede that documenting these random sampling events in nature is exceedingly difficult (*11*, *15*, *19*–*21*). Without knowledge of founder attributes and repeated sampling of colonized islands, the relative contributions of founder effects, population bottlenecks, natural selection, and gene flow to evolutionary divergence are impossible to disentangle (*19*–*21*).

We capitalized on the extensive knowledge of how *Anolis* lizards adapt to their environment, combined with the opportunity to use small islands in the Bahamas, recently cleared of lizards by a hurricane, as experimental units in a natural setting. Our focus was on limb length and the extent to which lizard populations would adapt to the novel environments on these small and scrubby islands. Extensive comparative and experimental research supports an adaptive explanation for the positive relationship between hindlimb length and perch diameter (i.e., the width of the cross section of the substrate that a lizard perches on, such as a branch or trunk) that is found among populations of anoles. Functional studies show a clear biomechanical basis: Lizards with relatively longer hindlimbs run faster on broad substrates, whereas lizards with shorter limbs for a given body size move more adeptly on narrow surfaces. Such performance probably aids in capturing prey, defending territories, and escaping from predators. Indeed, field studies in this system show that hindlimb length is under selection, favoring longer hindlimbs to run faster when exposed to terrestrial predators and shorter hindlimbs after lizards become arboreal and shift to narrower perches [reviewed in (*22*)].

To assess the relative importance of founder effects versus natural selection, we introduced lizards to replicate islands to which we predicted they were not well adapted because of differences in structural habitat from their source, thereby simulating founding events and altering the selective regime for limb length. Specifically, founding propagules were established on small experimental islands, all of which are sparsely vegetated and covered primarily with short, narrow-diameter vegetation as compared to the more forested habitat of the lizards' source area on a nearby larger island (Fig. 1 and figs. S1 and S2). Our prediction is that if natural selection is the dominant force, then we would expect all populations to evolve shorter hindlimbs as they adapt to using narrower

[1]Department of Organismic and Evolutionary Biology and Museum of Comparative Zoology, Harvard University, 26 Oxford Street, Cambridge, MA 02138, USA. [2]Department of Biology, Duke University, Durham, NC 27708, USA. [3]Section of Evolution and Ecology and Center for Population Biology, One Shields Avenue, University of California Davis, Davis, CA 95616, USA.

*To whom correspondence should be addressed. E-mail: jjkolbe@gmail.com

†Present address: Department of Biological Sciences, University of Rhode Island, Kingston, RI 02881, USA.

substrates; moreover, vegetation differences among experimental founder islands would be expected to produce a relationship between hindlimb length and perch diameter [reviewed in (*22*)]. Conversely, if founder effects are dominant, then we would expect no general trend in limb length evolution, with some populations increasing in limb length and others decreasing with respect to the source population, and limb variation being unrelated to vegetation differences among islands.

In May 2005, we randomly selected one male and one female brown anole from lizards collected on a nearby larger island (Iron Cay, Bahamas, vegetated area >150,000 m^2) to found populations on seven small islands (vegetated area 35 to 175 m^2). The storm surge from Hurricane Frances in September 2004 submerged these small islands near Great Abaco, extirpating their lizard populations (*23*). We took morphological measurements and tissue samples for later genetic analysis from these founders. Over the next 4 years, we characterized the environment and repeatedly sampled lizards from the source population (Iron Cay), from the seven experimental founder islands, and from 12 nearby reference islands (vegetated area 74 to 324 m^2) having *A. sagrei* and a composition of spider, insect, and plant species similar to that of the experimental islands (*24*). All lizard populations increased in size for the first 2 years (averaging a 13-fold increase) and fluctuated in size thereafter (Fig. 2).

A founder effect was immediately apparent, conforming to theoretical expectations and previous empirical studies of genetic variation (*25*–*27*). In 2006, 1 year after introduction, multilocus genotypes from six microsatellite loci revealed an average decrease of 46% in allelic diversity and 23% in heterozygosity on experimental founder islands as compared to their source. Furthermore, allele frequencies differed significantly among all pairs of populations, including the source on Iron Cay (Stouffer's z method of combining probabilities from exact G tests of six microsatellite loci; all $P < 0.05$; table S1). Founder populations were dispersed around the mean value of the source population (Iron Cay) and varied fivefold in their amount of divergence from it; moreover, among-islands genotype frequencies in subsequent years were correlated with the genotypes of the two founding individuals [correlation coefficient (r) = 0.80 to 0.97 on principal coordinates (PCo) axes 1 to 3 for 2006, 2007, and 2009, all $P < 0.05$; Fig. 3]. Islands differed significantly from each other in genotype frequencies (analyses of variance for PCo 1 to 3 separately, $F_{6,248}$ = 16.5 to 41.7, all $P < 0.0001$), whereas differences both across years and among islands across years were not significant. In all but one case (the island N3–Iron Cay comparison), pairwise fixation index (F_{ST}) values indicated significant genetic differentiation between islands (table S2), although F_{ST} values should be interpreted cautiously because of the likelihood of nonequilibrium conditions in these recently established populations. Moreover, genetic diversity was sustained after the founding event; only 1 locus out of 42 on the seven islands (six loci per island) showed a net decrease in the number of alleles from founding in 2005 to 2009. These results support the persistence of the initial founder effect without subsequent genetic drift through time.

A founder effect also was evident for hindlimb length, with experimental founder islands differing significantly in 2006 ($P = 0.0015$; table S3 and Fig. 4, inset). As with the genetic data, hindlimb values for island populations were dispersed around the mean value of the source population on Iron Cay (fig. S3). Furthermore, there was no relationship between perch diameter and relative hindlimb length among islands in 2006 ($r^2 = 0.15$, $P = 0.39$), supporting the interpretation that differences in hindlimb length among islands resulted from the founder event rather than adaptive divergence.

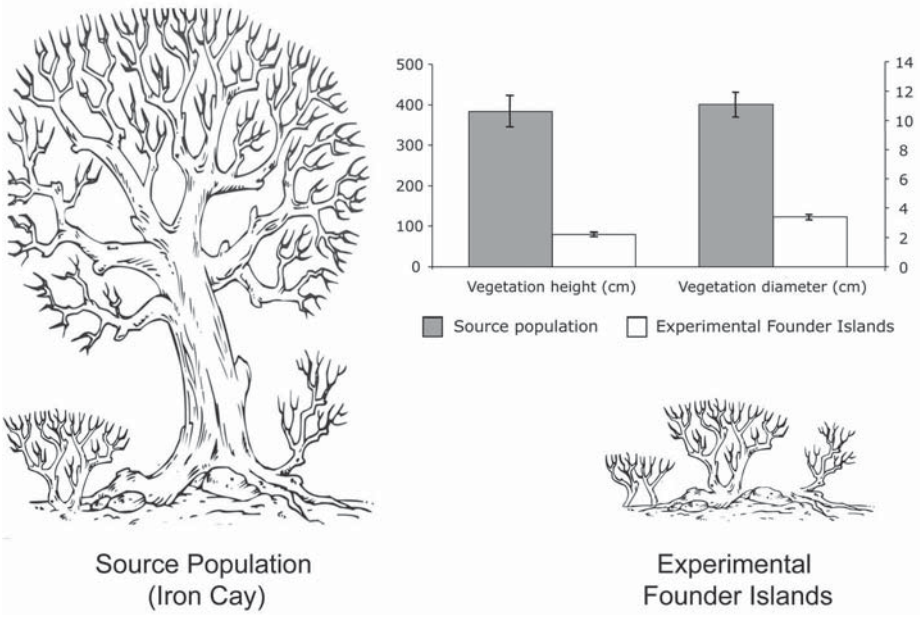

Fig. 1. Vegetation differences between the source population and those of the experimental founder islands. The schematic cartoon shows the change in the vegetation profile for lizards introduced from the source population on the more forested Iron Cay to the sparsely vegetated experimental founder islands. The vegetation illustrated is scaled to the mean values of vegetation height for Iron Cay and the pooled experimental founder islands, respectively. Bar graphs show the difference (mean ± SE) in available vegetation height and diameter from systematic transects on each island. We predicted that the change in vegetation profile would result in lizards using narrower perches on experimental founder islands, which would alter the selective regime to favor shorter hindlimbs.

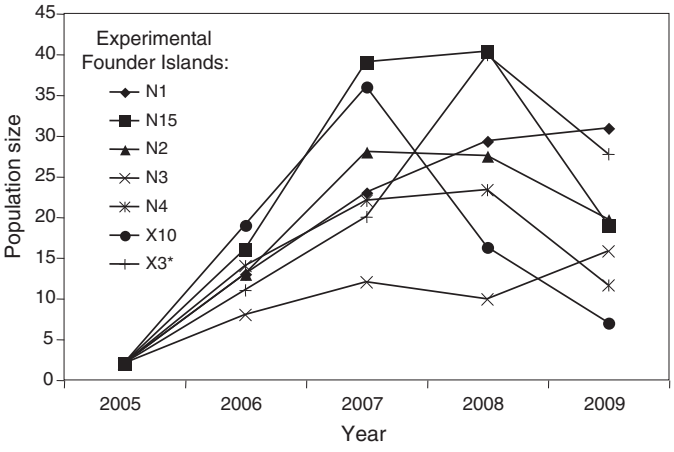

Fig. 2. Population size estimates for experimental founder islands. Surveys were conducted in May of each year from 2005 to 2009 [see (*29*) for details]. Population size showed a positive relationship with vegetated area of each island in 2006 ($r^2 = 0.53$, $P = 0.06$) and 2007 ($r^2 = 0.74$, $P = 0.01$), suggesting an effect of habitat area on population growth over the first 2 years. Population size estimates from November 2006, which included hatchlings produced that year, ranged from 21.4 to 60.2 (not shown in this figure). In all but one case, the November 2006 size estimates greatly exceeded the population size in May 2007, suggesting high mortality rates. Rapid population expansion such as found here may produce conditions favorable to evolution by natural selection (*16*, *30*) and may also curtail the loss of genetic variation after the initial founder effect.

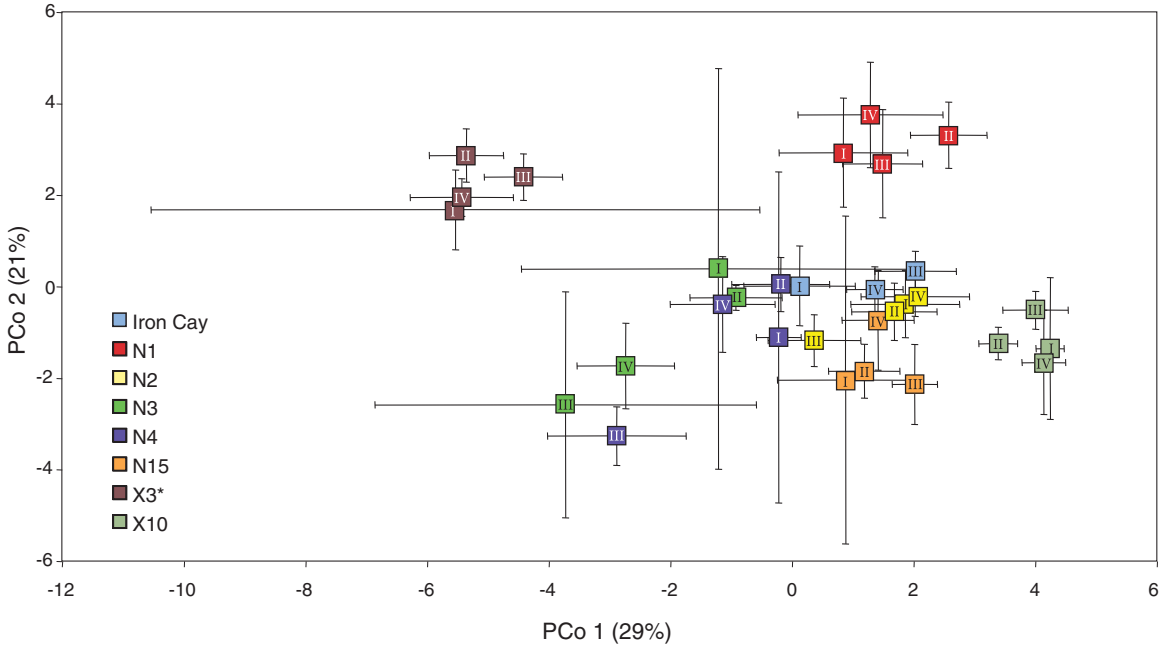

Fig. 3. Multilocus genotypic variation for the source population and those of the experimental founder islands. We conducted a PCo analysis of six microsatellite loci (mean ± SE of PCo values). Numbers within each symbol correspond to different sampling years: I, 2005 (i.e., the founding pair on each experimental founder island and these same founder individuals pooled for the source population estimate on Iron Cay); II, 2006 (no Iron Cay estimate); III, 2007; and IV, 2009. The percentage of variation explained for each PCo axis is in parentheses. Stored sperm use was detected in 6% of offspring through 2006, resulting in offspring fathered by a male other than the one introduced onto the island. However, all other individuals sampled during this time had multilocus genotypes consistent with being progeny of the founding pair (or founding female in the case of stored sperm use), and not until 2007 did we detect unambiguous immigrants.

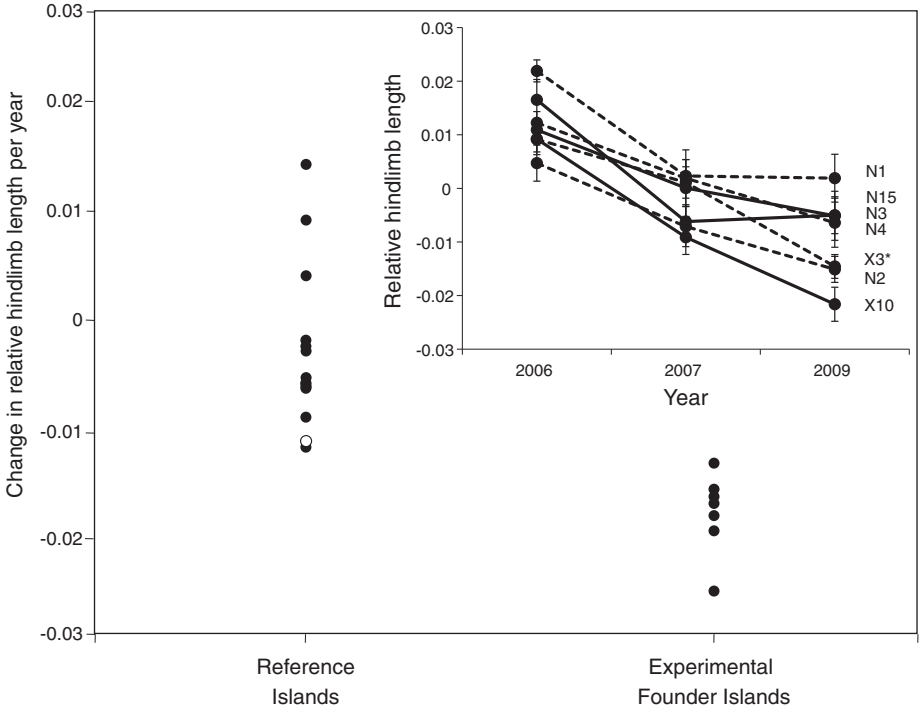

Fig. 4. Change in hindlimb length on reference and experimental founder islands. Change in mean relative hindlimb length [calculated as the residuals of the regression of log–hindlimb length on log-body length (i.e., snout-vent length), separately for each sex] per year for populations on experimental founder and reference islands, including the source population on Iron Cay (open circle). The inset in the upper right shows how the mean (±SE) relative hindlimb length decreases on the experimental founder islands in each year. Islands N1, N3, and X3* are shown with dotted lines for clarity. Immigration does not alter the results for hindlimb differentiation, which are virtually identical when putative immigrants are removed from analyses. Although the source population (Iron Cay) decreased in hindlimb length, all lizards on experimental founder islands exhibited even greater decreases than those on Iron Cay and on all other reference islands, with the mean rate of hindlimb change on reference islands not differing from zero.

We used systematic transects to quantify the available structural habitat (i.e., vegetation height and diameter). The vegetation profile of the source population on Iron Cay averaged substantially taller and broader vegetation (mean vegetation height = 384 cm and mean vegetation diameter = 11.1 cm) as compared to the experimental founder islands, which have much shorter and narrower vegetation (mean vegetation height ranged from 62 to 107 cm and mean vegetation diameter ranged from 1.6 to 5.4 cm) (Fig. 1 and figs. S1 and S2). In turn, the mean perch diameter used by lizards on all experimental founder islands (3.2 cm) was smaller than for the source population (4.6 cm).

As predicted by the adaptive relationship between hindlimb length and substrate diameter (*22*), relative hindlimb length decreased greatly over the course of 3 years on all seven experimental founder islands ($P < 0.0001$; table S4 and Fig. 4, inset), with a decrease of 6.5% for males and 4.0% for females (calculated at the median body size for each sex; table S5 and fig. S4). The magnitude of this decrease in hindlimb length was so great that mean values in 2006 are nearly nonoverlapping with 2009 values (Fig. 4, inset). We monitored nearby reference islands for the same length of time, and the decrease on experimental founder islands was five times greater than on the reference islands [mixed effects analysis of covariance (ANCOVA) test for an island type (reference versus experimental founder islands)–by–year interaction: $P < 0.0001$; table S6 and Fig. 4]. The rates of decrease on all seven founder islands were greater than the rates for all reference islands, including the source population on Iron Cay (Fig. 4), and the mean rate for the reference

islands did not differ significantly from zero (t = 1.55, df = 12, P = 0.15), whereas the mean rate for the experimental founder islands did (t = 11.53, df = 6, P < 0.0001).

Despite this substantial adaptive response, the mark of the founder event persisted, as illustrated by the significant difference among islands (ANCOVA: P < 0.0001; table S4) and the minimal change in the order of mean hindlimb length values among experimental founder islands from 2006 to 2009 (year-by-island interaction: P = 0.70; table S4 and Fig. 4, inset). Furthermore, multiple regression confirms the persistence of the founder effect by showing that mean relative hindlimb lengths among islands in 2006 had a positive relationship with values in 2009 (P = 0.046), and it demonstrates that no relationship existed between hindlimb lengths in 2009 and the diameter of either available vegetation (P = 0.17) or perches (P = 0.86), indicating that adaptation to differing environments cannot explain variation among islands in hindlimb length.

Hindlimb growth can be affected by environment during ontogeny in *A. sagrei* (*28*), but such phenotypic plasticity is unlikely to explain the large decreases in hindlimb length detected on the experimental founder islands from 2006 to 2009. If plasticity were important, we would have expected to see an immediate difference in hindlimb length between the founders and their first-generation descendants due to the latter developing in the new, narrow-vegetation environment, but the range in population means in 2006 overlapped completely with that of the male founders. Moreover, perch diameter did not change over time on experimental founder islands (year: P = 0.10, and year-by-island interaction: P = 0.13), even as hindlimb length progressively decreased, showing that the change in hindlimb length cannot be attributed to a change in a possible stimulus for plasticity. Finally, the magnitude of hindlimb divergence is three to five times greater than that produced by plasticity in *A. sagrei* raised on only narrow or broad surfaces in laboratory experiments (*28*) (fig. S5), even though the difference in perch diameter (1 versus 9 cm) imposed in the laboratory experiment was much greater than the differences in mean perch diameter observed between the source population and those of the experimental founder islands (4.6 cm and 2.6 to 4.5 cm for Iron Cay and the experimental founder islands, respectively).

Founder events generated among-island genetic and phenotypic differences that were similar in magnitude to those observed among populations on nearby islands (our reference islands), as well as among natural populations occurring throughout the Bahamas (tables S1 to S3, Fig. 3, and figs. S3 and S5). The strong genetic differentiation among founder islands, illustrated by allelic differentiation and F_{ST} values of similar magnitude to those seen among nearby reference islands, remained stable over the 4 years of the study (Mantel's r = 0.86 to 0.94 for correlations among pairwise F_{ST} matrices in 2006, 2007, and 2009, all P < 0.01; tables S1 and S2). The strong imprint of the founder effect and the stability of among-population genetic differentiation occurred despite evidence for ongoing immigration. Assignment tests and pedigree analyses revealed that 11% of individuals sampled on experimental founder islands in 2007 and 2009 had multilocus genotypes consistent with being first-generation immigrants. In terms of phenotypic differentiation, the level of hindlimb divergence observed among experimental founder islands was only slightly less than that seen both among nearby reference islands and among natural populations from across the Bahamas (fig. S5). These results did not change when putative immigrants were removed from analyses. That the magnitude of the genetic and phenotypic differentiation produced by founder events rivals that seen among populations on natural islands indicates that founder effects may, as some have suggested, be an important cause of variation among islands (*3*, *4*).

Our results indicate that founder effects persist, even in the face of substantial adaptive differentiation. The impacts of founder events on neutral genetic variation have long been recognized and are clearly evident here (*25*, *27*) (tables S1 and S2 and Fig. 3), but the impact of founder effects on phenotypic divergence is still debated. In support of the selectionist school, we show that differentiation from the source population is mostly the result of adaptation to the new environmental milieu on the experimental islands (*7–9*, *16–18*, *22*). However, the imprint of the founder effect remains apparent, even as this adaptive divergence has occurred; indeed, variation among experimental founder islands at the present time is better explained by initial phenotypes than by current environmental conditions (Fig. 4, inset). What remains to be seen is whether—or for how long—these founder effects will persist in the face of natural selection. One might expect that just as selection has driven a decrease in hindlimb length from that of the source population in response to the narrower vegetation on the founder islands, it will ultimately also drive smaller-scale differentiation among islands as their lizard populations similarly adapt to the much smaller differences in perch diameter and erase the signal of the founder event. This prediction is not a foregone conclusion: Not only are habitat differences among experimental founder islands small, but the ultimate outcome is dependent on the interaction of changing demographic, environmental, and genetic factors.

We here show that founder effects can play an important role in the divergence of island populations, even as adaptation occurs. By measuring the phenotypic values of founders and their descendents, we have distinguished between the influences of the founder effect and of adaptation; thus, we provide clear evidence of a rarely characterized dimension of evolutionary divergence among populations.

References and Notes

1. P. R. Grant, Ed., *Evolution on Islands* (Oxford Univ. Press, Oxford, 1998).
2. R. G. Gillespie, D. A. Clague, Eds., *Encyclopedia of Islands* (Univ. of California Press, Berkeley, CA, 2009).
3. E. Mayr, in *Evolution as a Process*, J. Huxley, A. C. Hardy, E. B. Ford, Eds. (Allen & Unwin, London, 1954), pp. 157–180.
4. E. Mayr, *Animal Species and Evolution* (Harvard Univ. Press, Cambridge, MA, 1963).
5. H. L. Carson, *Stadler Genet. Symp.* **3,** 51 (1971).
6. A. R. Templeton, *Genetics* **94**, 1011 (1980).
7. J. A. Endler, *Natural Selection in the Wild* (Princeton Univ. Press, Princeton, NJ, 1986).
8. N. H. Barton, in *Evolution on Islands*, P. R. Grant, Ed. (Oxford Univ. Press, Oxford, 1998), pp. 102–123.
9. D. Schluter, *The Ecology of Adaptive Radiation* (Oxford Univ. Press, Oxford, 2000).
10. T. Price, *Speciation in Birds* (Roberts & Co., Greenwood Village, CO, 2007).
11. N. H. Barton, B. Charlesworth, *Annu. Rev. Ecol. Syst.* **15**, 133 (1984).
12. P. R. Grant, B. R. Grant, K. Petren, *Genetica* **112-113**, 359 (2001).
13. M. Travisano, J. A. Mongold, A. F. Bennett, R. E. Lenski, *Science* **267**, 87 (1995).
14. P. Simões *et al.*, *Evolution* **62**, 1817 (2008).
15. J. A. Coyne, N. H. Barton, M. Turelli, *Evolution* **51**, 643 (1997).
16. D. N. Reznick, C. K. Ghalambor, *Genetica* **112-113**, 183 (2001).
17. S. M. Clegg *et al.*, *Evolution* **56**, 2090 (2002).
18. M. T. Kinnison, N. G. Hairston Jr., *Funct. Ecol.* **21**, 444 (2007).
19. C. W. Kilpatrick, in *Mammalian Population Genetics*, M. H. Smith, J. Joule, Eds. (Univ. of Georgia Press, Athens, GA, 1981), pp. 28–59.
20. R. J. Berry, in *Evolution on Islands*, P. R. Grant, Ed. (Oxford Univ. Press, Oxford, 1998), pp. 35–50.
21. P. R. Grant, *Proc. Natl. Acad. Sci. U.S.A.* **99**, 7818 (2002).
22. J. B. Losos, *Lizards in an Evolutionary Tree: Ecology and Adaptive Radiation of Anoles* (Univ. of California Press, Berkeley, CA, 2009).
23. The patterns of lizard extinction were similar to those documented for Hurricane Floyd in (*31*).
24. D. A. Spiller, T. W. Schoener, *Ecology* **88**, 37 (2007).
25. M. Nei, T. Maruyama, R. Chakraborty, *Evolution* **29**, 1 (1975).
26. R. Chakraborty, M. Nei, *Evolution* **31**, 347 (1977).
27. C. L. Tarr, S. Conant, R. C. Fleischer, *Mol. Ecol.* **7**, 719 (1998).
28. J. B. Losos *et al.*, *Evolution* **54**, 301 (2000).
29. T. W. Schoener, D. A. Spiller, J. B. Losos, *Ecol. Monogr.* **72**, 383 (2002).
30. D. Reznick, H. Rodd, L. Nunney, in *Evolutionary Conservation Biology*, R. Ferrière, U. Dieckmann, D. Couvet, Eds. (Cambridge Univ. Press, Cambridge, 2004), pp. 101–118.
31. T. W. Schoener, D. A. Spiller, J. B. Losos, *Science* **294**, 1525 (2001).

Acknowledgments: We thank B. Pinder, J. Piovia-Scott, D. Steinberg, Y. Stuart, C. Thornber, and C. White for assistance; the National Geographic Society (grant 8704-09), NSF (grants DEB-0444763 and DEB-0949415), and Duke University for funding; and the Bahamas Ministry of Agriculture and the Bahamas Environment, Science & Technology Commission of the Ministry of the Environment for permission to conduct this research. This material was based on work supported by NSF while one of the authors (D.A.S.) was working at NSF. Any opinions, findings, and conclusions or recommendations expressed in this material are those of the authors and do not necessarily reflect the views of NSF.

Supporting Online Material

www.sciencemag.org/cgi/content/full/science.1209566/DC1
Materials and Methods
Figs. S1 to S5
Tables S1 to S6
References (*32–45*)

9 June 2011; accepted 17 November 2011
10.1126/science.1209566

Pollinator-Mediated Selection on Flower Color Allele Drives Reinforcement

Robin Hopkins* and Mark D. Rausher

Reinforcement is the process by which reduced hybrid fitness generates selection favoring the evolution of stronger prezygotic reproductive barriers between emerging species. Using common-garden field experiments, we quantified the strength of reinforcing selection in nature by demonstrating strong selection favoring an allele conferring increased pigment intensity in the plant *Phlox drummondii* in areas of sympatry with the closely related species *Phlox cuspidata*. Incomplete hybrid sterility between the two species generates selection for traits that decrease interspecies hybridization. In contrast, selection on this locus is undetectable in the absence of *P. cuspidata*. We demonstrate that reinforcing selection is generated by nonrandom pollinator movement, in which pollinators move less frequently between intensely pigmented *P. drummondii* and *P. cuspidata* than between lightly pigmented *P. drummondii* and *P. cuspidata.*

Reinforcement is the evolution of increased prezygotic reproductive isolation due to selection favoring decreased hybridization between diverging groups of individuals or emerging species (*1*–*4*). A. R. Wallace first proposed that selection against hybrids might favor the evolution of novel prezygotic isolating barriers (subsequently termed the Wallace effect) in 1889 (*5*). Although this idea has been controversial, recent theoretical and empirical work suggests that reinforcement may often play an important role in increasing reproductive isolation in nature (*1*, *3*, *4*, *6*, *7*). However, the magnitude of reinforcing selection in nature is generally unknown, as are the genes upon which such selection acts. Theoretical models have demonstrated that direct environmental selection can be more effective in influencing trait evolution than reinforcing selection (*6*, *8*–*11*), but previous investigations of reinforcement have rarely differentiated between these two types of selection [but see (*12*, *13*)].

Flower color variation in *Phlox drummondii* has been hypothesized to be an example of reinforcement (*14*). The geographic range of this species partly overlaps with that of a congener, *P. cuspidata*, in eastern Texas. Both species have the light-blue (sometimes called violet or pink) flower color characteristic of most *Phlox* species in allopatric areas of their ranges, whereas *P. drummondii* has dark-red flowers in regions sympatric with *P. cuspidata* (*15*). In the region of sympatry, populations of the two species frequently grow in close proximity; produce hybrids in nature that have high, but not complete, ovule and pollen sterility; and exhibit some interspecific gene flow (*16*, *17*). In *P. drummondii*, the difference between the ancestral light-blue flower color and the derived dark-red flower color is caused by mutations in the *cis*-regulatory regions of two genes (*18*). Down-regulation of the gene coding for the enzyme Flavonoid 3′5′-hydroxylase (*F3′5′h*) alters the anthocyanin pigment composition of flowers and changes them from blue to red. At this hue locus, the ancestral "blue" allele (*H*) is dominant to the derived "red" allele (*h*). Up-regulation of an *R2R3-Myb* transcription factor increases the amount of pigments produced, resulting in increased color intensity. At this intensity locus, the derived "dark" allele (*I*) is dominant to the ancestral "light" allele (*i*). Western, allopatric *P. drummondii* populations are fixed for the *i* and *H* alleles, whereas eastern, sympatric populations are fixed or nearly fixed for the *I* and *h* alleles, and the two recombinant flower colors, light-red (*iihh*) and dark-blue (*I-,H-*), occur only near the boundary between allopatric and sympatric populations (*15*).

Patterns of neutral genetic variation across the range of *P. drummondii* suggest extensive gene flow between allopatric and sympatric populations, indicating that natural selection and not genetic drift is likely responsible for the geographic pattern of flower color variation (*15*). To determine whether selection in sympatry is due primarily to environmental factors acting directly on flower color variation, rather than to effects of reinforcement, we performed a common-garden field experiment designed to detect selection in the absence of *P. cuspidata.* We measured average fitness of the four flower-color double-homozygote genotypes in their natural habitat. Three generations of crosses were performed to produce seeds of known flower-color genotype and to randomize the genetic background of loci unlinked to the two flower-color loci (*19*). For clarity, we will refer to the homozygous color genotypes by their corresponding flower color throughout the remainder of this paper. A total of 2720 seeds were planted in a randomized block design, with 170 individuals per genotype per block, at the University of Texas Stengl research station (Smithville, Texas). This station is located within the sympatric region of *P. drummondii* and *P. cuspidata* and contains natural populations of both species (*19*).

No significant differences in survival or reproductive success among the flower-color genotypes were observed (table S2). We noted that survival was slightly lower for two derived genotypes (dark-blue and dark-red), compared with the ancestral genotype (light-blue), whereas it was slightly higher for the derived genotype light-red (Fig. 1A). The number of fruits produced was slightly higher for all three derived genotypes compared with light-blue (Fig. 1B), but these differences were also not statistically significant (table S3). There were no detectable differences among genotypes for number of seeds per fruit (table S4). Female fitness, the product of survival and fruit production, was also slightly higher for the derived genotypes, compared with light-blue genotype (Fig. 1C), but again none of these differences were statistically significant (*19*). Overall, we did not detect environmental effects acting directly on flower color favoring the derived allele at either the hue or the intensity locus in the area of sympatry.

To examine whether reinforcing selection generated by hybridization with *P. cuspidata* favors the derived allele at either flower-color locus, we established blocks consisting of 30 plants of one of the double-homozygous genotypes ("focal plants"), as well as 105 light-blue plants of a stock line. We followed 30 of the light-blue stock individuals as "reference plants" to control for environmental variation among blocks. In addition, we planted 115 *P. cuspidata* plants in each block. We collected fruits from reference and focal plants and randomly chose 100 to 150 seeds from each

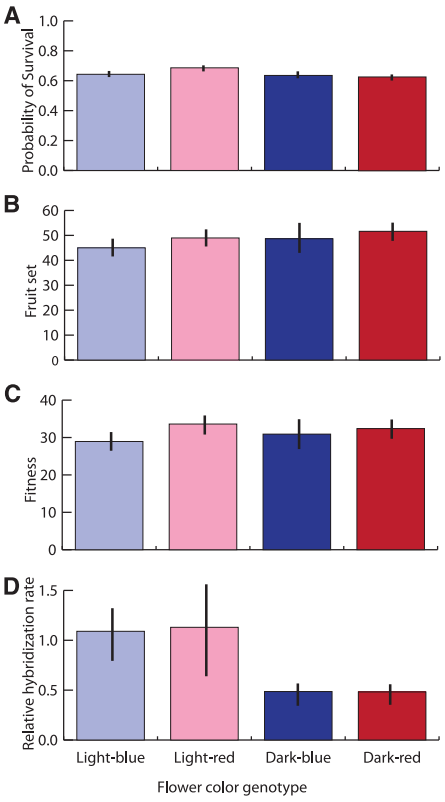

Fig. 1. Fitness components for each flower color genotype. (**A**) Survival probability (n = 1909). (**B**) Fruit production (n = 1240). (**C**) Fitness (n = 1909). (**D**) Relative hybridization rate (n = 931). Bars indicate 1 SE.

Department of Biology, Box 90338, Duke University, Durham, NC 27708, USA.

*To whom correspondence should be addressed. E-mail: robin.hopkins@duke.edu

focal and reference genotype in each block to genotype and determine whether the paternal parent was *P. drummondii* or *P. cuspidata* (*19*). Using this paternity test, we calculated the hybridization rate for focal and reference genotypes within each block.

Across the four blocks, the hybridization rate (proportion of seeds sired by *P. cuspidata*) varied between 28 and 44% for the light-blue reference plants, which indicated substantial overall interspecific hybridization. The hybridization rates of the light-blue and light-red focal plants were similar to those of their respective reference plants (Fig. 1D and table S5, a and b). In contrast, the hybridization rates of dark-blue and dark-red focal plants were more than 50% lower than the reference plants (Fig. 1D and table S5, a and b). Thus, we conclude that the dark allele (*I*) at the intensity locus significantly decreases hybridization between *P. drummondii* and *P. cuspidata*. Given conservative empirical estimates of hybrid sterility of ~90% (*17*) and the average light-blue reference plant hybridization rate of 0.43, the reduction in hybridization translates into a selection coefficient of 0.32 favoring the dark allele (*19*). The two species of *Phlox* are commonly found in intermixed populations with spatial proximity similar to that in our experiments. In these populations, the strong reinforcing selection documented here would increase the frequency of the dark allele rapidly to fixation. Extensive gene flow between *P. drummondii* populations (*15*), including those without nearby *P. cuspidata*, has likely resulted in the subsequent spread of the dark allele throughout the sympatric region. To our surprise, there appeared to be no effect of the red allele at the hue locus on hybridization, even though this allele is fixed in sympatric populations. Taken together with the lack of difference in fitness among genotypes in the first experiment, the difference in hybridization rates between dark and light plants supports the hypothesis that reinforcing selection is responsible for the fixation of the dark allele in sympatric populations.

Manual pollen transfers indicate that there is no difference between light and dark flowered plants in fertilization success of *P. cuspidata* pollen (*14*). These data suggest that dark-flowered individuals are not less compatible with *P. cuspidata* pollen than light-flowered individuals. It is therefore likely that nonrandom patterns of pollinator visitation between *Phlox* species with different flower colors explain our observed variation in hybridization. We examined patterns of pollinator visitation in experimental arrays to test this hypothesis. We constructed three arrays containing light-blue plants, *P. cuspidata* plants, and either light-red, dark-red, or dark-blue focal plants (*19*). We observed a total of 181 pollinators making a total of 2301 transitions between plants.

The primary visitors to both *Phlox* species in these arrays, as in natural populations, were *Battus philenor* butterflies (108 individuals observed) and various species of skippers (Lepidoptera, family Hesperiidae) (73 individuals observed) (table S6a). Both types of pollinators displayed similar movement patterns and visited both *Phlox* species extensively (table S6b). In arrays with light-red plants, there is no evidence of pollinator constancy, as measured by the Bateman's Constancy Index (*19*, *20*) (table S6c). Pollinators were equally likely to visit light-blue and light-red plants after visiting *P. cuspidata* (Table 1A) (*19*). This pattern is consistent with finding no difference in hybridization rates between these two genotypes. In addition, pollinators were equally likely to visit a *P. cuspidata* plant after visiting a light-blue or a light-red plant, which suggested that pollen wastage through interspecific fertilization does not differ between these two genotypes (Table 1A) (*19*).

In contrast, pollinators in arrays containing either dark-blue or dark-red plants exhibited a significantly higher species-level Bateman Constancy Index for dark-flowered genotypes compared with light-flowered genotypes (table S6c). In particular, pollinators were half as likely to visit dark plants as light-blue plants after visiting a *P. cuspidata*—a pattern that explains the reduced hybridization observed in plants with dark pigmentation (Table 1, B and C) (*19*). Pollinators were also substantially less likely to visit a *P. cuspidata* after visiting a dark-blue or dark-red plant than after visiting a light-blue plant (Table 1, B and C) (*19*), which suggested that darkly pigmented plants waste less pollen on interspecific pollination. Although we did not directly measure male fitness in our field experiments, this observation indicates that the dark allele may significantly increase male fitness, in addition to female fitness, relative to the light allele. It is possible that pollinators could be responding to pleiotropic effects of the intense allele (e.g., nectar volume or concentration), but this seems unlikely given the visual orientation of the primary pollinator, *B. philenor* (*21*).

Our investigations provide no explanation for why sympatric populations of *P. drummondii* have evolved red flowers. Although previously we used patterns of genetic variation at this locus and at neutral markers to show that natural selection drove the fixation of the red (*h*) allele in the region of sympatry (*15*), in the current study, we detected neither fitness differences nor differences in levels of interspecific hybridization between genotypes at the hue locus. One possible explanation for these contrasting results is that selection due to environmental factors favors the red allele in sympatry but that the magnitude of this selection is too small to detect given the power of our analysis (as may be evidenced by Fig. 1C). A second possibility is that environmental selection operates only intermittently on this locus and was absent during our experiments. Finally, a third possibility is that a selective agent, such as another type of pollinator, generated selection in the past on the hue locus but is no longer present. Although hitchhiking by the red allele in a selective sweep involving a closely linked gene is a formal possibility, this seems unlikely because it would have required that the favored mutation arose on a rare haplotype carrying the red allele.

Table 1. The percentage of transitions by pollinators across flower types. (**A**) Pollinator movement between colors and species within arrays containing light-red *P. drummondii*. (**B**) Pollinator movement between colors and species within arrays containing dark-blue *P. drummondii*. (**C**) Pollinator movement between colors and species within arrays containing dark-red *P. drummondii*. The percentages of transitions between *P. cuspidata* and *P. drummondii* plants are in bold.

A Pollinators in arrays with the light-red *P. drummondii* moved

	To (%)		
From	**Light-red**	**Light-blue**	***P. cuspidata***
Light-red (252)	32	44	**24**
Light-blue (219)	50	22	**28**
P. cuspidata (185)	**34**	**31**	35

B Pollinators in arrays with the dark-blue *P. drummondii* moved

	To (%)		
From	**Dark-blue**	**Light-blue**	***P. cuspidata***
Dark-blue (222)	51	38	**11**
Light-blue (198)	42	18	**40**
P. cuspidata (274)	**7**	**32**	61

C Pollinators in arrays with the dark-red *P. drummondii* moved

	To (%)		
From	**Dark-red**	**Light-blue**	***P. cuspidata***
Dark-red (255)	37	50	**13**
Light-blue (335)	37	25	**38**
P. cuspidata (378)	**9**	**33**	58

By measuring reinforcing selection acting on the dark flower–color allele in *P. drummondii* under natural sympatric conditions and by quantifying selection in the absence of *P. cuspidata*, we were able to compare the relative strengths of direct selection by other environmental factors and by reinforcing selection on a trait conferring increased premating isolation in a region of sympatry. The absence of detectable fitness differences among flower color genotypes in the absence of *P. cuspidata* indicates that another agent of selection is unlikely to be involved in flower color divergence in *P. drummondii*. Although we cannot rule out small, statistically undetectable differences in survival or reproductive success favoring these genotypes, such differences would be of minor importance compared with the strong reinforcing selection acting on the intensity locus.

Many plants have evolved premating reproductive isolation by switching pollinator types (e.g., from bees to hummingbirds) (*22*–*24*). Our work suggests that increased reproductive isolation can also be achieved by a single pollinator species through constancy of individual pollinators. In particular, if pollinators transition between flowers with similar phenotypes more frequently then between flowers with unlike phenotypes, this will decrease gene flow between unlike flowers. Constancy is commonly studied in bumble bees but rarely investigated in butterfly pollinators (*20*, *25*). That the primary pollinator *Battus philenor* exhibits this type of constancy is not surprising, given that females of this species exhibit constancy for leaf shape when searching for oviposition sites (*21*).

Theoretical models indicate that the likelihood of successful reinforcement is greater when selection is strong, because this will counteract gene flow and recombination, which tend to reduce premating isolation (*26*–*28*). Our results indicate that, at least in some cases, very strong reinforcing selection may act on a single allele and lead to increased reproductive isolation.

Theory also indicates that reinforcement is more easily achieved by a one-allele mechanism (*4*, *29*), but empirical assessment of this prediction has been difficult because the genetic basis of reinforcement is understood in few systems (*7*). Our current demonstration of reinforcing selection acting on the dark allele indicates that reinforcement in *P. drummondii* involves a two-allele reinforcement mechanism. The intensity locus causes reproductive isolation only if the dark allele is present in *P. drummondii* and the light allele is present in *P. cuspidata*. Consistent with theory, we find that strong selection and high levels of hybrid sterility cause the spread of the dark allele through sympatric *P. drummondii* populations. We suspect all reinforcement mechanisms involving different floral phenotypes to which pollination vectors must respond will be two-allele assortative mating mechanisms, because pollinators must be able to discriminate between the novel phenotype in one species and the ancestral phenotype in both species.

Although reinforcement has been studied primarily in animals (*3*, *7*), our work indicates that it may also be an important contributor to speciation in plants. If so, this phenomenon may provide a partial explanation for the tremendous diversity of floral color, floral morphology, and inflorescence structure that characterize flowering plants.

References and Notes

1. R. Butlin, *Trends Ecol. Evol.* **2**, 8 (1987).
2. T. Dobzhansky, *Genetics and the Origin of Species* (Columbia Univ. Press, New York, 1937).
3. D. J. Howard, in *Hybrid Zones and the Evolutionary Process*, R. G. Harrison, Ed. (Oxford Univ. Press, New York, 1993), pp. 46–69.
4. M. R. Servedio, M. A. F. Noor, *Annu. Rev. Ecol. Evol. Syst.* **34**, 339 (2003).
5. A. R. Wallace, *Darwinism: An Exposition of the Theory of Natural Selection, with Some of Its Applications* (Macmillan, London, 1889).
6. M. Kirkpatrick, V. Ravigné, *Am. Nat.* **159** (suppl. 3), S22 (2002).
7. D. Ortiz-Barrientos, A. Grealy, P. Nosil, *Ann. N. Y. Acad. Sci.* **1168**, 156 (2009).
8. M. Kirkpatrick, *Proc. R. Soc. London Ser. B* **267**, 1649 (2000).
9. M. Kirkpatrick, M. R. Servedio, *Genetics* **151**, 865 (1999).
10. M. R. Servedio, *Evolution* **55**, 1909 (2001).
11. M. R. Servedio, *Evolution* **58**, 913 (2004).
12. A. Y. K. Albert, D. Schluter, *Evolution* **58**, 1099 (2004).
13. P. Nosil, B. J. Crespi, C. P. Sandoval, *Proc. R. Soc. London Ser. B* **270**, 1911 (2003).
14. D. A. Levin, *Evolution* **39**, 1275 (1985).
15. R. Hopkins, D. A. Levin, M. D. Rausher, *Evolution* **66**, 469 (2012).
16. D. A. Levin, *Am. J. Bot.* **54**, 1122 (1967).
17. L. G. Ruane, K. Donohue, *Evol. Ecol.* **22**, 229 (2008).
18. R. Hopkins, M. D. Rausher, *Nature* **469**, 411 (2011).
19. Material and methods are available as supporting material on *Science* Online.
20. N. M. Waser, *Am. Nat.* **127**, 593 (1986).
21. M. D. Rausher, *Science* **200**, 1071 (1978).
22. H. D. Bradshaw Jr., D. W. Schemske, *Nature* **426**, 176 (2003).
23. D. R. Campbell, N. M. Waser, E. J. Melendez-Ackerman, *Am. Nat.* **149**, 295 (1997).
24. M. E. Hoballah *et al.*, *Plant Cell* **19**, 779 (2007).
25. L. Chittka, J. D. Thomson, N. M. Waser, *Naturwissenschaften* **86**, 361 (1999).
26. M. Caisse, J. Antonovics, *Heredity* **40**, 371 (1978).
27. J. Felsenstein, *Evolution* **35**, 124 (1981).
28. L. W. Liou, T. D. Price, *Evolution* **48**, 1451 (1994).
29. M. R. Servedio, *Evolution* **54**, 21 (2000).

Acknowledgments: We thank M. Kirkpatrick, S. Otto, M. Whitlock, D. Des Marais, and members of the Rausher and Kirkpatrick laboratory group for advice on this manuscript and S. Scarpino for statistical consultation. We thank the University of Texas Stengl Research Station for field experiment support. This work was supported by NSF grant 0841521 to M.D.R. and a NSF Doctoral Dissertation Improvement Grant to R.H. and M.D.R. R.H. was supported by the NSF Graduate Research Fellowship Program. All data presented here are available in the supporting material.

Supporting Online Material

www.sciencemag.org/cgi/content/full/science.1215198/DC1
Materials and Methods
Figs. S1 and S2
Tables S1 to S9
References

12 October 2011; accepted 12 January 2012
Published online 2 February 2012;
10.1126/science.1215198

Generation of Leaf Shape Through Early Patterns of Growth and Tissue Polarity

Erika E. Kuchen,[1]* Samantha Fox,[1]* Pierre Barbier de Reuille,[2] Richard Kennaway,[2] Sandra Bensmihen,[1] Jerome Avondo,[1] Grant M. Calder,[1] Paul Southam,[2] Sarah Robinson,[1] Andrew Bangham,[2]† Enrico Coen[1]†

A major challenge in biology is to understand how buds comprising a few cells can give rise to complex plant and animal appendages like leaves or limbs. We address this problem through a combination of time-lapse imaging, clonal analysis, and computational modeling. We arrive at a model that shows how leaf shape can arise through feedback between early patterns of oriented growth and tissue deformation. Experimental tests through partial leaf ablation support this model and allow reevaluation of previous experimental studies. Our model allows a range of observed leaf shapes to be generated and predicts observed clone patterns in different species. Thus, our experimentally validated model may underlie the development and evolution of diverse organ shapes.

The shapes of many plant and animal appendages are thought to develop under the influence of orthogonal organizing systems (i.e., systems with axes that intersect at right angles) (*1*–*4*). However, it is unclear how these orthogonal systems lead to changes in tissue shape and how shape changes may themselves feed back to deform the organizing systems. Consider a square piece of tissue that deforms during growth (Fig. 1A). The tissue has an initial linear orthogonal system that organizes the pattern of morphogenesis (Fig. 1B, arrows). We might en-

[1]John Innes Centre, Norwich Research Park, Norwich, NR4 7UH, UK. [2]School of Computing Sciences, University of East Anglia, Norwich Research Park, Norwich, NR4 7TJ, UK.

*These authors contributed equally to this work.
†To whom correspondence should be addressed. E-mail: enrico.coen@jic.ac.uk (E.C.); a.bangham@uea.ac.uk (A.B.)

visage two extreme possibilities as the tissue deforms. One is that the organizing system retains its original arrangement despite the change in tissue shape (Fig. 1C). Another possibility is that the change in shape of the tissue feeds back to deform the organizing system during growth (Fig. 1D).

Here, we exploit live imaging of fluorescently marked *Arabidopsis* leaves to distinguish these possibilities. We concentrated on growth of leaf 1, from when the leaf primordium had a simple dome shape [3 days after initiation (DAI)] to the stage at which the characteristic leaf shape was evident (9 DAI) (fig. S1). We first determined areal growth rates for different regions of the leaf by tracking cell vertices over time. Areal growth rate is lower toward the distal tip of the leaf (Fig. 1J), consistent with previous tracking studies at later stages of growth (*5*–*7*). Areal growth rates also tend to be higher in lateral compared to medial domains (Fig. 1J).

To understand how the observed patterns of growth could be generated, we first considered growth rates in the proximodistal direction along the midline of the leaf lamina (Fig. 1, E to I). At early stages, growth rates parallel to the midline show an almost linear decrease from proximal to distal regions (Fig. 1, E and F). At later stages, the proximodistal gradient in growth rates becomes shallower throughout most of the leaf but maintains a steep decline near the tip (Fig. 1, G to I). To account for these observations, we used a one-dimensional (1D) model with a factor, PGRAD, that declines from proximal to distal positions with an initial linear gradient (fig. S2, A and B) and promotes specified growth rate K (Fig. 1P). PGRAD levels are maintained locally and deform with the tissue during growth. The output of this model is a gradient in growth rates that becomes shallower proximally because these regions extend more rapidly (Fig. 1, E to G, black lines; Fig. 1, H and I, gray lines). Thus, the initial linear gradient is transformed into a curve that dips more steeply toward the distal end.

Although this model generates curves that match the data at early stages (Fig. 1, E to G), observed growth rates at later stages are lower than those predicted by the model (Fig. 1, H and I, gray lines). We therefore introduced a uniformly distributed factor into the model, LATE, that increases during later stages and inhibits the specified growth rates (Fig. 1P and fig. S2C). With this modification, the resulting proximodistal growth rates show a better match to the data (Fig. 1, H and I, black lines).

We next extended the model to 2D, using the growing polarized tissue framework (*8*), in which growth rates can be specified by a distribution of factors over a tissue. Regions of the tissue are mechanically connected, forming a canvas, allowing the deformation resulting from specified local growth patterns to be computed.

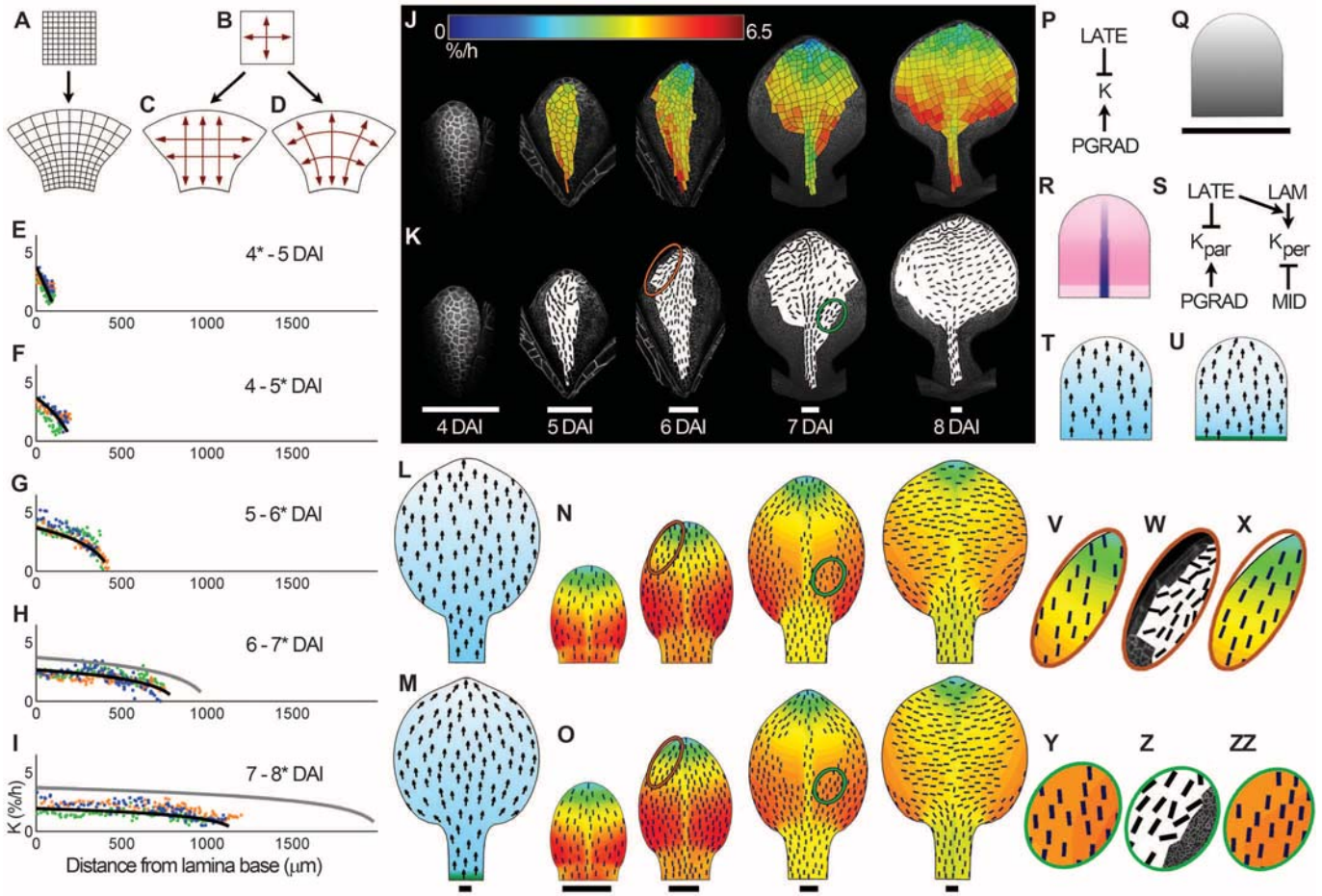

Fig. 1. Leaf growth analysis. (**A**) Tissue deforms through growth. (**B**) Orthogonal organizing system which (**C**) retains its original arrangement or (**D**) deforms during growth. (**E** to **I**) Midline proximodistal growth rates for three replicates (orange, green, and blue), and 1D models (black and gray lines). Distances from lamina base correspond to those on the day indicated by an asterisk. (**J**) Areal growth rates (heat map) and (**K**) principal directions of growth (black lines, where anisotropy > 10%) at the end of each period. (**L**) Resultant shape, POL levels and specified growth orientations (arrows) for nondeforming and (**M**) deforming (organizer-based) models. (**N**) Resultant shapes, areal growth rates, and directions of growth (black lines, where anisotropy > 5%) for 2D nondeforming and (**O**) deforming (organizer-based) models. Heat map and staging as in (J). (**P**) 1D model regulatory network. (**Q**) 2D distribution of PGRAD (gray). (**R**) MID (blue) and LAM (magenta) distributions. (**S**) 2D model regulatory network. (**T**) Initial POL (cyan) distribution for nondeforming and (**U**) deforming models. PROXORG in green. (**V** to **X**) Enlargement of brown ellipses in (N) (K), and (O), respectively. (**Y**, **Z**, and **ZZ**) Enlargement of green ellipses in (N), (K), and (O), respectively. Scale bars, 100 μm.

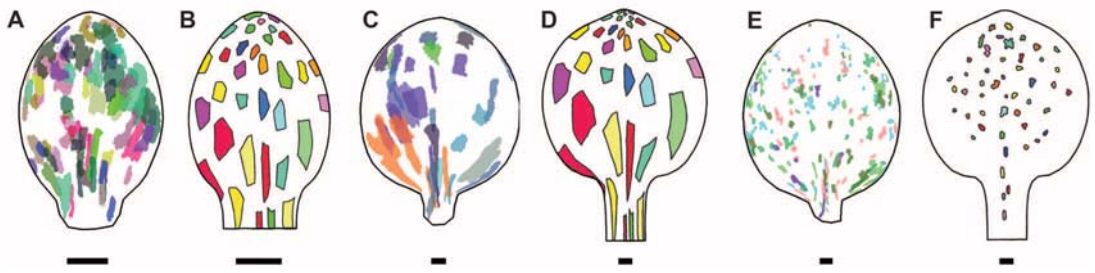

Fig. 2. Clonal analysis. (**A**, **C**, and **E**) Clones induced at 3 DAI (A and C) or 6 DAI (E) and imaged at 6 DAI (A) or 9 DAI (C and E). Clones from several leaves are superimposed. (**B**, **D**, and **F**) Clonal patterns generated by the organizer-based model at stages corresponding to those shown on their left. Scale bars, 100 μm.

Each model has three components: (i) an initial canvas shape with distributed factors; (ii) a system for specifying polarity; and (iii) a growth regulatory network. The starting shape for the canvas is based on a simplified leaf primordium shape (Fig. 1Q and fig. S3). To account for the observed pattern of growth rates (Fig. 1J), the initial canvas has spatial domains defined by three factors: (i) PGRAD is expressed as a linear gradient along the proximodistal axis (as for the 1D model); (ii) LAM is expressed everywhere but at a lower level in a narrow region at the base (which will form the petiole); and (iii) MID is expressed along the midline (Fig. 1, Q and R). For all these factors, levels are maintained locally and deform with the canvas during growth.

Growth orientations depend on a proximodistal gradient of a factor, POLARISER (POL), distributed throughout the canvas (Fig. 1T, arrows). The gradient of POL provides the axiality information needed to specify local growth orientations. We first assumed that growth orientations are specified according to a nondeforming system (Fig. 1C) with axes parallel (proximodistal axis) or perpendicular (mediolateral axis) to the midline (*9*, *10*). This corresponds to keeping the POL gradient parallel to the midline throughout growth (Fig. 1L). There is thus no feedback between tissue deformation and specification of growth orientations. The growth regulatory network controls two specified growth rates: parallel (K_{par}) and perpendicular (K_{per}) to the POL gradient (fig. 1S). K_{par} is controlled by PGRAD and LATE as for the 1D model (Fig. 1P). To account for the higher areal growth rates in the lateral domains, K_{per} is promoted by LAM and inhibited by MID. The extent to which LAM promotes K_{per} is further enhanced by LATE; otherwise, growth rates in the lamina drop below observed levels.

Running this nondeforming model leads to canvas shape changes and patterns of areal growth that are broadly similar to those observed experimentally (Fig. 1N). The principal orientations of resultant growth (Fig. 1N, black lines) switch from being mainly parallel to the midline at early stages to being mainly perpendicular to the midline in the lamina. The switch occurs because LATE enhances the effect of LAM on K_{per} (Fig. 1S).

The principal orientatins of growth predicted by the nondeforming model of leaf development were compared with observed orientations,

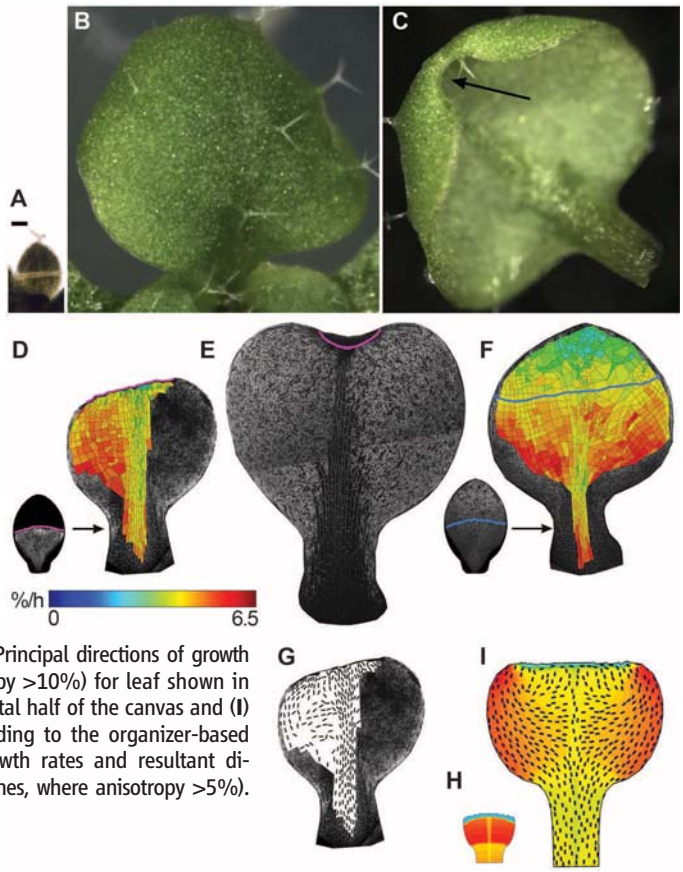

Fig. 3. Distal leaf excision. (**A**) Excision of the distal half of leaf 1 lamina at 6 DAI. Distal region was removed after laser cut (pale line). (**B**) Leaf 1, 6 days after distal excision, viewed from the top and (**C**) from lower (abaxial) side, showing a curved indentation at the tip (arrow). (**D**) Leaf 1 cut at 6 DAI (left) and tracked until 9 DAI (right). Areal growth rates (heat map) calculated over the last 24 hours of tracking. Boundary of cut highlighted with magenta line. (**E**) Leaf after tracking growth for 5 days after distal excision. (**F**) Tracked uncut leaf with a blue line shown at a similar position to the cut in (D). (**G**) Principal directions of growth (black lines, where anisotropy >10%) for leaf shown in (D). (**H**) Excision of the distal half of the canvas and (**I**) output after growth according to the organizer-based model, showing areal growth rates and resultant directions of growth (black lines, where anisotropy >5%). Scale bar, 100 μm.

obtained from the measured displacement of cell vertices (*11*). The observed principal directions of growth are mainly oriented proximodistally at early stages and switch in the lamina toward a more mediolateral orientation during later stages of growth (Fig. 1K), consistent with the nondeforming model (Fig. 1N). However, observed orientations converge toward the leaf tip at early stages much more than those of the model (brown ellipses, Fig. 1, K, N, V, and W, and fig. S4, A and B). Also, in the proximal lamina regions near the midvein, principal orientations of growth are oblique and diverge from the midline at later stages (green ellipses, Fig. 1, K and Z and fig. S4, C and D), in contrast to the largely parallel or perpendicular orientations predicted by the model (green ellipse, Fig. 1, N and Y).

We next considered an organizer-based model in which POL distribution arises by propagation through the canvas and then deforms during growth. POL production is promoted at the base of the canvas through an identity factor PROXORG (proximal organizer) and is degraded everywhere at a constant rate (Fig. 1U). Propagation of POL through the canvas generates a proximodistal field of polarities that is initially parallel to the midline in the basal half of the canvas and converges toward the tip (Fig. 1U and fig. S5A) but then deforms (Fig. 1M and fig. S5B). The initial canvas, distribution of factors, and growth regulatory network are the same as in the nondeforming model (Fig. 1, Q to S). The resulting shape changes and growth patterns are also similar (Fig. 1O and fig. S5C). However, resultant growth orientations give a better match to the experimental data (table S1): Orientations converge toward the leaf tip (brown ellipse, Fig. 1, O and X) and have oblique orientations of growth that diverge from the midline at later

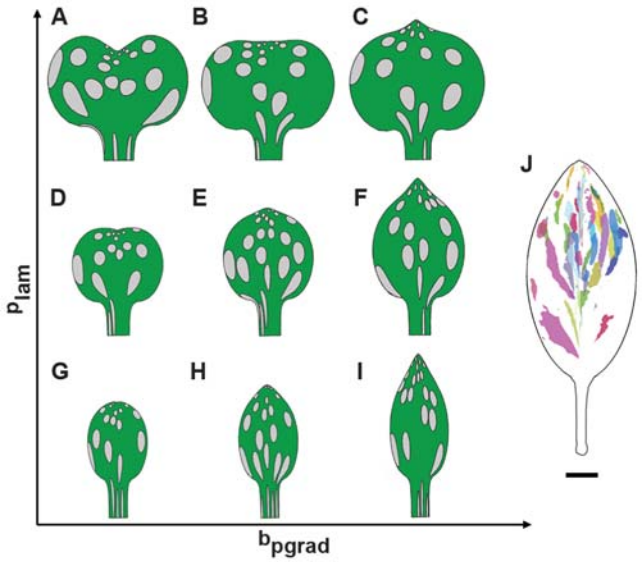

Fig. 4. Generation of diverse leaf shapes. (**A** to **I**) Morphospace generated from the organizer-based model, varying two growth parameters; the strength of promotion by LAM, p_{lam}, and the level of PGRAD at the distal end b_{pgrad}. *Arabidopsis* leaf 1 corresponds to (E). Clones induced as circles on day 3. (**J**) Clones on mature leaf (metamer 4) of *Antirrhinum*, induced when the leaf primordium is about 50 to 100 μm wide. Clones on the petiole were not recorded. Scale bar for *Antirrhinum* leaf, 1 cm.

stages due to deformation of the canvas (green ellipse, Fig. 1, O and ZZ).

An organizer-based model is also consistent with patterns of polarity observed in young leaf primordia. PIN1 (PIN-FORMED1) auxin transporters at this stage are oriented in a proximodistal pattern, with cell polarity pointing distally and converging toward the tip in the epidermis or pointing proximally in internal tissues (*12*). Both polarity patterns are consistent with an organizer-based model, because specifying growth orientation depends only on the axiality component of the polarity field, not the sense in which the polarity points (*8*). The mechanism determining PIN polarity is still unclear (*13*). One possibility is that auxin plays a primary role in establishing this pattern and would therefore be influenced by organizers of polarity. Alternatively, the PIN polarity pattern may be a read-out of a separate underlying polarity system.

The organizer-based model should account for growth patterns across the entire leaf as well as in regions accessible to tracking. This additional requirement was evaluated through clonal analysis. Clones were induced at 3 DAI (Fig. 2, A and C) or 6 DAI (Fig. 2E) using a heat shock–inducible Cre-Lox system (*14*). For regions accessible to tracking, the resulting clones were in good agreement with the fate of individually tracked cells (fig. S6). Clonal patterns were also compared with those generated by the organizer-based model. This was achieved by superimposing outlines of leaf cells on the canvas (fig. S3) and then growing the canvas to its final shape (Fig. 2, B, D, and F). The shapes and orientations of predicted and observed clones showed a good qualitative match: Clones diverge near the lamina base and converge toward the tip.

A key assumption of the above models is that the spatial pattern of growth rates is established at an early stage of leaf development. This assumption does not rule out modulations in growth pattern at later stages but seems inconsistent with the claim that leaves regenerate after excision of the distal half at a time after patterning has been established according to our models (*15*). To investigate this discrepancy, we repeated the excision experiment by removing the distal half of the leaf at a similar developmental stage to that previously reported to give regeneration (6 DAI) (Fig. 3A and fig. S7A) (*15*). As with the previously published experiments, the cut edge was clearly evident after 2 days of growth but seemed to have disappeared after a further 4 days of growth when the leaf was viewed from above (Fig. 3B). However, examination of the underside of the leaf revealed a semicircular edge at the tip similar in length to the original cut, suggesting that regeneration from the cut edge may not have occurred (Fig. 3C). Tracking leaf development after distal excision revealed a similar spatial pattern of growth rates to a control uncut leaf, except for regions near the cut, where growth rates were reduced (Fig. 3, D and F). There was no evidence of tip regeneration (Fig. 3, D and E). The superficial resemblance to regeneration (Fig. 3B) is a consequence of the high contribution that proximal regions of the leaf primordium make to the mature leaf, and the reduced growth rate of the cut edge.

To determine whether the organizer-based model could account for the observed effects of distal excision, we grew the canvas until day 6 and then removed the distal half (Fig. 3H and fig. S2, D and E). Growth is assumed to be unaffected except at the cut margin, where growth is inhibited. The final shape and growth patterns generated by the model are broadly similar to that observed experimentally after distal excision (Fig. 3, G and I). Thus, distal excision validates the model rather than refuting it.

To determine whether the organizer-based model could account for leaf shapes other than leaf 1 in *Arabidopsis*, we varied each of the model's growth parameters (fig. S8). The effect of varying b_{pgrad} (the level of PGRAD at the distal end) and p_{lam} (the strength of K_{per} promotion by LAM) in various combinations is shown in Fig. 4. The resulting morphospace includes many botanically described leaf shapes, such as obcordate (Fig. 4, A and D), ovate (Fig. 4F), and elliptic (Fig. 4, H and I) (*16*). Thus, the model may underlie a wide range of leaf forms.

As a further test of the model's generality, we compared the pattern of clones predicted to those observed in *Antirrhinum*, a species with an elliptic leaf shape amenable to clonal analysis (*9*). Clones were induced at an early stage of leaf development in *Antirrhinum*, using a temperature-sensitive transposon, and visualized in the mature leaf. The pattern of clones observed is in broad agreement with those generated by the model with low p_{lam}: Large narrow clones diverge outward from the lamina base, and small clones converge toward the tip (Fig. 4, H and J).

These results show that a relatively simple model can broadly account for the growth dynamics and shape changes observed during normal and perturbed growth of *Arabidopsis* and may also underlie a variety of other leaf shapes. The model assumes that growth orientations are specified through a tissue polarity system that deforms during growth and that a basic pattern of growth rates across the leaf is established from an early stage. This raises the question of how these features are specified at the cellular scale and what genes may underlie them. Candidate genes for LAM are *LEAFY PETIOLE* (*17*) and members of the *YABBY* family (*18*), which are expressed in the lamina and promote its lateral growth. Candidate organizers of tissue polarity are the *CUP-SHAPED COTYLEDON* (*CUC*) genes, which are expressed at the base of the leaf (*19*) and play a key role in leaf development (*20*, *21*). Thus, our model provides a simple unifying framework for the control of organ shape that can be further tested experimentally, elaborated through the incorporation of genes and cellular properties, and extended to cover more complex leaf shapes.

References and Notes

1. L. I. Held, *Imaginal Discs: The Genetic and Cellular Logic of Pattern Formation* (Cambridge Univ. Press, Cambridge, 2002).
2. G. T. Kim, K. H. Cho, *Physiol. Plant.* **126**, 494 (2006).
3. G. F. Stopper, G. P. Wagner, *Dev. Biol.* **288**, 21 (2005).
4. L. Wolpert, C. Tickle, *Principles of Development* (Oxford Univ. Press, Oxford, ed. 4, 2011).
5. G. S. Avery, *Am. J. Bot.* **20**, 565 (1933).
6. D. Schmundt, M. Stitt, B. Jahne, U. Schurr, *Plant J.* **16**, 505 (1998).
7. S. D. Wolf, W. K. Silk, R. E. Plant, *Am. J. Bot.* **73**, 832 (1986).
8. R. Kennaway, E. Coen, A. Green, A. Bangham, *PLOS Comput. Biol.* **7**, e1002071 (2011).
9. A.-G. Rolland-Lagan, J. A. Bangham, E. Coen, *Nature* **422**, 161 (2003).
10. A. J. Fleming, *Plant Biol.* **5**, 341 (2003).
11. Z. Hejnowicz, J. A. Romberger, *J. Theor. Biol.* **110**, 93 (1984).

12. E. Scarpella, D. Marcos, J. Friml, T. Berleth, *Genes Dev.* **20**, 1015 (2006).
13. Y. Boutté, Y. Ikeda, M. Grebe, *Curr. Opin. Plant Biol.* **10**, 616 (2007).
14. J. L. Gallois, C. Woodward, G. V. Reddy, R. Sablowski, *Development* **129**, 3207 (2002).
15. G. Sena, X. Wang, H.-Y. Liu, H. Hofhuis, K. D. Birnbaum, *Nature* **457**, 1150 (2009).
16. F. Swink, G. Wilhelm, *Plants of the Chicago Region* (Indiana Academy of Science, Indianapolis, ed. 4, 1994).
17. E. van der Graaff, A. D. Dulk-Ras, P. J. J. Hooykaas, B. Keller, *Development* **127**, 4971 (2000).
18. R. Sarojam *et al.*, *Plant Cell* **22**, 2113 (2010).
19. M. Aida, T. Ishida, M. Tasaka, *Development* **126**, 1563 (1999).
20. A. Hasson *et al.*, *Plant Cell* **23**, 54 (2011).
21. G. D. Bilsborough *et al.*, *Proc. Natl. Acad. Sci. U.S.A.* **108**, 3424 (2011).

Acknowledgments: This work was funded by the U.K. Biotechnology and Biological Sciences Research Council (BBSRC). We thank S. Sauret-Güeto, C. Hindle, and J. Chan for help in developing the tracking chamber; K. Lee for imaging cut leaves with OPT; and S. Grandison for mathematical support. The authors declare no competing financial interests.

Further information and software can be downloaded at www.uea.ac.uk/cmp/research/cmpbio/Gftbox.

Supporting Online Material
www.sciencemag.org/cgi/content/full/335/6072/1092/DC1
Materials and Methods
SOM Text
Figs. S1 to S8
Table S1
References (*22*–*31*)

30 September 2011; accepted 24 January 2012
10.1126/science.1214678

Elastic Domains Regulate Growth and Organogenesis in the Plant Shoot Apical Meristem

Daniel Kierzkowski,[1]* Naomi Nakayama,[1]* Anne-Lise Routier-Kierzkowska,[1]* Alain Weber,[1]* Emmanuelle Bayer,[2] Martine Schorderet,[3] Didier Reinhardt,[3] Cris Kuhlemeier,[1] Richard S. Smith[1]†

Although genetic control of morphogenesis is well established, elaboration of complex shapes requires changes in the mechanical properties of cells. In plants, the first visible sign of leaf formation is a bulge on the flank of the shoot apical meristem. Bulging results from local relaxation of cell walls, which causes them to yield to internal hydrostatic pressure. By manipulation of tissue tension in combination with quantitative live imaging and finite-element modeling, we found that the slow-growing area at the shoot tip is substantially strain-stiffened compared with surrounding fast-growing tissue. We propose that strain stiffening limits growth, restricts organ bulging, and contributes to the meristem's functional zonation. Thus, mechanical signals are not just passive readouts of gene action but feed back on morphogenesis.

The plant shoot apical meristem is composed of two regions, the slow-growing central region, which contains the stem cell niche, and the surrounding periphery, where cells divide rapidly and new organs are initiated (*1*–*4*). New organ primordia initiate at accumulation points of the plant hormone auxin (*5*–*7*). In addition to triggering gene regulatory pathways, auxin induces cell wall acidification (*8*), which increases expansin activity (*9*) that modifies cross-links in the cell wall matrix. Disruption of auxin signaling suppresses organ initiation, which can be restored by the local application of auxin (*7*, *10*, *11*). Bulging in the meristem flank can also be triggered by local cell wall loosening with expansin (*12*, *13*) or pectin methyl-esterase (PME) (*14*, *15*). These bulges can develop into normal organs, which suggests that a mechanical signal is involved in primordium differentiation. Additional support for mechanical signals in this pathway comes from the recent hypothesis that stress in the cell wall is the signal that orients the microtubule network and the PIN-FORMED 1 (PIN1) auxin transporter (*16*, *17*). Yet despite the accumulating evidence for an instructive role for mechanical signals in organogenesis, the mechanical properties of the shoot apex have only recently begun to be explored (*15*, *18*). Here, we examine both the elastic and plastic properties of the shoot apex and link them to growth dynamics.

Tomato vegetative shoot apices were imaged at 11-hour intervals by confocal microscopy in order to monitor their growth. Images were analyzed with MorphoGraphX (*19*) (Fig. 1) to compute relative changes in cell surface area (Fig. 2). Cell surface expansion was 25% on average in the central region and between 45 and 80% on average in the periphery, depending on the stage of development of the adjacent primordium. The boundary region between the primordium and the meristem displayed little growth. Our data closely resembled growth patterns in other species (*1*–*4*).

In order to examine meristem material properties, we induced tissue deformation by manipulating turgor pressure with osmotic treatments using mannitol and NaCl. Experiments started by adapting the samples in solutions of 0.2 M osmotically active molecules. Subsequent immersion in hypo-osmotic medium (0 M) resulted in a relative increase in total surface area of 6 ± 2% (n = 20). The treatment revealed regional differences, with cells in the central and boundary regions expanding less than those in the periphery (Fig. 3B, fig. S1A, and fig. S2B). Deflation in hyperosmotic solution (0.4 M) resulted in average shrinkage of 6 ± 2% (n = 17). The relative area decrease was high for cells at the apex summit and variable on the flank (Fig. 3C, fig. S1B, and fig. S2C). The effects were independent of the type of osmolyte used. In order to distinguish between elastic and plastic deformations resulting from hypo-osmotic treatments, we performed sequential treatment with 0 M medium followed by a return to 0.2 M. Whereas the hypo-osmotic treatment resulted in a 7 ± 1% (n = 5) total area increase, after returning to 0.2 M solution, the apices were irreversibly expanded by 2 ± 1%. Therefore, the total expansion after an increase in turgor pressure is primarily an elastic response.

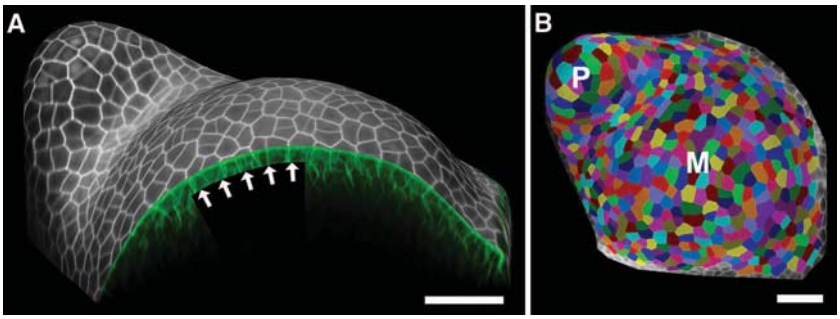

Fig. 1. Quantitative analysis of tissue deformation with MorphoGraphX (www.MorphoGraphX.org). (**A**) Cell wall signal from the epidermal layer was projected onto a curved surface mesh of the apex. (**B**) The surface is then segmented into cells and used to track local tissue deformation. P, youngest primordium; M, meristem, Scale bars, 40 μm.

[1]Institute of Plant Sciences, University of Bern, Altenbergrain 21, CH-3013 Bern, Switzerland. [2]CNRS—Laboratoire de Biogenèse Membranaire, UMR5200, 146 rue Leo Saignat, F-33076 Bordeaux, France. [3]Department of Biology, University of Fribourg, Chemin de Musée 10, CH-1700 Fribourg, Switzerland.

*These authors contributed equally to this work.
†To whom correspondence should be addressed. E-mail: richard.smith@ips.unibe.ch

Sequential hypo- to hyperosmotic treatments were then used to track inflation and deflation patterns on the surface of the same apices (Fig. 3, B and C, and fig. S2, B and C). At the apex summit, the same cells that expanded by only 4 ± 3% when treated with pure water shrank by 9 ± 3% upon plasmolysis (268 cells, three apices). In the periphery, relative areal cell expansion was significantly higher (9 ± 5%) than the shrinkage (4 ± 4%) (535 cells, three apices). Comparison between deflation and inflation for individual cells shows that cells from the central region and immediate surroundings consistently shrink more than they expand (Fig. 3, D and E; fig. S2, D and E; and fig. S3).

To test whether the observed mechanical properties of the cell wall correlate with functional zones of the shoot apex, we compared growth with osmotically induced expansion and shrinkage in apices at similar stages of development (Fig. 3 and fig. S2). The regions of slow and fast growth coincided with areas defined by elastic properties (Fig. 3, A to D and fig. S2, A to D). The results show that surface growth rates, which vary in the functional zones of the meristem, correspond to very different elastic behavior.

The pressure inside cells increases linearly with the osmotic potential; thus, a uniform increase or decrease in extracellular osmotic potential will raise or lower the pressure in all cells equally, barring osmoregulation. Changing the osmolarity by 0.2 M is equivalent to modifying the pressure by ~5 bars (0.5 MPa). If the elastic behavior was linear, we would expect the cells to expand and shrink roughly by the same amount. In the slow-growing areas, cells shrank more than they expanded (by a factor of about 2), which showed a strongly nonlinear elastic behavior (see supplementary material 4.3). This type of mechanical behavior, known as strain stiffening, is ubiquitous in biomaterials (*20*–*22*).

We explored several hypotheses to explain why fast-growing areas in the peripheral region expand more. At the organ level, mechanical stress is commonly thought to be borne mainly by the tunica, the outermost layer or layers of cells (*23*–*27*). This abstraction is supported by transmission electron microscopy (TEM) sections that show the outer cell wall is about seven times as thick as the inner walls (fig. S6). Under this assumption, a uniform material property would predict more stress in the flank because of lower

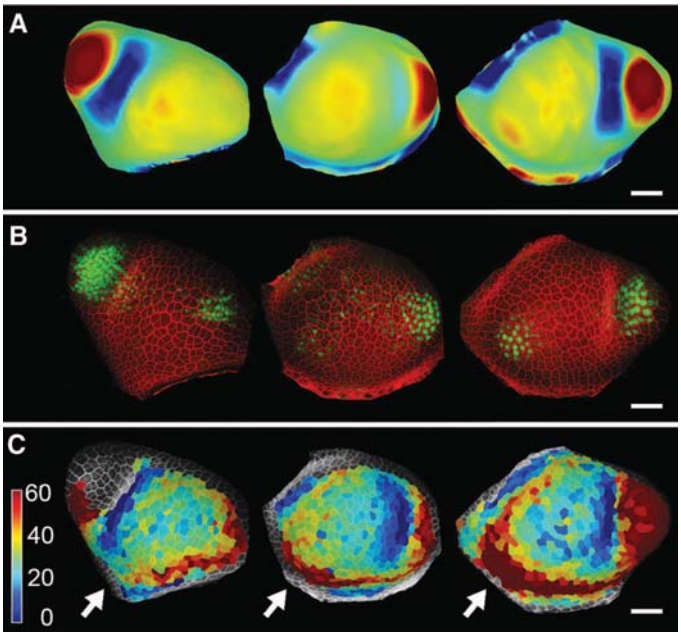

Fig. 2. Patterns of growth in tomato shoot apex. Three apices at consecutive stages of primordium development. (**A**) Gaussian curvature (red, positive; blue, negative). (**B**) Propidium iodide (PI) signal (red) combined with pDR5::VENUS expression (green) in the epidermis. (**C**) Heat maps of relative surface area increase over 11 hours of growth (color bar: percentage increase). Arrows indicate the site of next primordium initiation. Scale bars, 40 μm.

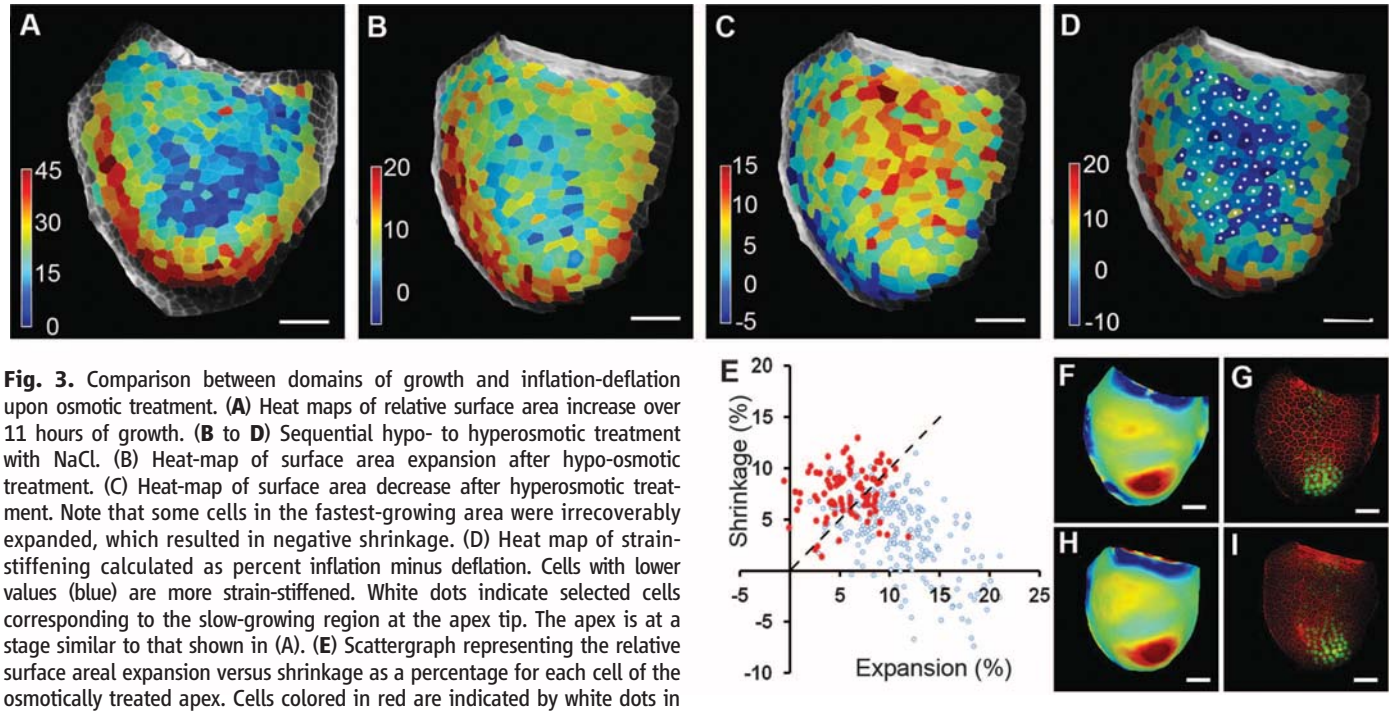

Fig. 3. Comparison between domains of growth and inflation-deflation upon osmotic treatment. (**A**) Heat maps of relative surface area increase over 11 hours of growth. (**B** to **D**) Sequential hypo- to hyperosmotic treatment with NaCl. (B) Heat-map of surface area expansion after hypo-osmotic treatment. (C) Heat-map of surface area decrease after hyperosmotic treatment. Note that some cells in the fastest-growing area were irrecoverably expanded, which resulted in negative shrinkage. (D) Heat map of strain-stiffening calculated as percent inflation minus deflation. Cells with lower values (blue) are more strain-stiffened. White dots indicate selected cells corresponding to the slow-growing region at the apex tip. The apex is at a stage similar to that shown in (A). (**E**) Scattergraph representing the relative surface areal expansion versus shrinkage as a percentage for each cell of the osmotically treated apex. Cells colored in red are indicated by white dots in (D). Dashed line is the boundary where cells shrink as much as they expand. (**F** and **H**) Gaussian curvature and (**G** and **I**) PI signal (red) combined with pDR5::VENUS expression (green) in the epidermis of the apex used for the growth assay (F and G) or for osmotic treatment (H and I). Gaussian curvature (red, positive; blue, negative) was used to compare stages of development between apices with the pDR5::VENUS signal marking the youngest primordia. Color bar (A to D): Relative surface area increase or decrease as a percentage. Scale bars, 40 μm.

curvature in this area (fig. S8). This could cause it to expand more relative to the center with increasing pressure. However, decreasing the pressure to zero should also make the peripheral region shrink more, which we did not observe. Thus, geometry alone cannot explain higher expansion in fast-growing areas of the flank.

Next, we asked if differential turgor pressure between regions could explain our results. The deflation assay shows that if there is a turgor difference, then the slow-growing tip region must have higher pressure because it deflates more (Fig. 3C, fig. S1B, and fig. S2C). However, in the sequential hypo- to hyperosmotic treatment, the periphery shrinks more (fig. S4), which indicates that pressure is lower in the central part. Therefore, turgor differences between the regions also do not explain our results.

Although complex hypotheses involving multiple mechanisms might explain the differential behaviors of the fast- and slow-growing regions, we suggest that the data can be explained by simply assuming different strain-stiffening behaviors in the two regions. The following analogy shows how our model works. Suppose two common hair elastic bands of the same length are tied together. If they are stretched from the ends, the load acting on both bands is equal (Fig. 4A). One band, which we call heavier, is harder to expand than the other for small deformations. At first, the lighter band will stretch more; however, at some point, the lighter elastic is strained beyond its linear range of deformation, and its stiffness increases greatly. If we continue to stretch the bands further, the heavier band stretches more easily than the thinner one. During the shift, there exists a crossover point where the stiffness of the two bands is actually equal.

We propose a similar scenario for the shoot apex. The slow-growing apex summit behaves as the light band does, whereas the fast-growing area of the flank behaves like the heavier one. Under normal turgor pressure, the apex is close to the crossover point, where the central region actually becomes harder to expand than the periphery. This intuition can be verified by using a mechanical simulation of the shoot apex using the finite-element method (FEM) (*19*). We represent the apex as a hemispherical shell of constant thickness and impose two regions of different elastic behavior (Fig. 4B). The material in the center is softer than that in the periphery for small deformation; however, it becomes stiffer for higher strains. The material in the periphery remains in its linear range of deformation for the strain observed (Fig. 4, D and E, and fig. S7). The osmotic experiments were then simulated by increasing and reducing the pressure inside the shell (Fig. 4C). The model was able to explain experimental results by using a simple assumption—a strain-stiffening material that is "heavier" in the periphery (Fig. 4, D and E). As in the experiments, the center shrank more than the flank when we reduced the pressure, whereas it expanded less than the flank when we increased the pressure (Fig. 4, F and G).

Our results show that there is a link between the elastic behavior of the shoot apex and its growth and organogenesis. We find that slow-growing areas of the apex tip are substantially strain-stiffened compared with fast-growing areas in the flank. Although the peripheral region is dynamic, with growth patterns and material properties that change on the basis of the developmental stage of primordia, the central region is consistently slow growing and strain-stiffened. Differential growth between regions may be a direct result of their elastic properties—that is, cells must be able to deform elastically in order to grow. Our data support this hypothesis; they suggest that expansion in slow-growing areas, including the central region, is limited by substantial strain-stiffening.

Recent work using atomic force microscopy microindentation techniques showed that cell walls in plasmolysed meristems were stiffer in the central part than at the flanks (*18*) or primordia (*15*). Although these studies largely measure compressibility of cell walls, modifying cell turgor pressure allows us to directly assess cell wall stretch under different levels of tension. We expect the response to tension and compression to be different in a reinforced soft material such as the cell wall, where in-plane tension is highly relevant for growth.

We have measured surface deformation, and the simplest interpretation of the results is based on the assumption that the surface layers of cells control growth in the shoot apex (*23*–*27*). There are, however, other possible interpretations. For example, mechanical variations in inner tissues may influence the surface deformability. Recently, the subepidermal tissue in the areas of incipient primordia has been reported to be easier to compress than the rest of the meristem (*15*). Although we did not detect a distinct behavior on these regions on the surface in our experiments, differential surface deformation seen in osmotic assays likely reflects the combined mechanical behavior of the several outermost layers of cells.

Although traditional models relate growth to stress (*28*), it appears that differential growth in the shoot apex is not because of differential stress, but rather changes in other parameters, such as plasticity or the threshold of stress required for yielding. This has implications for organogenesis and could reinforce the insensitivity of the central region to auxin (*7*, *11*, *29*) or to exogenous application of the wall-modifying enzyme PME (*14*). Differences in elastic properties may in turn be reinforced by the cell wall

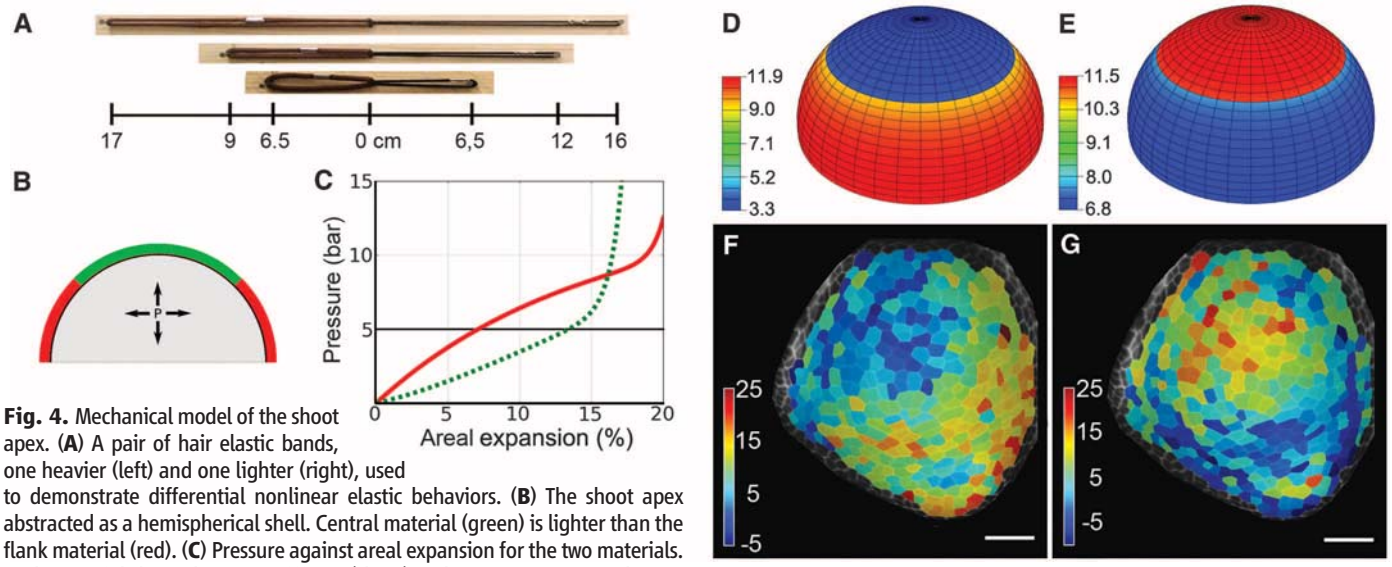

Fig. 4. Mechanical model of the shoot apex. (**A**) A pair of hair elastic bands, one heavier (left) and one lighter (right), used to demonstrate differential nonlinear elastic behaviors. (**B**) The shoot apex abstracted as a hemispherical shell. Central material (green) is lighter than the flank material (red). (**C**) Pressure against areal expansion for the two materials. Both materials have the same stiffness (slope) at the crossover point, close to 5 bar (0.5 MPa). (**D** and **E**) FEM simulation of the apex compared with osmotic treatments (**F** and **G**). Upon inflation (D), the central area expands less than the flank as in hypo-osmotic treatment (F). Upon deflation (E), the central area shrinks more as in hyperosmotic treatment (G). Color bars: Area increase or decrease as a percentage. Scale bars, 40 μm.

loosening needed for growth. Increased wall remodeling is expected to change elastic properties, which explains why fast-growing areas in the peripheral region can stay in their linear range of elasticity for larger deformations (*20*–*22*); while at the same time, they are stiffer than slow-growing regions for small strains. Our data suggest that the functional distinction between slow- and fast-growing regions in the shoot apex is not only genetically defined (*30*, *31*) but is enhanced by mechanical feedbacks. Such a mechanism would stabilize and protect the critically important stem cell niche from the numerous sources of noise inherent in the chemistry of biological systems.

References and Notes

1. T. Steeves, I. Sussex, Eds., *Patterns in Plant Development* (Cambrige Univ. Press, New York, 1988).
2. D. Kwiatkowska, J. Dumais, *J. Exp. Bot.* **54**, 1585 (2003).
3. O. Grandjean *et al.*, *Plant Cell* **16**, 74 (2004).
4. G. V. Reddy, M. G. Heisler, D. W. Ehrhardt, E. M. Meyerowitz, *Development* **131**, 4225 (2004).
5. S. Vanneste, J. Friml, *Cell* **136**, 1005 (2009).
6. M. G. Heisler *et al.*, *Curr. Biol.* **15**, 1899 (2005).
7. D. Reinhardt *et al.*, *Nature* **426**, 255 (2003).
8. D. L. Rayle, R. E. Cleland, *Plant Physiol.* **99**, 1271 (1992).
9. D. J. Cosgrove, *Nat. Rev. Mol. Cell Biol.* **6**, 850 (2005).
10. T. Vernoux, J. Kronenberger, O. Grandjean, P. Laufs, J. Traas, *Development* **127**, 5157 (2000).
11. D. Reinhardt, T. Mandel, C. Kuhlemeier, *Plant Cell* **12**, 507 (2000).
12. A. Fleming, S. McQueen-Mason, T. Mandel, C. Kuhlemeier, *Science* **276**, 1415 (1997).
13. S. Pien, J. Wyrzykowska, S. McQueen-Mason, C. Smart, A. Fleming, *Proc. Natl. Acad. Sci. U.S.A.* **98**, 11812 (2001).
14. A. Peaucelle *et al.*, *Curr. Biol.* **18**, 1943 (2008).
15. A. Peaucelle *et al.*, *Curr. Biol.* **21**, 1720 (2011).
16. M. G. Heisler *et al.*, *PLoS Biol.* **8**, e1000516 (2010).
17. O. Hamant *et al.*, *Science* **322**, 1650 (2008).
18. P. Milani *et al.*, *Plant J.* **67**, 1116 (2011).
19. Materials and methods are available as supporting material on *Science* Online
20. C. Storm, J. J. Pastore, F. C. MacKintosh, T. C. Lubensky, P. A. Janmey, *Nature* **435**, 191 (2005).
21. S. E. Whitney, M. G. Gothard, J. T. Mitchell, M. J. Gidley, *Plant Physiol.* **121**, 657 (1999).
22. R. R. Vincent, D. N. Pinder, Y. Hemar, M. A. Williams, *Phys. Rev. E Stat. Nonlin. Soft Matter Phys.* **76**, 031909 (2007).
23. J. Dumais, C. R. Steele, *J. Plant Growth Regul.* **19**, 7 (2000).
24. J. M. Selker, G. L. Steucek, P. B. Green, *Dev. Biol.* **153**, 29 (1992).
25. R. Vandiver, A. Goriely, *Philos. Transact. A Math. Phys. Eng. Sci.* **367**, 3607 (2009).
26. V. Mirabet, P. Das, A. Boudaoud, O. Hamant, *Annu. Rev. Plant Biol.* **62**, 365 (2011).
27. U. Kutschera, K. J. Niklas, *J. Plant Physiol.* **164**, 1395 (2007).
28. J. A. Lockhart, *J. Theor. Biol.* **8**, 264 (1965).
29. T. Vernoux *et al.*, *Mol. Syst. Biol.* **7**, 508 (2011).
30. R. Sablowski, *Curr. Opin. Plant Biol.* **10**, 639 (2007).
31. R. K. Yadav, T. Girke, S. Pasala, M. Xie, G. V. Reddy, *Proc. Natl. Acad. Sci. U.S.A.* **106**, 4941 (2009).

Acknowledgments: We thank J. Dumais, A. Fleming, S. Robinson, D. Kwiatkowska, and P. Wojtaszek for reading the manuscript. This work was supported by the Swiss National Science Foundation, SystemsX.ch, and the European Union New and Emerging Science and Technology grant MechPlant. N.N. received European Molecular Biology Organization Long-Term and Roche Research Foundation fellowships.

Supporting Online Material

www.sciencemag.org/cgi/content/full/335/6072/1096/DC1
Materials and Methods
Figs. S1 to S8
References (*32*–*41*)

24 August 2011; accepted 30 January 2012
10.1126/science.1213100

Global Network Reorganization During Dynamic Adaptations of *Bacillus subtilis* Metabolism

Joerg Martin Buescher,[1]* Wolfram Liebermeister,[2]* Matthieu Jules,[3]* Markus Uhr,[4]* Jan Muntel,[5]* Eric Botella,[7] Bernd Hessling,[5] Roelco Jacobus Kleijn,[1] Ludovic Le Chat,[3] François Lecointe,[3] Ulrike Mäder,[5] Pierre Nicolas,[6] Sjouke Piersma,[8] Frank Rügheimer,[15] Dörte Becher,[5] Philippe Bessieres,[6] Elena Bidnenko,[3] Emma L. Denham,[8] Etienne Dervyn,[3] Kevin M. Devine,[7] Geoff Doherty,[9] Samuel Drulhe,[15] Liza Felicori,[10] Mark J. Fogg,[11] Anne Goelzer,[6] Annette Hansen,[7] Colin R. Harwood,[12] Michael Hecker,[5] Sebastian Hubner,[7] Claus Hultschig,[13] Hanne Jarmer,[14] Edda Klipp,[2] Aurélie Leduc,[6] Peter Lewis,[9] Frank Molina,[10] Philippe Noirot,[3] Sabine Peres,[10] Nathalie Pigeonneau,[3] Susanne Pohl,[12] Simon Rasmussen,[14] Bernd Rinn,[13] Marc Schaffer,[5] Julian Schnidder,[1] Benno Schwikowski,[15] Jan Maarten Van Dijl,[8] Patrick Veiga,[6] Sean Walsh,[13] Anthony J. Wilkinson,[11] Jörg Stelling,[4]† Stéphane Aymerich,[3]† Uwe Sauer[1]†

Adaptation of cells to environmental changes requires dynamic interactions between metabolic and regulatory networks, but studies typically address only one or a few layers of regulation. For nutritional shifts between two preferred carbon sources of *Bacillus subtilis*, we combined statistical and model-based data analyses of dynamic transcript, protein, and metabolite abundances and promoter activities. Adaptation to malate was rapid and primarily controlled posttranscriptionally compared with the slow, mainly transcriptionally controlled adaptation to glucose that entailed nearly half of the known transcription regulation network. Interactions across multiple levels of regulation were involved in adaptive changes that could also be achieved by controlling single genes. Our analysis suggests that global trade-offs and evolutionary constraints provide incentives to favor complex control programs.

A major challenge in biology is to understand the organization and interactions of the various functional and regulatory networks in cells. The underlying complexity arises from the intertwined nonlinear and dynamic interactions among a large number of cellular components. To better understand these interacting molecular networks, the acquisition of appropriate, preferably time-resolved quantitative data is a prerequisite (*1*–*3*). Because the acquisition of such data is technically demanding, few studies have reported transcript, protein, and metabolite abundances, and most studies have been restricted to steady-state conditions (*4*–*8*). Consequently, only subsets of components have been monitored dynamically for very short- (*9*, *10*) or long-term responses (*11*, *12*) to environmental perturbations. These studies typically revealed coordinated abundance changes (*11*, *12*), major transcriptional reconfigurations in response to environmental change (*9*, *11*), and an unanticipated complexity of unicellular organisms (*7*). Data interpretation, however, has generally been restricted to multivariate statistical analysis methods that indicate general but not mechanistic relationships between different molecular entities. Focusing on single data types with sophisticated computational analysis has been informative (*3*) but increases the risk of missing the functionally relevant multilevel control mechanisms (*2*), limiting the description of the underlying molecular mechanisms and, hence, the depth of biological insight.

[1]Institute of Molecular Systems Biology, ETH Zurich, 8093 Zurich, Switzerland. [2]Theoretical Biophysics, Humboldt University Berlin, 10115 Berlin, Germany. [3]INRA, UMR1319 Micalis, Jouy-en-Josas F78350, France. [4]Department of Biosystems Science and Engineering, ETH Zurich, 4058 Basel, Switzerland. [5]Institute for Microbiology, Ernst-Moritz-Arndt-University Greifswald, 17487 Greifswald, Germany. [6]INRA, Mathématique Informatique et Génome UR1077, 78350 Jouy-en-Josas, France. [7]Smurfit Institute of Genetics, Trinity College Dublin, Dublin 2, Ireland. [8]Department of Medical Microbiology, University of Groningen and University Medical Center Groningen, 9700 RB Groningen, Netherlands. [9]School of Environmental and Life Sciences, University of Newcastle, Callaghan, NSW 2308, Australia. [10]Sysdiag CNRS Bio-Rad UMR 3145, Cap Delta/Parc Euromédecine, 34184 Montpellier Cedex 4, France. [11]York Structural Biology Laboratory, Department of Chemistry, University of York, York YO10 5YW, UK. [12]Institute, of Cell and Molecular Biosciences, Centre for Bacterial Cell Biology, University of Newcastle upon Tyne, Newcastle upon Tyne, NE2 4AX, UK. [13]Center for Information Sciences and Databases, Department of Biosystems Science and Engineering, ETH Zurich, 4058 Basel, Switzerland. [14]Center for Biological Sequence Analysis, Department of Systems Biology, Technical University of Denmark, 2800 Kgs. Lyngby, Denmark. [15]Institut Pasteur, Systems Biology Lab, Department of Genomes and Genetics, and CNRS URA 2171, F-75015 Paris, France.

*These authors contributed equally to this work.
†To whom correspondence should be addressed. E-mail: joerg.stelling@bsse.ethz.ch (J.S.); stephane.aymerich@grignon.inra.fr (S.A.); sauer@ethz.ch (U.S.)

To elucidate the dynamic interplay between metabolic and regulatory networks systematically, we investigated dynamic shifts in availability of the preferred carbon sources, glucose and malate, of the bacterium *Bacillus subtilis* (*13*). Because these nutrients repress the use of other substrates but are themselves used together, they represent a tractable model for analyzing dynamic decision-making by cells when faced with compounds of similar nutritional value. We induced dynamic shifts by adding glucose or malate to cultures of *B. subtilis* growing exponentially on the other substrate. To elucidate the cellular adaptation mechanisms, we determined transcript, protein, and absolute metabolite abundances, as well as promoter activities (Fig. 1 and table S1) (*14*), providing dynamic data with up to 24 time points for two shift experiments that cover short-term metabolic to longer-term protein-level adaptation (*15*).

To enable data integration, we developed problem-driven, yet generic solutions in three areas (table S1). To generate consistent data, we minimized biological variability (Fig. 1) by withdrawing samples from the same bioreactor culture in triplicate experiments (fig. S1) and, in a few cases, from standardized small-scale cultivations (fig. S2). We used naming and formatting conventions with unique identifiers for all considered constituents to permit the efficient exchange of data and knowledge. Furthermore, to maximize reliability and coverage for subsequent data analysis and modeling, we combined overlapping dynamic data acquired from different analytical platforms and on different time scales (Fig. 1). Data from the different transcript-array platforms did not require further consolidation (figs. S3 and S4), but we generated consensus proteomics data by calculating confidence-weighted averages of protein abundances obtained from two-dimensional gels and liquid chromatography–mass spectrometry (SOM 1). Replicate time series of transcript and protein data were then smoothed and interpolated by Bayesian multicurve regression analysis (SOM 1). Because metabolite data showed changes on various time scales, we developed a special algorithm that aligns time courses on the basis of Kalman smoothing (Fig. 2A and SOM 1) (*16*).

We exploited the profusion of data (table S1) to extend the genome annotation of *B. subtilis* by statistical data analysis and integration with prior knowledge (table S2). Analysis of mRNA

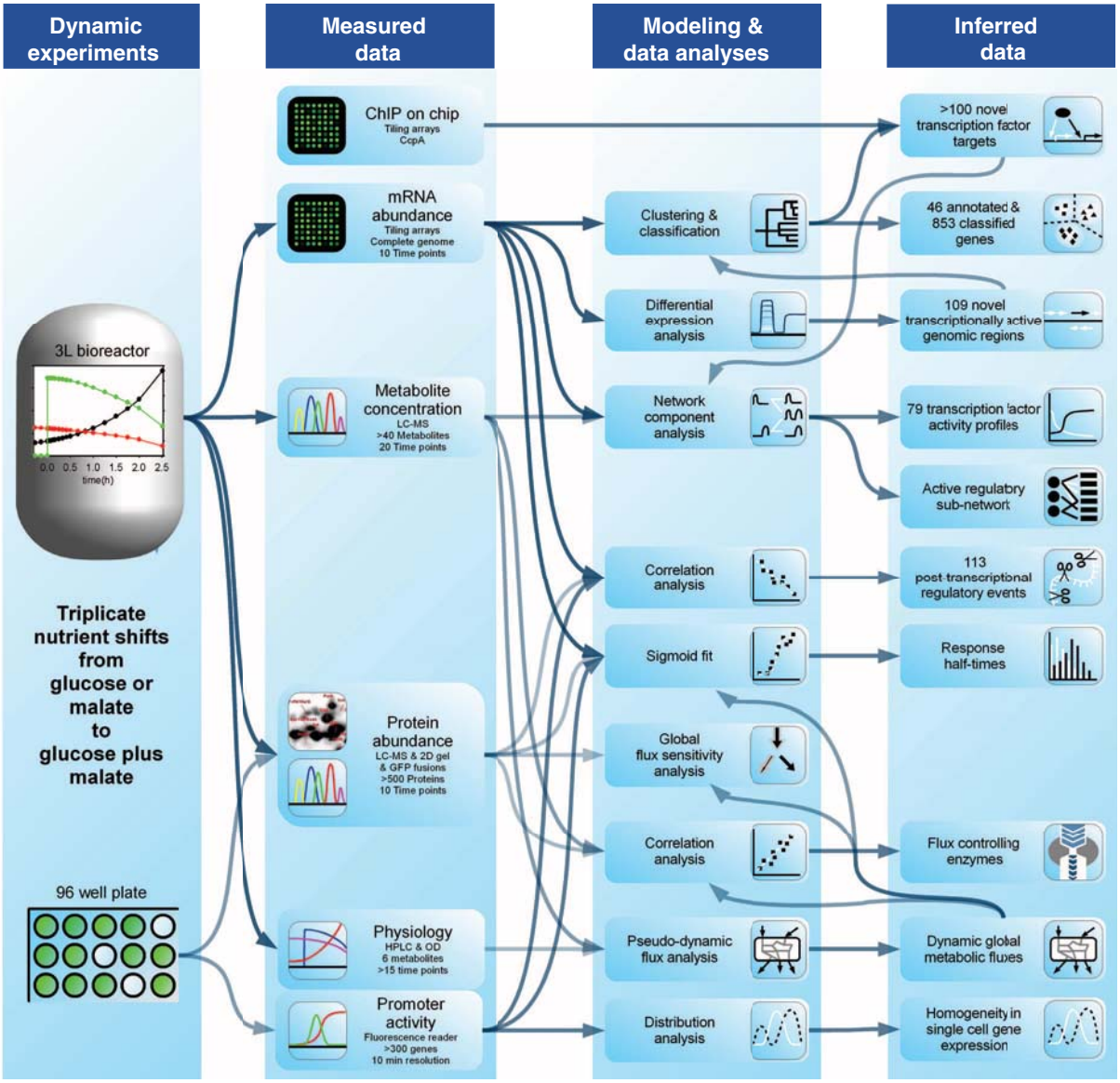

Fig. 1. Overview of our experimental design, computational analysis, and information flow. The dynamic shift experiments yielded measured data from which nonmeasurable quantities were inferred by statistical and model-based analysis. Arrows show the flow of information, including the use of inferred data as parameters for subsequent modeling steps. ChIP, chromatin immunoprecipitation; LC-MS, liquid chromatography–mass spectrometry; GFP, green fluorescent protein; HPLC, high-performance liquid chromatography; OD, optical density.

abundances identified 4393 transcriptionally active genomic regions, 109 of which were not previously described, including 21 putative protein-coding sequences and 23 antisense RNAs (table S3). Additionally, 2422 genomic regions were differentially transcribed after the nutrient shifts (table S1). Clustering of mRNA profiles and functional classification of differentially transcribed genes enabled detailed functional annotation of 46 genes (table S4) and probable function assignment of 853 previously not annotated genes (table S1). For the metabolically important transcription factors CcpA, CcpC, CcpN, and CggR (*17*–*19*), we identified DNA binding sites by chromatin immunoprecipitation–on-chip analysis in malate plus glucose (table S1). We found 184 CcpA binding sites, most of which were located near to promoters of genes differentially expressed immediately after glucose addition (fig. S5). By filtering this group for high-scoring, previously undetected CcpA sites, we generated an improved regulatory network topology (SOM 2) for subsequent analysis of regulatory events.

Metabolomics data revealed instantaneous malate uptake into cells grown on glucose but substantially delayed uptake of glucose into cells grown on malate (Fig. 2, B and C). Sensitivity analysis of steady-state fluxes in the stoichiometric network model in combination with proteomic data predicted transcriptional regulation to be more important for the dynamics induced by glucose than by malate (Fig. 2D). Network component analysis (*20*) quantified the strengths of all 2900 transcription factor interactions with target genes, and 1488 of the interactions were implicated in at least one shift (689 for malate addition; 1244 for glucose addition) (SOM 2). Furthermore, we identified 110 posttranscriptional regulation events in protein synthesis (77 and 23 were specific to malate and glucose addition, respectively) through a dynamic model that correlates time profiles of promoter activity, mRNA abundance, and protein abundance for 300 genes for which all three data types were available (tables S5 to S7). Overall, our integrated analysis suggests that apparently similar adaptation processes are mediated by fundamentally different control mechanisms, namely a predominantly posttranscriptional regulation after malate addition and a greater reliance on transcriptional regulation after glucose addition.

Next, we inferred the dynamic activity profiles of 154 transcription factors by network-component analysis (*20*) from the transcript abundances of

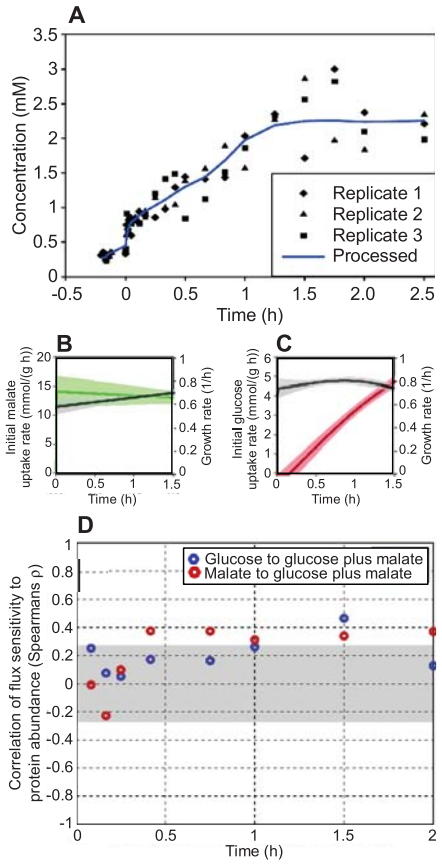

Fig. 2. (**A**) Processing of time-series data from parallel experiments. The example shown here is fructose 1,6-bisphosphate during the malate–to–glucose-plus-malate shift. Measurements from three independent cultures (black data points) yield an averaged and smooth time course (blue line). (**B** and **C**) Initial dynamic uptake rates of malate (green) and glucose (red) after addition to wild-type *B. subtilis* growing on the respective other substrate were obtained by fitting of splines. Black lines and shadings represent the specific growth rate and 95% confidence intervals, respectively (SOM 3). (**D**) The global importance of transcriptional regulation after glucose addition is confirmed by an increasing correlation (red) between flux sensitivity (measuring the impact of a change in environmental conditions on a metabolic flux) and protein abundance over time. This increase does not occur after malate addition (blue). White areas denote statistically significant correlation values with respect to an approximate 95% confidence interval; gray shaded areas denote the absence of statistically significant correlation.

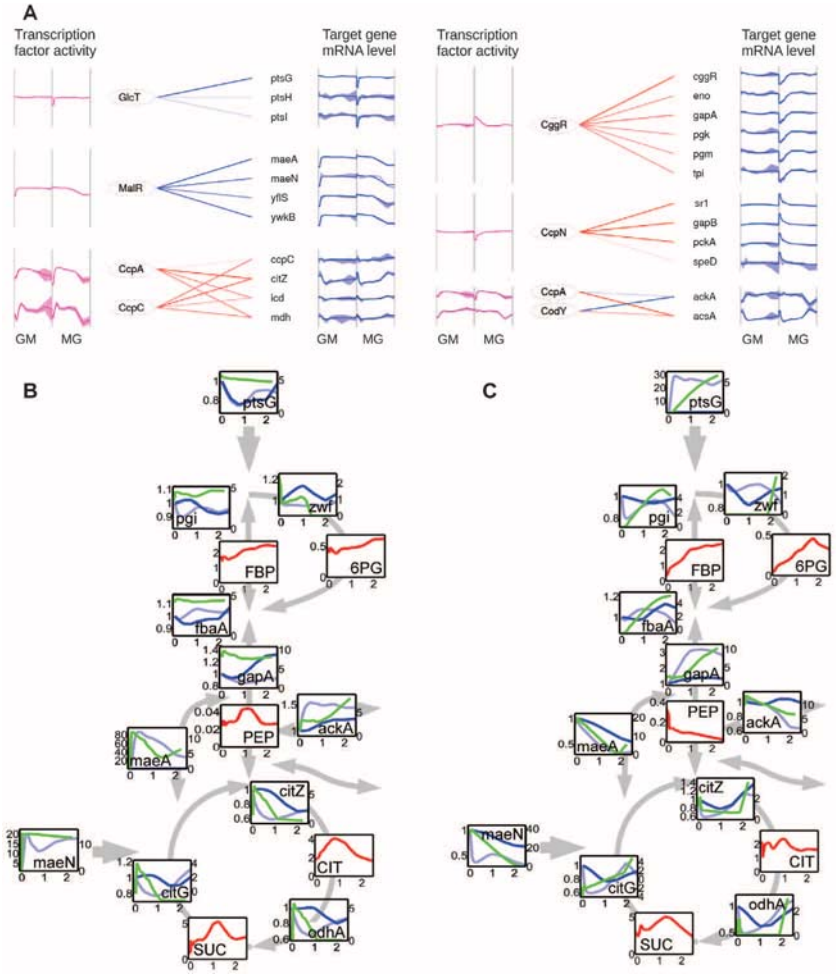

Fig. 3. (**A**) Activities of the main transcriptional regulators controlling central metabolism during the shifts of glucose (GM) or malate (MG) to glucose plus malate. Blue curves represent $\log_2$ expression profiles of target genes; purple curves denote the inferred transcription factor activities. Straight lines in the middle sections indicate the relative contribution (proportional to color intensity) of different transcription factors to target gene expression changes (blue, activation; red, repression). (**B** and **C**) Averaged time profiles of transcripts (light blue), proteins (dark blue), metabolic fluxes (green), and metabolites (red) during the dynamic shift experiments of glucose (B) or malate (C) to malate plus glucose.

their 1754 known target genes (Fig. 3A and SOM 2). One hundred twenty-seven transcription factors changed their activity profile significantly in at least one shift (61 for malate addition and 91 for glucose addition). A rapid change of activity (<5 min), most prominent for the transporter regulators MalR (malate) and GlcT (glucose), and the deviations between the inferred transcription factor activities and the measured transcription factor mRNA abundance provided evidence for posttranslational regulation (SOM 2). Network component analysis predicted that the activity of 51 transcription factors was modulated post-transcriptionally, and 39 of these (for example, NadR, KipR, CcpN, FruR) are regulated by yet unknown effectors. Overall, both nutrient shifts induced substantial, global network reconfiguration at all levels of regulation.

To identify the relevant primary changes in central metabolism, where essentially all genes were differentially expressed during one or both shifts, we correlated time courses of metabolic fluxes with those of the abundances of the corresponding enzymes. We estimated dynamic extracellular rates by interpolation (SOM 3) and network-wide pseudodynamic metabolic fluxes with a stoichiometric network model and the intracellular metabolite concentrations (Fig. 3, B and C, and SOM 4). Positive correlations between fluxes and enzyme abundances indicated genetic rather than metabolic regulation of the reaction rates (*21*). Upon the addition of malate, the abundances of only the nicotinamide adenine dinucleotide phosphate–dependent malic enzyme (YtsJ) and two acetate production enzymes (Pta and AckA) correlated with their respective reaction rates ($R > 0.8$) and thus putatively control flux (Fig. 4A). After the addition of glucose, enzymes for 11 central reactions putatively controlled flux, and in six cases increasing enzyme abundance potentially overcame the bottleneck in glucose uptake. The corresponding genes are organized in two operons: *ptsGHI* for glucose transport and phosphorylation and *cggR-gapA-pgk-tpiA-pgm-eno* for lower glycolysis. This focused analysis of multiple "omics" data sets suggested the *pts* and *cggR* operons as primary control targets for adaptation, where the half-maximal responses of the *pts* and *cggR* operon-encoded proteins within 30 to 60 min of glucose addition could account for the ~60-min delay in glucose uptake (Fig. 2, B and C). We evaluated the relative contributions of both operons to the delay with a *cggR* deletion mutant and a mutant with constitutive *ptsG* expression (Fig. 4B and SOM 5). When grown on malate, both mutants used glucose immediately without the delay of the wild-type strain. As the *cggR* or *ptsG* expression alone is sufficient to facilitate immediate glucose uptake, it is not obvious why *B. subtilis* does not express these genes constitutively.

B. subtilis needs to optimize its use of two qualitatively distinct substrates: Glucose results in high growth yields at low metabolic rates, whereas malate results in low growth yields at high metabolic rates (*13*). Similar trade-offs exist between respiratory and fermentative strategies in adenosine triphosphate generation, both of which can confer condition-specific evolutionary advantages (*22*). To investigate optimal control strategies for substrate usage in *Bacillus*, we developed a simplified dynamic model that describes the substrate and biomass dynamics of the shift experiments quantitatively (SOM 6). The maintenance cost for enzyme expression (ρ) is a key parameter in the model; the estimated value of $\rho_0 \approx 0.06$ implies that full expression of a metabolic (substrate) system would reduce the maximal specific growth rate by ≈5%. In silico

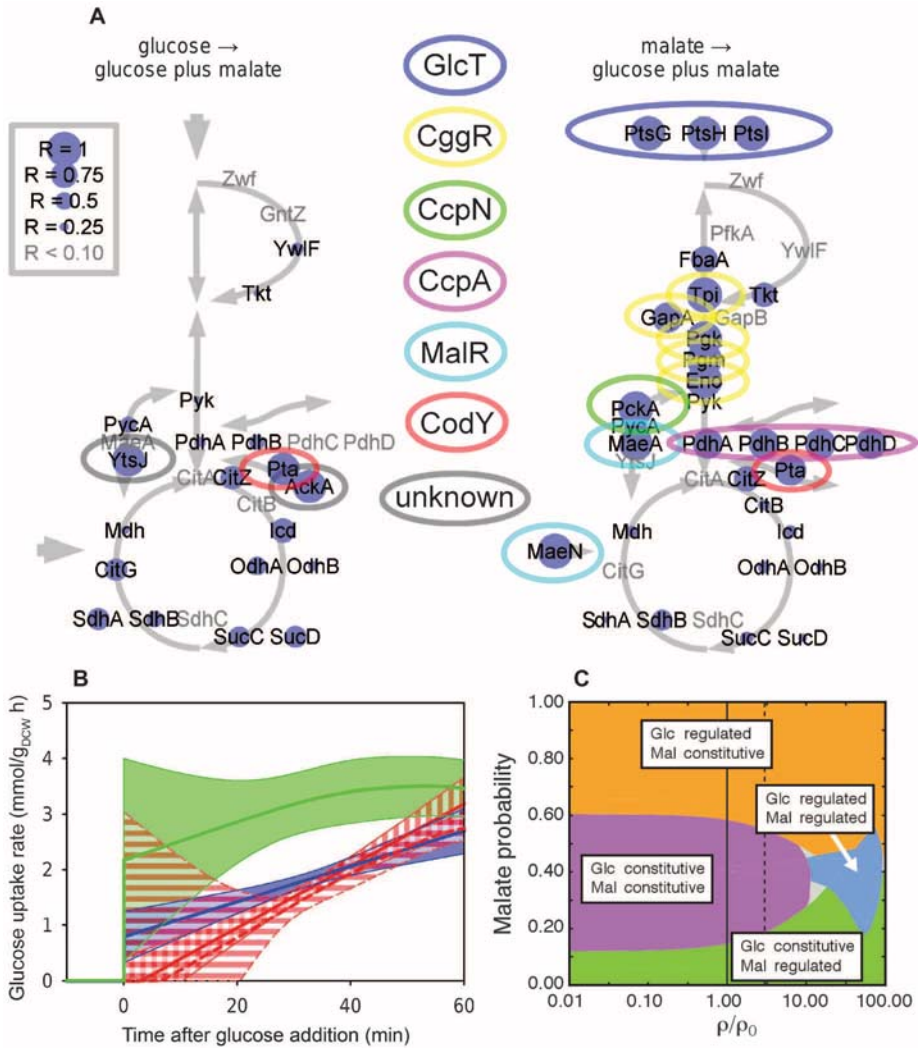

Fig. 4. (**A**) Regulatory mechanisms relevant for control of metabolic fluxes during the two shifts. Key controlling enzymes are indicated by a positive correlation between reaction rate and enzyme abundance after addition of malate (left) or glucose (right). Reactions were considered only if both enzyme abundance and flux changed by more than one standard deviation and if the correlation coefficient was positive. The size of the purple circles is proportional to the correlation coefficient (see inset). Transcription factors (middle) were identified by network component analysis to be responsible for changes in enzyme expression, as indicated by color coding (gray denotes unknown factors). (**B**) Dynamics of glucose uptake rate upon addition of glucose to a culture growing exponentially on malate in mutants with constitutive *ptsG* expression (green), *cggR* deletion (blue), and the respective parent strains (solid red, vertical shading and dashed red, horizontal shading). Shaded areas denote 95% pointwise confidence intervals. g_{DCW}, grams of dry cell weight. (**C**) Predicted growth effects of different control strategies using a simplified dynamic model. In silico competition experiments were carried out between two strains that differ in how they control malate and glucose uptake; both systems can be expressed constitutively or only upon substrate availability (SOM 6). Cocultures in a chemostat setting were pulsed every 3 hours with substrate (similar results were obtained with pulse frequencies of 1 and 9 hours), where the probability of selecting malate versus glucose as substrate was varied. The cost of metabolic system maintenance (ρ) normalized by the estimated cost for *B. subtilis* (ρ_0; the solid line indicates the estimated value of ρ; the dashed line to the right is the upper bound of the 95% confidence interval) constituted a free simulation parameter. Control strategies with higher growth rates were considered advantageous, and the best control strategies are identified by color coding.

competition of strains that either constitutively express the metabolic systems or induce their expression only upon substrate availability allowed us to quantify the dynamic control effects. In simulations of a dynamically changing environment, we varied the substrate probabilities and the maintenance cost ρ because of the uncertainties in the estimated ρ_0 (Fig. 4C). Surprisingly, there almost always existed a unique, evolutionarily dominating control strategy. The winning strategy depended on quantitative parameters. Hence, active regulation or constitutive subsystem expression are not advantageous per se. Even with the uncertainties in ρ_0, the experimentally observed strategy of constitutive malate usage capacity (Fig. 2B) but induced (and delayed) glucose-specific metabolism confers an evolutionary advantage if *B. subtilis* predominantly encounters malate (Fig. 4C). This is biologically plausible given the organism's habitat in the vicinity of plant root systems that often secrete carboxylic acids such as malate (*13*, *23*).

Our systems approach helps reveal how previously known regulatory mechanisms are combined to effect nutritional transitions. Despite more than half of the *B. subtilis* gene complement being involved in the adaptive response to glucose, our methodology could discern the key regulatory events. The overall control strategy of *B. subtilis* can be rationalized in terms of its evolutionary advantages; however, these advantages, and therefore the overall control design, depend on quantitative system characteristics—regulation is not beneficial per se. The dynamic data presented here may be used for further computational analyses such as multivariate statistics and large-scale structural or kinetic network models (*24*). We hope that our publicly available tools for mathematical analyses and modeling will facilitate future large-scale and dynamic systems biology studies in *B. subtilis* and other species.

References and Notes

1. U. Sauer, M. Heinemann, N. Zamboni, *Science* **316**, 550 (2007).
2. M. Ralser *et al.*, *Nat. Biotechnol.* **27**, 604 (2009).
3. G. Chechik *et al.*, *Nat. Biotechnol.* **26**, 1251 (2008).
4. N. Ishii *et al.*, *Science* **316**, 593 (2007).
5. E. Yus *et al.*, *Science* **326**, 1263 (2009).
6. M. Güell *et al.*, *Science* **326**, 1268 (2009).
7. J. F. Moxley *et al.*, *Proc. Natl. Acad. Sci. U.S.A.* **106**, 6477 (2009).
8. A. B. Canelas *et al.*, *Nat. Comm.* **1**, 145 (2010).
9. M. T. A. P. Kresnowati *et al.*, *Mol. Syst. Biol.* **2**, 49 (2006).
10. M. J. Brauer *et al.*, *Proc. Natl. Acad. Sci. U.S.A.* **103**, 19302 (2006).
11. S. Jozefczuk *et al.*, *Mol. Syst. Biol.* **6**, 364 (2010).
12. P. H. Bradley, M. J. Brauer, J. D. Rabinowitz, O. G. Troyanskaya, *PLOS Comput. Biol.* **5**, e1000270 (2009).
13. R. J. Kleijn *et al.*, *J. Biol. Chem.* **285**, 1587 (2010).
14. E. Botella *et al.*, *Microbiology* **156**, 1600 (2010).
15. Materials and methods are available as supporting material on *Science* Online.
16. S. Haykin, *Kalman Filtering and Neural Networks* (Wiley-Interscience, New York, 2001).
17. A. L. Sonenshein, *Nat. Rev. Microbiol.* **5**, 917 (2007).
18. T. Doan, S. Aymerich, *Mol. Microbiol.* **47**, 1709 (2003).
19. A. Goelzer *et al.*, *BMC Syst. Biol.* **2**, 20 (2008).
20. J. C. Liao *et al.*, *Proc. Natl. Acad. Sci. U.S.A.* **100**, 15522 (2003).
21. S. Rossell *et al.*, *Proc. Natl. Acad. Sci. U.S.A.* **103**, 2166 (2006).
22. T. Pfeiffer, S. Schuster, S. Bonhoeffer, *Science* **292**, 504 (2001).
23. H. P. Bais, T. L. Weir, L. G. Perry, S. Gilroy, J. M. Vivanco, *Annu. Rev. Plant Biol.* **57**, 233 (2006).
24. M. Heinemann, U. Sauer, *Curr. Opin. Microbiol.* **13**, 337 (2010).

Acknowledgments: This work was funded through the European Commission 7th Framework project BaSysBio (LSHG-CT-2006-037469), coordinated by P. Noirot, the Department of Education, Science and Training (CG110055), and the National Health and Medical Research Council (455646). Data, algorithms, and mathematical models have been deposited in a publicly accessible relational database (www.basysbio.eu/nutrientshift/ and table S1).

Supporting Online Material

www.sciencemag.org/cgi/content/full/335/6072/1099/DC1
Materials and Methods
SOM Text (SOM 1 to 6)
Figs. S1 to S20
Tables S1 to S8
References (*25*–*28*)
Database S1

12 April 2011; accepted 11 January 2012
10.1126/science.1206871

Condition-Dependent Transcriptome Reveals High-Level Regulatory Architecture in *Bacillus subtilis*

Pierre Nicolas,[1]* Ulrike Mäder,[2,3]* Etienne Dervyn,[4]* Tatiana Rochat,[4] Aurélie Leduc,[1] Nathalie Pigeonneau,[4] Elena Bidnenko,[4] Elodie Marchadier,[4] Mark Hoebeke,[1] Stéphane Aymerich,[4] Dörte Becher,[2] Paola Bisicchia,[5] Eric Botella,[5] Olivier Delumeau,[4] Geoff Doherty,[6] Emma L. Denham,[7] Mark J. Fogg,[8] Vincent Fromion,[1] Anne Goelzer,[1] Annette Hansen,[5] Elisabeth Härtig,[9] Colin R. Harwood,[10] Georg Homuth,[3] Hanne Jarmer,[11] Matthieu Jules,[4] Edda Klipp,[12] Ludovic Le Chat,[4] François Lecointe,[4] Peter Lewis,[6] Wolfram Liebermeister,[12] Anika March,[9] Ruben A. T. Mars,[7] Priyanka Nannapaneni,[3] David Noone,[5] Susanne Pohl,[10] Bernd Rinn,[13] Frank Rügheimer,[14] Praveen K. Sappa,[3] Franck Samson,[1] Marc Schaffer,[2] Benno Schwikowski,[14] Leif Steil,[3] Jörg Stülke,[15] Thomas Wiegert,[16] Kevin M. Devine,[5] Anthony J. Wilkinson,[8] Jan Maarten van Dijl,[7] Michael Hecker,[2] Uwe Völker,[3] Philippe Bessières,[1] Philippe Noirot[4]†

Bacteria adapt to environmental stimuli by adjusting their transcriptomes in a complex manner, the full potential of which has yet to be established for any individual bacterial species. Here, we report the transcriptomes of *Bacillus subtilis* exposed to a wide range of environmental and nutritional conditions that the organism might encounter in nature. We comprehensively mapped transcription units (TUs) and grouped 2935 promoters into regulons controlled by various RNA polymerase sigma factors, accounting for ~66% of the observed variance in transcriptional activity. This global classification of promoters and detailed description of TUs revealed that a large proportion of the detected antisense RNAs arose from potentially spurious transcription initiation by alternative sigma factors and from imperfect control of transcription termination.

Bacterial transcriptomes are surprisingly complex (*1*–*5*) and include diverse and abundant small RNAs and antisense RNAs (asRNAs). Because only a small number of environmental conditions have been investigated, the full extent of transcriptome complexity remains to be established for a single bacterial species. This prompted us to undertake a systematic and quantitative exploration of transcriptome changes in *Bacillus subtilis*, whose natural habitat, the soil, is subject to severe environmental fluctuations (*6*). *B. subtilis* is also a laboratory model for Gram-positive bacteria and is grown in industrial-scale fermentors for the production of enzymes and vitamins. We selected 104 conditions covering

[1]INRA, UR1077, Mathématique Informatique et Génome, F-78350 Jouy-en-Josas, France. [2]Institute for Microbiology, Ernst-Moritz-Arndt University Greifswald, D-17489 Greifswald, Germany. [3]Interfaculty Institute for Genetics and Functional Genomics, Ernst-Moritz-Arndt-University Greifswald, D-17489 Greifswald, Germany. [4]INRA, UMR1319 Micalis, F-78350 Jouy-en-Josas, France. [5]Smurfit Institute of Genetics, Trinity College Dublin, Dublin 2, Ireland. [6]School of Environmental and Life Sciences, University of Newcastle, Callaghan, NSW 2308, Australia. [7]Department of Medical Microbiology, University of Groningen and University Medical Center Groningen, 9700 RB Groningen, Netherlands. [8]York Structural Biology Laboratory, Department of Chemistry, University of York, York YO10 5YW, UK. [9]Institute of Microbiology, Technical University of Braunschweig, D-38106 Braunschweig, Germany. [10]Centre for Bacterial Cell Biology, Institute, of Cell and Molecular Biosciences, Newcastle University of Newcastle, Newcastle upon Tyne, NE2 4AX, UK. [11]Center for Biological Sequence Analysis, Department of Systems Biology, Technical University of Denmark, 2800 Kgs. Lyngby, Denmark. [12]Theoretical Biophysics, Humboldt University Berlin, 10115 Berlin, Germany. [13]Center for Information Sciences and Databases, Department of Biosystems Science and Engineering, ETH Zurich, 4058 Basel, Switzerland. [14]Systems Biology Lab and CNRS URA 2171, Institut Pasteur, 75724 Paris cedex 15, France. [15]Department of General Microbiology, Georg-August-University Göttingen, D-37077 Göttingen, Germany. [16]FN Biotechnologie, Hochschule Zittau/Görlitz, D-02763 Zittau, Germany.

*These authors contributed equally to this work.
†To whom correspondence should be addressed. E-mail: philippe.noirot@jouy.inra.fr

the use of various nutrients, aerobic and anaerobic growth, the development of motility, biofilm formation, adaptation to diverse stresses, high–cell-density fermentation, and hallmark adaptations of *B. subtilis*: the development of competence for genetic transformation, cell differentiation to form resistant spores, and germination from such spores.

In our labs, we grew a prototrophic strain under the selected conditions and hybridized 269 RNA samples to tiled microarrays with a resolution of 22 bases [supporting online material (SOM) 1 and table S1] (*7*). We then estimated strand-specific RNA signals from the raw data (Fig. 1A) (*8*) and computed an aggregated expression index for all transcribed regions (SOM 2 and table S2). The expression threshold was stringently set to reduce the number of potentially false short RNA features detected. Of the previously annotated coding sequences (CDSs), only 186 (4.4%) were not expressed under any condition. Most of these CDSs were of unknown function and predicted to originate from horizontal transfer (SOM 3 and table S3). The 30% of the CDSs most highly expressed under each condition were defined as "highly expressed" (SOM 3). Eighty-five percent of all CDSs were highly expressed in one or more conditions (fig. S3A), but only ~3% (144) of all CDSs were highly expressed under all conditions, indicating that most *B. subtilis* genes are differentially expressed. Genes in the latter group encode proteins with essential functions (*9*) and enzymes involved in glycolysis, iron sulfur metabolism, and detoxification pathways (table S3).

For each of the 269 profiles, we used the repertoire of high-confidence 5′ and 3′ mRNA ends to delineate the transcribed regions, which we derived directly from the positions of abrupt increases and decreases in RNA abundance, hereafter called up- and downshifts, respectively (Fig. 1A and SOM 2). More than 85% of previously known transcriptional start sites (*10*, *11*) mapped within ~12 base pairs (bp) of an upshift (SOM 4), indicating that most mRNAs have unprocessed 5′ ends. Therefore, most of the 3242 detected upshifts appear to correspond to genuine promoters, increasing ~threefold the number of promoters mapped in *B. subtilis*. Downstream of these promoters, 3000 transcription units (TUs) were defined and then decomposed into previously annotated genes and newly identified RNAs (SOM 2 and tables S4 and S5). This analysis revealed that ~46% of all annotated CDSs can be transcribed from more than one promoter. After manual validation, we classified 1583 previously unannotated RNAs (S1 to S1583) according to their structural relationships with neighboring annotated CDSs (Table 1). These RNAs considerably expand the registry of potential regulatory RNAs (SOM 5 and table S6) and increase the total number of potential genes in *B. subtilis* by 11% (Table 1). The condition-dependent experimental annotation can be queried at www.basysbio.eu/bsubtranscriptome/seb.

The 3′ ends of most mRNAs were associated with predicted intrinsic terminators (that is, an RNA hairpin followed by a U-track) at which RNA polymerase (RNAP) dissociates without the need for auxiliary proteins (SOM 6 and table S7). A subgroup of 174 TUs generated asRNAs due to the lack of a termination site and read-through transcription (categories Indep-NT, 3′NT, and 3′PT in Table 1). These mRNAs could extend up to 3.4 kb beyond the 3′ boundaries of their cognate CDS with a gradual decrease in signal intensity (Fig. 1B). Overall, 13% of *B. subtilis* CDSs are overlapped by asRNAs (table S11) that can potentially act to regulate their cognate sense mRNAs at the transcriptional, RNA stability, or translational levels (*12*). In a mutant strain lacking the termination factor Rho, which is not required for growth of *B. subtilis* in a rich medium (*13*), the mRNA extensions reached up to 12 kb (average ~2.8 kb) (Fig. 1C and table S9). Without Rho, additional asRNAs were formed by extension of a subset of TUs, many of which have only partially efficient intrinsic terminators

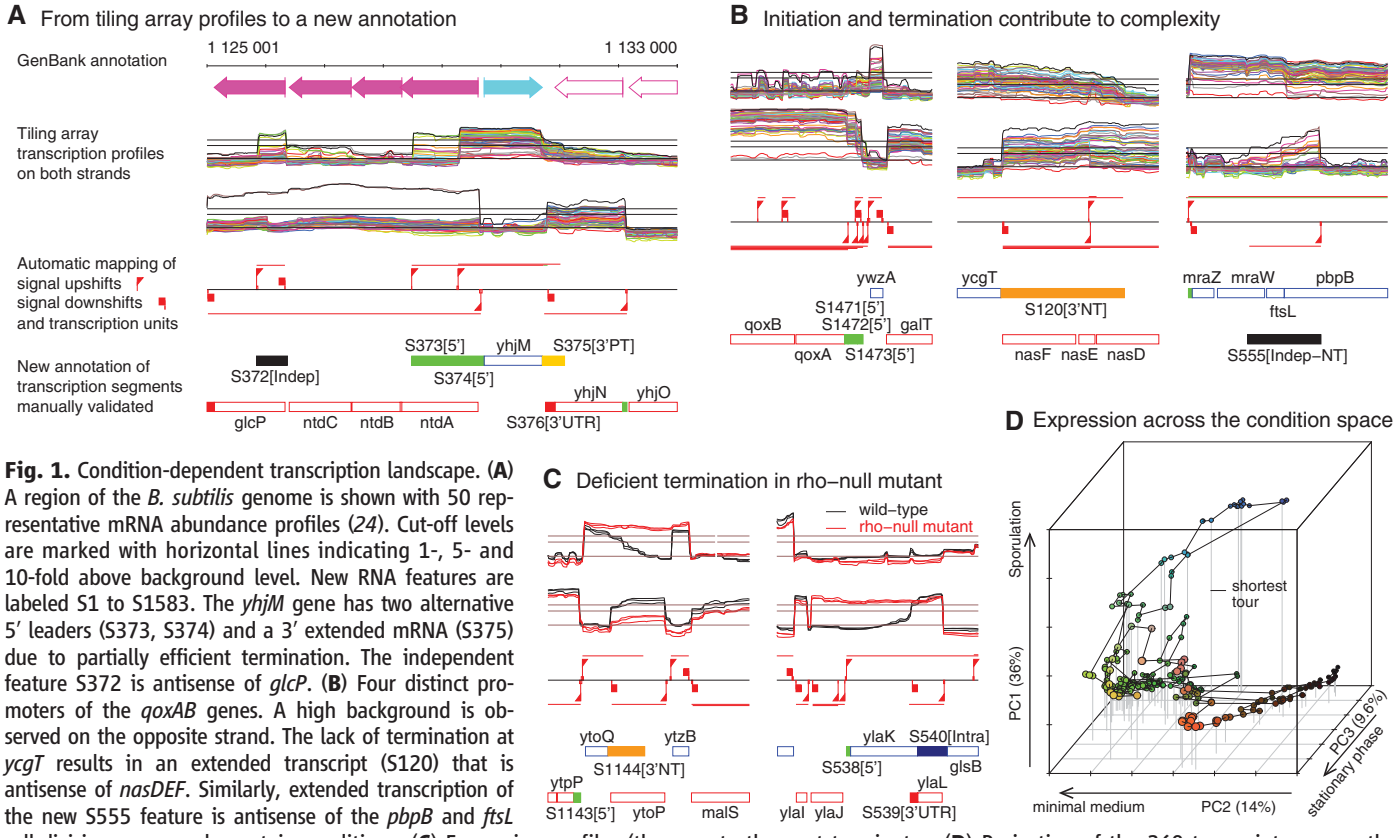

Fig. 1. Condition-dependent transcription landscape. (**A**) A region of the *B. subtilis* genome is shown with 50 representative mRNA abundance profiles (*24*). Cut-off levels are marked with horizontal lines indicating 1-, 5- and 10-fold above background level. New RNA features are labeled S1 to S1583. The *yhjM* gene has two alternative 5′ leaders (S373, S374) and a 3′ extended mRNA (S375) due to partially efficient termination. The independent feature S372 is antisense of *glcP*. (**B**) Four distinct promoters of the *qoxAB* genes. A high background is observed on the opposite strand. The lack of termination at *ycgT* results in an extended transcript (S120) that is antisense of *nasDEF*. Similarly, extended transcription of the new S555 feature is antisense of the *pbpB* and *ftsL* cell-division genes under certain conditions. (**C**) Expression profiles (three replicates) in the prototype strain (black) and its *rho*-null mutant derivative (red). In the mutant, the mRNA of *ytoQ* lacking an intrinsic termination site and that of *ylaL* with a termination site are elongated up to the next terminator. (**D**) Projection of the 269 transcriptomes on the three main axes of the principal component analysis (SOM 8). These axes are highly relevant to *B. subtilis* life-styles and account for up to 60% of the total variability of the data.

(Fig. 1C and SOM 7), indicating that Rho is a general inhibitor of antisense transcription.

The relations among the expression profiles revealed highly correlated changes in expression (Fig. 1D and SOM 8) and provided functional insights (SOM 9). To elucidate the global transcriptional regulatory network, we used the mRNA signal downstream of each of the 3242 detected upshifts to estimate pairwise correlations between promoter activities (SOM 10). The results are summarized in the form of a tree created by hierarchical clustering (Fig. 2A). In this tree built independently of DNA sequence information, the DNA binding sites for different RNAP sigma subunits (*11*) are clustered (Fig. 2B), highlighting the prominent role of sigma factor–mediated promoter recognition in differential gene expression.

For de novo genome-wide identification of sigma factor regulons, we developed an unsupervised algorithm combining information from the DNA sequences near the upshifts and from the clustering of promoters to model the bipartite degenerate motifs recognized by the sigma-containing RNAP (SOM 10). This approach is an alternative to the targeted search for motifs in prespecified clusters (*14*). A predicted sigma factor binding site could be assigned to the majority (2935/3242) of promoters identified (Fig. 2B and table S12). The promoters expected to bind SigA formed six clusters reflecting substantial motif diversity (*15*), and SigA bound in vivo to all six motifs (SOM 11). The promoters recognized by the other sigma factors formed either distinct clusters, each with a distinctive DNA binding motif (SigB, SigD, SigH, SigI, SigK, and SigL), or clusters that grouped several sigma factors that displayed similar DNA binding motifs (Fig. 2B and SOM 12). This de novo classification is consistent with the cross-recognition observed between the sporulation-specific SigE, SigF, and SigG factors (*16*, *17*) and the extracellular function sigma-factors SigM, SigW, SigX, and SigY (*18*, *19*).

The comprehensive definition of regulons allows quantification of the contribution of each sigma factor to transcriptome plasticity in *B. subtilis*. The global activity of a single motif cluster was estimated as the average transcription signal for all the promoters of the cluster (Fig. 2C). Assuming a simple linear relation between individual promoters and cluster activities, we computed the fraction of the transcriptome variance explained by each cluster motif (SOM 10). Overall, ~66% of the observed variance was attributed to variations in the activity of sigma factors mainly associated with sporulation and responses to stress, processes that are essential for adaptation and survival in nature (Fig. 2D and table S12). The proportion of variation attributed to sigma factor activities varied considerably. The highest values (>0.75) were obtained for SigB, SigD, and the sporulation sigma factors. In contrast, the lowest value (0.24) was obtained for SigA, suggesting that condition-specific regulation of SigA-dependent promoters relies mostly on other transcription factors (TFs). Our classification captured biologically meaningful regulatory information on TF function, despite the multilevel organization of the TF regulatory network (SOM 13) (*20*). It also provides leads for further functional analyses and biotechnological applications (SOM 14).

asRNAs exhibited diverse condition-dependent expression profiles (Fig. 3). Indeed, asRNAs are more often initiated from non-SigA promoters (48%) than protein-coding RNAs (26%) (SOM 15 and table S14). asRNAs also tend to be expressed in lower amounts than protein-coding RNAs (fig. S19), and expression of sense and asRNA pairs displays mutual exclusion more often than coexpression (47% negative correlation

Table 1. Summary of mRNA features. The 1583 previously unidentified RNA features were categorized according to size (columns) and their structural relationships with annotated genes (SOM 2): 5′ and 3′ regions; Indep, RNA independent of previously annotated features; Inter, mRNA segment lying between two genes with distinct promoters; Intra, portion of a polycistronic mRNA from a single promoter. The 3′ RNAs comprised three subgroups: 3′ untranslated regions (3′UTR) and 3′ extended transcripts with either no termination (3′NT) or partial termination (3′PT). Similarly, the Indep RNAs displayed either termination at a site (Indep) or no termination (Indep-NT) (Fig. 1B). *L*, length; nt, nucleotides; *n*, number of features. Pred.; predicted.

	50 ≤ *L* < 150 nt			*L* ≥ 150 nt			
Features	***n***	**asRNA***	**Pred. CDSs†**	***n***	**asRNA***	**Pred. CDSs†**	**Genes‡**
5′	462	5	2	214	85	13	105
3′UTR	64	5	0	61	26	5	36
3′NT	2	0	0	44	40	1	40
3′PT	4	1	0	74	69	0	70
Indep	17	3	2	62	21	14	79
Indep-NT	2	0	0	72	64	1	74
Inter	182	3	0	137	86	3	90
Intra	132	0	1	54	15	2	18
Total	865	17	5	718	406	39	512

*asRNAs are segments overlapping ≥100 bp (or 50% for short segments) with the sense RNA. †Putative unannotated CDSs (≥10 amino acids) predicted by the software SHOW with a confidence score above 90% (*25*). ‡Previously unidentified genes include all Indep, Indep-NT, asRNAs, and predicted CDSs. Four genes encoded both asRNAs and potential CDSs. The RNA features are listed in table S5.

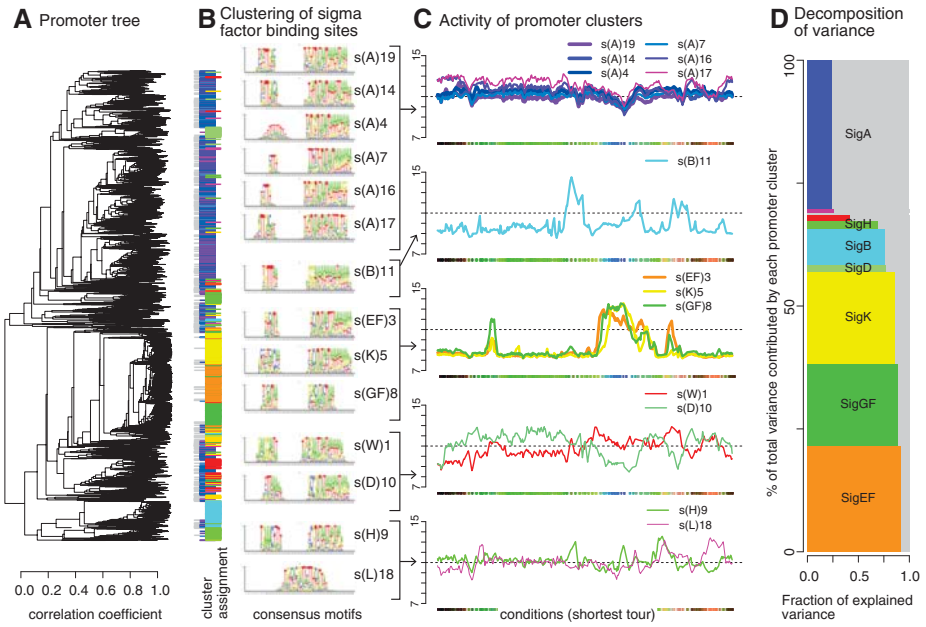

Fig. 2. Classification of promoters. (**A**) Hierarchical clustering tree summarizing the correlations (*x* axis) between promoter pairs arranged on the *y* axis. Detailed information on each promoter and its neighbors can be found in table S4. (**B**) Each promoter is shown as a horizontal bar that is colored according to the distinct clusters revealed by the unsupervised identification of bipartite motifs. Color coding of clusters is as displayed in Fig. 2C, and promoters with low-confidence cluster assignment are shown in gray. For each cluster, the defined consensus motif is labeled with the sigma factor name (letter) and motif number (as in table S4). (**C**) Estimated activity of clusters (*y* axis, log2 scale) across the conditions that are arranged on the *x* axis according to the "shortest tour" (SOM 8 and fig. S4). (**D**) Decomposition of the total variance of promoter activity (SOM 10 and table S12). Unexplained variance is shown in gray.

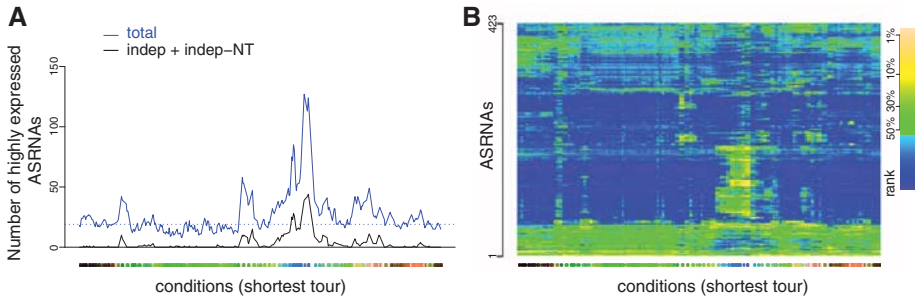

Fig. 3. Patterns of natural antisense transcription across conditions. (**A**) Variation of the number of highly expressed (upper 30%) asRNAs across the conditions (*x* axis). (**B**) Heat map representation: asRNAs are ordered as in table S11 and are colored according to their expression levels.

versus 30% positive correlation). The predominance of negative correlation results primarily from the differential expression of sense and antisense transcripts from SigA and non-SigA promoters, respectively (SOM 15 and fig. S20). Transcription extending beyond the boundaries of CDSs often generates asRNAs (Fig. 1B). Importantly, inefficient termination of a subset of TUs is globally counteracted by the action of Rho, consistent with its role in matching transcription to translational needs (*21*–*23*). Altogether, ~80% of asRNAs result from transcription initiated by alternative sigma factors or from imperfect transcription termination (table S14). We propose that many asRNAs arise from spurious transcriptional events, which are more prevalent when driven by alternative sigma factors. Supporting this hypothesis, the sigma factor binding sites appear to be less evolutionarily conserved in promoters driving potentially spurious asRNAs than in those driving protein-coding RNAs (SOM 15 and fig. S23). Nevertheless, some asRNAs might have important biological functions (*12*). We detected asRNAs with established or potential functions (table S6), the latter including the asRNAs expressed in amounts sufficient to regulate their target genes (SOM 15 and fig. S19). In conclusion, our quantitative analysis of the condition-dependent transcriptome defined the contribution of the sigma factor complement to *B. subtilis* transcriptome plasticity. It revealed that asRNAs generated by inefficient control of transcriptional events might be a drawback of this plasticity, though they might contribute to the creation of previously unknown regulatory functions.

References and Notes

1. B. K. Cho *et al.*, *Nat. Biotechnol.* **27**, 1043 (2009).
2. M. Güell *et al.*, *Science* **326**, 1268 (2009).
3. C. M. Sharma *et al.*, *Nature* **464**, 250 (2010).
4. A. Toledo-Arana *et al.*, *Nature* **459**, 950 (2009).
5. O. Wurtzel *et al.*, *Genome Res.* **20**, 133 (2010).
6. A. L. Sonenshein, J. A. Hoch, R. Losick, Bacillus subtilis *and Its Closest Relatives: From Genes to Cells* (American Society for Microbiology Press, Washington, DC, 2002).
7. S. Rasmussen, H. B. Nielsen, H. Jarmer, *Mol. Microbiol.* **73**, 1043 (2009).
8. P. Nicolas *et al.*, *Bioinformatics* **25**, 2341 (2009).
9. K. Kobayashi *et al.*, *Proc. Natl. Acad. Sci. U.S.A.* **100**, 4678 (2003).
10. I. Irnov, C. M. Sharma, J. Vogel, W. C. Winkler, *Nucleic Acids Res.* **38**, 6637 (2010).
11. N. Sierro, Y. Makita, M. de Hoon, K. Nakai, *Nucleic Acids Res.* **36**, D93 (2008).
12. M. K. Thomason, G. Storz, *Annu. Rev. Genet.* **44**, 167 (2010).
13. P. G. Quirk, E. A. Dunkley Jr., P. Lee, T. A. Krulwich, *J. Bacteriol.* **175**, 647 (1993).
14. P. T. McGrath *et al.*, *Nat. Biotechnol.* **25**, 584 (2007).
15. J. D. Helmann, *Nucleic Acids Res.* **23**, 2351 (1995).
16. P. Eichenberger *et al.*, *PLoS Biol.* **2**, e328 (2004).
17. S. T. Wang *et al.*, *J. Mol. Biol.* **358**, 16 (2006).
18. J. D. Helmann, *Adv. Microb. Physiol.* **46**, 47 (2002).
19. W. J. Lane, S. A. Darst, *PLoS Biol.* **4**, e269 (2006).
20. A. Goelzer *et al.*, *BMC Syst. Biol.* **2**, 20 (2008).
21. C. J. Cardinale *et al.*, *Science* **320**, 935 (2008).
22. B. M. Burmann *et al.*, *Science* **328**, 501 (2010).
23. S. Proshkin, A. R. Rahmouni, A. Mironov, E. Nudler, *Science* **328**, 504 (2010).
24. M. Hoebeke, P. Nicolas, P. Bessières, *Bioinformatics* **19**, 859 (2003).
25. M. Ibrahim *et al.*, *Microbiology* **153**, 3631 (2007).

Acknowledgments: The data are deposited in the Gene Expression Omnibus (GEO) database (accession numbers GSE27219, GSE27303, GSE27419, and GSE27652), and are tabulated in the SOM and at www.basysbio.eu/bsubtranscriptome. This Web page provides links to the data archived in the GEO and Openbis databases. This study was supported by the European Commission–funded BaSysBio project (LSHG-CT-2006-037469), the SysMO network funded by the German Federal Ministry of Education and Research (0313978B), Department of Education, Science and Training (CG110055), and the National Health and Medical Research Council (455646). We are grateful to N. Pelé, B. Giovani, C. Sautot, and B. Diep for management support. The authors declare no competing interests.

Supporting Online Material

www.sciencemag.org/cgi/content/full/335/6072/1103/DC1
SOM Text (SOM 1 to 15)
Figs. S1 to S23
Tables S1 to S14
References (*26*–*102*)
Database S1

11 April 2011; accepted 11 January 2012
10.1126/science.1206848

Biased Signaling Pathways in β_2-Adrenergic Receptor Characterized by ^{19}F-NMR

Jeffrey J. Liu,[1]* Reto Horst,[1]* Vsevolod Katritch,[1] Raymond C. Stevens,[1]† Kurt Wüthrich[1,2]†

Extracellular ligand binding to G protein–coupled receptors (GPCRs) modulates G protein and β-arrestin signaling by changing the conformational states of the cytoplasmic region of the receptor. Using site-specific ^{19}F-NMR (fluorine-19 nuclear magnetic resonance) labels in the β_2-adrenergic receptor (β_2AR) in complexes with various ligands, we observed that the cytoplasmic ends of helices VI and VII adopt two major conformational states. Changes in the NMR signals reveal that agonist binding primarily shifts the equilibrium toward the G protein–specific active state of helix VI. In contrast, β-arrestin–biased ligands predominantly impact the conformational states of helix VII. The selective effects of different ligands on the conformational equilibria involving helices VI and VII provide insights into the long-range structural plasticity of β_2AR in partial and biased agonist signaling.

Signaling through G protein–coupled receptors (GPCRs) is a fundamental component of eukaryotic cellular communication. As a result, GPCRs make up a large fraction of the "druggable proteome," with more than 30% of available pharmaceuticals targeting GPCRs (*1*). In performing their functions, GPCRs such as the β_2-adrenergic receptor (β_2AR) recognize a diverse array of ligands and transmit signals through the cellular membrane to cytoplasmic G proteins. In parallel to G protein signaling, activated β_2AR can be phosphorylated and binds to β-arrestin, initiating desensitization, endocytosis of β_2AR, and β-arrestin–dependent signaling (*2*). A number of β_2AR ligands, including the U.S. Food and Drug Administration–approved β-blocker carvedilol (*3*) and the agonist isoetharine (*4*), have been shown to impart differing degrees of signaling in G protein and arrestin pathways, a phenomenon called "functional selectivity" or "biased signaling" (*5*). Understanding the mechanism of biased signaling can provide leads for designing more specific and efficient drugs.

Crystal structures have been determined for β_2AR with bound inverse agonists, antagonists,

[1]Department of Molecular Biology, The Scripps Research Institute, 10550 North Torrey Pines Road, La Jolla, CA 92037, USA. [2]Skaggs Institute of Chemical Biology, The Scripps Research Institute, 10550 North Torrey Pines Road, La Jolla, CA 92037, USA.

*These authors contributed equally to this work.
†To whom correspondence should be addressed. E-mail: stevens@scripps.edu (R.C.S.); wuthrich@scripps.edu (K.W.)

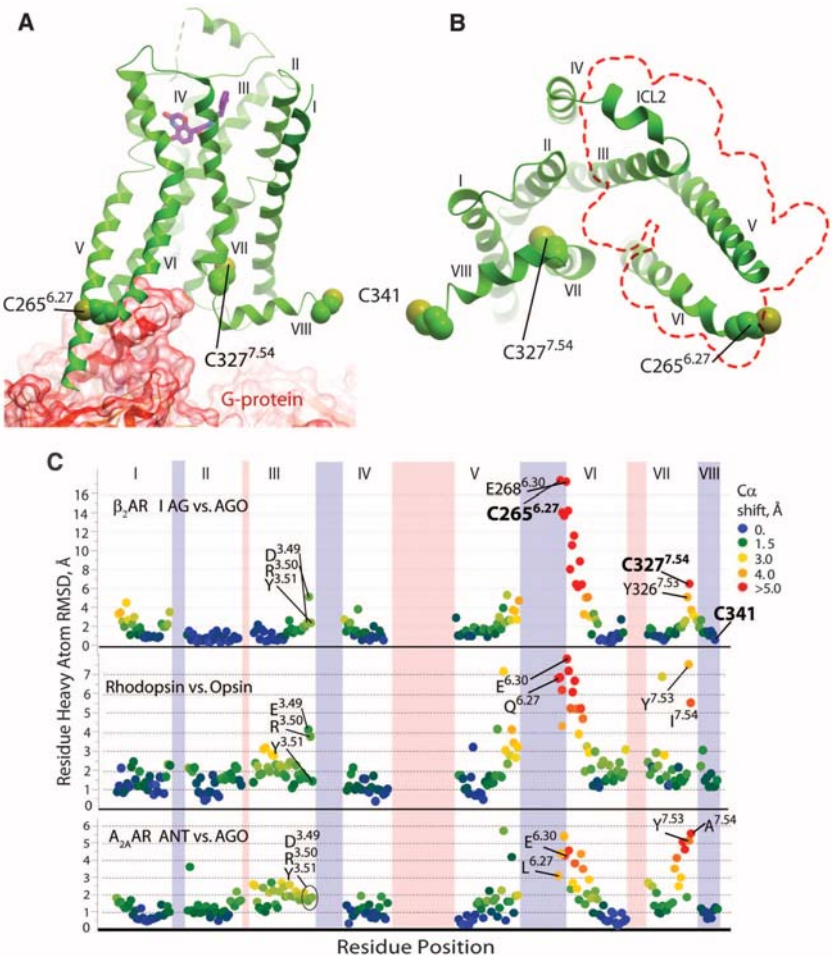

Fig. 1. Locations of ^{19}F-NMR labels in β_2AR and activation-related changes in GPCR crystal structures. (**A**) Side view of β_2AR in the active G protein–bound form [Protein Data-Bank (PDB) ID 3SN6], shown in green. The transmembrane helices I to VII and the C-terminal helix VIII are identified. The full agonist BI-167107 in the ligand-binding site is shown as a stick diagram. Green and yellow spheres highlight the three cysteine residues used for TET labeling, i.e., $Cys265^{6.27}$ and $Cys327^{7.54}$ at the cytoplasmic ends of helices VI and VII, respectively, and Cys341 at the C terminus. The bound G protein heterotrimer is shown as red ribbons and surfaces. (**B**) Cytoplasmic view of the structure in (A), with the G protein contact sites outlined by a broken red line. (**C**) Plot of distance root mean square deviations (RMSDs) of individual residues between crystal structures of inactive and active states of three GPCRs. Crystal structures used are as follows (from top to bottom): β_2AR (PDB IDs 2RH1 versus 3SN6), rhodopsin (PDB IDs 1GZM versus 3DQB), and A_{2A}AR (PDB IDs 3EML versus 3QAK). The horizontal axes represent the amino acid sequences (β_2AR residues 34 to 341, bovine rhodopsin residues 38 to 320, and A_{2A}AR residues 6 to 302). The vertical axis shows all-heavy-atom RMSDs per residue, and the color code defined in the upper right corner of the panel indicates corresponding C^{α} deviations. For each protein, selected residues are identified. The locations of the helices I to VIII are indicated at the top. Periplasmic loop regions are highlighted in red, and cytoplasmic loops and helix VIII are highlighted in blue. The cytoplasmic ends of helices VI and VII, which contain $Cys265^{6.27}$ and $Cys327^{7.54}$, are "hot spots" with large conformational rearrangements between the crystal structures of inactive and active states; other transmembrane helices and intracellular helix VIII, which includes Cys341, show only small displacements. Single-letter abbreviations for the amino acid residues are as follows: A, Ala; C, Cys; D, Asp; E, Glu; F, Phe; G, Gly; H, His; I, Ile; K, Lys; L, Leu; M, Met; N, Asn; P, Pro; Q, Gln; R, Arg; S, Ser; T, Thr; V, Val; W, Trp; and Y, Tyr.

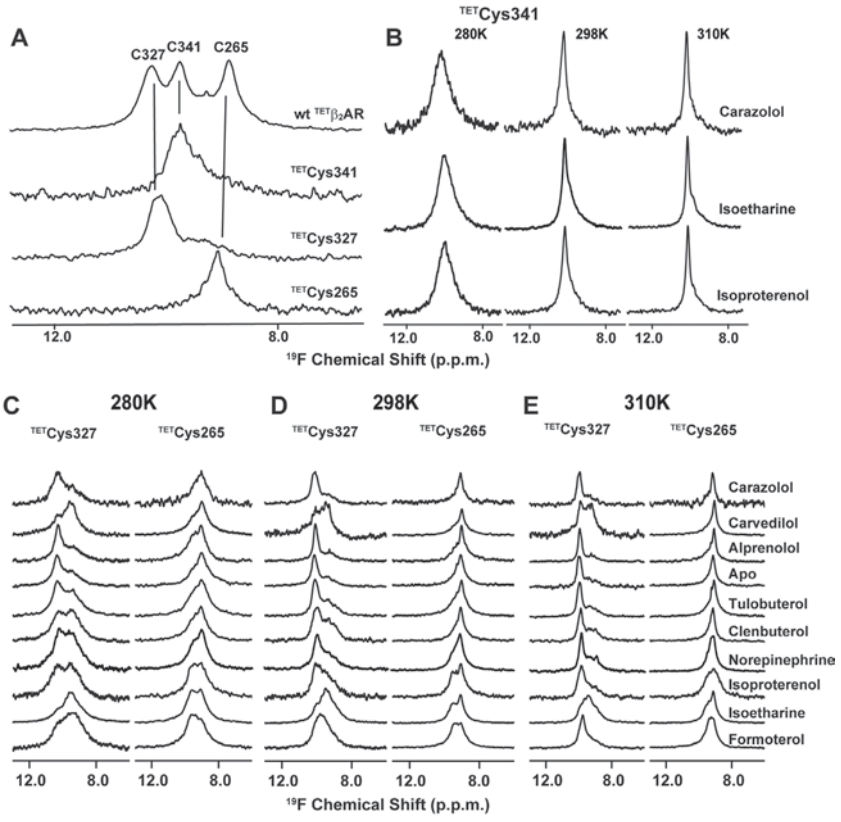

Fig. 2. One-dimensional ^{19}F-NMR spectra of different TET-labeled β_2AR constructs under variable solution conditions. (**A**) ^{19}F-NMR resonance assignments for carazolol-bound $^{TET}\beta_2$AR at 298 K. Spectra of the following constructs were recorded: wild-type (wt) $^{TET}\beta_2$AR; β_2AR(^{TET}C265, C327S, C341A); β_2AR(C265A, ^{TET}C327, C341A); and β_2AR(C265A, C327S, ^{TET}C341). The vertical lines connect peaks in the ^{19}F-NMR spectrum of $^{TET}\beta_2$AR with the corresponding peaks in the spectra of the single-residue TET-labeled mutants. At the top, the peak assignments are indicated by the one-letter amino acid code and the residue number. (**B**) β_2AR(C265A, C327S, ^{TET}C341) in complex with an inverse agonist (carazolol), a biased agonist (isoetharine), and a full agonist (isoproterenol) at 280, 298, and 310 K. (**C**, **D**, and **E**) β_2AR(^{TET}C265, C327S, C341A) and β_2AR(C265A, ^{TET}C327, C341A) free and bound to nine different ligands at 280, 298, and 310 K. In (B) to (E), the temperature and the ligands are indicated at the top and on the right, respectively. For all experiments, the following parameter settings were used to collect and process the spectra: data size 1024 complex points, acquisition time 51 ms, and 24576 scans per increment. The data were multiplied with an exponential function with a line-broadening factor of 30 Hz and zero-filled to 2048 points before Fourier transformation.

and agonists (*6*–*10*), including active-state β_2AR complexes with a G protein mimetic nanobody (*8*) and with a heterotrimeric G protein (*11*). The β_2AR–G protein structure, which has also been analyzed by electron microscopy (EM) (*12*), reveals the location of the G protein binding site, showing that the G protein interacts with helices V and VI, and the intracellular loops ICL2 and ICL3, but makes no substantial contacts with helices VII and VIII (Fig. 1, A and B). A comparison of inactive and active-state crystal structures of β_2AR, rhodopsin (*13*), and the A_{2A} adenosine receptor (*14*, *15*) suggests a common pattern of structural differences between inactive and active states in GPCRs (Fig. 1C), where a coupled motion of helices V and VI, and changes in helices III and VII, are accompanied by distinct side-chain rotamer switches on the cytoplasmic side of the protein (*16*, *17*). Activation of β_2AR has been investigated previously with fluorescence-based biophysical experiments (*18*–*25*) and nuclear magnetic resonance (NMR) (*26*), and conformational changes during receptor activation were observed in helix VI and the cytoplasmic surface.

To probe for subtle conformational changes involved in receptor-ligand binding (*27*), ^{19}F-NMR spectroscopy was employed. This highly sensitive method was used to provide information based on the observation of line shapes and chemical shifts of strategically located ^{19}F labels in the cytoplasmic region of the receptor (Fig. 1, A and B) (*28*). Similar approaches have previously been successfully applied to studies of a number of membrane proteins (*29*–*31*). Three native cysteine residues (Cys265$^{6.27}$, Cys327$^{7.54}$, and Cys341) (*32*) of β_2AR (*33*) in the cytoplasmic region of the receptor are accessible for covalent labeling with 2,2,2 trifluoroethanethiol (TET) (*31*), and their NMR signals were unambiguously assigned through the use of site-specific mutagenesis of these residues and all other native cysteine residues that might be affected by TET (Fig. 2A) (*34*). To probe for structural changes, we primarily used singly labeled receptors, which have reduced complexity of the ^{19}F-NMR spectra when compared with wild-type $^{TET}\beta_2$AR (Fig. 2A). Cys265$^{6.27}$ and Cys327$^{7.54}$ are located at the cytoplasmic ends of helices VI and VII, respectively, both of which are known to undergo large conformational changes during receptor activation (Fig. 1C). In contrast, Cys341 is located in the nontransmembrane helix VIII at the C terminus, and β_2AR(C265A, C327S, ^{TET}C341) was observed to be unresponsive to binding of different ligands (Fig. 2B). This C-terminal probe therefore served as an internal negative control relative to Cys265$^{6.27}$ and Cys327$^{7.54}$ in studies of the effects from the binding of different pharmacological ligands.

The ^{19}F-NMR spectra of β_2AR(^{TET}C265, C327S, C341A) and β_2AR(C265A, ^{TET}C327, C341A) (Fig. 2, C to E) show prominent changes upon addition of saturating concentrations of a collection of ligands (table S1) that represent a full spectrum of ligand efficacy (*35*). In general, the signals at 280 K of both β_2AR(^{TET}C265, C327S, C341A) and β_2AR(C265A, ^{TET}C327, C341A) consist of two components, suggesting that the β_2AR structure contains two independent equilibria between locally different conformations manifested at these two amino acid positions. Whereas ligand-free and inverse agonist-bound $^{TET}\beta_2$ARs have almost identical spectra, in which the populations of C327^{I} and C265^{I} are much more prominent than those of C327^{A} and C265^{A}, spectra of $^{TET}\beta_2$AR bound to the full agonist isoproterenol exhibit approximately equal populations at both residues (Fig. 3A). Shifts of this equilibrium are observed with different agonists bound to $^{TET}\beta_2$AR, suggesting that the peaks A and I are likely to represent the active and inactive state of both helices VI and VII of β_2AR, respectively. The temperature dependence of the ^{19}F signals with regard to line width and peak intensity (Fig. 2, C to E, and fig. S4) suggests that the active state of both helices VI and VII of β_2AR exhibits a larger degree of conformational plasticity than the inactive state; that is, the active state samples a wider range of conformers with slightly different chemical shifts, either in a static ensemble or in a manifold of conformers that also includes conformational exchange.

The ^{19}F-NMR data were analyzed with a double-Lorentzian function to obtain quantitative information on the conformational equilibria (Fig. 3A). This revealed that positions and widths of the NMR peaks remain practically unchanged for all ligands studied and confirmed that the major effects of agonist binding are population shifts from inactive state peaks (I) to those of active state (A). A plot of relative peak volumes for Cys265^{A} versus those for Cys327^{A}, which represent the populations of the active state in helix VI and helix VII, respectively, reveals varying degrees of agonist-mediated shifts toward the active state manifested by Cys265$^{6.27}$ and Cys327$^{7.54}$ (Fig. 3B). For most agonists, the shifts along the two axes follow the same overall trend as their reported pharmacological efficacy on G protein activation (*36*). For instance, the partial agonists tulobuterol, clenbuterol, and norepinephrine have a less pronounced effect on Cys265$^{6.27}$ than the full agonist isoproterenol, whereas the full agonist formoterol elicits a greater shift in conformational equilibrium on Cys265$^{6.27}$. These results suggest that the degree to which agonists shift the equilibrium toward the active state of helix VI results in differing G protein signaling

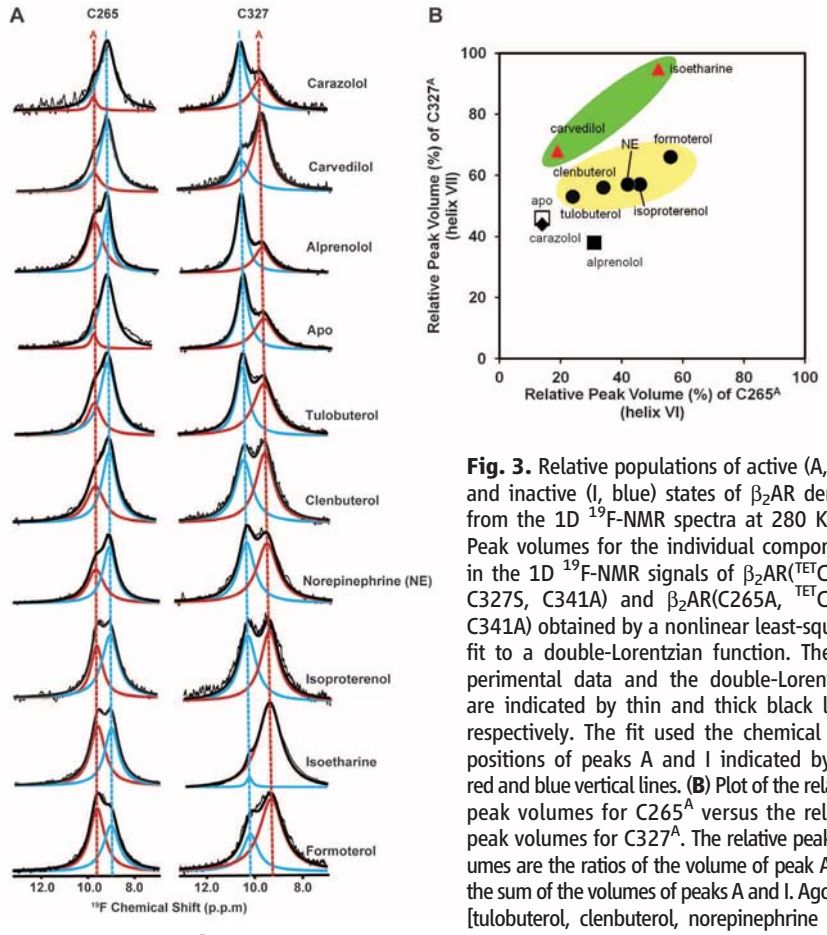

Fig. 3. Relative populations of active (A, red) and inactive (I, blue) states of β_2AR derived from the 1D ^{19}F-NMR spectra at 280 K. (**A**) Peak volumes for the individual components in the 1D ^{19}F-NMR signals of β_2AR(^{TET}C265, C327S, C341A) and β_2AR(C265A, ^{TET}C327, C341A) obtained by a nonlinear least-squares fit to a double-Lorentzian function. The experimental data and the double-Lorentzian are indicated by thin and thick black lines, respectively. The fit used the chemical shift positions of peaks A and I indicated by the red and blue vertical lines. (**B**) Plot of the relative peak volumes for C265^{A} versus the relative peak volumes for C327^{A}. The relative peak volumes are the ratios of the volume of peak A and the sum of the volumes of peaks A and I. Agonists [tulobuterol, clenbuterol, norepinephrine (NE), isoproterenol, and formoterol] are shown as black circles highlighted by a yellow background, biased ligands (carvedilol, isoetharine) as red triangles highlighted by a green background, a neutral antagonist (alprenolol) as a black square, an inverse agonist (carazolol) as a black diamond, and apo as an open square.

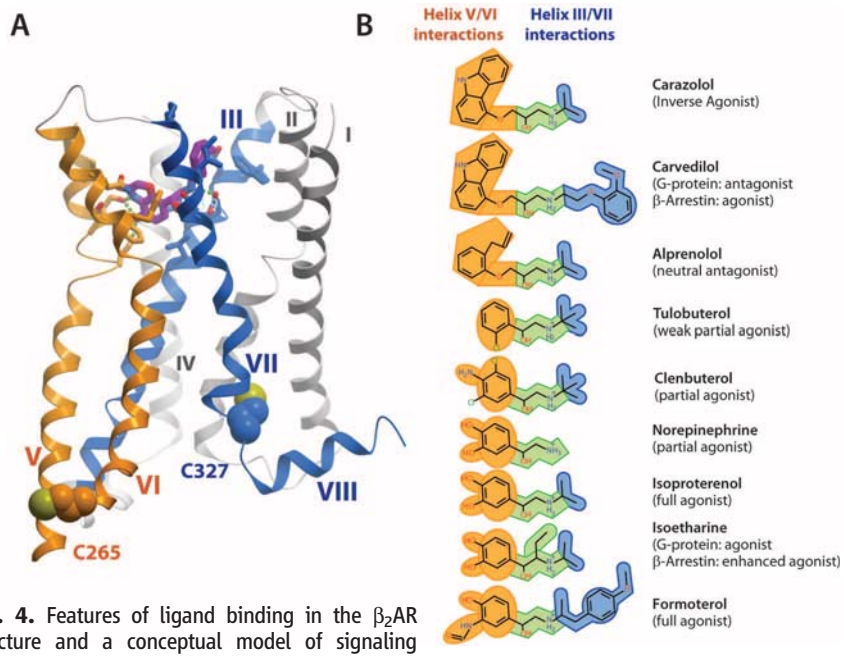

Fig. 4. Features of ligand binding in the β_2AR structure and a conceptual model of signaling pathways to G proteins and arrestins in β_2AR activation. (**A**) Side view of the structure of active-state β_2AR in the complex with the agonist BI-167107 (PDB ID 3SN6), with helices V/VI and III/VII color-coded orange and blue, respectively, to indicate that they interact with the correspondingly colored fragments of the ligands in (B). (**B**) Chemical structures of the ligands used in the current ^{19}F-NMR studies. Orange highlights the head groups, green the common ethanolamine moieties, and blue the substituents to the amino group of the ethanolamine tail. Ligand names are shown on the right, with published pharmacological efficacy indicated in parentheses.

capacity. The antagonist/weak partial agonist alprenolol can induce a small shift on Cys265$^{6.27}$ but has a minimal effect on Cys327$^{7.54}$, in agreement with previous findings that it is a weak partial agonist (*25*, *37*). The inverse agonist carazolol, on the other hand, induces no apparent shifts as compared to the apo form. In contrast, the two β-arrestin–biased ligands, isoetharine and carvedilol, cause large shifts of the equilibria in Cys327$^{7.54}$ toward the active state. Interestingly, carvedilol, like other antagonists and inverse agonists, has little influence on the equilibrium of Cys265$^{6.27}$, whereas isoetharine, like other agonists, also produces a prominent shift of Cys265$^{6.27}$ toward the active state.

The large activation changes in Cys327$^{7.54}$ caused by carvedilol and isoetharine suggest that helix VII primarily affects β-arrestin signaling pathways. This is consistent with the result of a previous study that β_2AR phosphorylation by GPCR kinases, which is a prerequisite for β-arrestin binding, primarily targets a region directly adjacent to helix VII on helix VIII (*38*). Furthermore, recent crystallographic (*11*) and EM studies (*12*) of a β_2AR-$G_{\alpha\beta\gamma}$ heterotrimer complex show that the G_α subunit makes major contact with helices V and VI of β_2AR, resulting in a 14 Å outward movement of the cytoplasmic ends of these helices, whereas there is no contact between $G_{\alpha\beta\gamma}$ and helix VII (Fig. 1, A and B), suggesting that the conformational changes in helix VII are not directly involved in G protein binding and signaling.

To further characterize the environment of Cys327$^{7.54}$ in the active state, we evaluated the effect of the water-soluble paramagnetic relaxation agent gadopentetic dimeglumine (Magnevist, Bayer HealthCare Pharmaceuticals, New Jersey, USA) (*39*) on individual resonances of β_2AR(C265A, ^{TET}C327, C341A) bound to isoproterenol. A comparison of the line widths of peaks A and I in the one-dimensional (1D) ^{19}F-NMR spectra at various Magnevist concentrations revealed that peak I is more susceptible to the line broadening by Magnevist than peak A (fig. S1A), indicating that Cys327$^{7.54}$ in the inactive state is more readily solvent-accessible than in the active state. This interpretation is consistent with crystal structure data, where Cys327$^{7.54}$ was found to be solvent-exposed in the carazolol-bound structure (*6*) but buried in the transmembrane helix bundle of the receptor in its complexes with a nanobody (*8*) or the G protein (*11*) (fig. S1B).

Additional insight from analysis of the ^{19}F-NMR results can be obtained by examining the chemical structures of the agonists and their interactions with the individual helices in the β_2AR binding pocket (Fig. 4). The majority of known high-affinity adrenergic ligands have a common structural motif consisting of an aromatic "head group" and an ethanolamine "tail group". The head group (e.g., catechol) of agonists is directly connected to the ethanolamine tail, whereas antagonists and inverse agonists—both of which act as competitive inhibitors to agonists and either have no impact or a negative impact on the receptor basal activity—have an additional two-atom linker between the head and tail groups. Crystal structures of the β_2AR complexes with various ligands (*6*–*11*), as well as biochemical (*40*–*42*) and modeling studies (*43*, *44*) have established that the aromatic head groups interact with helices V and VI, whereas the ethanolamine tails are anchored by ionic and polar interactions at helices III and VII (Fig. 4A and fig. S2). For agonists, polar interactions of their head groups with helix V side chains thereby mediate an inward shift of Pro211$^{5.50}$, and subsequent conformational changes involving Ile121$^{3.40}$ and Phe282$^{6.44}$ (*8*) result in the activation move of the cytoplasmic tip of helix VI.

The changes observed by ^{19}F-NMR (Fig. 3) provide additional insight into correlations between the chemical structure of the ligands and their interactions with β_2AR. Binding of full agonists (such as isoproterenol and formoterol) imparts a large shift in the conformational equilibrium of both helices VI (Cys265$^{6.27}$) and VII (Cys327$^{7.54}$). Binding of partial agonists, which either completely lack (as in tulobuterol) or have much weaker (as in clenbuterol) polar features on their aromatic heads, has a smaller influence on the conformational equilibrium of helix VI than full agonists but has almost as much impact on helix VII. In addition, the β-arrestin–biased ligands carvedilol and isoetharine, which differ from their corresponding "unbiased" prototypes (inverse agonist carazolol and full agonist isoproterenol, respectively) only in the tail moieties, strongly affect the helix VII equilibrium. Another important observation is that the 1D ^{19}F-NMR spectrum of β_2AR(C265A, C327S, ^{TET}C341) bound to isoetharine, which is one of the most potent biased agonists, is similar to those of β_2AR(C265A, C327S, ^{TET}C341) bound to carazolol and isoproterenol (Fig. 2B). This shows that the C terminus of the nontransmembrane helix VIII, where Cys341 is located, is not directly involved in the β-arrestin signaling pathway. In the absence of structural data on a complex of β_2AR with β-arrestin, it is tempting to further hypothesize from this data that the position of Cys341 on helix VIII is located outside of the interface with bound arrestin.

These observations on structure-activity relationships for β-arrestin–biased β_2AR ligands, and unbiased full and partial agonists, provide insights into β_2AR signaling pathways that suggest the existence of parallel pathways for G protein and β-arrestin signaling (fig. S3). Although these pathways appear interconnected on several levels and may involve other activation-related rearrangements in the cytoplasmic and periplasmic loops (*45*), the present ^{19}F-NMR results point to a high level of decoupling of the two pathways. The implicated links between ligand structure and function may serve as a platform for future rational design of specific ligands.

Given the above observations on the correlation between ligand structure and receptor response, a connection can now be made between

the chemical structures of pharmacological ligands and their signaling pathways acting either through G proteins or β-arrestins. The general principle that links the chemical space of the ligands to the specific changes in conformational plasticity at the signaling cytoplasmic receptor surface may be preserved in other GPCRs. The use of ^{19}F-NMR may thus prove to be a widely applicable tool for structure-activity relationship studies of GPCR ligands.

References and Notes

1. A. L. Hopkins, C. R. Groom, *Nat. Rev. Drug Discov.* **1**, 727 (2002).
2. K. Rajagopal, R. J. Lefkowitz, H. A. Rockman, *J. Clin. Invest.* **115**, 2971 (2005).
3. S. K. Shenoy, R. J. Lefkowitz, *Trends Pharmacol. Sci.* **32**, 521 (2011).
4. M. T. Drake *et al.*, *J. Biol. Chem.* **283**, 5669 (2008).
5. J. D. Urban *et al.*, *J. Pharmacol. Exp. Ther.* **320**, 1 (2007).
6. V. Cherezov *et al.*, *Science* **318**, 1258 (2007).
7. M. A. Hanson *et al.*, *Structure* **16**, 897 (2008).
8. S. G. Rasmussen *et al.*, *Nature* **469**, 175 (2011).
9. D. M. Rosenbaum *et al.*, *Nature* **469**, 236 (2011).
10. D. Wacker *et al.*, *J. Am. Chem. Soc.* **132**, 11443 (2010).
11. S. G. Rasmussen *et al.*, *Nature* **477**, 549 (2011).
12. G. H. Westfield *et al.*, *Proc. Natl. Acad. Sci. U.S.A.* **108**, 16086 (2011).
13. P. Scheerer *et al.*, *Nature* **455**, 497 (2008).
14. V. P. Jaakola *et al.*, *J. Biol. Chem.* **285**, 13032 (2010).
15. F. Xu *et al.*, *Science* **332**, 322 (2011).
16. X. Deupi, J. Standfuss, *Curr. Opin. Struct. Biol.* **21**, 541 (2011).
17. R. Nygaard, T. M. Frimurer, B. Holst, M. M. Rosenkilde, T. W. Schwartz, *Trends Pharmacol. Sci.* **30**, 249 (2009).
18. U. Gether *et al.*, *J. Biol. Chem.* **272**, 2587 (1997).
19. P. Ghanouni *et al.*, *J. Biol. Chem.* **276**, 24433 (2001).
20. P. Ghanouni, J. J. Steenhuis, D. L. Farrens, B. K. Kobilka, *Proc. Natl. Acad. Sci. U.S.A.* **98**, 5997 (2001).
21. S. Granier *et al.*, *J. Biol. Chem.* **282**, 13895 (2007).
22. G. Swaminath *et al.*, *J. Biol. Chem.* **280**, 22165 (2005).
23. G. Swaminath *et al.*, *J. Biol. Chem.* **279**, 686 (2004).
24. X. Yao *et al.*, *Nat. Chem. Biol.* **2**, 417 (2006).
25. X. J. Yao *et al.*, *Proc. Natl. Acad. Sci. U.S.A.* **106**, 9501 (2009).
26. M. P. Bokoch *et al.*, *Nature* **463**, 108 (2010).
27. M. A. Danielson, J. J. Falke, *Annu. Rev. Biophys. Biomol. Struct.* **25**, 163 (1996).
28. Materials and methods are available as supporting material on *Science* Online.
29. F. Evanics, J. L. Kitevski, I. Bezsonova, J. Forman-Kay, R. S. Prosser, *Biochim. Biophys. Acta* **1770**, 221 (2007).
30. J. J. Falke, L. A. Luck, J. Scherrer, *Biophys. J.* **62**, 82 (1992).
31. J. Klein-Seetharaman, E. V. Getmanova, M. C. Loewen, P. J. Reeves, H. G. Khorana, *Proc. Natl. Acad. Sci. U.S.A.* **96**, 13744 (1999).
32. Ballesteros-Weinstein numbering is shown as a superscript. The most conserved residue in each transmembrane helix is designated as x.50, where x is the number of the transmembrane helix, and the second number (50) indicates the relative position of the specific residue. The second number decreases toward the N terminus and vice versa. Only residues on transmembrane helices are noted.
33. To produce β_2AR samples that are stabilized enough for NMR measurement, the C terminus was truncated, the part of intracellular loop 3 that is not involved in G protein recruitment was removed, and a stabilizing E122W mutation was added. Constructs containing these modifications were also crystallized and characterized as functionally similar to the unmodified β_2AR.
34. The three ^{19}F signals in labeled wild-type $^{TET}\beta_2$AR/carazolol were identified by comparison with signals from β_2AR constructs containing single-labeled residues, i.e., β_2AR(^{TET}C265, C327S, C341A); β_2AR(C265A, ^{TET}C327, C341A); and β_2AR(C265A, C327S, ^{TET}C341).
35. Ligand-binding properties of the cysteine mutants were examined on the membranes from β_2AR expressing *Sf9* cells. Radioligand binding assay used [^{3}H]Dihydroalprenolol as the reporter ligand, and competition assay used isoproterenol as the competing ligand. The binding affinity of antagonist to the wild-type receptor (1.4 nM) is identical to all cysteine mutants (Cys265 = 1.1 ± 0.1 nM; Cys327 = 1.4 ± 0.4 nM; and Cys341 = 1.1 ± 0.1 nM), and the affinity of full agonist to the wild-type receptor (323 nM) is similar to all cysteine mutants (Cys265 = 100nM; Cys327 = 118 nM; and Cys341 = 138 nM).
36. J. G. Baker, *Br. J. Pharmacol.* **160**, 1048 (2010).
37. J. W. Wisler *et al.*, *Proc. Natl. Acad. Sci. U.S.A.* **104**, 16657 (2007).
38. K. N. Nobles *et al.*, *Sci. Signal.* **4**, ra51 (2011).
39. C. Hilty, G. Wider, C. Fernández, K. Wüthrich, *Chem. Bio. Chem.* **5**, 467 (2004).
40. G. Liapakis *et al.*, *J. Biol. Chem.* **275**, 37779 (2000).
41. C. D. Strader, M. R. Candelore, W. S. Hill, I. S. Sigal, R. A. Dixon, *J. Biol. Chem.* **264**, 13572 (1989).
42. C. D. Strader *et al.*, *J. Biol. Chem.* **263**, 10267 (1988).
43. C. de Graaf, D. Rognan, *J. Med. Chem.* **51**, 4978 (2008).
44. V. Katritch *et al.*, *J. Mol. Recognit.* **22**, 307 (2009).
45. A. W. Kahsai *et al.*, *Nat. Chem. Biol.* **7**, 692 (2011).

Acknowledgments: This work was supported in part by NIH Roadmap Initiative grant P50 GM073197 for technology development and purchase of the ^{19}F-NMR probe, and by PSI:Biology grant U54 GM094618 for GPCR biology studies. The authors thank J. Velasquez for help on molecular biology; C. Cornillez-Ty, T. Trinh, and K. Allin for help on baculovirus expression; J. Gatchalian for ligand-binding assays; P. Stanczak for assistance with the paramagnetic titration experiment; V. Cherezov for helpful discussions; I. Wilson for careful review and scientific feedback on the manuscript; K. Kadyshevskaya for assistance with figure preparation; and A. Walker for assistance with manuscript preparation. R.C.S. is a founder and member of the board of directors of Receptos, a GPCR structure–based drug discovery company.

Supporting Online Material

www.sciencemag.org/cgi/content/full/science.1215802/DC1
Materials and Methods
Figs. S1 to S4
Tables S1 and S2
References (*46*–*54*)

26 October 2011; accepted 11 January 2012
Published online 19 January 2012;
10.1126/science.1215802

Catalysis and Sulfa Drug Resistance in Dihydropteroate Synthase

Mi-Kyung Yun,[1]* Yinan Wu,[1,2]* Zhenmei Li,[1] Ying Zhao,[3] M. Brett Waddell,[4] Antonio M. Ferreira,[1,5] Richard E. Lee,[3] Donald Bashford,[1,2] Stephen W. White[1,2]†

The sulfonamide antibiotics inhibit dihydropteroate synthase (DHPS), a key enzyme in the folate pathway of bacteria and primitive eukaryotes. However, resistance mutations have severely compromised the usefulness of these drugs. We report structural, computational, and mutagenesis studies on the catalytic and resistance mechanisms of DHPS. By performing the enzyme-catalyzed reaction in crystalline DHPS, we have structurally characterized key intermediates along the reaction pathway. Results support an S_N1 reaction mechanism via formation of a novel cationic pterin intermediate. We also show that two conserved loops generate a substructure during catalysis that creates a specific binding pocket for *p*-aminobenzoic acid, one of the two DHPS substrates. This substructure, together with the pterin-binding pocket, explains the roles of the conserved active-site residues and reveals how sulfonamide resistance arises.

Drug resistance has led to a decrease in the clinical utility of virtually all marketed antibacterial agents (*1*), and the sulfonamide class of antibiotics (sulfa drugs) was an early victim of this phenomenon (*2*, *3*). Sulfa drugs interrupt the essential folate pathway in bacteria and primitive eukaryotes; they target the enzyme dihydropteroate synthase (DHPS), which catalyzes the condensation of 6-hydroxymethyl-7,8-dihydropterin pyrophosphate (DHPP) with *p*-aminobenzoic acid (PABA) in the production of the folate intermediate, 7,8-dihydropteroate (*4*). Sulfa drugs target both Gram-positive and Gram-negative bacterial infections, and combination therapies such as co-trimoxazole—a mixture of the sulfa drug sulfamethoxazole (SMX) and the dihydrofolate reductase (DHFR) inhibitor trimethoprim—are effective against many pathogenic microorganisms (*5*). However, DHPS mutations have been frequently characterized in many clinical isolates, relegating sulfonamide-based therapies to second- or third-line options.

Co-trimoxazole has proven to be effective against several emerging threats, including community-acquired multidrug-resistant *Staphylococcus aureus* (MRSA) (*6*, *7*) and *Pneumocystis jiroveci* infections in immune-compromised patients (*8*). DHPS therefore remains an important drug target, and we are developing new inhibitors that target the DHPP-binding pocket of the enzyme (*9*–*11*). Understanding the DHPS catalytic mech-

[1]Department of Structural Biology, St. Jude Children's Research Hospital, Memphis, TN 38105, USA. [2]Integrated Program in Biomedical Sciences, University of Tennessee Health Science Center, Memphis, TN 38163, USA. [3]Department of Chemical Biology and Therapeutics, St. Jude Children's Research Hospital, Memphis, TN 38105, USA. [4]Hartwell Center for Bioinformatics and Biotechnology, St. Jude Children's Research Hospital, Memphis, TN 38105, USA. [5]Department of Information Sciences, St. Jude Children's Research Hospital, Memphis, TN 38105, USA.

*These authors contributed equally to this work.
†To whom correspondence should be addressed. E-mail: stephen.white@stjude.org

anism and the mechanistic basis of sulfa drug resistance is crucial for these drug discovery efforts. DHPS has a TIM barrel α/β structure, and many of the drug resistance point mutations are located within two flexible and conserved loops that appear to make important contributions to the active site (*9*, *11*–*15*). The inability to observe these loops in their catalytic and/or substrate-bound conformations in the available crystal structures has hampered efforts to understand the structural basis of catalysis and sulfa drug resistance.

DHPS catalyzes the formation of a bond between the amino nitrogen of PABA and the C9 carbon of DHPP, with pyrophosphate as the leaving group. It has been suggested that the reaction proceeds by an S_N2-like mechanism (*14*), but the NH_2 group of PABA is a poor nucleophile, and crystal structures of DHPS with the substrate analog 6-hydroxymethyl pterin pyrophosphate (PtPP) and the product analog pteroate suggest that the required attack geometry is sterically disfavored (*9*). To visualize DHPP and PABA in the active site, we soaked both compounds into *Bacillus anthracis* DHPS (BaDHPS) crystals (table S1) (*16*). We found that both molecules in the asymmetric unit (molecules A and B) performed catalysis, leaving the product 7,8-dihydropteroate bound at the active site (Fig. 1A). This was unexpected because these crystals are grown at pH 9.0 and in 1.4 M sulfate, conditions that would be expected to hinder catalysis. The costructure closely resembles the pteroate costructure (*9*), and both have a sulfate ion instead of the eliminated pyrophosphate of DHPP in the anion-binding pocket. A new feature is the partial ordering of loop 2 in molecule A that packs onto the PABA moiety, which is now sandwiched between loop 2 and Lys^{220}. This is the first indication that one role of loop 2 is to stabilize the binding of PABA at the active site.

To investigate whether PABA is locked into place before product formation, we replaced PABA with *p*-hydroxybenzoic acid (PHBA), a less reactive PABA analog (*16*). The structure (table S1) showed that PHBA indeed binds in the same location as PABA, with a partially ordered loop 2 clamping it in place (Fig. 1B). The structure also revealed that DHPP had lost its pyrophosphate group in both molecules A and B, leaving the dihydropterin core in the pterin-binding pocket. There is no evidence of an OH group at C9 that would result from hydrolysis of an unstable carbocation. This structure confirms that the pyrophosphate is not removed by an S_N2 nucleophilic attack but is eliminated in a manner consistent with an S_N1 reaction.

We explored alternatives to an S_N2 mechanism by performing quantum chemical modeling of the initial step of a "pure" S_N1 reaction: the cleavage of the C9–O bond of DHPP in the absence of PABA (figs. S1 and S2) (*16*). Three key results resulted from these computational analyses: (i) The barrier to bond breaking is only ~24 kcal mol^{-1}; (ii) the essential Mg^{2+} ion (*17*) adds the leaving pyrophosphate α-oxygen to its coordination shell, thereby acting as a Lewis acid and assisting pyrophosphate elimination; and (iii) the carbocation formed at the C9 position is stabilized by charge delocalization into the pterin ring. This predicted scenario is analogous to the S_N1 mechanism of the prenyltransferases (*18*, *19*). Natural bond order analyses (*20*) before and after bond breaking indicate resonance stabilization of the carbocation that includes a partial iminium character of N8. We propose that this cationic intermediate, which we term DHP^+, is the dihydropterin core species that we observe in the crystal structure.

The calculations suggest that DHPS can slowly release pyrophosphate from DHPP independent of PABA binding at the active site. To test this, we soaked BaDHPS crystals in DHPP without PABA (*16*), and the structure (table S1) revealed that pyrophosphate had indeed been released from DHPP (Fig. 1C). Loop 2 was completely disordered, which supports its role in helping to lock PABA onto the surface of Lys^{220}. The calculations also support the essential role of the Mg^{2+} ion (*17*), and we confirmed this experimentally for BaDHPS (fig. S3A) (*16*). To visualize the effect of removing Mg^{2+}, we presoaked crystals in EDTA to remove Mg^{2+}, and then added EDTA and DHPP for a further 3 hours of soaking (*16*). The resulting structure (table S1) showed that pyrophosphate is still cleaved from DHPP but remains trapped in the anion-

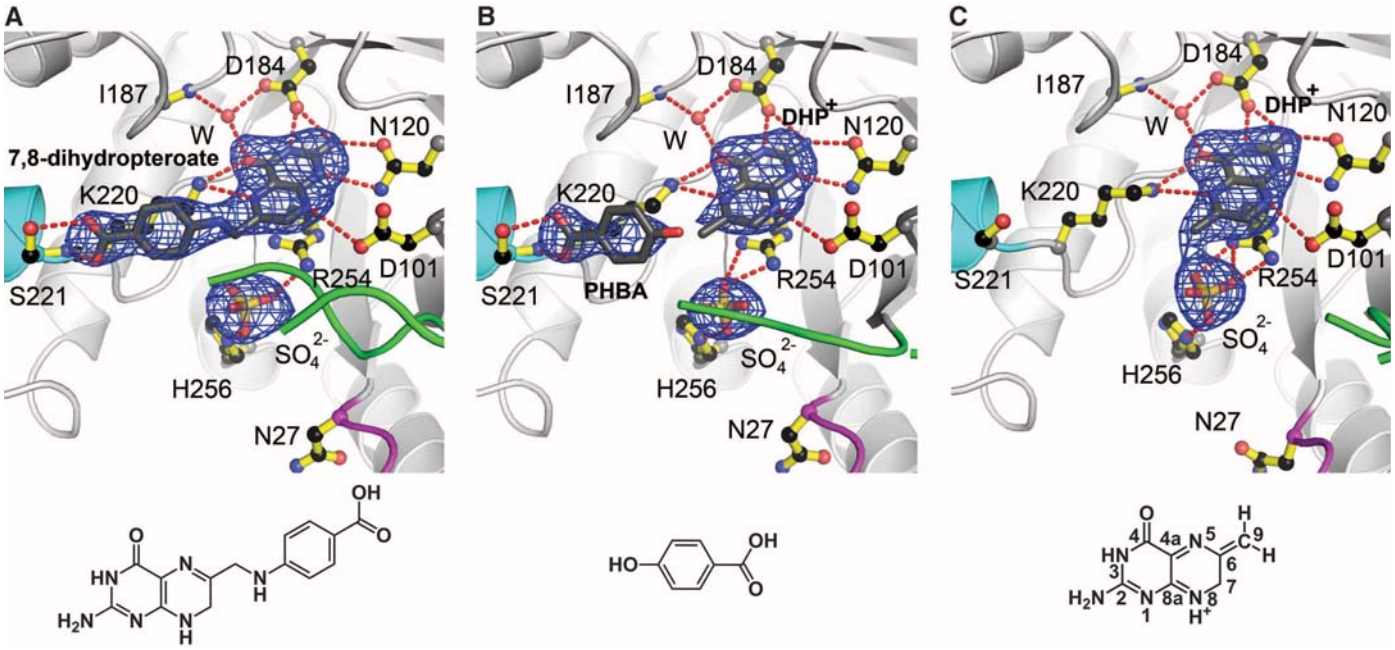

Fig. 1. Products generated by crystalline BaDHPS. (**A**) The product 7,8-dihydropteroate after soaking crystals in DHPP, PABA, and Mg^{2+}. (**B**) DHP^+ and PHBA after soaking crystals in DHPP, PHBA, and Mg^{2+}. (**C**) DHP^+ after soaking crystals in DHPP and Mg^{2+}. In each figure, loop 1 is shown in magenta, loop 2 in green, and the N terminus of helix αloop7 in teal; a sulfate ion (yellow/red) occupies the anion-binding pocket. The surrounding protein is shown in light gray; carbon, oxygen, and nitrogen atoms are shown as black, red, and blue balls, respectively; covalent bonds are shown in yellow, and hydrogen bonds are shown with red dashes. The $F_{obs} - F_{calc}$ electron densities were generated from refined structures in which the indicated ligands were omitted and are contoured at 3σ. Below each panel is the structure of the key molecule bound in the complex. DHP^+ is bound in both (B) and (C), but the structure is only shown in (C) with the pterin ring atoms numbered. W indicates an ordered water molecule in the pterin-binding pocket. Abbreviations for amino acids: D, Asp; H, His; I, Ile; K, Lys; N, Asn; R, Arg; S, Ser.

binding pocket, where it appears to stabilize the conformations of loop 1 and loop 2 (fig. S4). Therefore, Mg^{2+} is not absolutely required for the cleavage of pyrophosphate from DHPP but may play a key role in its release from the enzyme.

We also completed two crystal structures of *Yersinia pestis* DHPS (YpDHPS) (*16*): the apo structure (fig. S5A and table S2) and the complex with pteroate (fig. S5B and table S2). Although both structures closely resemble those of BaDHPS (*9*), two features particularly recommend them for mechanistic studies: Loop 1 and loop 2 are both unconstrained by crystal contacts in the apo structure and are free to adopt functional conformations, and the crystals are grown in more physiological conditions (pH 6 to 7 and 12% PEG 20,000).

Soaking DHPP and PABA into YpDHPS crystals gave a structure (table S2) that apparently shows the enzyme near the transition state (Fig. 2A, fig. S6A, and movie S1). In both molecules in the asymmetric unit, PABA, DHP^+, pyrophosphate, and a Mg^{2+} ion are all present within a highly organized loop 1 and loop 2 substructure prior to product formation. The released pyrophosphate occupies a pocket comprising residues Ser^{32}, Ser^{34}, and Asp^{35} from loop 1 (the latter two residues via an ordered water molecule), Ser^{66} and Thr^{67} from loop 2, and Arg^{254} and His^{256} from the anion-binding site (we use BaDHPS numbering; the sequence alignment is shown in fig. S7). The Mg^{2+} ion is octahedrally coordinated with the two distal oxygen atoms of the pyrophosphate, the Oδ1 oxygen of Asn^{27}, and three water molecules. The entire active site is covered by the distal end of loop 1 encompassing Pro^{30} to Gly^{37}, which forms a β-ribbon structure. The component residues make a number of stabilizing interactions; Asp^{31} is clamped between Arg^{68} and Arg^{82}, Ser^{32} interacts with the pyrophosphate as noted above, Ser^{34} interacts with Arg^{219}, and Asp^{35} interacts with Asn^{27}.

The YpDHPS complex structure (Fig. 2A) explains three key features of the catalytic mechanism and the active site. First, it explains that an essential role of Mg^{2+} is to order the loop 1–loop 2 substructure, as well as to stabilize the leaving pyrophosphate. The conformations and locations of the active-site residues, the bound substrates, and the Mg^{2+} ion closely match those of the computed state in which the C–O bond has been broken (fig. S2D, RMSD = 0.77 Å) (*16*). Second, it explains why the residues within the two loops are so highly conserved. Finally, it explains why the PABA-binding site has been so difficult to visualize: It is only fully formed in this complex. Phe^{33} from loop 1, Pro^{69} from loop 2, and Lys^{220} and Phe^{189} are all highly conserved, and they combine to form the PABA-binding pocket. Also, loop 1 forms a protective lid over the active site with a restricted entrance that matches the shape and chemistry of PABA. Consistent with our previous results (*9*), the carboxylate moiety of PABA is accommodated by Ser^{221} and the helix dipole of helix αloop7.

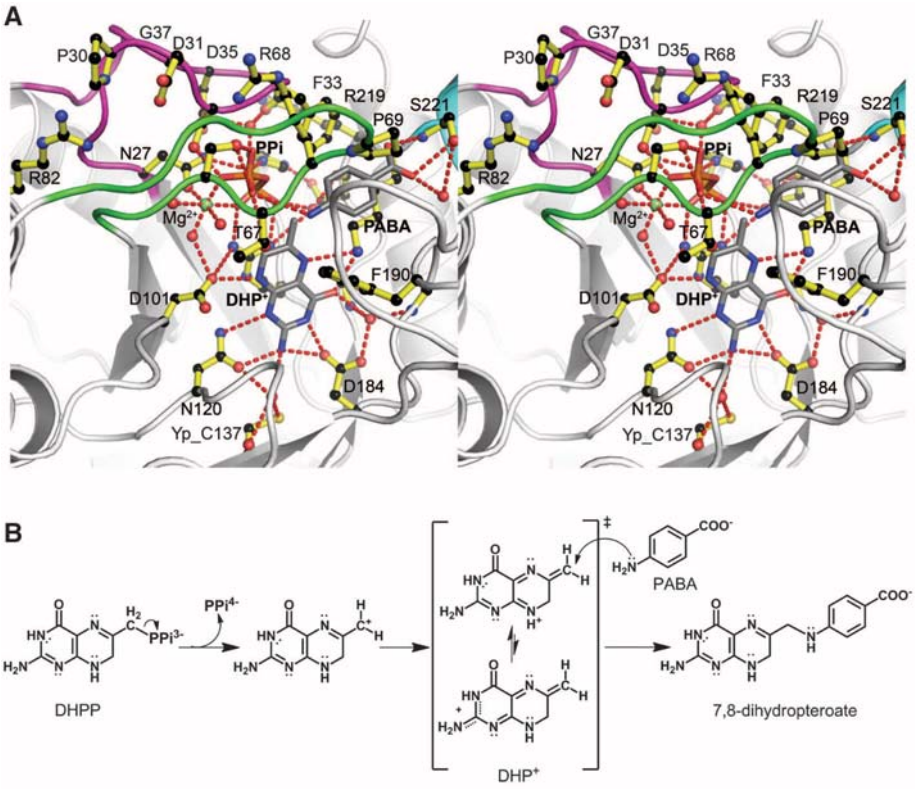

Fig. 2. The DHPS catalytic mechanism. (**A**) Stereo view of the *Y. pestis* (Yp) DHPS ordered active site generated from YpDHPS crystals soaked in DHPP, PABA, and Mg^{2+}. Loop 1 (magenta), loop 2 (green), and an octahedrally coordinated Mg^{2+} ion (green ball) are all organized by the pyrophosphate (PPi; orange/red), and a PABA molecule is bound within a specific binding pocket. Note that loop 1 caps the active site via a distal β-ribbon substructure, and the distal Pro^{69} of loop 2 engages the bound PABA. The residue numbering corresponds to BaDHPS. (**B**) The proposed S_N1 chemical reaction catalyzed by DHPS. Pyrophosphate is first removed from DHPP. The resulting cationic intermediate species can adopt the DHP^+ resonance forms shown in the square brackets in which the positive charge is delocalized into the pterin rings and stabilized by the pterin-binding pocket. The amine group of PABA finally attacks DHP^+ at the C9 carbon atom to generate the product 7,8-dihydropteroate. Abbreviations for amino acids: C, Cys; D, Asp; F, Phe; G, Gly; H, His; I, Ile; K, Lys; N, Asn; P, Pro; R, Arg; S, Ser; T, Thr.

Table 1. Kinetic parameters of wild-type and mutant BaDHPS. k_{obs}, observed turnover number; K_m, Michaelis constant; ND, activity too low to detect.

Enzyme	DHPP		PABA	
	k_{obs} (s^{-1})	K_m (μM)	k_{obs} (s^{-1})	K_m (μM)
Wild type	0.545 ± 0.0068	3.16 ± 0.150	0.520 ± 0.0136	1.78 ± 0.218
N27A	0.007 ± 0.0001	5.82 ± 0.237	ND	
F33A	0.239 ± 0.0032	3.94 ± 0.192	0.789 ± 0.0327	507.90 ± 33.070
F33L	0.318 ± 0.0041	4.83 ± 0.210	0.563 ± 0.0086	185.90 ± 6.422
D35A	1.100 ± 0.0156	4.24 ± 0.210	0.999 ± 0.0117	71.21 ± 2.956
S66A	0.443 ± 0.0086	2.76 ± 0.215	0.459 ± 0.0088	14.45 ± 0.767
D101N	0.087 ± 0.0021	1.63 ± 0.192	0.086 ± 0.0010	3.57 ± 0.141
D184N	ND		ND	
K220Q	0.086 ± 0.0023	35.47 ± 1.735	0.177 ± 0.0111	410.20 ± 42.480

Our data show that the role of the pterin-binding pocket is to first bind DHPP and then promote the release of pyrophosphate by stabilizing a carbocation on the C9 carbon. The likely roles of the conserved Asp^{184} and Asp^{101} are to stabilize resonance forms that move the positive charge away from this primary carbocation and toward the N3/2-amino and N8 nitrogen atoms, respectively, either by ionic interactions or by proton abstraction (*16*). The electrophilic DHP^+ intermediate can then react with the incoming PABA nitrogen via nucleophilic conjugate addition. We showed experimentally (*16*) that the release of pyrophosphate, and presumably the dis-

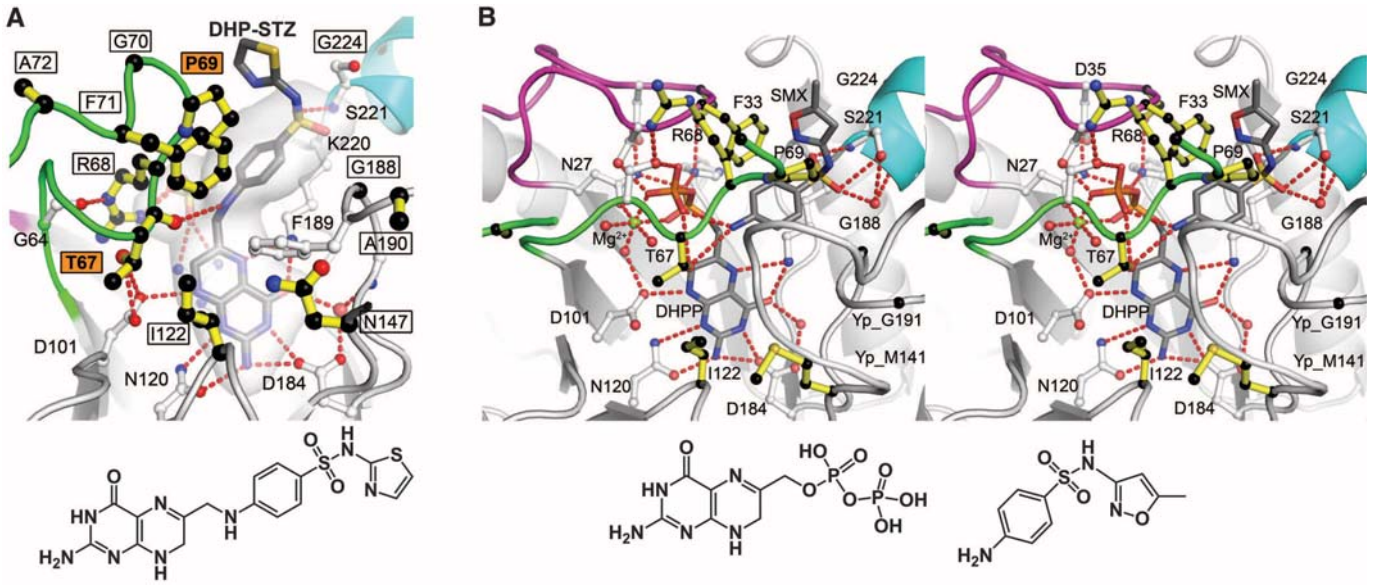

Fig. 3. Sulfa drug mechanism and resistance. (**A**) *B. anthracis* (Ba) DHPS crystals soaked in DHPP and STZ reveal a covalent DHP-STZ adduct bound at the active site and stabilized by an ordered loop 2. The boxed labeled residues are sites of sulfa drug resistance, and two major sites are labeled in boxed orange. The molecular envelope (light gray) encompasses the binding pockets for pterin, PABA, and the anion (PPi or sulfate). Note that the thiazole ring of STZ extends outside this pocket directly adjacent to Pro^{69}. The structure of DHP-STZ is shown below. (**B**) Stereo view of the *Y. pestis* (Yp) DHPS active site occupied by DHPP, sulfamethoxazole (SMX), and an octahedrally coordinated Mg^{2+} ion. The structure is very similar to that shown in Fig. 2A with PABA in place of SMX. One difference from the PABA structure is that DHPP is intact with the pyrophosphate covalently attached. The residue numbering corresponds to BaDHPS. The structures of DHPP and SMX are shown below. In both figures, loop 1 is shown in magenta, loop 2 in green, and the N terminus of helix αloop7 in teal. Abbreviations for amino acids: A, Ala; D, Asp; F, Phe; G, Gly; I, Ile; K, Lys; N, Asn; P, Pro; R, Arg; S, Ser; T, Thr.

solution of the intermediate-state substructure, is promoted by PABA (fig. S3B). The S_N1 mechanism that we propose is shown in Fig. 2B.

We prepared eight active-site BaDHPS mutants to test this proposal (*16*). The kinetic parameters were measured using an assay that monitors pyrophosphate release (*16*), and the results are summarized in Table 1. Parallel assays were performed in the presence of high (200 μM) PABA and high (50 μM) DHPP to allow independent measurements of the binding affinities of the two substrates. In general, the mutations support the proposed mechanism and the intermediate-state substructure shown in Fig. 2A. Loop 1 mutations Asn^{27} → Ala (N27A), Phe^{33} → Ala (F33A), Phe^{33} → Leu (F33L), and Asp^{35} → Ala (D35A) and loop 2 mutation Ser^{66} → Ala (S66A) all primarily affected the binding of PABA and had little effect on the binding of DHPP. Each of these residues, directly or indirectly, contributes to the PABA-binding site. The pterin-pocket mutants, Asp^{101} → Asn (D101N) and Asp^{184} → Asn (D184N), were designed to investigate the effect of removing these negative charges. D184N was unable to bind DHPP because the asparagine side chain adopts a rotamer that prevents its interaction with the pterin ring (table S1 and fig. S8). However, D101N showed efficient binding to both DHPP and PABA but had a much reduced k_{obs}. Finally, Lys^{220} → Gln (K220Q) showed reduced binding to PABA and DHPP, consistent with the role of Lys^{220} in binding both substrates.

To investigate the mechanism of the sulfa drugs, we soaked BaDHPS crystals in DHPP and sulfathiazole (STZ) and determined the structure (table S1) (*16*). Molecule A revealed a clear DHP-STZ product (Fig. 3A) similar to that of the normal product (Fig. 1A), whereas molecule B revealed the bound drug before complex formation, similar to the PHBA complex (Fig. 1B). This finding is consistent with previous studies showing that sulfa drugs can replace PABA as DHPS substrates (*21*, *22*). We then soaked DHPP and SMX into YpDHPS crystals and obtained a structure (Fig. 3B, fig. S6B, table S2, and movie S2) similar to that observed with DHPP and PABA (Fig. 2A) (*16*). In molecules A and B, DHPP is bound and loop 1 and loop 2 are ordered by pyrophosphate and an octahedrally coordinated Mg^{2+} ion, but only molecule B contains SMX in the PABA-binding pocket. A difference from the YpDHPS PABA/DHPP structure (Fig. 2A) is that pyrophosphate remains attached to DHPP, but this has little effect on the loop conformations because both the location and Mg^{2+} coordination of the pyrophosphate are unaffected.

The YpDHPS sulfa drug complex reveals the drug binding site. SMX perfectly fits the PABA-binding pocket, with the negatively charged oxygen atoms of the sulfonyl group matching the PABA carboxyl group and their common phenyl groups engaging the same hydrophobic pocket in the loop 1–loop 2 substructure. Figure 3B shows that the common sites of resistance are all clustered around this substructure. Phe^{33}, Thr^{67}, and Pro^{69} are frequently observed sites of resistance mutations (*14*) and form key elements of the PABA-binding site. It has been observed that resistance is typically associated with regions of a drug that extend beyond the substrate envelope (*23*). Figure 3A reveals that the thiazole and methoxazole rings of STZ and SMX, which have no counterparts in PABA, are positioned outside the DHPS substrate envelope and are located such that mutations at Phe^{33} and Pro^{69} can impede sulfa drug binding.

References and Notes

1. L. B. Rice, *Curr. Opin. Microbiol.* **12**, 476 (2009).
2. O. Sköld, *Drug Resist. Updat.* **3**, 155 (2000).
3. P. Huovinen, *Clin. Infect. Dis.* **32**, 1608 (2001).
4. N. Anand, in *Burger's Medicinal Chemistry and Drug Discovery, Vol. 2, Therapeutic Agents*, M. E. Wolff, Ed. (Wiley-Interscience, New York, ed. 5, 1996), pp. 527–573.
5. P. A. Masters, T. A. O'Bryan, J. Zurlo, D. Q. Miller, N. Joshi, *Arch. Intern. Med.* **163**, 402 (2003).
6. D. Y. Hyun, E. O. Mason, A. Forbes, S. L. Kaplan, *Pediatr. Infect. Dis. J.* **28**, 57 (2009).
7. G. Pappas, A. P. Athanasoulia, D. K. Matthaiou, M. E. Falagas, *J. Chemother.* **21**, 115 (2009).
8. S. Merali, Y. Zhang, D. Sloan, S. Meshnick, *Antimicrob. Agents Chemother.* **34**, 1075 (1990).
9. K. Babaoglu, J. Qi, R. E. Lee, S. W. White, *Structure* **12**, 1705 (2004).
10. K. E. Hevener *et al.*, *J. Med. Chem.* **53**, 166 (2010).
11. C. W. Pemble 4th *et al.*, *PLoS ONE* **5**, e14165 (2010).
12. A. Achari *et al.*, *Nat. Struct. Biol.* **4**, 490 (1997).
13. I. C. Hampele *et al.*, *J. Mol. Biol.* **268**, 21 (1997).
14. A. M. Baca, R. Sirawaraporn, S. Turley, W. Sirawaraporn, W. G. Hol, *J. Mol. Biol.* **302**, 1193 (2000).
15. C. Levy, D. Minnis, J. P. Derrick, *Biochem. J.* **412**, 379 (2008).
16. See supporting material on *Science* Online.
17. F. Rébeillé, D. Macherel, J. M. Mouillon, J. Garin, R. Douce, *EMBO J.* **16**, 947 (1997).
18. E. A. Mash, G. M. Gurria, C. D. Poulter, *J. Am. Chem. Soc.* **103**, 3927 (1981).
19. C. D. Poulter, P. L. Wiggins, A. T. Le, *J. Am. Chem. Soc.* **103**, 3926 (1981).
20. A. E. Reed, L. A. Curtiss, F. Weinhold, *Chem. Rev.* **88**, 899 (1988).

21. L. Bock, G. H. Miller, K. J. Schaper, J. K. Seydel, *J. Med. Chem.* **17**, 23 (1974).
22. S. Roland, R. Ferone, R. J. Harvey, V. L. Styles, R. W. Morrison, *J. Biol. Chem.* **254**, 10337 (1979).
23. K. P. Romano, A. Ali, W. E. Royer, C. A. Schiffer, *Proc. Natl. Acad. Sci. U.S.A.* **107**, 20986 (2010).

Acknowledgments: We thank R. DuBois, C. Pemble, S. Gajewski, and D. Miller for assistance with the YpDHPS structure determination; J. Bollinger and E. Enemark for technical assistance; D. Hammoudeh and C. Rock for helpful discussions; and staff at SERCAT for assistance with synchrotron data collection. Supported by NIH grant AI070721 (S.W.W. and R.E.L.), NIH Cancer Center (CORE) support grant CA21765, and ALSAC (the American Lebanese Syrian Associated Charities). The content is solely the responsibility of the authors and does not necessarily represent the official views of the NIH. Data were collected at Southeast Regional Collaborative Access Team (SER-CAT) 22-ID and 22-BM beamlines at the Advanced Photon Source, Argonne National Laboratory. Supporting institutions may be found at www.ser-cat.org/members.html. Use of the Advanced Photon Source was supported by the U.S. Department of Energy, Office of Science, Office of Basic Energy Sciences, under contract W-31-109-Eng-38. Coordinates and structure factors for all the structures described have been deposited in the Protein Data Bank, and the PDB accession codes are listed in tables S1 and S2.

Supporting Online Material

www.sciencemag.org/cgi/content/full/335/6072/1110/DC1
Materials and Methods
Figs. S1 to S8
Tables S1 and S2
References (*24*–*40*)
Movies S1 and S2

29 September 2011; accepted 11 January 2012
10.1126/science.1214641

Identification of the Social and Cognitive Processes Underlying Human Cumulative Culture

L. G. Dean,[1] R. L. Kendal,[2]* S. J. Schapiro,[3] B. Thierry,[4] K. N. Laland[1]*

The remarkable ecological and demographic success of humanity is largely attributed to our capacity for cumulative culture, with knowledge and technology accumulating over time, yet the social and cognitive capabilities that have enabled cumulative culture remain unclear. In a comparative study of sequential problem solving, we provided groups of capuchin monkeys, chimpanzees, and children with an experimental puzzlebox that could be solved in three stages to retrieve rewards of increasing desirability. The success of the children, but not of the chimpanzees or capuchins, in reaching higher-level solutions was strongly associated with a package of sociocognitive processes—including teaching through verbal instruction, imitation, and prosociality—that were observed only in the children and covaried with performance.

The success of humanity in colonizing virtually every terrestrial habitat on the planet and resolving countless ecological, social, and technological challenges is widely attributed to our species' unique capability for "cumulative culture"—the extensive accumulation of knowledge, and iterative improvements in technology, over time (*1*, *2*). Although many animals—especially mammals, birds, and fishes—acquire knowledge and skills from others (often manifest in behavioral traditions), in no instance have these unambiguously exhibited "ratcheting" in complexity (*2*). Given that the adaptive value of cumulative learning is well established (*1*, *3*, *4*), the question as to why social learning is so much more widespread than cumulative culture constitutes a major evolutionary puzzle (*1*, *4*–*7*).

Although claims have been made for cumulative culture in other species (*8*–*10*), the evidence is circumstantial and contested (*2*, *5*, *6*, *11*). The resulting debate has spawned a large number of distinct hypotheses concerning the cognitive capabilities, or social conditions, thought to be necessary for cumulative culture. These explanations include a hypothesized critical dependency of cumulative culture on aspects of social cognition deemed to be exclusive to (or substantially enhanced in) humans, including teaching (henceforth hypothesis 1, or *H1*), language (*H2*), imitation (*H3*), and prosociality (*H4*) (*1*, *2*, *4*, *5*, *11*–*14*). Other explanations stress features of social structure that mitigate against the spread of superior solutions in animals other than humans, including scrounging (kleptoparasitism; *H5*), which can hinder social learning and demotivate resource production (*15*); the tendency of dominant individuals to monopolize resources, thereby preventing subordinates from learning (*H6*) (*16*); and a lack of attention to low-status inventors (*H7*) (*17*, *18*). A further (nonsocial cognition) hypothesis is that satisficing, or conservative behavior, hinders ratcheting in nonhumans (*H8*) (*8*, *19*). Large social networks (*20*, *21*) may enhance cultural diversity and promote cumulative culture, but we do not consider this hypothesis because it presupposes the existence of the necessary cognitive capabilities.

Cumulative culture has been investigated through historical analysis (*22*), in the psychological laboratory (*23*), and through experimentation in chimpanzees (*14*). However, until now, there has been no extensive and rigorous experimental investigation of the capacity for cumulative cultural learning that simultaneously tests humans and other animals using the same apparatus and that is capable of evaluating all of the aforementioned hypotheses. Here, we present such an investigation.

We designed a puzzlebox (Fig. 1) that could be solved at three stages of difficulty, with success at stage 2 building on stage 1 and success at stage 3 building on stage 2. We presented appropriately scaled versions, under a variety of conditions, to groups of children ($N = 35$, eight groups of 3- to 4-year-olds from three nurseries in Fife, UK), chimpanzees (*Pan troglodytes*; $N = 74$, eight mixed juvenile and adult groups at the Michale E. Keeling Center for Comparative Medicine and Research, University of Texas), and capuchin monkeys (*Cebus apella*; one group over 2 years, year 1 $N = 22$, year 2 $N = 18$, at the Centre de Primatologie, Strasbourg) (see supporting online material). All stages could be completed through two parallel options (Fig. 1), allowing us to investigate cooperation, tolerance, and social learning at the task; presentation in social groups allowed solutions to each level to spread among individuals. Experiment 1 included two conditions: an "open" condition, where groups could gain access to all stages and a "scaffolded" condition, where guards prevented access to the manipulandi associated with higher stages until performance at the lower stage reached criterion. In experiment 2, conducted only with chimpanzees, one female from each of four additional groups was isolated from her group and trained to use the puzzlebox to stage 3. The use of trained females of differing status as demonstrators allowed investigation of how social rank affected the spread of solutions.

Chimpanzees and capuchins were selected because the evidence for cultural traditions is as strong in these species as in any nonhuman (*24*, *25*), maximizing the chances of observing cumulative cultural learning. Moreover, chimpanzees, as our closest relative, provide an appropriate comparator to humans, with the performance of capuchins aiding interpretation of any chimpanzee-human differences. Children are widely used in comparative studies [e.g., (*26*)] to help tease out the effects of culture, as adults have been greatly enculturated by society.

We anticipated that children, but not chimpanzees or capuchins, would exhibit evidence of cumulative cultural learning, and the study was designed to sort between alternative explanations

[1]Centre for Social Learning and Cognitive Evolution, School of Biology, University of St. Andrews, Queen's Terrace, St. Andrews, Fife KY16 9TS, UK. [2]Centre for the Coevolution of Biology and Culture, Department of Anthropology, University of Durham, Durham DH1 3LE, UK. [3]Michale E. Keeling Center for Comparative Medicine and Research, University of Texas M.D. Anderson Cancer Center, Bastrop, TX 78602, USA. [4]Département Ecologie, Physiologie et Ethologie, Institut Pluridisciplinaire Hubert Curien, Centre National de la Recherche Scientifique, Université de Strasbourg, F-67087 Strasbourg, France.

*To whom correspondence should be addressed. E-mail: rachel.kendal@durham.ac.uk (R.L.K.); knl1@st-andrews.ac.uk (K.N.L.)

for this. For a hypothesis to be deemed supported (i.e., not falsified), we specified that it should satisfy two criteria: (i) Differences in the relevant predictor variable should covary with differences in species' mean performance in the cumulative task, in the predicted direction; and (ii) within-species variation in the relevant predictor should covary with variation in individual performance within species, in the predicted direction. Thus, we used analyses of covariation, both between and within species, to reject causal hypotheses that were inconsistent with the data. We further assumed that the manner in which social or cognitive processes currently operate is qualitatively similar to the manner in which they operated in ancestral environments. Hence, although our study sought to identify the proximate processes underlying cumulative cultural learning in contemporary populations, the same processes were potentially ancestral sources of selection.

Performance with the puzzlebox is summarized in Fig. 2A. After 30 hours of presentation of the task to each of four chimpanzee groups, only 1 of 33 individuals reached stage 3, with a further 4 having reached stage 2, and with each group having witnessed multiple solvers at stage 1 (experiment 1). Chimpanzee performance was not greatly enhanced by trained demonstrators (experiment 2), who performed stages 1 to 3 proficiently. A similar pattern was observed in the capuchins: After 53 hours, no individual reached stage 3 and only two individuals reached stage 2. Thus, the experiments provide no evidence for cumulative cultural learning in chimpanzees or capuchins. These findings stand in stark contrast to those of the children, where despite a far shorter exposure to the apparatus (2.5 hours), five of the eight groups had at least two individuals (out of a maximum of five) who reached stage 3, with multiple solvers at stages 2 or 3 in all but two groups (see supporting online material).

Analyses revealed support for four of the eight hypotheses (Fig. 2, B to E), suggesting that teaching, communication, observational learning, and prosociality all played important roles in human cultural learning but were absent (or played an impoverished role) in the learning of chimpanzees and capuchins.

A total of 23 unambiguous instances of teaching by direct instruction (i.e., referencing part of the puzzlebox) were observed ($\bar{x} = 0.69 \pm 0.32$), exclusively in the children (*H1*) (Fig. 2B), of which all involved task-relevant communication (e.g., "push that button there") and approximately one-third involved gesture. A strong positive relationship was observed between the amount of instruction received and the stage reached by a child [Spearman's $\rho = 0.598$, $P = 0.0001$ (*27*)]. Such an analysis fails to consider teaching precursors, or subtle processes similar to teaching, such as "pedagogical cuing" (*28*) or "scaffolding" (*29*). To explore whether chimpanzees or capuchins might facilitate learning in others (e.g., through enlisting offspring's interest in the task), we examined rates of both provisioning and food-calling by "knowledgeable" individuals. However, we observed substantially greater rates of tolerated theft of extracted food by mothers from offspring than vice versa in chimpanzees (Wilcoxon $W = 16$, $P = 0.026$) and no tolerated theft in mother-infant pairs of capuchins. Moreover, neither chimpanzees (Wilcoxon $W = 6.5$, $P = 0.77$) nor capuchins ($W = 9$, $P = 0.45$) exhibited any difference in the rate of recruitment of others to the puzzlebox before, versus immediately after, a food call, and low rates of calling were observed; in contrast, children who received verbal instruction outperformed those who did not (*H2*) (Mann-Whitney $U = 41$, $P = 0.002$; Fig. 2C).

We also compared the rate at which individuals from each species, in their first response or during the subsequent minute, performed a matching manipulation (e.g., copy push down button on left) to that observed being performed by another individual departing the box (*H3*). Matching (table S6) could constitute copying the actions of others (i.e., imitation) or making the same manipulandi move in the same way (i.e., emulation). Children alone performed more matching than nonmatching manipulations (Wilcoxon $W = 163$, $P = 0.003$), they produced a significantly greater proportion of matching actions than both chimpanzees and capuchins (Kruskal-Wallis $\chi^2 = 18.13$, df = 2, $P = 0.001$; Fig. 2D), and the degree of matching they exhibited correlated positively with performance (Spearman's $\rho = 0.41$, $P = 0.01$). We observed chimpanzee social learning at stage 1 (option-bias analysis, $\chi^2 = 941.6$, $P = 0.021$) (*30*) but not at higher stages.

Regarding prosociality (*H4*), we hypothesized that if individuals voluntarily give rewards to others, this signifies an understanding that others share the motivation of achieving the goal that they had achieved. We observed 215 altruistic events where a child spontaneously gave another child a retrieved reward ($\bar{x} = 6.14 \pm 2.32$; 47% of children exhibited altruism), but not a single instance of the voluntary donation of food in either the chimpanzees or capuchins (Fig. 2E). The number of prosocial acts received covaried strongly with the stage that a child reached (Spearman's $\rho = 0.54$, $P = 0.001$). Moreover, the proportion of manipulations that children performed at the same time that another individual was in proximity was significantly greater than in either chimpanzees or capuchins, indicating greater tolerance of others, cooperation, and shared motivation among children.

The other four hypotheses failed to satisfy our criteria, providing little evidence that the capability for cumulative culture is affected by either social structure or nonsocial cognition. There was a positive, rather than the predicted negative, correlation between the amount of

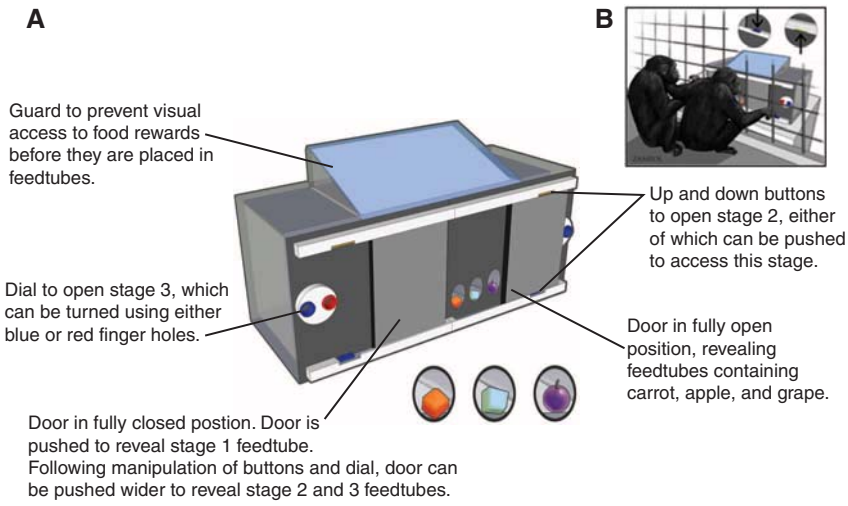

Fig. 1. (**A**). The cumulative culture puzzlebox, which could be solved at three sequential stages, each building on the preceding stage. (**B**) Illustration of puzzlebox use. Stage 1 required individuals to push a door in the horizontal plane to reveal a chute through which a low-grade reward was delivered. Stage 2 required individuals to depress a button and slide the door further to reveal a second chute for a medium-grade reward. Stage 3 required the solver to rotate a dial, releasing the door to slide still further to reveal a third chute containing a high-grade reward. All stages could be completed through two parallel options (alternative doors could be slid left or right at stage 1, alternative buttons at the top or bottom could be depressed at stage 2, and alternative colored finger holes enabled rotation of the dial at stage 3), with sets of three chutes on both left and right sides. This two-action, two-option design aided evaluation of alternative social learning mechanisms and allowed two individuals to operate the puzzlebox simultaneously. Replenishment of the chutes by the experimenter allowed the apparatus to be continuously used for long periods. Pilot work established an unambiguous ascendancy in the desirability of reward with stage (food stage 1 = carrot, 2 = apple, 3 = grapes for chimpanzees and capuchins; stickers of increasing size and attractiveness for children).

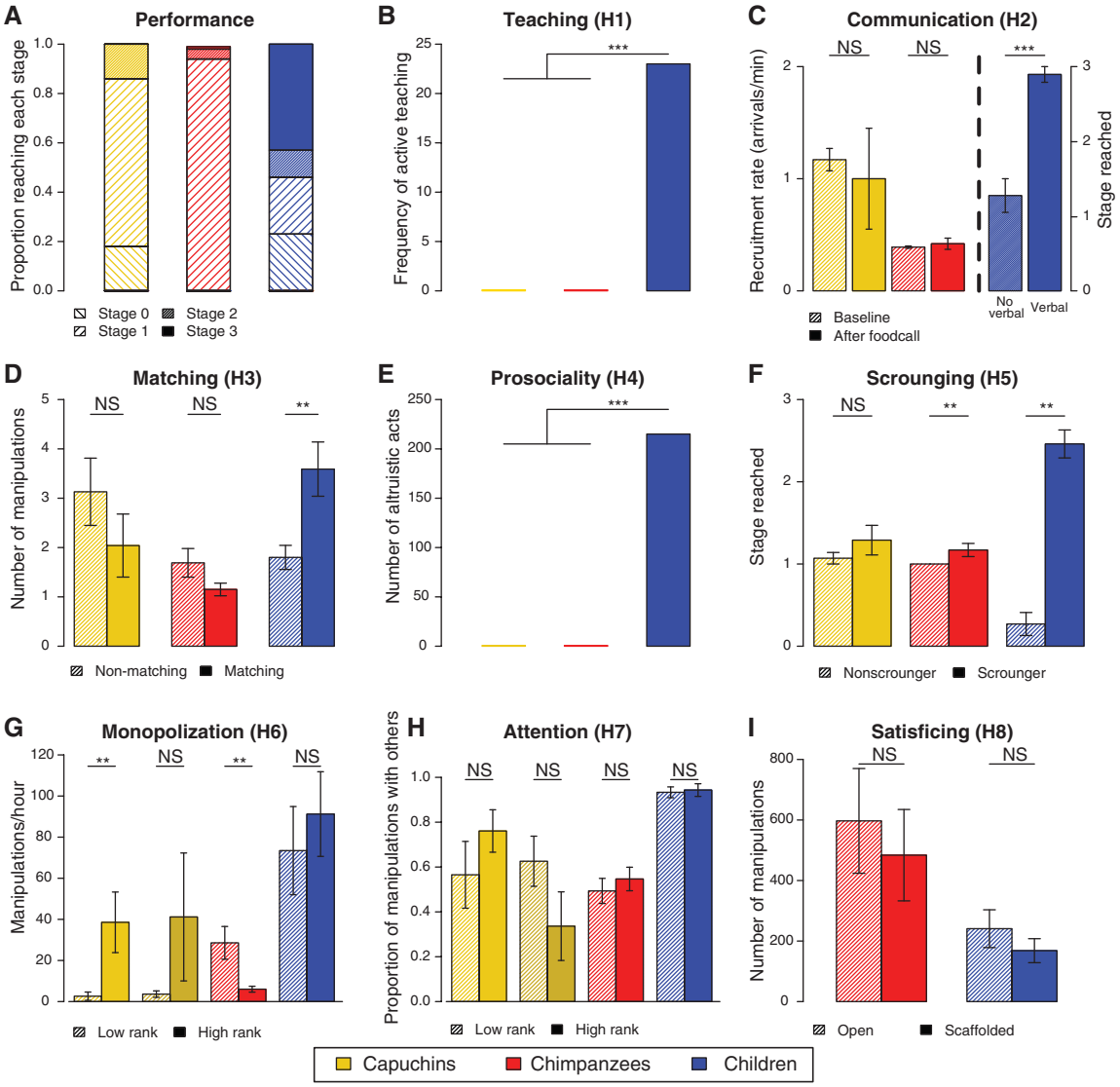

Fig. 2. (**A**) Attainment of stages 2 and 3 was exceptionally rare or absent in capuchins and chimpanzees but common in human children. (**B**) We observed 23 unambiguous instances of teaching, by direct instruction, exclusively in children. (**C**) In neither chimpanzees nor capuchins was there greater recruitment to the task after, versus before, a food call. Conversely, children who received verbal instruction outperformed those who did not. (**D**) Children alone performed more matching than nonmatching manipulations, and they produced a greater proportion of matching actions than did either chimpanzees or capuchins. (**E**) We observed 215 altruistic events (giving an extracted reward to others), exclusively in children. (**F**) There was no evidence that scrounging hindered performance in any species; children who were victims of scrounging outperformed children who were not. (**G**) Dominant children and chimpanzees did not monopolize the task, and high-ranking capuchins monopolized the puzzlebox in 2007 but not 2008. (**H**) Low-rankers did not receive less attention than high-rankers when manipulating the task. (**I**) In the open condition, where they received rewards at all stages, neither chimpanzees nor children manipulated the puzzlebox less than individuals in the scaffolded condition. In (G) and (H), capuchins (2007 and 2008 pale and dark yellow, respectively) and chimpanzees were split into three (high-, mid-, low-) rank categories, although for clarity and comparability with the child data, we present only analysis of high- versus low-ranked individuals. $^{**}P \leq 0.05$; $^{***}P \leq 0.01$; NS, not significant.

Table 1. Numbers (and percentages) of children reaching each stage, together with the amount of teaching, matching (e.g., imitation), and prosociality (altruism) exhibited.

Stage reached	Number of individuals (from *N* groups)	Number that received teaching	Number with more matching than nonmatching manipulations	Number that received altruism	Number that received no social support
0	8 (5)	0	1 (12.5%)	0	7 (87.5%)
1	8 (3)	0	4 (50%)	4 (50%)	3 (37.5%)
2	4 (3)	1 (25%)	1 (25%)	2 (50%)	1 (25%)
3	15 (5)	9 (60%)	11 (73%)	11 (73%)	0

scrounging an individual falls victim to and performance in capuchins (Spearman's $\rho = 0.71$, $P = 0.0002$), chimpanzees ($\rho = 0.312$, $P = 0.008$), and children ($\rho = 0.8$, $P = 6.87 \times 10^{-9}$), and no sign that scrounging hindered performance (*H5*) (Fig. 2F). Dominant children (Wilcoxon $W = 186$, $P = 0.15$) and chimpanzees [analysis of variance (ANOVA) $F_{2,72} = 3.49$, $P = 0.036$] did not monopolize the puzzlebox (*H6*), and although there was a positive correlation between rank and puzzlebox use among capuchins in 2007 (Kruskal-Wallis $\chi^2 = 8.23$, df = 2, $P = 0.016$), this was not repeated in 2008 ($\chi^2 = 0.13$, df = 2, $P = 0.93$) (Fig. 2G). When manipulating the box, low-rankers did not receive less attention (defined as having others within 1.5 m of the task) than high-rankers (*H7*) (Fig. 2H; capuchins 2007, Kruskal-Wallis $\chi^2 = 2.49$, df = 2, $P = 0.29$; capuchins 2008, $\chi^2 = 2.08$, df = 2, $P = 0.35$; chimpanzees, ANOVA $F_{2,72} = 1.22$, $P = 0.3$; children, Wilcoxon $W = 100$, $P = 0.61$), nor was there any evidence for satisficing or conservatism (*H8*) (Fig. 2I; chimpanzees, Mann-Whitney $U = 166.5$, $P = 0.42$; children, $U = 163$, $P = 0.54$), with individuals continuing to manipulate the dials and buttons of the puzzlebox after they had found the solution to stage 1. In the open condition, where they received rewards at all stages, both chimpanzees and children manipulated the puzzlebox slightly more, rather than less, than individuals in the scaffolded condition, despite the latter being unrewarded at the previous stage(s). Although we did not find a significant difference between the proportions of rewards scrounged at each stage in chimpanzees, they expressed clear and strong preferences for the three foodstuffs in pilot work, and olfactory holes in the doors allowed these foods to be detected in the apparatus prior to their extraction. Moreover, many of the chimpanzees performed failed attempts to access the foods by "termiting" (inserting stalks through the olfactory holes), and all 29 cases involved an attempt to reach the highest-stage food that was available. In the children and capuchins, more low-stage than high-stage rewards were scrounged, which reflects a greater motivation to retain high-grade rewards.

Thus, we found no support for the hypotheses that cumulative culture is absent in chimpanzees or capuchins because in these species the social transmission of superior solutions is hindered by scrounging, because dominant individuals monopolize key resources, because of a lack of attention to low-status innovators, because these animals satisfice, or because these animals were unable to discriminate higher-quality from lower-quality rewards. Nor can the results be easily dismissed as an artifact of captivity testing, as wild chimpanzees and capuchins have been subjected to long-term studies that reveal no unambiguous evidence for cumulative culture (*24*, *25*). Likewise, our animals cannot be described as "dysfunctional" because they have performed effectively in previous studies demonstrating social learning and tradition of noncumulative tasks (*31*, *32*).

Closer inspection of the children's behavior supports the conclusion that a package of social cognitive capabilities, encompassing teaching (largely through verbal instruction) as well as matching (e.g., imitation) and prosociality (altruism), was critical for performance at the highest level. Table 1 reveals that all children who reached level 3 received at least one form of social support and 86% received at least two types. Conversely, children who did not benefit from social support generally performed poorly in the task. These data not only provide clear and strong evidence for a cumulative cultural capability in the children but strongly link their elevated performance to their social cognition.

The puzzlebox experiment reveals clear and characteristic differences in cumulative cultural learning and patterns of social interaction among children, chimpanzees, and capuchin monkeys, highlighting sociocognitive processes that may be important for cultural transmission to "ratchet." The children responded to the apparatus as a social exercise, manipulating the box together, matching the actions of others, facilitating learning in others through verbal instruction and gesture, and engaging in repeated prosocial acts of spontaneous gifts of the rewards they themselves retrieved. In contrast, the chimpanzees and capuchins appeared to interact with the apparatus solely as a means to procure resources for themselves, in an entirely self-serving manner, largely independent of the performance of others, and exhibiting restricted learning that appeared primarily asocial in character.

Our findings, based on confirmation of predicted patterns of covariation both between and within species, constitute strong support for the view (*2*, *11*, *12*) that cumulative culture requires a package of key psychological processes—specifically, teaching through verbal instruction, imitation, and prosocial tendencies—that are present in humans but are absent or impoverished in chimpanzees and capuchins. The claim that these sociocognitive processes, rather than other effects, were directly responsible for the pattern of cumulative cultural learning observed in the children is supported by the positive relationships found between the stage reached and the amount of teaching, verbal instruction, and prosocial acts received, as well as between the stage reached and the amount of observational learning that took place (Table 1).

We reject as improbable the alternative causal hypotheses that performing well in the task caused elevated levels of the predictor variables or that some unspecified factor elevated both performance and the predictors. It is not clear why success in solving the task should cause children to imitate, be taught by, or receive rewards from others, nor how an unspecified third variable might account for our within-species data. For instance, although it is possible that the relationship between imitation and performance reflects the child's cognitive ability, this explanation cannot account for the relationships of both teaching and prosociality with performance, because in both cases the donor (of knowledge or reward) is a different individual from the learner. The most likely explanation is that aspects of human social cognition are directly responsible for the cumulative culture capability.

Human cultural traditions accumulate refinements over time, thereby producing both technology and other cultural achievements of astonishing complexity and diversity unprecedented in the rest of nature. Although numerous hypotheses have been proposed for this phenomenon, the explanation has for many years remained elusive. Our experiment provides a clear answer to this conundrum, providing strong support for the position advanced by Tomasello and colleagues (*2*, *11*, *12*, *33*) that "human social learners focus to a much greater degree than other nonhuman primates on the actual actions performed by others …[and]… that uniquely human forms of cooperation ... teaching and norms of conformity contribute to the cultural ratchet" [(*11*), p. 2413]. These findings pave the way for an exciting avenue of research into when and why this particular "package" of other-regarding sociocognitive capacities evolved.

References and Notes

1. R. Boyd, P. Richerson, *Culture and the Evolutionary Process* (Univ. of Chicago Press, Chicago, 1985).
2. M. Tomasello, in *Chimpanzee Cultures*, R. W. Wrangham, W. C. McGrew, F. B. M. de Waal, P. G. Heltne, Eds. (Harvard Univ. Press, Cambridge, MA, 1994), pp. 301–377.
3. M. Enquist, S. Ghirlanda, *J. Theor. Biol.* **246**, 129 (2007).
4. R. Boyd, P. Richerson, *Proc. Br. Acad.* **88**, 77 (1996).
5. B. G. Galef, *Hum. Nat.* **3**, 157 (1992).
6. C. M. Heyes, *Anim. Behav.* **46**, 999 (1993).
7. C. Boesch, M. Tomasello, *Curr. Anthropol.* **39**, 591 (1998).
8. C. Boesch, *Evol. Anthropol.* **12**, 82 (2003).
9. G. R. Hunt, R. D. Gray, *Proc. Biol. Sci.* **270**, 867 (2003).
10. C. Sanz, D. Morgan, *Int. J. Primatol.* **30**, 411 (2009).
11. C. Tennie, J. Call, M. Tomasello, *Philos. Trans. R. Soc. London Ser. B* **364**, 2405 (2009).
12. M. Tomasello, *The Cultural Origins of Human Cognition* (Harvard Univ. Press, Cambridge, MA, 1999).
13. K. N. Laland, *Learn. Behav.* **32**, 4 (2004).
14. S. Marshall-Pescini, A. Whiten, *Anim. Cogn.* **11**, 449 (2008).
15. L. Giraldeau, L. Lefebvre, *Anim. Behav.* **35**, 387 (1987).
16. S. Coussi-Korbel, D. Fragaszy, *Anim. Behav.* **50**, 1441 (1995).
17. S. Reader, K. Laland, *Int. J. Primatol.* **22**, 787 (2001).
18. D. Biro *et al.*, *Anim. Cogn.* **6**, 213 (2003).
19. C. Hrubesch, S. Preuschoft, C. van Schaik, *Anim. Cogn.* **12**, 209 (2009).
20. J. Henrich, *Am. Antiq.* **69**, 197 (2004).
21. K. R. Hill *et al.*, *Science* **331**, 1286 (2011).
22. G. Basalla, *The Evolution of Technology*, G. Basalla, W. Coleman, Eds. (Cambridge Univ. Press, Cambridge, 1988).
23. C. Caldwell, A. Millen, *Evol. Hum. Behav.* **29**, 165 (2008).
24. A. Whiten *et al.*, *Nature* **399**, 682 (1999).
25. S. Perry *et al.*, *Curr. Anthropol.* **44**, 241 (2003).
26. E. Herrmann, J. Call, M. V. Hernàndez-Lloreda, B. Hare, M. Tomasello, *Science* **317**, 1360 (2007).
27. We conducted two classes of analyses, cross-species comparisons and single-species analyses exploring the relationship between a predictor variable and performance. For the latter analyses, to render the

distribution continuous, we computed an "achievement rank" by combining the number of the stage reached and the number of successful manipulations (see supporting online material).
28. G. Csibra, G. Gergely, in *Processes of Change in Brain and Cognitive Development*, Y. Munakata, M. Johnson, Eds. (Oxford Univ. Press, Oxford, 2006), pp. 249–274.
29. D. Wood, J. S. Bruner, G. Ross, *J. Child Psychol. Psychiatry* **17**, 89 (1976).
30. R. L. Kendal, J. R. Kendal, W. Hoppitt, K. N. Laland, *PLoS ONE* **4**, e6541 (2009).
31. A. Whiten *et al.*, *Curr. Biol.* **17**, 1038 (2007).
32. M. Dindo, B. Thierry, A. Whiten, *Proc. R. Soc. B* **275**, 187 (2008).
33. M. Tomasello, M. Carpenter, J. Call, T. Behne, H. Moll, *Behav. Brain Sci.* **28**, 675 (2005).

Acknowledgments: Supported by the CULTAPTATION project (European Commission contract FP6-2004-NESTPATH-043434), a European Research Council Advanced Grant (EVOCULTURE, 232823) (K.N.L.), and a Royal Society Dorothy Hodgkin Fellowship (R.L.K.). Chimpanzees at M. D. Anderson Cancer Center were supported by NIH Cooperative Agreement RR-15090. We thank S. Pavonetti, A. Whiten, C. Caldwell, C. Tennie, M. Tomasello, C. van Schaik, the CCBC/EARG journal club (Durham), and members of the Laland lab for advice and/or useful comments on earlier drafts of our manuscript, and J. Zampol for drawing Fig. 1. All research was approved by the ethics committee at the University of St. Andrews and the relevant committees at the research facilities and follows the relevant legislation in the UK, USA, and France. Data are available from the authors upon request.

Supporting Online Material
www.sciencemag.org/cgi/content/full/335/6072/1114/DC1
Materials and Methods
Figs. S1 and S2
Tables S1 to S6

14 September 2011; accepted 23 January 2012
10.1126/science.1213969

The Effects of Experience and Attrition for Novice High-School Science and Mathematics Teachers

Gary T. Henry,[1]* C. Kevin Fortner,[2] Kevin C. Bastian[3]

Because of the current high proportion of novice high-school teachers, many students' mastery of science and mathematics depends on the effectiveness of early-career teachers. In this study, which used value-added models to analyze high-school teachers' effectiveness in raising test scores on 1.05 million end-of-course exams, we found that the effectiveness of high-school science and mathematics teachers increased substantially with experience but exhibited diminishing rates of return by their fourth year; that teachers of algebra 1, algebra 2, biology, and physical science who continued to teach for at least 5 years were more effective as novice teachers than those who left the profession earlier; and that novice teachers of physics, chemistry, physical science, geometry, and biology exhibited steeper growth in effectiveness than did novice non–science, technology, engineering, and mathematics teachers.

In the past two decades, the teacher labor market has dramatically changed in response to more employment opportunities for women, increased demand for teachers, and policies opening new pathways into the profession (*1*). For instance, the modal value of experience for U.S. teachers dropped from 15 years in 1987–1988 to 1 year in 2007–2008 (*2*). Additionally, turnover for beginning teachers is high: After just 5 years, nearly 50% of all novice teachers have exited the profession (*3*). This churn of beginning teachers in and out of public schools results in more students, particularly poor and/or ethnic minority students, being taught by novice teachers (*4*, *5*), and that in turn leads to reduced student achievement (*6*–*11*). Investigating the consequences of these teacher labor market conditions for high-school students' science and mathematics achievement—specifically, the effects of experience and attrition among novice teachers—will shed light on challenges facing education and career preparation in science and mathematics.

We quantified the growth in effectiveness of high-school science and mathematics teachers and the effects of those teachers who exit public school classrooms. We analyzed effectiveness using scores on standardized tests given to high-school students in three mathematics courses and four science courses. We define teachers' effectiveness in terms of the increases in their students' test scores, adjusted for the prior achievement of the individual students and for other student, classroom, and school covariates. Prior research shows that the average effectiveness of novice teachers increases during their first 3 years and flattens thereafter (*12*–*14*); and that after differences in effectiveness that are attributable to experience are removed, less effective teachers are more likely to exit the profession (*10*, *15*, *16*). We extended this research to investigate teacher effectiveness in specific high-school courses and addressed three questions: (i) To what extent do novice high-school science and mathematics teachers become more effective with additional experience? (ii) Are novice high-school science and mathematics teachers who exit public schools more or less effective than those who stay? [There is little published research on where teachers who exit public schools are subsequently employed, but it suggests that leaving for higher-paying jobs in the private sector is relatively rare (*17*).] (iii) Do the rates of change in effectiveness for high-school science and mathematics teachers vary by course?

Student outcomes are related to variations in many school-related factors, including leadership; an orderly environment; high student expectations; a focus on student outcomes; a positive school culture; parental involvement; and, most closely, to teachers' effectiveness (*18*, *19*). Teachers are the most important school-related variable explaining variation in student achievement (*12*, *18*, *20*), and teacher experience positively affects student performance (*6*–*11*). Most gains in effectiveness occur in the first 3 years of teachers' careers, with minimal increases thereafter (*13*).

It is likely that through teaching experience, trial and error, professional development, mentoring, and/or collaboration with fellow educators, teachers learn rapidly during their first few years on the job. However, some of the average increases in effectiveness that have been attributed to experience may be a statistical artifact caused by the exit of less effective early-career teachers, thereby overstating the year-to-year differences in the statistics related to experience. Recent research supports this second explanation, finding that exiting teachers are less effective than comparable teachers who remain in the profession (*10*, *15*, *16*). Here we disentangle the effects of teacher development from differential attrition among high-school teachers of science and mathematics courses.

To assess the effectiveness and attrition of novice science and mathematics teachers, we developed a data set from North Carolina containing end-of-course test scores for seven science and mathematics courses—algebra 1, algebra 2, geometry, biology, chemistry, physical science, and physics—and three other courses—English 1, U.S. history, and civics/economics—which we grouped together for the purposes of our analysis and label non-STEM (science, technology, engineering, and mathematics) courses. Our study sample included all teachers in tested subjects with less than 5 years of experience employed in any regular North Carolina public high school from 2005–2006 through 2009–2010. The most crucial feature of the data set is that students and teachers were linked on the basis of actual classroom rosters, which allowed us to match approx-

[1]Department of Public Policy and Education Policy Initiative at Carolina, University of North Carolina at Chapel Hill, Abernethy Hall, Campus Box 3435, Chapel Hill, NC 27599–3435, USA. [2]Department of Educational Policy Studies, College of Education, Georgia State University, 30 Pryor Street, Atlanta, GA 30303–3083, USA. [3]Department of Public Policy and Education Policy Initiative at Carolina, University of North Carolina at Chapel Hill, Abernethy Hall, Campus Box 3279, Chapel Hill, NC 27599–3435, USA.

*To whom correspondence should be adddressed. E-mail: gthenry@unc.edu

imately 93% of high-school teachers to students in their courses; to construct student, teacher, and classroom covariates; and to account for students who had multiple teachers for any course. In total, the sample included 1.05 million test scores, 624,842 unique students, and 7961 unique teachers with less than 5 years of experience.

The outcome variable analyzed was the students' score on a standardized exam: the North Carolina End-of-Course Tests. These exams are designed to test students' knowledge and skills based on the North Carolina Standard Course of Study objectives for each course, which follow the frameworks of the National Assessment of Educational Progress and recommendations from national standard-setting groups (*21*, *22*). The items on these tests covered a range of cognitive skills, from remembering to analyzing and evaluating; included four potential response options; and were designed to cover a range of difficulty from easy (25%) to medium (50%) to hard (25%). Multiple versions of each test with different items reduce teachers' ability to predict the items, while providing equivalent scores across different versions. For example, there were 12 versions of the chemistry test, each of which included 92 unique items, meaning that a total of 1104 items were in use during the study period (*21*). To remove any year-to-year differences in test scores and to estimate effects in standard deviation units (SDUs), we standardized all tests within course and year by centering observations on the mean and dividing by the standard deviation.

To assess the development and attrition of novice science and mathematics teachers, we estimated two sets of subject-specific models, in which focal development variables were four dichotomous experience indicators coded 1 for teachers with the designated experience level (1, 2, 3, or 4 years, respectively) and 0 for teachers with other experience levels (comparisons were to teachers with 0 prior years of experience). The two sets of models included different focal variables to measure the impact of teacher attrition and separate its effect from teacher development. Based on certified salary files supplied by the North Carolina Department of Public Instruction, the focal variable in model 1, labeled "leaves within 5 years," was coded 1 for teachers who leave North Carolina public schools before beginning a sixth year of service and 0 for all others; the focal variable in model 2, labeled "last year," was coded 1 for teachers in a given year who will not be paid as teachers in the following school year and 0 for all others. In model 1, the coefficient on "leaves within 5 years" provided an estimate of the overall average effectiveness of exiting teachers, while netting out the effects of attrition [see eq. 1 in the supporting online material (SOM)]. In model 2, the coefficient on the "last year" indicator estimated the average effectiveness of novice teachers in their final year, while removing the effect of teachers who will leave at the end of the year (which is commonly known as the marginal rate of return to experience). In addition, model 2 included interaction terms between experience and "last year" to allow the average effectiveness of departing teachers to vary based on the year of exit (see eq. 2 in the SOM).

To estimate differences in the rates of change of teachers' effectiveness by course, we combined all courses in a third model and substituted a continuous measure of experience and its squared term into the value-added models. In model 3, we interacted both experience measures with course indicator variables to compare slopes and rates of change by subject (see eq. 3 in the SOM). Results from this model compare the average returns to experience for novice science and mathematics teachers to those of novice teachers in non-STEM courses. All model specifications use value-added models with student, classroom, and school covariates, including students' prior test scores (Table 1).

We find (Table 2) that teachers of all four science subjects experience gains of at least 0.11 SDU ("2nd Year Teachers") between their first and second year of teaching, as compared to lesser gains of 0.06 to 0.09 SDU for all three mathematics courses and non-STEM courses. Second-year physics teachers post the largest gains of 0.38, with chemistry, physical science, and biology teachers posting gains of 0.17, 0.16, and 0.12 SDU, respectively. For all teachers, returns to experience diminish rapidly. The effectiveness of novice algebra 2, geometry, biology, and chemistry teachers peaks in their fourth year, whereas algebra 1, physics, and non-STEM teachers continue to increase in effectiveness through their fifth and final year that is included in this data set. In the middle panels of Table 2, the coefficients on the experience variables quantify the marginal rates of return to experience, separating out the effects of teachers who leave the next year, which are either larger or smaller than the coefficients on experience in model 1, depending on the effectiveness of teachers who exited.

Comparing average effectiveness, novice teachers who will remain teaching beyond 5 years are more effective in four of seven science and mathematics courses than teachers who will leave before completing 5 years (Table 2). In courses where differences are significant, the average difference in effectiveness for teachers who exit within 5 years ranges from −0.102 for physical science

Table 1. Covariates used in analyses.

Student Covariates	Classroom Covariates	School Covariates
1) Prior test scores (mathematics and reading)	1) Class size	1) School size
2) Classmates' prior test scores	2) Heterogeneity of prior achievement within the class	2) School size squared
3) Days absent	3) Advanced curriculum	3) Violent acts per 1,000 students
4) Structural mobility	4) Remedial curriculum	4) Total per-pupil expenditures
5) Within year mobility	5) Teacher out-of-field status	5) Average district teacher supplement
6) Other between year mobility		6) Racial/ethnic composition
7) Race/ethnicity		7) Concentration of poverty
8) Gender		
9) Poverty status		
10) Gifted		
11) Disability		
12) Currently limited English proficient		
13) Was limited English proficient		
14) Overage for grade		
15) Underage for grade		
16) Model 3 only: High school EOC exam (non-STEM courses as the reference group)		

Table 2. Average effectiveness of novice teachers who stay and who exit by course (focal variables only). All results are in comparison to first-year teachers who stay in North Carolina public schools for at least a second year. *, **, and *** indicate significance at the $P < 0.05$, $P < 0.01$, and $P < 0.001$ levels, respectively.

Focal Variables	Algebra 1	Algebra 2	Geometry	Biology	Chemistry	Physical Science	Physics	Non-STEM
2nd Year Teachers	0.056***	0.058*	0.091***	0.115***	0.168**	0.158***	0.378***	0.058***
3rd Year Teachers	0.066***	0.082**	0.125***	0.114***	0.197***	0.159***	0.311***	0.081***
4th Year Teachers	0.067***	0.098***	0.160***	0.122***	0.242***	0.156***	0.321***	0.084***
5th Year Teachers	0.084***	0.091**	0.142***	0.105***	0.236***	0.114**	0.393***	0.089***
Leaves within 5 Years	-0.071***	-0.074**	0.018	-0.036 *	-0.013	-0.102**	0.068	-0.013
2nd Year Teachers	0.050***	0.045	0.076***	0.104***	0.129*	0.101**	0.276**	0.051***
3rd Year Teachers	0.061***	0.083**	0.129***	0.106***	0.159**	0.145***	0.343***	0.079***
4th Year Teachers	0.075***	0.104***	0.133***	0.128***	0.233***	0.138**	0.306***	0.085***
5th Year Teachers	0.092***	0.102**	0.137***	0.110***	0.204***	0.108**	0.370***	0.089***
Last Year	-0.079*	-0.133**	-0.074*	-0.045	-0.192	-0.237***	0.007	-0.052**
2nd Year* Last Year	0.029	0.123	0.125*	0.049	0.248	0.270**	0.270	0.066*
3rd Year* Last Year	0.050	0.016	-0.006	0.048	0.275	0.096	-0.132	0.025
4th Year* Last Year	-0.063	0.018	0.206***	-0.030	-0.131	0.141	0.063	-0.001
5th Year* Last Year	-0.017	-0.017	-0.046	-0.024	0.393	0.041	-0.097	0.010
Cases	163,621	77,999	93,715	125,643	30,452	58,863	4,878	494,970
1st Year Teachers	882	316	364	455	146	293	53	1,479
2nd Year Teachers	848	324	378	507	199	311	60	1,653
3rd Year Teachers	666	268	305	426	155	260	47	1,492
4th Year Teachers	596	272	243	357	137	228	49	1,316
5th Year Teachers	496	208	220	297	128	195	46	1,138
Will Leave	470	184	195	366	116	239	51	904

to −0.036 for biology when compared to teachers with the same level of experience who stay. Exiting geometry, chemistry, and physics teachers are neither more nor less effective than those who stay.

In the middle panels of Table 2, we examine the effectiveness of exiting teachers in their final year of teaching ("last year"). Teachers in four science and mathematics courses—algebra 1, algebra 2, geometry, and physical science—and the non-STEM courses who leave the profession within 5 years are less effective in their last year on the job.

For non-STEM courses, novice teachers exhibit a positive slope and diminishing returns to experience (Table 3). Novice algebra 1 and algebra 2 teachers exhibit patterns similar to those of non-STEM teachers. Novice biology and physical science teachers exhibit higher rates of growth, but also rates of return to experience that dampen more quickly than those of non-STEM teachers. Finally, novice geometry, chemistry, and physics teachers show steeper slopes but diminishing returns to experience similar to those of non-STEM teachers.

Figure 1 shows the average effectiveness of teachers in each of their first 5 years in the profession, by subject, to allow effectiveness trajectories to be directly compared. On average, novice teachers' trajectories plateau or fall by their fifth year. Furthermore, the order of the lines indicates the consequences of the loss of experienced science and mathematics teachers when they are replaced by first-year teachers. These consequences, in terms of student achievement, are most sizable for physics and chemistry, representing losses of approximately 0.25 to 0.4 SDU, on average; then physical science, geometry, and algebra 2, representing losses between 0.1 and 0.2 SDU, on average; and finally, algebra 1, biology, and non-STEM, representing losses of less than 0.1 SDU, on average.

Table 3. Returns to experience for novice high-school teachers by course. *, **, and *** indicate significance at the $P < 0.05$, $P < 0.01$, and $P < 0.001$ levels, respectively.

Main Effects	Coefficient
Teaching Experience	0.0527***
Teaching Experience Squared	-0.0085***
Interaction Effects	**Coefficient**
Physics × Teaching Experience	0.1820*
Physics × Teaching Experience Squared	-0.0286
Chemistry × Teaching Experience	0.1026*
Chemistry × Teaching Experience Squared	-0.0135
Physical Science × Teaching Experience	0.0860**
Physical Science × Teaching Experience Squared	-0.0184**
Geometry × Teaching Experience	0.0549**
Geometry × Teaching Experience Squared	-0.0083
Biology × Teaching Experience	0.0357*
Biology × Teaching Experience Squared	-0.0094*
Algebra 2 × Teaching Experience	0.0306
Algebra 2 × Teaching Experience Squared	-0.0028
Algebra 1 × Teaching Experience	-0.0060
Algebra 1 × Teaching Experience Squared	0.0023

Overall, novice teachers of high-school science and mathematics exhibit significant returns to experience early in their careers that diminish after 4 years of teaching. This indicates that (i)

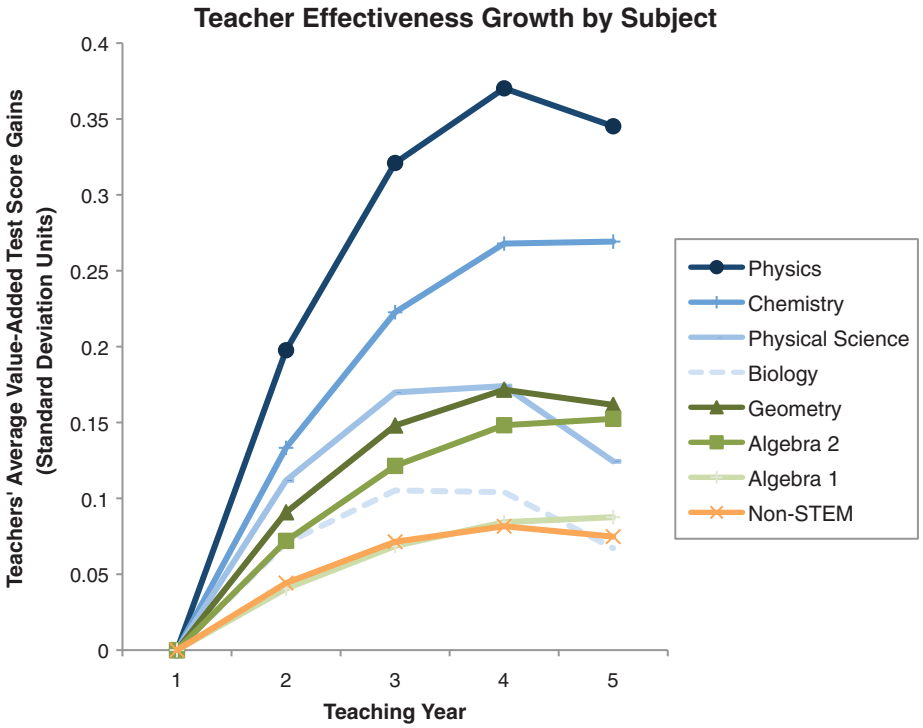

Fig. 1. Average effectiveness of novice high-school teachers.

beginning teachers have a tremendous capacity for improving quickly, and (ii) students of beginning teachers will not achieve at the same levels as students with more experienced teachers. Our results show that increased reliance on novice teachers leads to lower average teacher effectiveness. In light of current teacher labor market conditions, key questions include the following: (i) How to get more effective science and mathematics teachers into high-school classrooms? (ii) Can science and mathematics teachers be better prepared through more preservice experience in classrooms, increased focus on instructional skills, and deeper knowledge of content by the time they begin teaching?

Different high-school subjects show different impacts of teacher turnover. For courses with steeper effectiveness growth curves—physics, chemistry, and geometry—the loss of these experienced teachers has the greatest consequences for student performance. For courses with less steep growth curves—algebra 1, algebra 2, biology, and physical science—the loss of more experienced teachers has less severe consequences. But both cases call for recruiting more able, motivated, and committed teachers. Could these teachers be better screened by evaluating their academic performance, persistence, ability to engage audiences, and projected commitment to teaching, specifically teaching STEM courses to high-school students? Would incentives, such as higher salaries, assignment to fewer courses per year, or paid opportunities for research with university faculty during summers or semester leaves, help retain more of the experienced teachers?

The current churn of the teacher labor market is working against higher student achievement in STEM courses. Although most current education policies that affect teachers do not distinguish between teachers of different types of courses, our results strongly suggest that distinctions between STEM and non-STEM teachers, and even among STEM teachers who teach different courses, may be warranted.

References and Notes

1. M. Bacolod, *Rev. Econ. Stat.* **89**, 737 (2007).
2. R. Ingersoll, L. Merrill, *Educ. Leadership* **67**, 14 (2010).
3. R. Ingersoll, T. Smith, *Educ. Leadership* **60**, 30 (2003).
4. H. Lankford, S. Loeb, J. Wyckoff, *Educ. Eval. Policy Anal.* **24**, 37 (2002).
5. C. Clotfelter, H. Ladd, J. Vigdor, *Econ. Educ. Rev.* **24**, 377 (2005).
6. D. Boyd, P. Grossman, H. Lankford, S. Loeb, J. Wyckoff, *Educ. Finance Policy* **1**, 176 (2006).
7. C. Clotfelter, H. Ladd, J. Vigdor, *Econ. Educ. Rev.* **26**, 673 (2007).
8. C. Clotfelter, H. Ladd, J. Vigdor, *J. Hum. Resour.* **45**, 655 (2010).
9. D. Goldhaber, *J. Hum. Resour.* **42**, 765 (2007).
10. G. T. Henry, K. C. Bastian, C. K. Fortner, *Educ. Res.* **40**, 271 (2011).
11. S. Rivkin, E. Hanushek, J. Kain, *Econometrica* **73**, 417 (2005).
12. J. Rockoff, *Am. Econ. Rev.* **94**, 247 (2004).
13. D. Staiger, J. Rockoff, *J. Econ. Perspect.* **24**, 97 (2010).
14. M. Chingos, P. Peterson, *Econ. Educ. Rev.* **30**, 449 (2011).
15. D. Goldhaber, B. Gross, D. Player, *J. Policy Anal. Manage.* **30**, 57 (2011).
16. J. Krieg, *Econ. Educ. Rev.* **25**, 13 (2006).
17. B. Scafidi, D. Sjoquist, T. Stinebrickner, *Adv. Econ. Anal. Policy* **6**, 1 (2006).
18. C. Teddlie, D. Reynolds, *The International Handbook of School Effectiveness Research* (Falmer Press, London, 2000).
19. D. Reynolds, P. Sammons, B. De Fraine, T. Townsend, J. Van Damme, *Educational Effectiveness Research (EER): A State of the Art Review,* paper presented at the annual meeting of the International Congress for School Effectiveness and Improvement, Cyprus, 2011.
20. J. S. Coleman *et al.*, *Equality of Educational Opportunity* (U.S. Government Printing Office, Washington, DC, 1966).
21. North Carolina Department of Public Instruction, *North Carolina Mathematics Tests. Ed. 3: Technical Report* (Raleigh, NC); downloaded 29 December 2011 from www.dpi.state.nc.us/docs/accountability/reports/mathtechmanualdrafted2.pdf (2008).
22. North Carolina Department of Public Instruction, *North Carolina Science Tests: Technical Report* (Raleigh, NC); downloaded 29 December 2011 from www.dpi.state.nc.us/docs/accountability/testing/reports/eocsciencetechmanual.pdf (2009).

Acknowledgments: We recognize ongoing financial support for this research from the Teacher Quality Research Initiative provided by the University of North Carolina General Administration.

Supporting Online Material

www.sciencemag.org/cgi/content/full/335/6072/1118/DC1
SOM Text
Tables S1 and S2

17 October 2011; accepted 30 January 2012
10.1126/science.1215343

New Products: Toxicology

CELL ANALYZER

The innovative Muse Cell Analyzer system can be used for real-time quantitative assessment of cell concentration, cell health, apoptosis, and cell cycle with greater accuracy and precision than manual hemocytometry or image-based automated analysis. By providing real-time, multidimensional information on cell populations, the Muse cell analyzer enables faster, more accurate decision-making, more productive workflows, and greater insight into cell health. The Muse system delivers high performance cell analysis using miniaturized fluorescent detection and microcapillary technology, which occupy one-tenth the space of a typical cytometer. Laser-based fluorescence detection of each cell event can evaluate up to three cellular parameters. As a result, Muse provides accurate quantitative results compared to imaging-based systems, which only examine up to two parameters, are time-consuming, and ultimately provide less quantitative data. The system is capable of analyzing both suspension and adherent cells from 2 to 60 µm in diameter. Intuitive software and simple touchscreen interface enable rapid setup and analysis.

EMD Millipore

For info: 800-645-5476 | www.millipore.com

ENDOCRINE-ACTIVE CHEMICALS TEST

The ToxInsight Endocrine Profiler Panel (EPP) is a groundbreaking new tool for assessing the risk of human exposure to endocrine-active chemicals in the environment. EPP cartridges measure estrogen and androgen receptor activity in human cell lines. Each cartridge includes all the cell lines, reagents, assay protocols, growth media, plasticware, analysis, and data-reporting capabilities to profile compounds for endocrine activity with high sensitivity and specificity. EPP cartridges, coupled to the ToxInsight CHPS platform, offer a high throughput, quantitative prescreen for primary toxicology assessment, as well as a selection of chemicals for follow-up animal studies, in a simple mix-and-read format that is easily standardized. This automated, benchtop platform is easy-to-use and provides physiologically relevant toxicity assays in vitro, reducing the reliance on late-stage histopathology or animal studies. The ToxInsight CHPS platform not only profiles compounds for their toxicity risk, but also determines the mechanism of action of any toxicity detected.

Thermo Fisher Scientific

For info: 800-432-4091 | www.thermoscientfic.com

IMAGE DATA STORAGE AND ANALYSIS

Researchers in the areas of cancer and stem cells, predictive toxicity, neuroscience, and developmental biology can benefit from the improved capabilities of the updated Columbus 2.3 Image Data Storage and Analysis System, which are intended to enable faster and more powerful high content analysis-based research applications. The Columbus 2.3 platform now enables scientists to perform their high content analysis on one powerful platform, from image analysis through to secondary analysis, regardless of which high content screening (HCS) instrument they have. The secondary analysis capabilities can enable scientists to select small interfering RNA (siRNA) or compounds with desirable inhibition or activation effects, by proving the statistical significance of the observations made at the image analysis stage of a HCS campaign. Multiple plates or batches are analyzed, filtering out anomalies, and identifying trends. The software's improved morphology analysis capability is designed to give scientists a more complete understanding of the effects different treatments have on cell samples.

PerkinElmer

For info: 800-762-4000 | www.perkinelmer.com

MICROBIAL COLONY PICKERS

The QPix 400 series, the next generation of microbial colony pickers, offers unmatched performance and productivity enabling scientists to manage large, diverse populations, including 98% efficiency in colony picking, far surpassing the industry standard. The QPix 400 series features the unique option to simultaneously detect colonies and quantify fluorescent markers. This prescreening step enables the colonies of interest to be objectively identified and selected. Together with highly accurate robotics and organism-specific colony picking pins, scientists can ensure that the right colony is picked every time, thus eliminating unnecessary work and expense downstream. An agar height sensor further increases accuracy at the picking stage. Application-driven software includes tools to easily track sample histories throughout a workflow. Applications include areas such as protein expression, biofuel research, enzyme evolution, phage display, DNA sequencing, and library generation and management.

Molecular Devices

For info: 800-635-5577 | www.moleculardevices.com

APOPTOTIC BODY DNA ANALYSIS

The D-Pop Kit simplifies the capture of DNA-containing particles from cell-free biological samples such as blood serum and plasma, urine, and eukaryotic cell culture media as well as the extraction of DNA from the captured particles. Using the D-Pop Kit, apoptotic bodies and potentially other large particles are captured from biological fluids in minutes by passing them through a filter in a syringe format. The filter is then removed to a microfuge tube and the DNA is extracted from it using a rapid solid-phase extraction of DNA with non-organic reagents. The D-Pop Kit also includes control polymerase chain reaction primers for the hTERT gene to verify concentration and recovery of DNA from the sample.

Bioo Scientific

For info: 888-208-2246 | www.biooscientific.com

Electronically submit your new product description or product literature information! Go to **www.sciencemag.org/products/newproducts.dtl** for more information.

Newly offered instrumentation, apparatus, and laboratory materials of interest to researchers in all disciplines in academic, industrial, and governmental organizations are featured in this space. Emphasis is given to purpose, chief characteristics, and availability of products and materials. Endorsement by *Science* or AAAS of any products or materials mentioned is not implied. Additional information may be obtained from the manufacturer or supplier.

SHIMADZU

PITTCON 2012 Heritage Award Honoring

Shimadzu – accepting the award on their behalf,
Shigehiko Hattori, Chairman of the Board of Shimadzu

Genzo Shimadzu, Sr. (1839-1894) and Genzo Shimadzu, Jr. (1868-1951)

Japan's rapid modernization
in the nineteenth and twentieth centuries
was made possible by such people of vision
as Genzo Shimadzu, Sr. and Jr.

PITTCON CONFERENCE & EXPO 2012

PITTCON SHIMADZU Booth #1806
March 11-15, 2012
Orange County Convention Center Orlando, FL USA








Shimadzu Scientific Instruments
North America

7102 Riverwood Drive Columbia, MD 21046 U.S.A.
Phone Number: 1-800-477-1227 Fax Number: 410-381-1222

You have demands. Shimadzu delivers.

www.ssi.shimadzu.com

Everything you need to measure mitochondrial (dys)function in cells

XF Cell Mito Stress Test Kit
for use with the XF Analyzer

Webinars On-Demand
See our mitochondrial profiling webinars at seahorsebio.com/science

With the XF Cell Mito Stress Test Kit and the XF Analyzer you can confidently identify mitochondrial (dys)function, and measure mitochondrial response to stress.

XF Cell Mito Stress Test Kit

- Complete easy-to-use kit, including pre-calibrated, pre-tested reagents for 6 microplates
- Software wizard guides assay optimization, design, and interpretation
- Designed for use with the XF Analyzer
- Provides metrics essential to understanding cancer, aging, and metabolic, cardiovascular, and neurodegenerative diseases

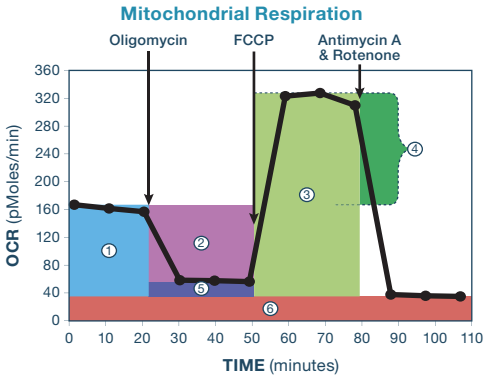

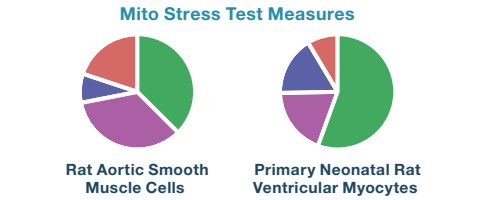

1. Basal Respiration
2. ATP Production
3. Maximal Respiration
4. Spare Respiratory Capacity
5. Proton Leak
6. Non-mitochondrial Respiration

Measuring **cell metabolism** is so easy now!

www.seahorsebio.com/science • +1-978-671-1600 • info@seahorsebio.com
16 Esquire Road, North Billerica, MA 01862, USA

Seahorse *Bioscience*

NEW ENGLAND BioLabs® Inc.
enabling technologies in the life sciences

Mix it up.

RE-Mix™ Restriction Enzyme Master Mixes

Restriction enzyme digests are now even easier! The same high quality restriction enzymes that you have come to trust from New England Biolabs are now available in master mix format, including enzyme, buffer and loading dye; simply add your DNA and digest.

With RE-Mix Master Mixes take advantage of:

- Simplified and shortened protocols
- Fast digestion in 15 minutes (Time-Saver qualified)
- High product quality with reproducible results

RE-Mix Master Mixes – just add your DNA and mix

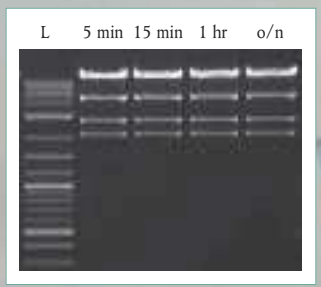

pXba DNA was digested with EcoRV-HF™ RE-Mix™ according to the recommended protocol. Lane L is the TriDye™ 2-Log DNA Ladder (NEB #N3270). The same results are obtained whether incubated for 5–15 minutes, 1 hour or overnight.

For more information, visit
www.NEBREMIX.com

Blue-footed Booby (Sula nebouxii)
© Tui De Roy

Toxicology

Animal-Free Toxicology

Sometimes, in Vitro is Better

The next time you use shampoo, air freshener, or moisturizing cream, consider this: How do you know it's safe? In all likelihood, whatever toxicologic screening its component ingredients were subjected to involved laboratory animals, the method of choice for decades and the industry's reigning "gold standard." Yet as Bob Dylan once put it, the times, they are a-changing. Animal-based testing is expensive and time-consuming, morally and ethically troubling, and most significantly, often a poor predictor of human toxicity. Animals aren't going anywhere just yet. But their numbers are dropping. Driven both by legislative mandate and scientific need, a new suite of in vitro and cell culture-based animal-free methods are gaining a foothold in toxicology labs. **By Jeffrey M. Perkel**

One key player in the modernization of toxicology screening is automation.

In 2010, as oil gushed from the broken wellhead beneath the stricken *Deepwater Horizon*, the **U.S. Environmental Protection Agency** (**EPA**) struggled to assess the safety of the chemical dispersants being used to treat that oil.

Eight commercial dispersants and 23 reference compounds were put through the analytical ringer, being probed for their cytotoxicity and activity on some 73 transcription factors, and—because one component of several of these dispersants was nonylphenol ethoxylate, a known "endocrine disruptor"—for their ability to activate estrogen and/or androgen-responsive pathways.

The take-home message from this analysis was that the compound then in use, Corexit 9500 appeared relatively safe, at least regarding endocrine activity.

But perhaps the bigger take-home message concerns how those data were collected. Rather than laboratory animals, the traditional go-to method of toxicity testing, the research team used a high throughput cell culture-based approach, finishing their analysis in about two weeks.

These days, an ever-increasing number of researchers, government agencies, and commercial entities have adopted a similar strategy. Partly, that's due to ethical considerations. But there are others as well.

For one thing, observes toxicologist Thomas Hartung, "We are not 70 kg rats." But time, cost, and practicality also loom large. Some 55,000 chemicals or more were grandfathered in when the U.S. Congress first passed the Toxic Substances Control Act in 1976. About 100,000 chemicals are similarly situated in Europe. No toxicological data has ever been filed on most of those, a "knowledge gap" that represents the vast majority of compounds in use today.

Filling that gap, at least with animals, is both financially and practically impossible. According to Robert Kavlock, director of the U.S. EPA National Center for Computational Toxicology (NCCT), "the capacity of the U.S. industry to test is probably in the hundreds of chemicals a year at best." And it can cost a company upwards of $10 million and take five years to fully test just a single pesticide, at which point the EPA then needs a million dollars or so to review those data and make a safety determination "If you extrapolate that to 80,000 chemicals, the math doesn't work very well," Kavlock says.

But this huge backlog represents just one reason for pushing alternative methods. The European Union (EU) has for years been promoting a move away from animal-based testing in industries such as cosmetics, with a testing ban on cosmetic products and ingredients being implemented in stages since 2004. And where Europe goes, so goes the world, because U.S.-based companies that use animal testing, for instance, can no longer sell their cosmetics in Europe. But cosmetics testing represents only about 0.2 percent of the animals used for safety assessment testing in Europe, estimates Mathieu Vinken, of the Department of Toxicology at **Vrije Universiteit Brussel.** Another piece of European legislation, called REACH, covers the giant chemical backlog, suggesting that if animal-free alternative methods exist, they should be used there, as well.

"European legislation at the moment is the pacemaker worldwide on some of the demands in regulatory testing," says Hartung, the Doerenkamp-Zbinden Professor and Chair for evidence-based toxicology at **Johns Hopkins University Bloomberg School of Public Health.**

The EU has, since 1986, invested some $300 million on the development and validation of alternative approaches, Hartung estimates. A new initiative, called Safety Evaluation Ultimately Replacing Animal Testing (SEURAT) dedicates another 50 million euro specially to investing animal-free methods to long-term toxicity endpoints.

The United States has been slower to react, but a 2007 report by the National Research Council's Committee continued>

UPCOMING FEATURES

Polymer Science: Creating Synthetic Materials—March 16

Innovation in Japan—April 13

Proteomics: Protein Chip Arrays—May 11

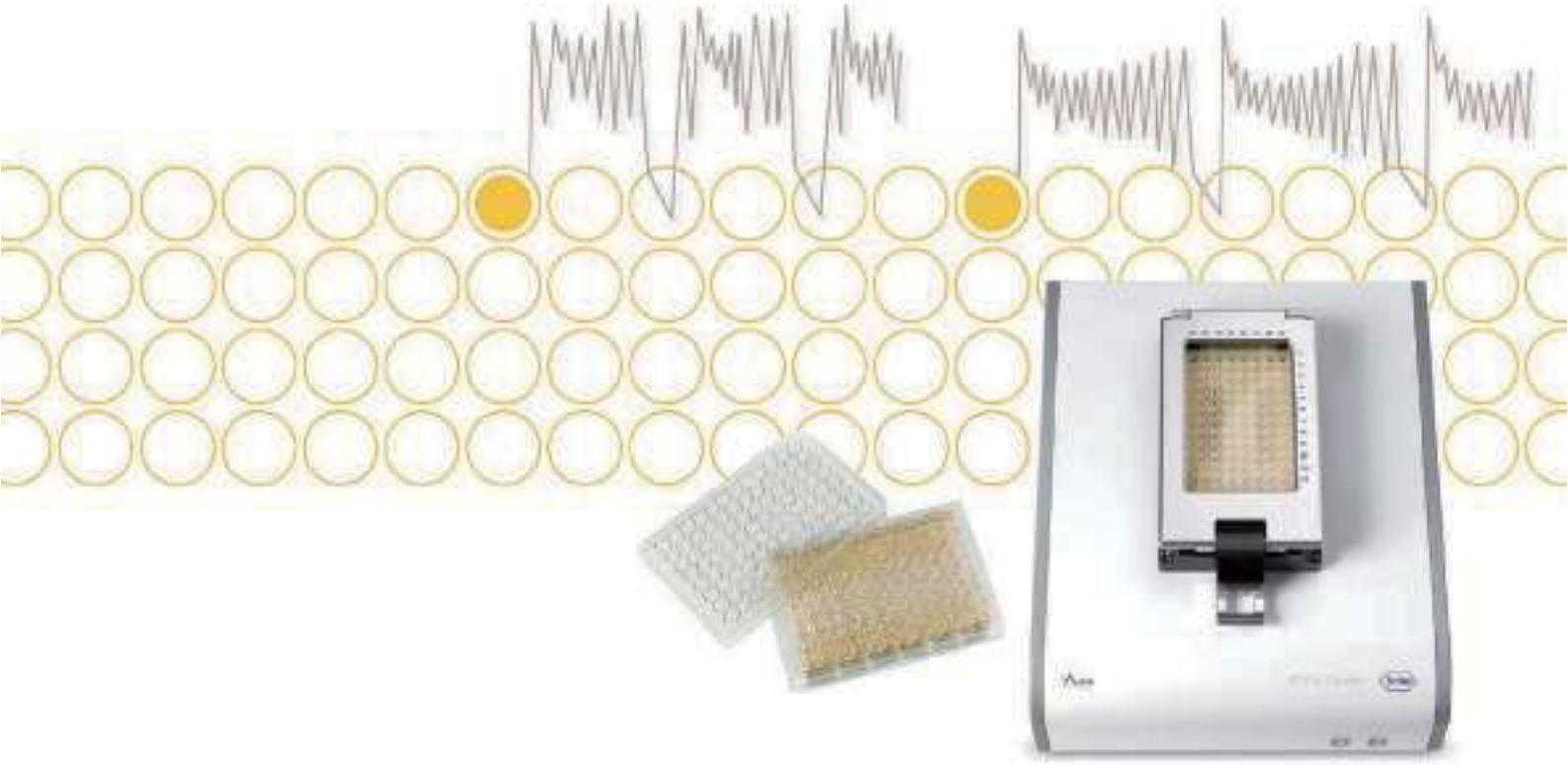

xCELLigence

xCELLigence RTCA Cardio Instrument

Fail faster – Avoid launching the next drug with unforeseen cardiotoxic effects.

Drug	Beating Profile (after Addition of Drug)
Control	
Domperidone	
Droperidol	
Cisapride	
Chloroquine	

Evaluate compounds for hERG modulation.

- Rule out cardiotoxic compounds earlier in drug development.
- Obtain physiologically relevant data through non-invasive, label-free monitoring of cardiomyocyte beating.
- Use a 96-well format to analyze both acute and long-term effects on a cell population.

Visit **www.xcelligence.roche.com** or call **800 262 4911** to learn more.

ACEA Biosciences, Inc.

For life science research only.
Not for use in diagnostic procedures.

Roche Diagnostics Corporation
Roche Applied Science
Indianapolis, Indiana

Roche

Toxicology

"There's only a certain number of critical infrastructures in the cell where you can harm the cell, and whatever we are using which is perturbing the physiology is somehow converging towards these critical infrastructures."

on Toxicity Testing and Assessment of Environmental Agents, called *Toxicity Testing for the 21st Century: A Vision and a Strategy* (http://scim.ag/zEJou2), says Hartung, "was really a game-changer." Laying out the issues with animal-based testing, the report "suggested to [researchers that they] embrace new technologies to overcome this problem."

Today, from automated screening platforms to the incorporation of 'omics technologies, the toxicology world is doing just that.

TOXICITY FORECASTING

One key player in the modernization of toxicology screening is automation. For instance, the European Union Reference Laboratory for Alternative Methods to Animal Testing uses automated imaging on a **Cellomics** ArrayScan vTi platform and robotics in its work validating proposed animal-free testing methods. "Our aim is to challenge the assay with sets of reference chemicals/substances which have been well characterized in terms of their toxicity and preferably [with respect to] their mode-of-action," says Maurice Whelan, head of the systems toxicology unit at the **European Commission Joint Research Centre,** which operates the lab.

Using such a system and 96-well plates, Whelan says his team has been able to reduce the time required to test a complete set of 90-plus reference compounds from 18 months (performed manually) to about eight weeks.

Automation plays an even bigger role at the EPA's NCCT, which developed the Toxicity Forecaster (ToxCast) panel used in the oil dispersant study.

According to Kavlock, the NCCT, formed in 2005, was "basically given a blank wall" regarding the creation of a "more efficient, more effective, and maybe more intelligent" way to assess chemical hazards. The team's strategy was to borrow the tools of the pharmaceuticals industry, pushing tens of thousands of compounds through automated, high throughput platforms.

In the first phase of ToxCast, the NCCT applied a battery of more than 500 tests to some 309 chemicals, using computational methods to develop what they call "predictive signatures" of some harmful biological action, which may then be used to infer the behavior of other chemicals. Three signatures have already been published, including one 36-assay signature of reproductive toxicity in rats.

Phase 2 of ToxCast, which currently is ongoing, extends this work to 1,061 chemicals (including pesticides, failed pharmaceuticals, industrial chemicals, and so on) and 700 tests.

According to Kavlock, those 700 assays represent some 10 platforms, including cell-free assays (such as receptor-binding assays); reporter gene assays; and co-culture assays in which activation of one-cell type produces a response in the second—plus one zebrafish-based test.

ToxCast's first task, Kavlock says, is prioritizing chemicals for animal testing, specifically for endocrine toxicity. Currently, EPA is using the so-called Tier 1 Endocrine Disruptor Screening Battery of 11 animal and in vitro tests for that purpose. But each chemical costs between half-a-million and a million dollars to run, Kavlock says, and the full battery takes about a year. The full ToxCast panel costs about $30,000 per compound, and EPA is testing another thousand compounds (in addition to the 1,000 Phase 2 compounds) on a subset of 80 or so endocrine-focused ToxCast tests at a cost of about $4,000 apiece.

"We'll have basically 2,000 chemicals we've tested through all of these different endocrine assays, and we'll be able to rank order those and provide that information to the EPA program office to say, these are the ones you ought to ask industry to look at first, because they look like chemicals that we know can cause endocrine effects."

TOWARDS A HUMAN TOXOME

ToxCast is part of a broader federal program called Tox21, in which the EPA, the **National Institutes of Health** (**NIH**), and the **U.S. Food and Drug Administration** (**FDA**) are collaborating to rapidly put some 10,000 compounds (including the 1,000 Phase 2 ToxCast compounds) through 30 assays in 1,536-well plates on a robotic platform at the NIH Chemical Genomics Center in Rockville, Maryland. The goal is to map the complete set of biochemical pathways implicated in toxicologic responses, so that more targeted assays of toxicity may be developed.

Hartung calls those "pathways of toxicity" the "toxome" and is using a $6 million NIH Director's Grant to help map them. His primary tools: transcriptomics and mass spectrometry-based metabolomics.

Hartung's team will use **Agilent Technologies'** gene expression microarrays and liquid chromatography-mass spectrometry to map the gene expression and metabolome changes that result from exposure of two human breast cancer cell lines to some 53 pro-estrogenic agents, compounds like bisphenol A that activate estrogen-responsive pathways. They will use chemical inhibitors and RNAi to validate the identified pathways.

Hartung says he expects to find no more than perhaps a few hundred such pathways that, when mapped, could form the foundation for a set of simple cell and in vitro assays that almost any lab could run. "There's only a certain number of critical infrastructures in the cell where you can harm the cell," he explains, "and whatever we are using which is perturbing the physiology is somehow converging towards these critical infrastructures."

Of course, his initial toxome efforts per se won't be able to map all those mechanisms—it focuses only on two cell lines and "a handful" of toxicants, he says. But by moving onto other cell systems and inhibitor classes, Hartung can broaden his search. For instance, he was recently awarded another grant by the FDA to study mechanisms of developmental neurotoxicity. And he anticipates other researchers will join him, inputting data on still more pathways into their database through a kind of open wiki

system. "In a process which has some quality control as joint governance, but a process which is open, we hope more and more of these pathways will get into the system," he says.

ANIMAL-FREE INDUSTRY

Industry, too, is moving away from animal testing. **Proctor & Gamble** (**P&G**), for instance, has been developing animal-free alternatives to toxicology testing for nearly 30 years, says Len Sauers, the company's vice president for global sustainability.

"The ethical and moral issue is a primary driver, but there are some real business drivers for wanting to get out of animal testing," he says. Over the years, he says, P&G's toxicologists—there currently are 150 on staff—have developed some 50 methods and published nearly 1,000 papers on the subject.

P&G employs a multi-tiered process for toxicology testing. The first step, says Sauers, is structure-activity relationship (SAR) analysis.

To feed those SAR studies, the company has compiled a database of "every toxicity study that's ever been run and is in the public literature," says George Daston, a Victor Mills Society Research Fellow at P&G, including published papers, public domain EPA submissions, and so on. "That literally results in hundreds of thousands if not one million or so line item pieces of information on the toxicity of materials," he says.

That database allows the company to make intelligent predictions about possible toxicities, and to test them directly. For instance, Daston says, perhaps some new ingredient has a structural fragment that previously has been associated with thyroid peroxidase inhibition. "We'll just set up an assay and evaluate the new chemical and see whether it does that."

Now, says Daston, the company has turned its sights on gene expression analysis, a technology P&G is "investing pretty heavily in." In one recent study, the company's researchers identified a 71-gene signature of uterine cell response by 17-alpha-ethynyl estradiol. "These results indicate that transcript profiling can serve as a viable tool to select reliable in vitro systems to evaluate potential estrogenic activities of target chemicals and to identify genes that are relevant for the estrogen response," the authors wrote.

REDUCE, REFINE, REPLACE

For P&G, this emphasis of animal-free testing has reduced animal testing dramatically, says Sauers. "Ninety-nine percent of our assessments today are done without animal testing."

As the toxome comes into focus and the platforms become more widespread, the broader research community can likewise reduce their animal usage. Several such assays are commercially available, including the MucilAir assay from **Epithelix** (a cell culture system that includes the three cell types found in airway epithelium) and **Thermo Fisher Scientific**'s ToxInsight Endocrine Profiler Panel (a fluorescence-based cell culture test for endocrine disruptors).

Yet no matter how sophisticated the system, cell culture and in vitro assays—not to mention computer models—are just no match for live animals whose many organ systems and cell types can react differently to chemical agents. For instance, researchers cannot reliably predict a priori a chemical's bioavailability and biodistribution as well as how it will be processed in the liver. "We're very good with in vitro methods at telling you, assuming a chemical reaches a cell, what happens," says Whelan. "We're not very good at saying how much of that chemical will be bioavailable in a certain tissue over time based on the exposure."

Some animal testing is thus inevitable, especially as pharmaceuticals are not covered by the European testing bans. But that doesn't mean there won't be improvements. For decades, the mantra in the world of laboratory animals has been the so-called 3Rs, which encourages researchers to *Reduce* the number of animals they use, *Refine* the assays to reduce distress, pain, and suffering, and ultimately, *Replace* animals with alternative methods.

Europe's cosmetics testing ban focuses just on one *R*, says Vinken: replacement. But a more realistic approach to limiting animal testing would focus on all three, he explains.

Take, for instance, the local lymph node assay (LLNA). The LLNA is a reduced and refined skin sensitization test that uses mice instead of guinea pigs and is based on the extent of stimulation of lymphocyte proliferation in regional lymph nodes draining the site of application of the test substance. The major refinement, Vinken says, is that the actual end stage of the sensitization process—erythema and edema—doesn't occur in the experimental animal, reducing its distress. That is not the case for conventional animal-based skin sensitization tests.

The U.S. regulatory body charged with validating animal-free alternatives, called ICCVAM, has to date approved 44 such methods. The equivalent European body has validated six more in such areas as eye irritation and reproductive toxicity. Yet one area for which no alternatives exist is long-term toxicity testing—mimicking, for instance, the allergic responses that might result from repeated, long-term exposure to a chemical.

Researchers are on the case, but the bottom line, says Kavlock, "is we're a long way away from animal-free toxicology."

Jeffrey M. Perkel is a freelance science writer based in Pocatello, Idaho.

DOI: 10.1126/science.opms.p1200062

FEATURED PARTICIPANTS

Agilent Technologies
www.agilent.com

Cellomics
www.cellomics.com

Epithelix
www.epithelix.com

European Commission Joint Research Centre
ec.europa.eu/dgs/jrc/index.cfm

Johns Hopkins University Bloomberg School of Public Health
www.jhsph.edu

National Institutes of Health
www.nih.gov

Procter and Gamble
www.pg.com

Thermo Fisher Scientific
www.thermoscientific.com

U.S. Environmental Protection Agency
www.epa.gov

U.S. Food and Drug Administration
www.fda.gov

Vrije Universiteit Brussel
www.vub.ac.be/english/index.php

New Products: Toxicology

CELL ANALYZER

The innovative Muse Cell Analyzer system can be used for real-time quantitative assessment of cell concentration, cell health, apoptosis, and cell cycle with greater accuracy and precision than manual hemocytometry or image-based automated analysis. By providing real-time, multidimensional information on cell populations, the Muse cell analyzer enables faster, more accurate decision-making, more productive workflows, and greater insight into cell health. The Muse system delivers high performance cell analysis using miniaturized fluorescent detection and microcapillary technology, which occupy one-tenth the space of a typical cytometer. Laser-based fluorescence detection of each cell event can evaluate up to three cellular parameters. As a result, Muse provides accurate quantitative results compared to imaging-based systems, which only examine up to two parameters, are time-consuming, and ultimately provide less quantitative data. The system is capable of analyzing both suspension and adherent cells from 2 to 60 µm in diameter. Intuitive software and simple touchscreen interface enable rapid setup and analysis.

EMD Millipore

For info: 800-645-5476 | www.millipore.com

ENDOCRINE-ACTIVE CHEMICALS TEST

The ToxInsight Endocrine Profiler Panel (EPP) is a groundbreaking new tool for assessing the risk of human exposure to endocrine-active chemicals in the environment. EPP cartridges measure estrogen and androgen receptor activity in human cell lines. Each cartridge includes all the cell lines, reagents, assay protocols, growth media, plasticware, analysis, and data-reporting capabilities to profile compounds for endocrine activity with high sensitivity and specificity. EPP cartridges, coupled to the ToxInsight CHPS platform, offer a high throughput, quantitative prescreen for primary toxicology assessment, as well as a selection of chemicals for follow-up animal studies, in a simple mix-and-read format that is easily standardized. This automated, benchtop platform is easy-to-use and provides physiologically relevant toxicity assays in vitro, reducing the reliance on late-stage histopathology or animal studies. The ToxInsight CHPS platform not only profiles compounds for their toxicity risk, but also determines the mechanism of action of any toxicity detected.

Thermo Fisher Scientific

For info: 800-432-4091 | www.thermoscientfic.com

IMAGE DATA STORAGE AND ANALYSIS

Researchers in the areas of cancer and stem cells, predictive toxicity, neuroscience, and developmental biology can benefit from the improved capabilities of the updated Columbus 2.3 Image Data Storage and Analysis System, which are intended to enable faster and more powerful high content analysis-based research applications. The Columbus 2.3 platform now enables scientists to perform their high content analysis on one powerful platform, from image analysis through to secondary analysis, regardless of which high content screening (HCS) instrument they have. The secondary analysis capabilities can enable scientists to select small interfering RNA (siRNA) or compounds with desirable inhibition or activation effects, by proving the statistical significance of the observations made at the image analysis stage of a HCS campaign. Multiple plates or batches are analyzed, filtering out anomalies, and identifying trends. The software's improved morphology analysis capability is designed to give scientists a more complete understanding of the effects different treatments have on cell samples.

PerkinElmer

For info: 800-762-4000 | www.perkinelmer.com

MICROBIAL COLONY PICKERS

The QPix 400 series, the next generation of microbial colony pickers, offers unmatched performance and productivity enabling scientists to manage large, diverse populations, including 98% efficiency in colony picking, far surpassing the industry standard. The QPix 400 series features the unique option to simultaneously detect colonies and quantify fluorescent markers. This prescreening step enables the colonies of interest to be objectively identified and selected. Together with highly accurate robotics and organism-specific colony picking pins, scientists can ensure that the right colony is picked every time, thus eliminating unnecessary work and expense downstream. An agar height sensor further increases accuracy at the picking stage. Application-driven software includes tools to easily track sample histories throughout a workflow. Applications include areas such as protein expression, biofuel research, enzyme evolution, phage display, DNA sequencing, and library generation and management.

Molecular Devices

For info: 800-635-5577 | www.moleculardevices.com

APOPTOTIC BODY DNA ANALYSIS

The D-Pop Kit simplifies the capture of DNA-containing particles from cell-free biological samples such as blood serum and plasma, urine, and eukaryotic cell culture media as well as the extraction of DNA from the captured particles. Using the D-Pop Kit, apoptotic bodies and potentially other large particles are captured from biological fluids in minutes by passing them through a filter in a syringe format. The filter is then removed to a microfuge tube and the DNA is extracted from it using a rapid solid-phase extraction of DNA with non-organic reagents. The D-Pop Kit also includes control polymerase chain reaction primers for the hTERT gene to verify concentration and recovery of DNA from the sample.

Bioo Scientific

For info: 888-208-2246 | www.biooscientific.com

Electronically submit your new product description or product literature information! Go to **www.sciencemag.org/products/newproducts.dtl** for more information.

Newly offered instrumentation, apparatus, and laboratory materials of interest to researchers in all disciplines in academic, industrial, and governmental organizations are featured in this space. Emphasis is given to purpose, chief characteristics, and availability of products and materials. Endorsement by *Science* or AAAS of any products or materials mentioned is not implied. Additional information may be obtained from the manufacturer or supplier.

Ever wondered what cutting-edge technologies your peers across Europe are using?

Ever wondered how you could get access to their technology and expert support?

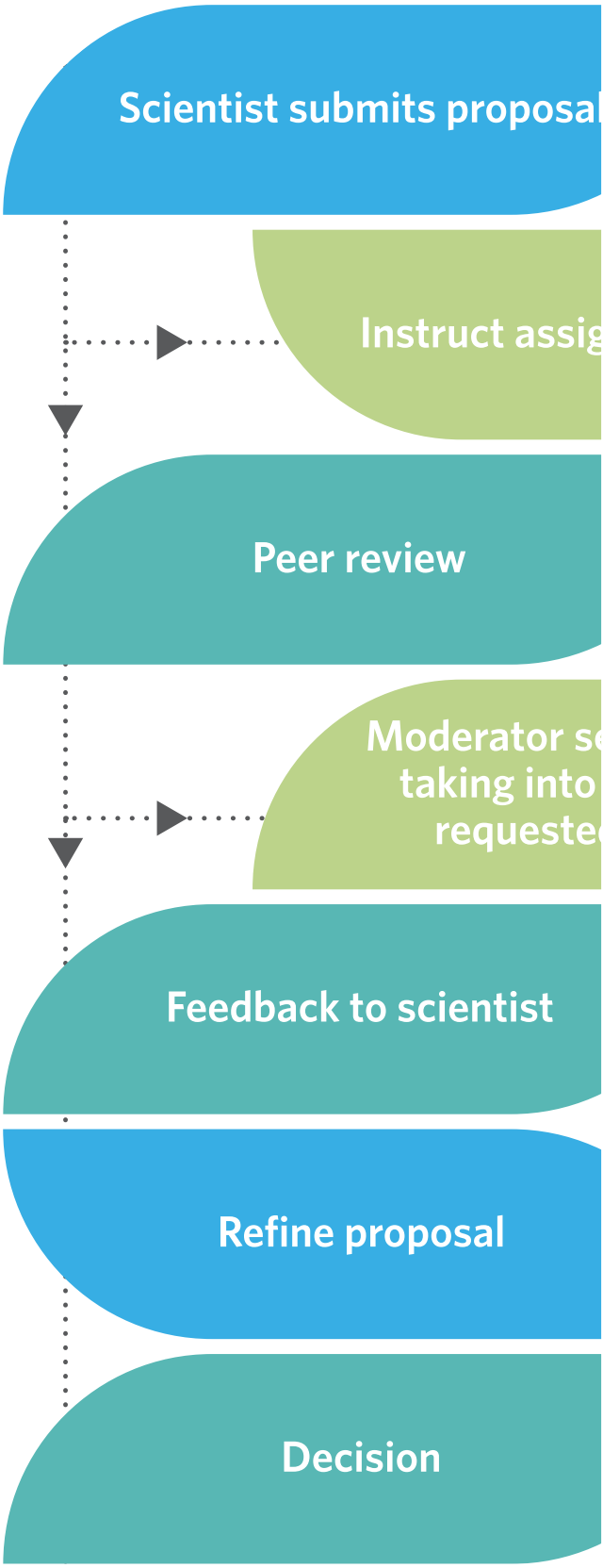

Instruct can answer both your wishes.

Across Europe, governments and leading research institutions have been investing in state-of-the-art equipment. At our online Instruct Hub you can browse the first catalogue of European technologies.

Delve into the details and compare one platform to another. Find the perfect mix of technology to further your research. Apply for access through our straightforward online process.

It isn't wishful thinking.
www.structuralbiology.eu

instruct
Integrating
Biology

Colorado State University

Position Announcement
(March 2, 2012)

Department of Microbiology, Immunology, and Pathology
Colorado State University
Fort Collins, Colorado

Tenure track faculty position: RNA Virology, Assistant or Associate Professor

The Department of MIP (**http://www.cvmbs.colostate.edu/mip/**) is seeking to fill a tenure track position (Assistant or Associate Professor) in RNA Virology. The successful candidate will have an established record in research and scholarly activity with arboviruses or other zoonotic RNA viral pathogens. Special consideration will be given to candidates with research programs in viral immunology (innate and/or acquired), emerging RNA viruses and virus diseases, epidemiology and control of virus diseases, and/or RNA biology in the context of the host-virus interaction.

The successful candidate will have multiple opportunities to collaborate and assume a leadership role in infectious disease programs at CSU, including the Arthropod-borne and Infectious Diseases Laboratory, the Infectious Disease Supercluster, the Rocky Mountain Regional Center of Excellence, the RM Regional Biocontainment Laboratory, and the Veterinary Teaching Hospital and Diagnostic Laboratory. S/he also will participate in the MIP undergraduate, graduate, and professional teaching programs as appropriate. The extraordinary research and teaching opportunities at CSU are enriched by the highly interactive and collaborative environment with world recognized infectious disease programs and scientists in CDC and USDA laboratories on and near campus.

Candidates must have the PhD, DVM or MD degree and an established record of extramural funding and scholarly activity in RNA virology. Salary and start up package are negotiable. More information about the position is available at **http://www.cvmbs.colostate.edu/ns/_docs/departments/mip/mip_job_rna_virologist.pdf**.

Applications and nominations will be considered until the position is filled; however, to ensure full consideration applications should be submitted by April 15, 2012. Candidates should submit either electronically or by mail a letter of application, curriculum vitae, and the names, mailing addresses, and e-mail addresses of three references to: **RNA Virologist Search Committee, c/o Andrea Guillory, Department of Microbiology, Immunology, and Pathology, 1619 Campus Delivery, Colorado State University, Fort Collins, CO 80523-1619; Andrea.Guillory@colostate.edu; 970-491-7861.**

CSU is an EO/EA/AA Employer and conducts background checks on all final candidates.

ASSISTANT, ASSOCIATE OR FULL PROFESSOR QUANTITATIVE BIOLOGIST

Job Opening ID Number: 5367

The Biology Department at City College of the City University of New York invites applications for a tenure-track or tenured position in Quantitative Biology at the level of Assistant, Associate, or Full Professor to begin Fall 2012. We seek an outstanding candidate performing cutting-edge research in landscape ecology, microbial ecology, evolutionary ecology, macroecology, or urban ecology. Candidates should have demonstrated research excellence and collaborative skills to interact with a vibrant, expanding Ecology, Evolution, and Behavior group. The candidate's research program should strengthen the current departmental research in tropical ecology, biogeography, evolutionary ecology, and conservation biology. The successful candidate will be expected to teach in both undergraduate and doctoral program and work collaboratively within the City University of New York. For areas of departmental strengths, see www.sci.ccny.cuny.edu/biology.

QUALIFICATIONS: Junior candidates should have a Ph.D., postdoctoral experience, and a strong record of publications; senior candidates should have a strong history of federal funding, research productivity, and teaching at the undergraduate and graduate level.

COMPENSATION: Commensurate with qualifications and experience. Competitive start-up package available.

HOW TO APPLY: If you are viewing this job posting in CUNYFirst, please click on "Apply Now" on the bottom of this page and follow the instructions.

If you are viewing this job posting externally, please apply as follows:
- Go to **www.cuny.edu** and click on "**Employment**"
- Click "Search job listings"
- Click on "More options to search for CUNY jobs"- Search by Job Opening ID number
- Click on the "Apply Now" button and follow the instructions.

To be considered for this position, you must include a curriculum vitae (CV), summary of past research accomplishments and future research plans, and a statement of teaching and mentoring experience in one document in any of the following formats: doc, docx, .pdf, .rtf, or text format.

Letters of recommendation from at least three referees should be sent directly to the search committee at: **Quantitative Biology Search Committee, Department of Biology, J526, The City College of New York, 160 Convent Avenue, New York, NY 10031, biosearches@sci.ccny.cuny.edu, fax: 212- 650-8585.**

EQUAL EMPLOYMENT OPPORTUNITY: *We are committed to enhancing our diverse academic community by actively encouraging people with disabilities, minorities, veterans, and women to apply. We take pride in our pluralistic community and continue to seek excellence through diversity and inclusion. EO/AA Employer.*

CITY COLLEGE IS CUNY

Assistant/Associate Professor of Biomedical and Pharmaceutical Sciences

Boise/Meridian, Idaho

The Department of Biomedical and Pharmaceutical Sciences of the Idaho State University College of Pharmacy invites applications for a tenure-track faculty position at the rank of Assistant or Associate Professor. The successful candidate will possess contemporary and competitive research expertise in any area of the biomedical and pharmaceutical sciences. However preference may be given to candidates with training and experience in proteomics or the ability to merge medicinal chemistry with other life sciences disciplines leading to structure-guided drug design. He or she must have a Ph.D. or equivalent degree and a rigorous postdoctoral experience leading to publications in top tier journals. The scholar chosen will participate in pharmacy (Pharm.D.) and graduate (M.S. and Ph.D.) education. A pharmacy degree, graduate or postdoctoral training in a college of pharmacy, or previous faculty rank in a college of pharmacy would be viewed most favorably. Applications for the rank of Associate Professor will be considered from individuals with funded research programs, evidence of academic leadership, publications in high impact journals, demonstrated excellence in teaching, and a history of some interdisciplinary collaboration. The ISU College of Pharmacy is located on both the ISU campus in Pocatello and in the Skaggs Pharmacy Complex in Meridian, Idaho, a municipality adjacent to Boise. This position will be located in Meridian.

Application Process: For full consideration, please apply through the Idaho State University Human Resources website (**www.isujobs.net**) and submit the following items: a cover letter; full curriculum vitae; list of three references; a summary of research and any teaching experience; and a statement of research plans not exceeding three pages. Priority consideration will be given to those applicants who apply by 6/30/2012. Review of applications will begin upon receipt; search will continue until position is filled.

ISU is an equal opportunity/affirmative action employer. We have an institution-wide commitment to inclusion and diversity and encourage all qualified individuals to apply. Veterans' preference.
Upon request, reasonable accommodations in the application process will be provided to individuals with disabilities.

Director

The University of Maryland Center for Environmental Science (UMCES) seeks a dynamic leader to serve as Director of the Appalachian Laboratory (AL) at the Associate or Full Professor level. Located in Frostburg, Maryland, AL is one of four UMCES laboratories, and is dedicated to advancing research in terrestrial and freshwater systems. With a focus on interdisciplinary research across the mountains-to-the-sea continuum, UMCES advances science and science education to transform the way society understands and manages the environment. The Director is expected to maintain a vigorous, extramurally funded research program; provide leadership of the laboratory's academic and research activities; and effectively execute administrative responsibilities, including oversight of personnel, physical and fiscal resources.

The ideal candidate for this position is an outstanding and experienced interdisciplinary researcher with demonstrated abilities to integrate research across scientific fields, including, for example: (1) interactions between human and natural systems across large spatial and temporal scales; (2) application of a genes-to-ecosystems perspective, addressing influences of genetic variation on population, community, and ecosystem processes and resilience to global change; and (3) interactions and feedbacks between terrestrial and coastal ecosystems. The successful candidate will exhibit potential for strong scientific leadership and must be prepared to lead the development, communication, and implementation of goals and strategic plans to advance AL's mission.

Excellent facilities for research, computing, and teaching are available at AL, including plant, soil, water, and molecular analysis laboratories with state-of-the-art analytical instrumentation, a new stable isotope facility, growth chambers, and a greenhouse. AL is located adjacent to Frostburg State University, and situated in the mountains of western Maryland within 2.5 hours from Baltimore, Washington D.C., and Pittsburgh. Applicants should send an electronic copy of a curriculum vitae; statement of research and leadership interests; selected reprints; and names and contact information of three references to **dirsearch@al.umces.edu**. Review of applications will begin on **April 16, 2012** and will continue until the position is filled. Information about AL and UMCES and this search can be found at: **http://www.umces.edu/**.

UMCES is an Affirmative Action/Equal Opportunity Employer; women and minorities are strongly encouraged to apply.

NANYANG TECHNOLOGICAL UNIVERSITY

Cheng Tsang Man Chair Professorship in Energy

The Cheng Tsang Man Professorship was established in 1999 by the Nanyang Technological University to mark a historical milestone in the Prima Group's philanthropic legacy. This is in line with the University's vision to advance the knowledge creation and discovery in the vital areas of Science and Technology for sustainable energy as well as to address the global urgency in ensuring a sustainable future through energy security.

This endowed position is open to all candidates worldwide who has interest to advance research efforts in sustainable energy. The candidate appointed will not only be a leader in his/her field but will also contribute to Singapore's drive towards energy efficiency and sustainable energy solutions by devoting his/her tenure to provide intellectual leadership and mentoring of younger scientists.

Join a dynamic team of faculty and world's students at what is one of the fastest advancing universities.

Applicant Profile:
- Credentials meriting a Full Professorship appointment
- An excellent publication record in any energy-related field
- A demonstrated leadership skill and ability in securing major research grants from external funding agencies and industry

We Provide:
- A vibrant research environment with excellent R & D infrastructure and opportunities for research funding
- Well-equipped state-of-the-art laboratories, attractive research start-up grants, PhD student scholarships
- Competitive remuneration package and attractive benefits

To Apply:
Electronic submission of application should be submitted to the Dean, College of Engineering at **d-coe@ntu.edu.sg**. It should consist of a cover letter, curriculum vitae, personal particulars form, teaching statement and evaluations, a statement of current and future research interest, selected publications and the names of at least 5 referees. For information on the submission guidelines, please refer to: **http://www.ntu.edu.sg/ohr/Career/SubmitApplications/Pages/Faculty.aspx**

Deadline: **March 31, 2012**

www.ntu.edu.sg

University of Hawai`i at Mānoa Department of Biology Marine Biologist

The Department of Biology at the University of Hawai'i at Mānoa seeks two tenure track faculty with expertise in the biology of marine organisms. Desirable specialties include marine conservation, coral reef ecology, and larval biology. The successful candidates will join a faculty with diverse research interests, a strong focus on evolutionary biology and native Hawaiian organisms, and will be expected to support our growing undergraduate and graduate programs in Marine Biology. Teaching responsibilities will include an upper level undergraduate course and a graduate course in the individual's specialty. Applicants must have a Ph.D. in biology or a related field, evidence of interest in teaching, evidence of research productivity and grantsmanship. Desirable qualifications include a developing record of publication, extramural funding, a minimum of two years of post-doctoral experience, and plans for a research program that would take advantage of the Hawaiian biota. Appointment will be at Assistant or Associate Professor level, depending on experience. Additional details can be found under position **no. 82434 and 83232** at: **http://workatuh.hawaii.edu**.

To apply, please send a single PDF document to **mbfacsch@hawaii.edu** that includes: a cover letter indicating your teaching and research interests and how you satisfy the minimum and desirable qualifications; a detailed curriculum vitae; three representative publications; and the names and contact information (including email address) for three professional references. Evidence of Ph.D. or other advanced degree must be provided. A hard copy of the complete application package should also be mailed to **Chair, Marine Biology Search Committee, Department of Biology, Rm. 2, Dean Hall, University of Hawai'i, 2450 Campus Road, Honolulu, HI 96822**. Review of applications will begin **March 23, 2012** and will continue until the position is filled.

The University of Hawai'i is an Equal Opportunity/Affirmative Action Institution and encourages applications from women and minority candidates.

WWW.NIH.GOV

Positions @ NIH

THE NATIONAL INSTITUTES OF HEALTH

Deputy Director of the Division of Extramural Activities

The National Institute of Allergy and Infectious Diseases (NIAID) is one of the largest Institutes of the world-renowned National Institutes of Health (NIH). With a budget approaching $4.5 billion annually, NIAID supports and conducts basic, applied, and clinical research to better understand, treat, and prevent infectious, immunologic, and allergic diseases. The Division of Extramural Activities (DEA) oversees grants, contracts, peer review, and extramural policy and information dissemination for NIAID. DEA also directly supports extramural research through research training and career development programs, small business research awards, and international extramural activities in the areas of allergy, immunology, transplantation, and infectious diseases.

DEA seeks applications from exceptional candidates for the position of deputy director of DEA.

The selected candidate will serve as deputy to the DEA director and fully share responsibility for managing DEA's grants, contracts, peer review, and policy functions. In collaboration with the director, the deputy participates in the planning, administration, development, and evaluation of DEA's research management programs and in directing, overseeing, and evaluating DEA's ongoing activities through subordinate supervisors, project leaders, program specialists, and contract employees. The deputy also has full responsibility to manage the DEA units and staff responsible for coordination of training and career development programs, small business innovative research, and international extramural research policies. The deputy represents the division at NIAID, NIH, national, and international meetings and conferences; makes scientific policy presentations at scientific/medical meetings; and serves as a key advisor to the directors of DEA and NIAID. The chosen candidate must have the ability to encourage participation and partnering with public and private/commercial entities to transition basic research knowledge into the development of products that will improve human health in the United States and globally.

Applicants must have an M.D., Ph.D., or equivalent degree, be a U.S. citizen, and exhibit a broad scientific management vision; an ability to lead staff; an outstanding ability to communicate with diverse audiences; flexibility in responding to multiple and rapidly emerging issues; and a demonstrated expertise in supervision and management of a broad and complex biomedical research program encompassing one or more of the following areas: biomedical research relevant to the NIAID mission, research training and career development, international research collaborations, or small business biotechnology research development. The chosen candidate will possess the supervisory, project management, interpersonal, and oral and written communication skills required to interact effectively with staff, representatives of academia, private industry, national and international research and health organizations, other units of NIH, the media, and the general public.

Candidates must be familiar with both standard university grantee processes as well as private laboratory and small business organizations with regard to conduct and management of complex biomedical research projects and training programs. They must have a clear understanding of regulatory requirements pertaining to such things as use of animals, human subjects, infectious agents, and other biohazards. Familiarity with research program initiative development, clinical regulatory affairs, and intellectual property issues, either as an NIH grantee or program director, would be a plus.

Salary is commensurate with experience, and a full package of benefits is available including retirement, health and life insurance, long term care insurance, leave, and savings plan (401K equivalent). Provide curriculum vitae, bibliography, and a three-page summary explaining 1) your vision of extramural research, 2) your reasons for being interested in the position, and 3) the specific leadership skills and experience you would bring to NIAID to Ms. Theresa D. Shrader, 6700B Rockledge Drive, Room 2145, Bethesda, MD 20892-7610 (FedEx: Bethesda, MD 20817). The application review process will begin **April 14, 2012**. Direct inquiries to Ms. Shrader at 301-496-3795 or tm25k@nih.gov.

To learn more about NIAID and how you can play a role in this exciting and dynamic research organization, visit us on the Web at www.niaid.nih.gov/careers/m.

NIAID

National Institute of Allergy and Infectious Diseases

US DEPARTMENT OF HEALTH AND HUMAN SERVICES
National Institutes of Health

National Institute of Allergy and Infectious Diseases
Proud to be equal opportunity employers

THE NIH IS DEDICATED TO BUILDING A DIVERSE COMMUNITY IN ITS TRAINING AND EMPLOYMENT PROGRAMS

REGIONAL CENTRE FOR BIOTECHNOLOGY
an institution of education, training & research

Adv. No. 2/2012

Career Opportunities in Plant Biology and Agriculture sciences

The Regional Centre for Biotechnology (RCB), a newly created institution in the National Capital Region (NCR) of Delhi, is looking for innovative faculty members working in the areas of plant biology such as plant-microbe interactions, genetic improvement of crops, molecular mechanism of abiotic stress responses, epigenomics, bioenergy, and other emerging areas linked with agriculture, climate science and environment, to develop novel research and teaching programmes in biotech science at the interface of multiple disciplines. RCB recognizes that expertise and innovation in these core domains is critical for the development of fresh perspectives in plant biology and agricultural sciences, and invites individuals with interdisciplinary profiles of the highest caliber and credibility to participate in this shared adventure to transform the biotech sciences.

Interested Scientists may send their CVs to the **Executive Director, Regional Centre for Biotechnology, 180, Udyog Vihar, Phase I, Gurgaon - 122016, Haryana, India** and e-mail the same at **office@rcb.res.in**. More information about RCB as also the details regarding faculty recruitment can be found on the website **http://www.rcb.res.in.**

UNIVERSITY OF OXFORD

www.ox.ac.uk/jobs

Halley Professorship of Physics

in association with Jesus College
Start date: 1 October 2012
or as soon as possible thereafter.

BRONZE
Athena SWAN

The Halley Professorship of Physics was established in 1991 as an upgrade of the long-standing statutory Readership in Atmospheric Physics and was renamed the Halley Professorship in 2000. The post has a history stretching back continuously to G. M. B. Dobson (discoverer of the Earth's ozone layer) in the 1920s. The person appointed will be an exceptional physicist with an international reputation in one or more areas of atmospheric, oceanic, climate and planetary physics and an outstanding research and publication record. He/she will exercise leadership in research and teaching, will be keen to interact with members of Atmospheric, Oceanic and Planetary Physics (AOPP) and other groups within the Department and the University, and will play a strategic role in advancing further the research portfolio of AOPP in Oxford. AOPP at Oxford has grown significantly in recent years and has consolidated its reputation in a range of research areas, including atmospheric and oceanic observations of the Earth and other solar system planets; remote sensing instrumentation and data analysis; numerical modelling of the Earth's climate system and of the climate of other planets; physical oceanography, climate dynamics and geophysical fluid dynamics.

Please see the further particulars at **http://www.ox.ac.uk/about_the_university/jobs/fp/** for more details about the post and for full instructions before making an application. Applications, including a covering letter and full CV, and naming three referees should be received no later than 30 April 2012 by Dr Gwen Booth, Personnel Officer, Senior Appointments at professorships@admin.ox.ac.uk If you have a query about how to apply, please contact Mrs Elaine Eastgate at professorships@admin.ox.ac.uk or telephone: +44 (0) 1865 280189.

Applications are particularly welcome from women and black and minority ethnic candidates, who are under-represented in academic posts in Oxford.

Committed to equality and valuing diversity

Gastrointestinal Immunologist

The Department of Medicine at Georgetown University seeks an outstanding MD, PhD or MD/PhD at the Assistant or Associate Professor rank. The ideal candidate will be a clinician and/or laboratory scientist with a strong interest in translational research in gastroenterology especially with a focus on immunological disorders such as inflammatory bowel disease. The candidate will have a successful program of research demonstrated by their publication record and participation as PI or co-I on peer-reviewed extramurally funded research. The candidate will establish and lead a translational immunology program that integrates with clinical and basic science investigators within the university community and benefits from the Georgetown - Howard Universities Center for Clinical and Translational Science. Nearby federal institutions including the NIH, FDA and VA serve to enrich the academic environment while our location in the heart of the Nation's capitol offers an unparalleled social, recreational and cultural lifestyle. Please send your cover letter and curriculum vitae by **May 31, 2012** to: **Ms. Tolise Miles (Tel: 202.687.7380; E-mail: tcm9@georgetown.edu**).

Georgetown University is an Affirmative Action/Equal Opportunity Employer.

Physician-Scientist Endocrinology

The Division of Endocrinology at the University of Texas Medical School – Houston is seeking a Physician-Scientist to develop a program in translational metabolic research focused on diabetes and obesity. Research opportunities include cross appointment in the Brown Foundation Institute of Molecular Medicine, access to the resources of the CCTS, and interactions with all of the affiliated schools of the UT Health Science Center including the School of Public Health and Center on Aging. The applicant must be ABIM-certified in Endocrinology and demonstrate ability for independent research. The position is full time, tenure track, and will require approximately 20% clinical effort.

Send CV, list of three references, and description of academic interests to **Philip Orlander, MD, Division of Endocrinology, University of Texas Medical School, 6431 Fannin, MSB 5.104, Houston, Texas 77030** or e-mail: **Philip.R.Orlander@uth.tmc.edu.**

UTHealth | The University of Texas Health Science Center at Houston is an EO/AA employer, M/F/D/V. This is a security sensitive position and thereby subject to Texas Education Code §51.215. A background check will be required for the final candidate.

UTHealth
The University of Texas
Health Science Center at Houston

COURSE

NEW INTERDISCIPLINARY SUMMER COURSE
Biophysics and Computation in Neurons and Networks
Directors: David W. Tank and Michael Berry, Princeton University

Course Date: June 17 – July 14, 2012
Application Deadline: April 1, 2012
Application Forms: www.princeton.edu/neuroscience/bcnn

This new course, supported by the Burroughs Wellcome Fund, will introduce students with quantitative training in the physical sciences, mathematics or engineering to the concepts and research methodologies of modern neuroscience. Topics covered will range from cellular biophysics to systems neuroscience, including particularly imaging methods for the study of single neurons, networks of neurons and human brain dynamics during execution of behavioral computations. The course will be unique in its focus on neural dynamics at several scales of complexity – cells, circuits, intact brains – and the combination of didactic lectures and laboratory exercises, including cellular biophysics, synaptic interactions and plasticity in neuronal networks, and fMRI imaging of targeted brain regions in human subjects. The capstone of this course will be one-week student-designed research projects integrating concepts and methodologies encountered during the initial formal lectures and laboratory exercises. Course work will include morning lectures and tutorials and laboratory exercises selected to complement and extend the themes presented in morning lectures.

Princeton Neuroscience Institute

COLLEGE of PHARMACY
THE UNIVERSITY OF TEXAS AT AUSTIN

FACULTY POSITION
Division of Pharmacology and Toxicology

The University of Texas at Austin College of Pharmacy invites applications for a tenure track position at the rank of Assistant Professor.

Candidates should have a well-developed research program that applies cutting edge research approaches to understanding the cellular, molecular, and/or biochemical mechanisms to define host responses to environmental toxicants. Research areas of interest include, but are not limited to: critical developmental periods/endocrine/hormone disruption; mechanisms of environmental carcinogenesis; and diet, energy balance and environmental disease risk. This position will be part of the Center for Molecular and Cellular Toxicology (website: **www.utexas.edu/pharmacy/cmct**), an interdisciplinary center that fosters the training of undergraduate, graduate, and postdoctoral fellows in toxicology. The CMCT administers an NIEHS-supported pre- and post-doctoral toxicology training program, and faculty are also joint participants in an NIEHS Environmental Center Grant (website: **http://cred.mdanderson.org/**) with faculty at The University of Texas M.D. Anderson Cancer Center.

A Ph.D. with at least two years of postdoctoral experience is required and preference will be given to individuals with a track record of independent research funding, including current grant funding, as well as Ph.D. training in toxicology or a relevant field. Instructional responsibilities in both the Pharm.D. and Ph.D educational programs is required. The deadline for receipt of applications is **April 1, 2012** and the search will continue until the position is filled. The position carries an exceptional salary, benefits, and start-up package. Applicants should submit electronically a letter of intent addressed to **Dr. John H Richburg**, search committee chair and include a, curriculum vitae, research synopsis, and a list of five references This position is security-sensitive as defined by the Texas Education Code and the Texas Government Code. Applicants will be required to submit all transcripts to complete the interview process. Background check conducted on applicant selected.

The University of Texas at Austin is an Affirmative Action/Equal Access/ Equal Opportunity Employer committed to diversity and excellence.

UNIVERSITY of WASHINGTON

Tenure Track Position in Synthetic Biology

The Department of Bioengineering at the University of Washington (UW) invites applications for a tenure track position in the area of **Synthetic Biology**. Successful candidates will have a plan to apply synthetic biology to problems with direct relevance to human health.

Applications are sought at all levels: Assistant, Associate and Full Professor, but those at the Assistant Professor level are particularly encouraged. Ph.D. or M.D. degrees are required. The successful candidate will be expected to develop an internationally recognized research program and to participate in the teaching and service missions of the department. Scientists and engineers who apply should show evidence of excellence, originality and productivity in research and potential for excellent teaching. In order to maximize the impact of this hire, successful candidates will be selected, in part, on the basis of their complementarity to existing UW faculty with expertise in synthetic biology, and to other synthetic biology faculty being hired in other departments at this time (see **http://synbio.washington.edu/**). These candidates will be expected to attract strong support from one or more additional departments within the UW and will be expected to follow UW's strong tradition of collaboration across disciplinary boundaries. Candidates with interests in translational medicine are also encouraged to take advantage of our active Coulter Translational Research Partnership.

Applications must be submitted electronically at **https://www.engr.washington.edu/facsearch/apply.phtml?pos_id=111**. Applicant review will begin immediately and continue until the position is filled. All positions are contingent on the availability of funding.

The University of Washington is a recipient of a National Science Foundation ADVANCE Institutional Transformation Award to increase the participation of women in academic science and engineering careers. UW faculty engage in teaching, research, and service. The University of Washington is building a culturally diverse faculty and strongly encourages applications from women and minority candidates. The University of Washington is an Affirmative Action, Equal Opportunity Employer.

Core-Funded Group Leader Positions

Paterson
Institute for Cancer Research

- **Reference Number: PI/12/11**
- **Competitive Salary**
- **2 vacancies**

The Paterson Institute for Cancer Research in Manchester is one of Europe's premier cancer research centres. The Institute is core-funded by Cancer Research-UK, the largest independent cancer research organisation in the world. It provides a highly interactive and vibrant research environment, facilitated by access to a comprehensive range of world-class and state-of-the-art core research services.

Its juxtaposition to The Christie, Europe's largest specialist cancer hospital, ensures ample opportunities for interaction from the basic to clinical research spectrum and the translation of basic research findings into patient benefit. The Institute is also at the heart of the Manchester Cancer Research Centre (MCRC), an exciting development that integrates cancer research within Manchester (www.mcrc.manchester.ac.uk).

We are seeking two outstanding individuals with demonstrated records of significant achievements and the ability to establish vigorous and ambitious independent research programmes in an area of cancer biology. The programme should complement and expand existing research strengths, which include molecular oncology, stem cells, cell signalling, cell cycle control and DNA damage responses. We are particularly interested in recruiting to posts focussed on our areas of priority, which currently include molecular pathology, lung cancer and women's cancers.

The positions come with generous start-up packages providing fully funded positions with running costs and substantial core research support. The successful applicant will manage a team of research scientists and laboratory technicians in their specific research area, and will be responsible for the professional development of their laboratory personnel.

Senior Group Leader:

Applicants to this position must have a PhD, a proven record in running an independent laboratory, normally including the ability to attract grant funding, and an excellent track record of publication in journals of excellence. Senior Group Leaders are reviewed by Cancer Research UK every five years. This position would be at Reader/Professorial level, and is non-time limited. The package includes:

- **Competitive personal salary**
- **Up to four additional posts plus running expenses**
- **Access to core-funded PhD students and clinical fellows**
- **Generous package for equipment**
- **High quality laboratory space for the group, with scope for expansion for additional staff secured by outside funding**
- **Access to all core facilities**

Junior Group Leader:

Applicants to this tenure track position will have a PhD plus relevant experience of post-doctoral training along with an excellent record of research including significant first author publications in high quality peer-reviewed journals. The position is at Lecturer/Senior Lecturer level, with review at five years for consideration for promotion to a Senior Group Leader position. The package includes:

- **Competitive personal salary**
- **Three additional positions plus running expenses**
- **Access to core-funded PhD students and clinical fellows**
- **Generous package for equipment**
- **High quality laboratory space for the group, with scope for expansion for additional staff secured by outside funding**
- **Access to all core facilities**

Informal enquiries should be addressed to Prof Richard Marais, Director of the Institute, email: rmarais@picr.man.ac.uk and applications including a CV, names of three referees, a short summary of past research and future plans and an Equal Opportunities form should be sent to the HR Department – jobs@picr.man.ac.uk quoting the reference number above.

Closing date: 30th March 2012

www.paterson.man.ac.uk

MANCHESTER 1824
The University of Manchester

POSITIVE ABOUT DISABLED PEOPLE

CANCER RESEARCH UK

POSITIONS OPEN

BCM
Baylor College of Medicine

FACULTY POSITION

The Department of Molecular Physiology and Biophysics at Baylor College of Medicine is seeking scientists employing advanced technologies for the cardiovascular system, neuromuscular function, metabolism/obesity, or cancer in vertebrate models of human disease. We are recruiting for **ASSISTANT** (tenure-track) or **ASSOCIATE PROFESSOR** with strong independent research programs (preferably with current NIH funding) and a commitment to excellence in graduate and medical student education. The department currently has strong research programs in both basic and translational biomedical research and has state-of-the-art facilities for confocal and multiphoton imaging, mouse MRI, computed tomography, and cores for the creation and phenotypic analysis of new mouse models. Baylor College of Medicine is a world-renowned research institution with ample opportunities for scientific interaction and collaborations within the department, throughout the College, and with the other world class institutions of the Texas Medical Center.

Applications must be received by April 15, 2012. Please electronically send your application materials to **e-mail: molphys@bcm.edu** and include a curriculum vitae and a description of your current and future research program. Additionally, have three letters of references sent separately to the same e-mail address.

SENIOR FACULTY POSITION in Developmental Neuroscience
Stark Neurosciences Research Institute
Wells Center for Pediatric Research
Indiana University School of Medicine

The Indiana University (IU) School of Medicine, in partnership with Indiana University Health, is undertaking a major expansion of neuroscience research and research facilities at its campus in Indianapolis. The Paul & Carole Stark Neurosciences Research Institute (SNRI) in partnership with the Herman B. Wells Center for Pediatric Research announces a search for an accomplished Senior-level Investigator for a position at the rank of **ASSOCIATE** or **FULL PROFESSOR** to direct and expand a multi-faculty research group in neurodevelopment and regeneration. Individuals with exceptional and well-funded research programs in any area of developmental neuroscience, particularly with direct translational potential, will have the opportunity to participate in hiring of additional junior and mid-career investigators and develop an internationally prominent research group. Of particular interest are candidates who combine cellular, molecular, or genetic approaches to investigate fundamental questions in human developmental disorders. Researchers employing interdisciplinary approaches including advanced imaging, structural biology, or electrophysiology are encouraged to apply. Primary departmental affiliation is anticipated to be in Pediatrics, Psychiatry, Neurology, or Genetics although appointments in other departments can be negotiated by mutual interest. An M.D. and/or Ph.D. degree and strong evidence of continuous productivity and grant support are required. A competitive initial support package will include ample startup funds and laboratory space in a new research building and access to exceptional core research facilities for animal and human imaging, molecular biology, chemical biology, transgenics, and computational biology and bioinformatics. More information about the SNRI (**website: http://www.snri.iusm.iu.edu**) and the Wells Center (**website: http://www.wellscenter.iupui.edu**) can be found on our websites. Interested individuals should send curriculum vitae, a research prospectus, and the names and addresses of five references. Application materials will only be accepted in electronic format by submission to the attention of **Dr. Gerry Oxford,** Executive Director, Stark Neurosciences Research Institute, IU School of Medicine at **e-mail: snri@iupui.edu.** *IU is an Equal Employment Opportunity/Affirmative Action Employer, Minorities/Females/Persons with Disabilities.*

POSITIONS OPEN

TENURE-TRACK/TENURED FACULTY
Microbiology & Infectious Diseases
Florida Atlantic University

The Charles E. Schmidt College of Medicine is seeking a tenure track/tenured faculty member at any rank to conduct research and teach microbiology and infectious diseases or a related topic to medical and graduate students. The applicant should have a well-developed research program focusing on molecular basis of human diseases and/or therapies. The successful candidate will have a Ph.D. and/or M.D.

Preferred candidates will have research interests that complement those of current faculty, a demonstrated ability to conduct innovative research, a strong record of external grant awards and must be currently funded with a NIH RO1 grant or equivalent.

Applications will be accepted until April 30, 2012 or until the position is filled. Application materials must be submitted electronically including: Administrative, Managerial and Professional (AMP) application, cover letter, curriculum vitae, a one-page statement of teaching experience and philosophy, a one-page summary of research interests and the names of three references to **website: https://jobs.fau.edu** (**position #981310**). Credentials will be subject to Florida Public Records Law. For accommodation, call **telephone: 561-297-4341.** A background check is required for the candidate selected for this position. *Equal Opportunity/Equal Access TTY/TDD 1-800-955-8771.*

MARKETPLACE